Technical Report

TR-06-25

Data report for the safety assessment SR-Can

Svensk Kärnbränslehantering AB

November 2006

Svensk Kärnbränslehantering AB
Swedish Nuclear Fuel
and Waste Management Co
Box 5864
SE-102 40 Stockholm Sweden
Tel 08-459 84 00
+46 8 459 84 00
Fax 08-661 57 19
+46 8 661 57 19

Data report for the safety assessment SR-Can

Svensk Kärnbränslehantering AB

November 2006

Preface

This document compiles and evaluates data and data uncertainties relevant to the long-term safety of a KBS-3 repository. It supports the safety assessment SR-Can, which is a preparatory step for a safety assessment that will support the licence application for a final repository in Sweden.

The report is authored by Fredrik Vahlund, SKB; Johan Andersson, JA Streamflow AB and Martin Löfgren, Kemakta Konsult AB.

The methodology, which builds on that used in SKB's most recent safety assessment, SR 97, was developed mainly by Johan Andersson, in collaboration with Fredrik Vahlund and the undersigned.

Several other experts and generalists have been involved in specific parts of the work, as is further described in Section 1.6 of the report.

The report has been reviewed by Mike Thorne, Mike Thorne and Associates Ltd, UK, Jordi Bruno, Enviros, Spain; John Hudson, Rock Engineering Consultants, UK; Ivars Neretnieks, Royal Institute of Technology, Sweden and Bill Dershowitz, Golder Associates Inc., USA.

Stockholm, November 2006

Allan Hedin

Project leader, SR-Can

Summary

This report is the data report derived within the project SR-Can. The purpose of the data report is to present input data, with uncertainty estimates, for the SR-Can assessment calculations. Data presented in the report have been derived using standardised procedures following a methodology which is presented in the initial part of the report. In this part, a template is presented that has been used when assessing input data in supporting documents as illustrated in subsequent chapters of the data report. By using the template, decisions by the SR-Can team are separated from expert input. This increases the traceability of assessment decisions.

The data report supplies assessment data for all parts of the repository system, the fuel, the canister, the buffer and backfill and the geosphere. For the geosphere, many of the data are based on information obtained during the site investigation programme.

Contents

1 Introduction

This report provides input data, with uncertainty estimates, to the safety assessment SR-Can. The data are provided for a wide selection of conditions and are assessed through standardised procedures based on a methodology in which input provided by experts is distinguished from judgements made by the SR-Can team, as further described in Chapter 2.

This chapter presents the purpose of the Data report, as well as general information needed when reading the report. This includes background information for the report and the SR-Can assessment, a description of the two sites which is needed when reading sections covering site-specific data, the different radionuclides identified to be of importance for the analysis and hence the requiring discussion in this Data report, and projects and reports related to the SR-Can assessment and the Data report.

1.1 Background

The SR-Can project is a preparatory stage for the SR-Site assessment, the assessment that will be used for SKB's application to build a final repository. The purposes of the safety assessment SR-Can are the following:

1. To assess the safety of potential KBS-3 repositories at Forsmark and Laxemar to dispose of canisters as specified in the application to build the encapsulation plant.
2. To provide feedback to design development, to SKB's R&D programme, to further site investigations and to future safety assessment projects.
3. To foster a dialogue with the authorities that oversee SKB's activities, i.e. the Swedish Nuclear Power Inspectorate, SKI, and the Swedish Radiation Protection Authority, SSI, regarding interpretation of applicable regulations, as a preparation for the SR-Site project.

The assessment relates to the KBS-3 disposal concept in which copper canisters with a cast iron insert containing spent nuclear fuel are surrounded by bentonite clay and deposited at approximately 500 m depth in saturated, granitic rock. Preliminary data from the Forsmark and Laxemar sites, presently being investigated by SKB as candidates for a KBS-3 repository are used in the assessment.

Because there are a large number of input data used in SR-Can, structured procedures for handling these data are needed.

Assessing input data – need for traceable expert decisions

All input data used in quantitative aspects of the safety assessment have uncertainties associated with them. The quality of the results of any calculation in the assessment will, among other factors, depend on the quality of the input data and on the rigour with which input data uncertainties have been handled. A methodological approach for the characterisation of input data with uncertainties and the subsequent handling of data uncertainty is therefore required.

In SR 97 (SKB's latest safety assessment), a standardised procedure was employed for all input data to radionuclide transport calculations. These data were presented in the SR 97 Data report /Andersson 1999/ which was jointly reviewed by the authorities as part of the SR 97 review /SKI/SSI 2001/. Following SR 97, both SKB /Hedin 2002, Hedin 2003/ and the authorities /Wilmot and Galson 2000, Wilmot et al. 2000, Hora 2002, Hora and Jensen 2002/ have performed investigations relevant to the data derivation process in safety assessment calculations.

The results of these studies and the general development work undertaken were initially reported and applied in the interim version of the SR-Can Data report /SKB 2004c/ which, as with all reports in the SR-Can interim series /SKB 2004defg/, was developed to show how the safety assessment methodology has been developed since SR 97.

Among other things, the reviewers of the SR 97 assessment required *quantification of uncertainties* into a form suitable for probabilistic assessment and *traceable records on the expert input* to data selection and uncertainty assessment. A new procedure, based on the one used in SR 97 and taking into account review comments, has therefore been established for SR-Can.

1.2 Objectives and scope of the Data report

The objective of this report is to compile input data, with uncertainty estimates, for the SR-Can assessment calculations for a wide selection of conditions. In contrast to SR 97, this SR-Can data report provides data not only for the radionuclide migration calculations, but also for some important aspects of the quantification of repository evolution. Furthermore, data are assessed through standardized procedures, adapted to the importance of the data, aiming at identifying the origins of uncertainties and in which the input provided by experts is distinguished from judgements made by the SR-Can team.

However, there are several issues related to data that are not covered in this report. Evaluation of processes and selection of models fit for use in the assessment process are made in the SR-Can process reports /SKB 2006cfg/. Selection of scenarios and calculation cases, which in turn define the conditions for which data need to be supplied, are made in the SR-Can main report /SKB 2006i/. The initial state of the fuel and the engineered components according to the reference design is given in an Initial state report /SKB 2006h/. Descriptions of the sites are given in the site descriptive reports /SKB 2005c, 2006k/, for Forsmark and Laxemar, respectively. The data report is based on the judgements made in those reports and does not repeat information given there, unless it is needed for the further assessment of the information or for readability. However, additional judgements are sometimes needed, in order to define input data in a form appropriate for use in the assessment.

1.3 Organisation of the report

This report is organised as follows; Chapter 1 presents the purpose of the report as well as general information needed when reading the report, such as background to the report and the SR-Can assessment in general, a description of the two sites, reasons for choosing particular radionuclides for inclusion in the assessment, and projects and reports related to the SR-Can assessment and the Data report. In Chapter 2, the methodology underpinning the data derivation process is presented. The chapter outlines the approach to data and uncertainty assessment by listing the inventory of parameters for which data are to be supplied, and describing the procedures for obtaining expert inputs and judgements made by the SR-Can team. However, all data are not equally important and it would require excessive effort to achieve the same precision and detail for all data. Various sensitivity analyses are used for determining the degree of characterisation needed in the data assessment. All factual information in this report is based on expert input provided in supporting documents, but in some cases the external expert input require substantial further evaluation by the SR-Can team. In such cases, it has not been considered helpful to have separate subsections on “Expert Input”, instead this input is clearly identified through standard referencing. Subsequent chapters (Chapter 3–6) assess the data according to the procedure described in Chapter 2, with each subsection covering one

or a few parameters for which data are to be supplied. These subsections follow a standardized outline covering:

- modelling in SR-Can,
- sensitivity of assessment results to the parameter or parameters,
- source of information,
- conditions for which data are supplied,
- conceptual uncertainties,
- data uncertainties,
- spatial and temporal variation,
- correlations,
- quantification of the data with uncertainty.

1.4 Related projects

Site-specific information in SR-Can is mainly obtained from the Site Descriptive Models, SDMs and presented in Site descriptions, e.g. /SKB 2005c, 2006k/. These are based on field data obtained from various investigation activities, such as surface based geophysics, borehole drilling and borehole testing. The data are quality controlled and then entered into the database, Sicada. The field data are interpreted and evaluated into a cross-disciplinary SDM being a synthesis of geology, rock mechanics, thermal properties, hydrogeology, hydrogeochemistry, bedrock transport properties and surface system properties

Preliminary repository layouts, from design step D1, based on the site descriptions, have been developed for the two sites. The layout considers a repository for 6,000 canisters. At Forsmark, the reference layout, assessed in SR-Can, is developed at the −400 m level. At Laxemar, the reference layout is developed at the −500 m level.

1.5 Key reports referenced

As previously indicated, the present report is one in a series of reports presenting the safety assessment SR-Can. The top document, which presents ideas central to the assessment, main results and conclusions is the Main report*. In addition to the Main report, the SR-Can series of reports also includes reports describing the initial state of the repository, three process reports describing processes in different parts of the repository system, and a FEP report presenting the features, events and processes considered in the analysis. The series also includes reports describing climate and biosphere-related issues. In Table 1-1, the different documents are identified, together with the abbreviations used when referring to these SKB authored documents in the text.

In addition to the documents in the SR-Can series of reports, SDM reports having SKB as main author are hereinafter referred to according to Table 1-2. These site reports have a uniform structure and the type of data given in one chapter in one report, can be found in the corresponding chapter in each of the reports in the site description series. In many cases, these reports also have supporting documents, for instance model documents written by experts on the different scientific areas. For clarity these are referred to as model documents using standard referencing.

* With the full title “Long-term safety for KBS-3 repositories at Forsmark and Laxemar – a first evaluation. Main Report of the SR-Can project”.

Table 1-1. Full titles and abbreviations used for documents in the SR-Can report series.

Full title	Abbreviation used in the present report	Reference
Long-term safety for KBS-3 repositories at Forsmark and Laxemar – a first evaluation. Main report of the SR-Can project	**Main report**	/SKB 2006i/
FEP report for the safety assessment SR-Can	**FEP report**	/SKB 2006e/
Initial state report for the safety assessment SR-Can	**Initial state report**	/SKB 2006h/
Fuel and canister process report for the safety assessment SR-Can	**Fuel and canister process report**	/SKB 2006f/
Buffer and backfill process report for the safety assessment SR-Can	**Buffer and backfill process report**	/SKB 2006c/
Geosphere process report for the safety assessment SR-Can	**Geosphere process report**	/SKB 2006g/
Climate related issues for the safety assessment SR-Can	**Climate report**	/SKB 2006d/
Model summary report for the safety assessment SR-Can	**Model summary report**	/SKB 2006j/

Table 1-2. Full titles and abbreviations used for site descriptive reports.

Full title	Abbreviation used in the present report	Reference
Preliminary site description. Forsmark area – version 1.2.	**Site descriptive report, Forsmark**	/SKB 2005c/
Preliminary site description. Simpevarp subarea – version 1.2.	**Site descriptive report, Simpevarp**	/SKB 2005d/
Preliminary site description. Laxemar area version 1.2	**Site descriptive report, Laxemar**	/SKB 2006k/

1.6 Distinction between experts and the SR-Can team

As further explained in Chapter 2 (which describes the methodology underpinning the present report) and especially in Section 2.2, all factual information in this report, with a few exceptions, is based on expert input provided in supporting documents. The experts are generally identified in these documents – see also the list of references, where the main references for each section are presented. In addition, the teams responsible for the site descriptions of the Forsmark and Laxemar areas /SKB 2005c, 2006k/, respectively, have provided the expert input to the site descriptions used herein. This information is primarily used in Chapter 6 but also in some other contexts, such as in relation to buffer and backfill migration where site data are required.

As some parts of the data report are SR-Can specific, which is the case for most of the site-specific data, there may not exist experts outside SKB. For parts of the data report, the sections "Input from Experts" have been omitted to clarify that all decisions actually are decisions either by the SR-Can assessment team or decisions reported in SKB authored documents and made by SKB staff.

Furthermore, the various inputs have been evaluated, including the making of final judgements on the selection of reference data values and distributions for the SR-Can calculations, by a subset of the SR-Can project group comprising the following.

- Fredrik Vahlund (SKB), Johan Andersson (JA Streamflow AB), and Martin Löfgren (Kemakta Konsult AB) – Compilation of this report and overall judgements.
- Patrik Sellin (SKB) – Sections 3.1, 3.4, and Chapter 5.
- Lars Werme (SKB) – Sections 3.2, 3.3, and Chapter 4.
- Ignasi Puigdomenech (SKB) – Section 6.1.
- Raymond Munier (SKB) – Section 6.3.

- Rolf Christiansson (SKB) – Section 6.4.
- Jan-Olof Selroos (SKB) – Sections 6.6 and 6.7.
- Allan Hedin (SKB) – SR-Can project management and overview.

This group is subsequently denoted the SR-Can team.

1.7 Review procedure

According to the objectives of the Data report, there should be a clear distinction between input provided by experts and judgements made by the SR-Can team needed for performing the safety analysis. This is reflected in the outline of the text. It is emphasised that the various experts have reviewed the compiled text and the judgements made by the SR-Can team. In addition, the data report has been reviewed by a relevant selection of members of SKB's external SIERG review group.

1.8 The sites

The site-specific data and the modelling interpretation of those data are generally described in the **Site descriptive reports**. However, the site description, and information in references given therein, cannot always be used directly in the safety assessment. There is sometimes a need also to consider non site-specific information, to add judgements on how to handle the uncertainties identified in the SDM and to make final selections of model input data. For this reason, all site data used in SR-Can is assessed in this Data report, mainly in Chapter 6, using the SDM reports as input. That chapter discusses rock mechanics, thermal, hydraulic, chemical and transport properties of importance for long-term safety. The site investigations are performed in the municipalities of Forsmark, north of Stockholm and Oskarshamn in the south. In Oskarshamn, two different subareas were initially studied, the Simpevarp and the Laxemar subareas. It was, however, later decided that SR-Can should be targeted on the Forsmark site and the Laxemar subarea (denoted the Laxemar site).

As a background, the present section presents a short overview of the site-specific information for the Forsmark and Laxemar sites. This information is mainly referred to in Chapter 6 where site-specific geosphere data are presented. In addition, data for the Simpevarp subarea have been used, where these are relevant to interpretation of the site-specific data.

The site lithology, i.e. the distribution of rock types, reveals important aspects of the structure of the site. In the SDM, the lithology is described in terms of rock domains, defined based on composition, grain size, homogeneity, and style and inferred degree of ductile deformation. Thermal, fracture and mechanical data (Sections 6.2, 6.3, and 6.4) presented in later sections of this report are all given per rock domain.

Deformation zones and fractures are important characteristics of the site, as they affect possible locations for the repository, mechanical stability, and groundwater flow. Furthermore, the deformation history and the geometry of the deformation zones affect the rock stress distribution and thereby also the properties of fractures in the volume. Understanding the deformation zones is thus key to understanding the fracturing, Section 6.3, the *in-situ* stress, Section 6.4, and the hydraulic properties, Sections 6.5.

1.8.1 The Forsmark Site

The Forsmark site is located in northern Uppland within the municipality of Östhammar, about 170 km north of Stockholm. The candidate area for site investigation, approximately 6 km long and 2 km wide, is located along the shoreline of Öregrundsgrepen, Figure 1-1.

The north-western part of the candidate area has been selected as the target location for a potential repository. Characterisation of the bedrock in the target area is undertaken by both surface-based investigations and by investigations in boreholes, the locations of which are also shown in Figure 1-1. The site information available for establishing version 1.2 of the Forsmark SDM, which is the main source for site-specific information in SR-Can, is further set out below and fully described in the **Site descriptive report, Forsmark** and supporting documents.

Lithology and division into rock domains

The candidate area is situated within the north-westernmost part of a tectonic lens in which folding, LS-tectonites, where linear ductile mineral fabrics dominate over planar equivalents, and a generally lower degree of ductile strain, are present. The lens which is ca. 25 km long and up to ca. 4 km wide extends along the Uppland coast from north-west of the nuclear power plant south-eastwards to Öregrund, Figure 1-2.

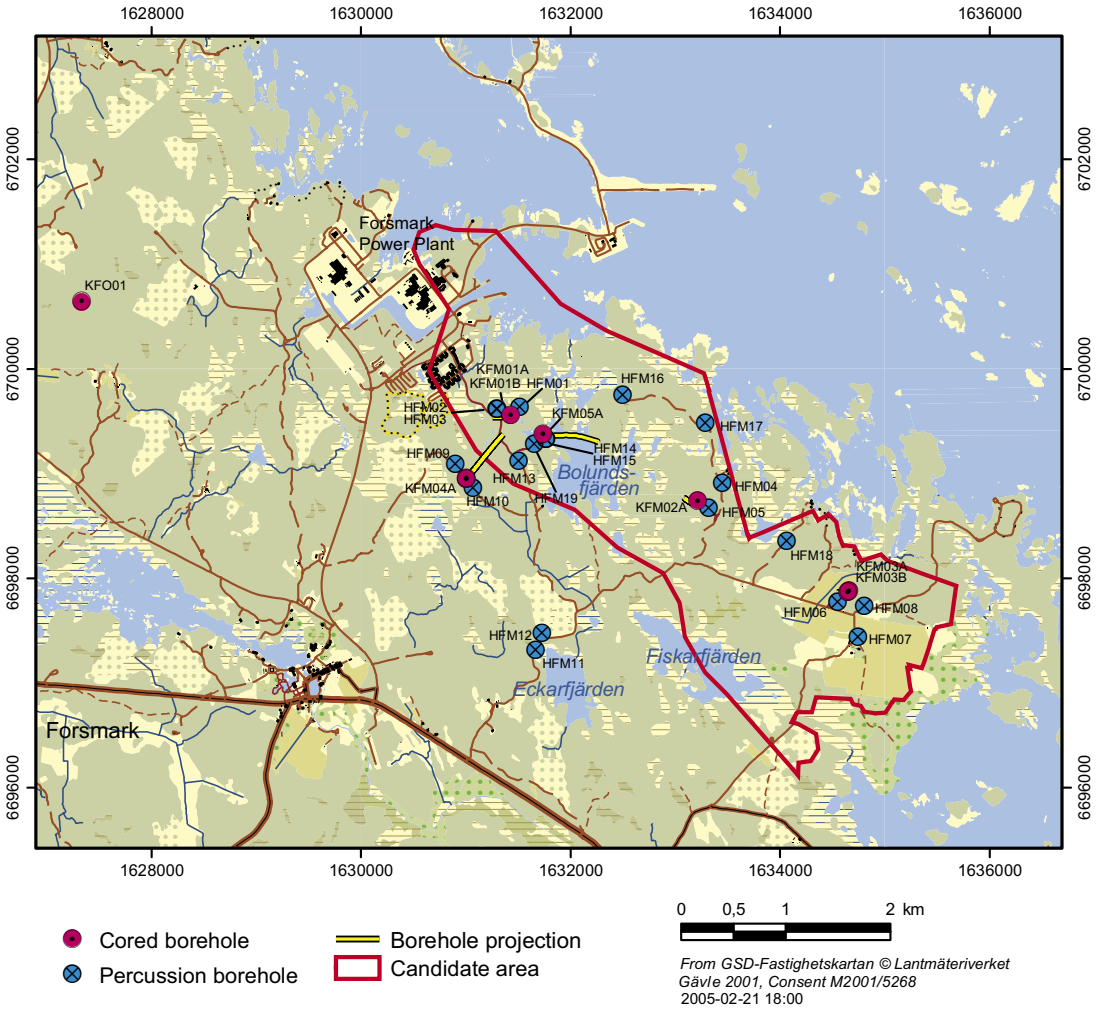

Figure 1-1. *The Forsmark site and location of deep boreholes defining the input to the SDM.*

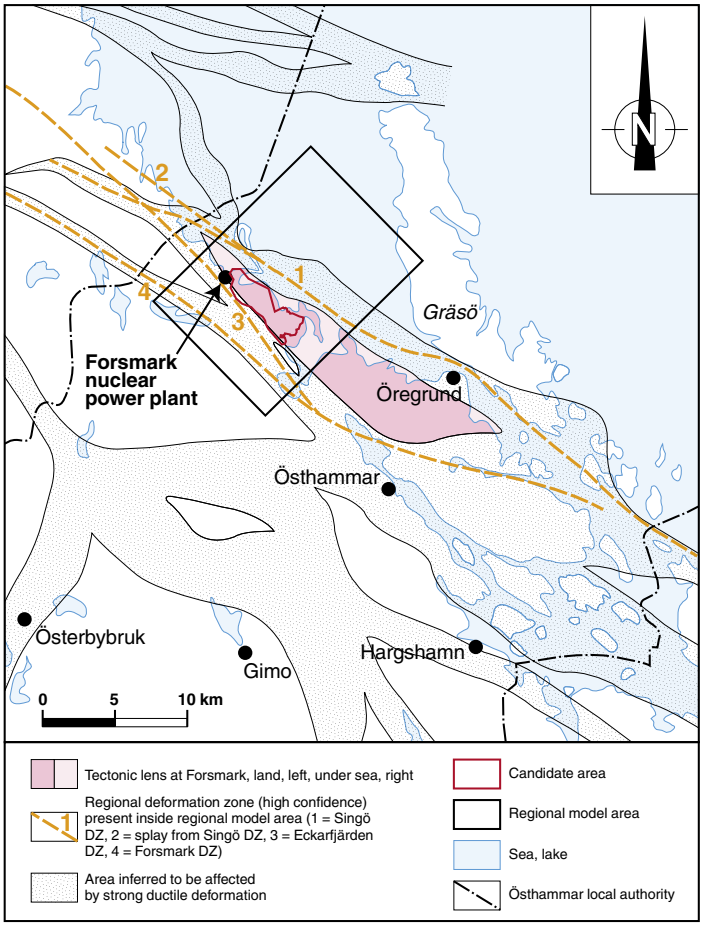

Figure 1-2. *Structural geological map of the coastal area in the local authority of Östhammar showing the extension of the tectonic lens within which the candidate area at Forsmark is situated.*

In the regional structural context of the coastal area in northern Uppland, the tectonic lens in which the candidate area is located is considered to be well established. The lens developed more than 1,800 million years ago, when the rock units were situated at mid-crustal depths and were affected by penetrative but variable degrees of ductile deformation under amphibolite-facies metamorphic conditions. The bedrock inside the lens is relatively homogeneous and is dominated by a metagranite. Although the bedrock inside the lens is relatively homogeneous, a more complex lithology and deformation pattern is considered to exist outside the lens.

A substantial amount of geologic data, both at the surface (obtained by mapping and geophysics) and from depth in the form of information from cored (5,600 m at six sites, denoted KFM*xx*) and percussion (2,850 m at 19 sites, denoted HFM*xx*) boreholes, underpins the rock domain model. Cored borehole data confirm that the character of the bedrock at approximately 1,000 m depth inside the candidate area is identical to that observed at the surface. Hence, the surface geology is the key to the geology at depths down to at least 1,000 m in the candidate area at Forsmark.

The site investigation data confirm that the tectonic lens makes up the larger part of the candidate area and, due its internal homogeneity, most of the lens can be described as a single rock domain denoted RFM029, Figure 1-3. The dominant rock type in this rock domain is medium-grained granite to granodiorite (84% of the domain volume). Subordinate rock types are fine- to medium-grained metagranodiorite or metatonalite, amphibolite, pegmatitic granite or pegmatite, and fine- to medium-grained granite. The dominant rock type and the subordinate rock types, except for amphibolite, have high quartz content (~ 20 to 50%). A foliation within the metagranite is folded, and both fold axis and mineral stretching lineations plunge towards the south-east.

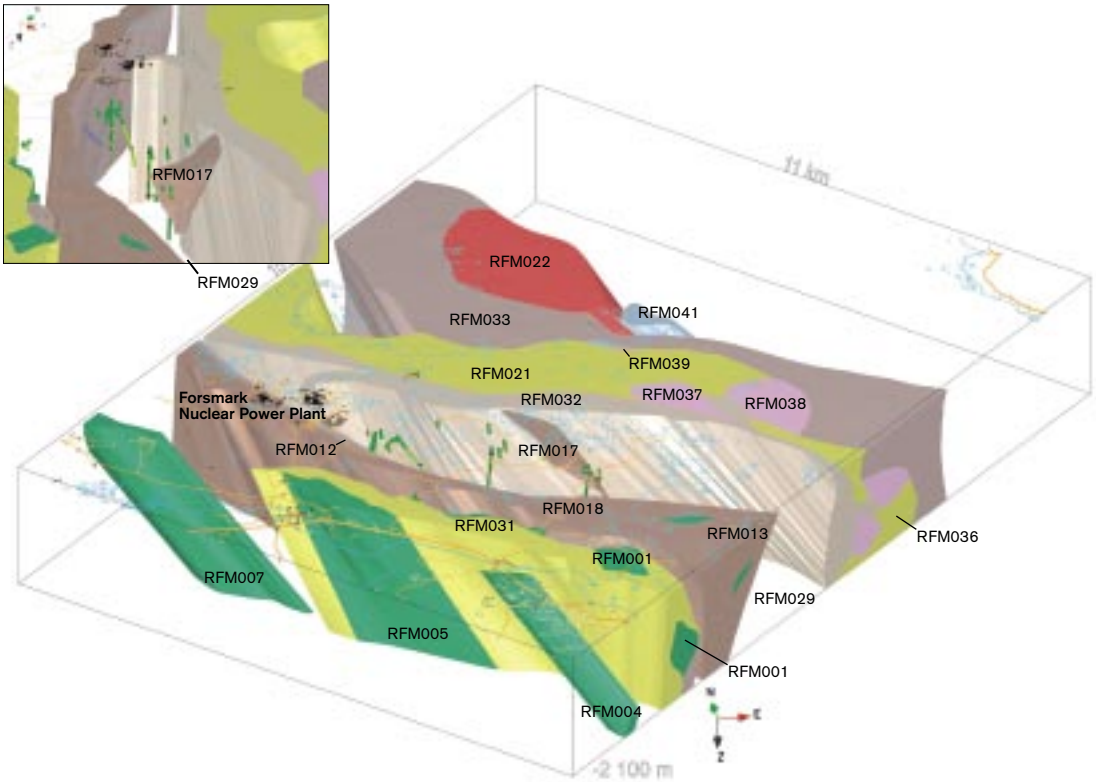

Figure 1-3. *3-D view of the rock domain model. The colours indicate the dominant rock type in each domain.*

The lens is surrounded by various domains that strike north-west, dip steeply to the south-west and are dominated by SL-tectonites, i.e. contain both planar and linear ductile mineral fabrics. In general, the rocks in these domains show a considerably higher degree of ductile deformation relative to that observed inside the tectonic lens and the bedrock is heterogeneous and composed of various types of felsic to intermediate metavolcanic rocks and metagranitoids. In the model, these are described as rock domains with strongly deformed, and also in part, banded and inhomogeneous rocks that occur along the south-western (e.g. RFM012, RFM018) and the north-eastern (e.g. RFM021, RFM032) margins of the lens. The rocks in these marginal domains dip steeply towards the south-west.

Deformation zones and fractures

Deformation zones and deformation history

Three major sets of deformation zones with distinctive orientations that have been recognised with high confidence at the Forsmark site are represented in the models. Vertical and steeply SW-dipping zones with WNW-NW strike, are regional and local major structures that show complex, ductile and brittle deformation. These zones define important structures at the boundary of the candidate volume, Figure 1-4. Vertical and steeply-dipping, brittle deformation zones with NE strike are local major (and local minor) in character. This set of zones is strongly dominated by sealed fractures and sealed fracture networks. These zones transect the candidate volume at Forsmark and are prominent in the Bolundsfjärden area, Figure 1-4 and Figure 1-5. Gently SE- and S-dipping brittle deformation zones are local major in character and occur more frequently in the south-eastern part of the candidate volume, Figure 1-5. Relative to the other three sets, there is an increased frequency of open fractures along the gently dipping set. These gently dipping zones seem to play an important role in determining the properties of the Forsmark site.

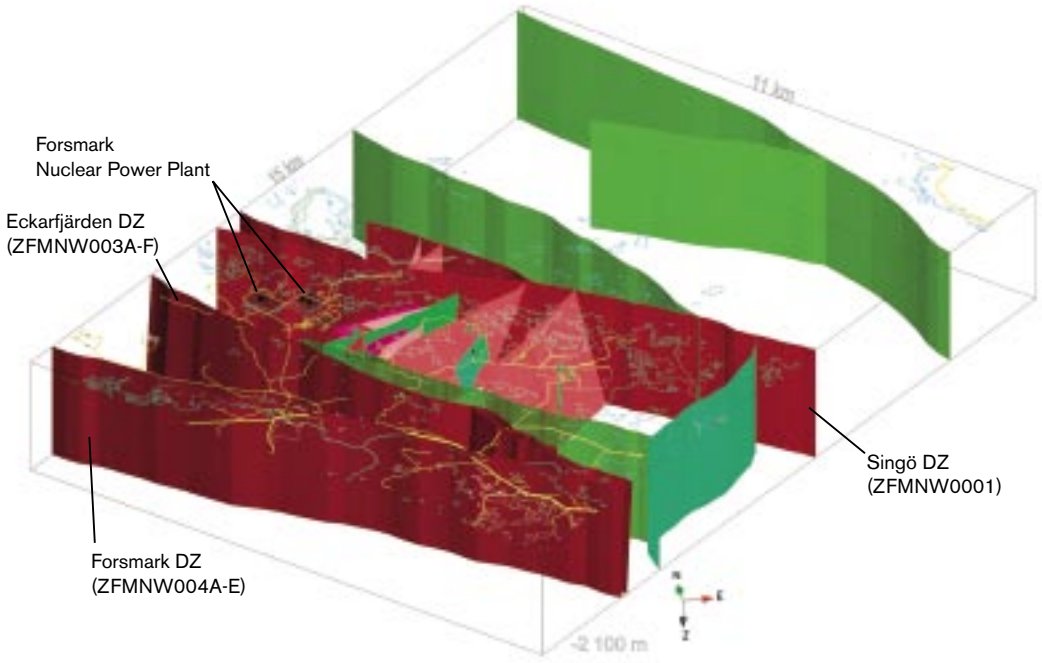

Figure 1-4. *Vertical and steeply dipping deformation zones in the version 1.2, base model (and its variant) for the site, viewed to the north. The zones coloured in red-brown shades are high confidence zones and the zones coloured in green shades are medium confidence zones. No low confidence zones are present in these two models.*

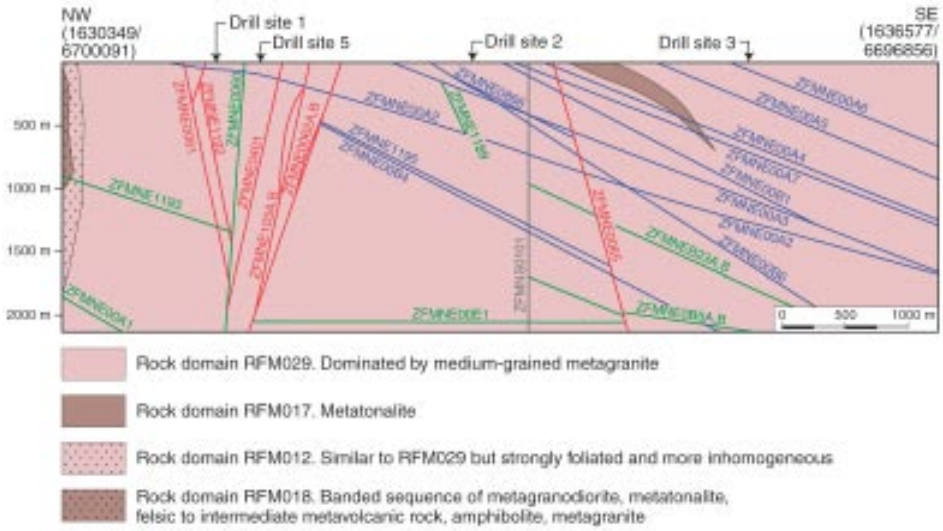

Figure 1-5. *NW-SE cross section through the candidate area in the structural model showing vertical and steeply dipping zones identified with high confidence (red), gently dipping zones identified with high confidence (blue), medium confidence zones (green) and a vertical zone identified with low confidence (grey).*

A fourth set of zones that strikes NS and is vertical or steeply dipping has also been recognized. However, only one local minor zone with a medium confidence of existence and a subordinate number of zones with a low confidence of existence have been included in model version 1.2, which is used for SR-Can. Relative to the other three sets, there is a limited number of such zones and a higher degree of uncertainty concerning the existence of this set of deformation zones.

Because of uncertainties concerning the geometry and character of deformation zones interpreted on the basis of linked lineaments, mainly in the regional domain outside the candidate area, as well as in the extension of the gently dipping deformation zones, three alternative deformation zone models were developed in version 1.2 of the SDM. These are referred to as the base model, the base model variant and the alternative model, see Figure 1-4. The difference between the base model and its variant only concerns the size of four gently dipping zones (ZFMNE00A1, ZFMNE00A2, ZFMNE00C1, ZFMNE00C2). In the alternative model (Figure 1-4), vertical and steeply-dipping zones that are generally longer than 1,000 m are described as deterministic features within the whole regional model volume. Outside the "target area" (a volume in the north-western part of the candidate area which has been the focus for more detailed investigations) virtually all these features have been identified solely on the basis of lineaments and have been assigned a low level of confidence in existence. It should be noted that the alternative model essentially only differs from the base model outside the "target area".

The deterministic deformation zone model builds on the integration of the understanding of the deformation history with surface seismic reflection data, lineament information, and fracture orientation, fracture mineralogical and bedrock alteration data from especially the cored boreholes. Gently dipping zones have mainly been detected by an integration of data from boreholes with the interpretation of seismic reflectors, see Figure 1-5. By contrast, vertical and steeply dipping zones have been recognised by an integration of data from boreholes and the surface with the interpretation of, mainly magnetic, lineaments.

Fractures and fracture domains

Smaller zones and fractures, not covered by the deformation zone model, are handled in a statistical way through discrete fracture network (DFN) models. The descriptions are based on fracture observations in the boreholes, mapped fractures at outcrops and from interpretation of lineaments.

Fracture data and analyses of these indicate a large spatial variability in the size, intensity and properties between different rock domains, but also within rock domain RFM029. The fracturing in RFM029 is of higher intensity in the upper part of the rock, but the fracture frequency shows no consistent depth dependence. Instead it seems that the fracturing is affected by the proximity to deformation zones. This is indicated by the higher frequency of fractures close to the gently dipping deformation zone ZFMNE00A2 that outcrops in the target area, and the existence of very few fractures at larger depth below this zone. This suggests that rock domain RFM029 should be subdivided into different fracture domains.

The possible need for division into fracture domains was identified as a result of the version 1.2 modelling work. Later versions of the SDM will consider dividing the volume into different fracture domains, but the version 1.2 DFN model does not make that division of rock domain RFM029 into sub-domains. Instead, one DFN model is produced for the entire rock domain. This is also the model used within SR-Can. More details of this model and associated uncertainties are given in Section 6.3.

1.8.2 The Laxemar site

The Laxemar site is part of the overall Simpevarp area located the municipality of Oskarshamn, about 300 km south of Stockholm. The Simpevarp area is divided into two parts, the Simpevarp subarea, concentrated on the Simpevarp Peninsula and the Laxemar subarea located on the mainland west of the Simpevarp Peninsula, see Figure 1-6.

The site investigations are being carried out in two stages, an initial investigation followed by a complete investigation, should the results after the initial stage be favourable. The initial stage has been completed for the Laxemar subarea and reported in the preliminary SDM version 1.2 for the Laxemar subarea /**Site descriptive report, Laxemar**/.

Figure 1-6. *Overview map of the locations of core-drilled and percussion-drilled boreholes in the Laxemar (on the left hand side) and Simpevarp (on the right hand side) subareas.*

The Simpevarp area is characterised by a relatively flat topography (ca. 0.4% overall topographical gradient), which largely reflects the surface of the underlying bedrock and is characterised by a high degree of bedrock outcrop (38%). Although flat, the landscape is interrupted by occasional narrow valleys, often associated with fracture zones in the bedrock. Till is the dominant Quaternary deposit, which covers about 35 % of the subarea.

Lithology and division into rock domains

The lithological domains defined in the Laxemar subarea, see Figure 1-7, are mainly domain RSMA primarily composed of Ävrö granite and dominating the northern and central parts of the subarea, domain RSMD consisting mainly of quartz-monzodiorite and a mixed domain RSMM (diorite to gabbro) dominating on the surface in the southwest and dipping in an arc-shape to the north, with the concave side to the north. A conspicuous rock domain (RSMP) is related to the north-easterly oriented set of shear zones that make up the eastern boundary of the subarea.

Deformation zones

The bedrock in the Simpevarp area, which generally is well preserved and non-deformed, has been exposed to a series of tectonic events that have involved shifts in the direction and magnitude of compressional forces exerted on the rock mass. The distributional pattern of deformation zones, see Figure 1-8, is different between the Simpevarp subarea, where the major deformation zones largely align with the belt of shear zones, and in the Laxemar subarea, where there is a strong element of NS and EW zones. The characteristic ductile features in the Simpevarp area are the occurrences of low-grade brittle-ductile shear zones comprising the north-easterly belt of zones associated with deformation zones ZSMNE005A (Äspö shear zone) and ZSMNE004A, which also make up the rock domain RSMP discussed above.

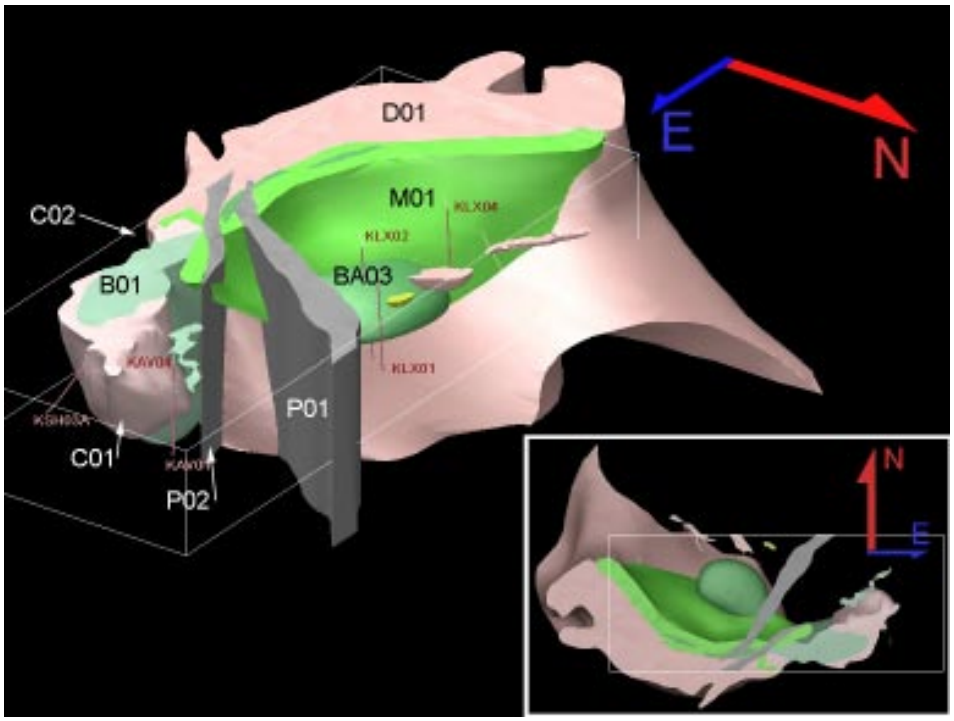

Figure 1-7. *Rock domain model of Laxemar subarea, viewed from the north east. Rock domains are indicated by short notation (i.e. B01, BA03, etc where the numbers indicate different geometrical units of the same domain). Rock domain RSMA is unshaded in order to show some of the major three-dimensional characteristics. The insert shows the model from above.*

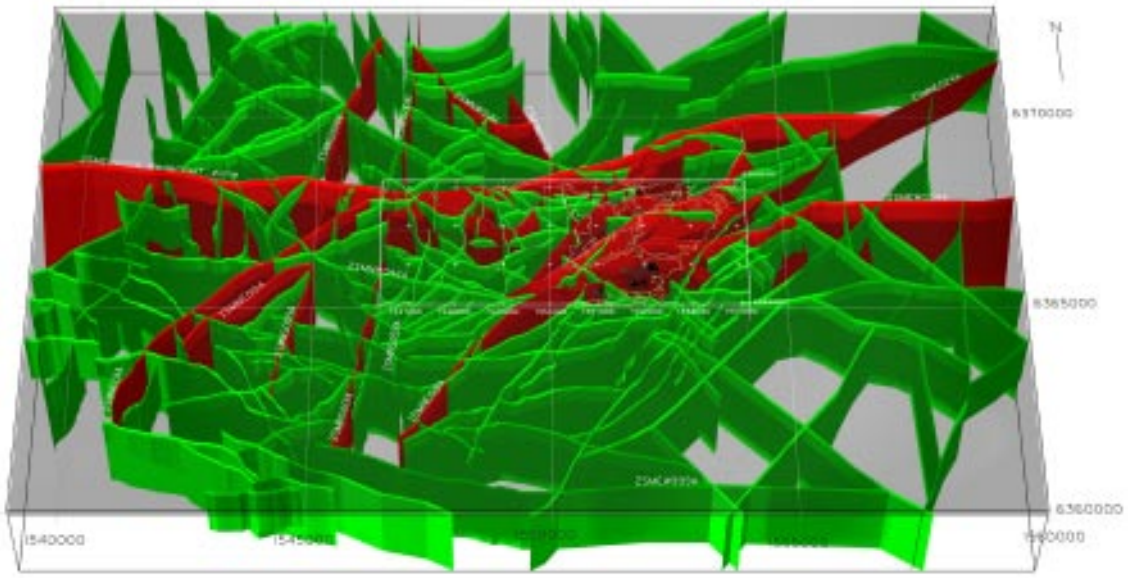

Figure 1-8. *Regional scale model of deformation zones at Laxemar. Red indicates zones with a high confidence of existence and green indicates intermediate confidence zones. The local scale model area is indicated for reference.*

Compared with the Simpevarp subarea, which is located within a belt of shear zones, the Laxemar subarea is set in a more tectonically stable environment. However, as usually observed in crystalline rock, statistical analyses of rock mass fractures between deformation zones indicate a large spatial variability in the size, intensity and properties both between and within the different rock domains. The derivation of fracture orientations has revealed five sets; three regional sets and two local sets typical of each subarea. More details of this model and associated uncertainties are given in Section 6.3.

1.9 Selection of radionuclides for the analysis

Spent nuclear fuels contain, at the time of deposition, a large number of radionuclides of which many have no or negligible importance for the overall safety of the repository due to short half life, immobility, or negligible amount present. In order to limit the number of radionuclides represented in the transport calculations and hence also the amount of input data that need to be provided, those relevant to consequence calculations are identified here and these only are discussed in subsequent chapters.

To select the important radionuclides for inclusion in SR-Can, a methodology corresponding to that used in SR 95 /SKB 1995/ and in SR 97 /SKB 1999a/ was adopted, based on considerations of radiotoxicity and the amount of each radionuclide present in the repository, Appendix A1 (discussion and quantification of the inventory and uncertainties in it are presented in Section 3.1). To simplify the analysis, two distinct groups of radionuclides have been identified, based on mobility and radiotoxicity:

1. Fission and activation products (which are highly mobile).
2. Actinides and their daughters (which have a high radiotoxicity).

For each group, the potential health hazard (defined as the product of the radiotoxicity and the amount) has calculated for each radionuclide from repository closure until one million years. This allows radioactive in-growth and decay to be taken into account in the evaluation. If the potential health hazard for a given radionuclide exceeds 0.1‰ of the total health hazard for that group at any point in time, the radionuclide is included in the assessment calculations. For the second group, only the heaviest member of each actinide chain is calculated this way. After that all the daughters in the chain are included. The 4*n* actinide chain could however be reduced to only incorporate Pu-240, since Cm-244 has a short half-life and U-236 and Th-232 will be present with such small activities that they can be neglected. However, data for thorium and uranium have to be supplied, since they appear in other chains.

The Nagra Opalinus clay safety assessment /Nagra 2002/ also included the radionuclides H-3, Be-10, Ca-41 and Mo-93. Of these, only Ca-41 is potentially important in SR-Can case, whereas the others are considered to be of negligible importance based in the methodology described above. The Finnish Radiation and Nuclear Safety Authority, STUK has issued constraints on activity releases to the environment. These are radionuclide specific and are defined for long-lived radionuclides only. All the nuclides mentioned by STUK are included in the lists above. Table 1-3 and Table 1-4 show the radionuclides considered based on the methodology described above.

In the early phase, Cs-137 dominates the potential health hazard. The radionuclides Co-60, Cd-113m and Eu-154 all have shorter half-lives than Cs-137 and are present in far smaller amounts in the waste at the time of deposition. They are also not expected to be more mobile in the repository environment than Cs-137. For the reasons mentioned, it is justified to exclude these three radionuclides from the assessment (provided that Cs-137 is not a dominant radionuclide in the assessment calculations) even though their potential health hazard is above the stimulated 0.1‰ of the total health hazard for the very short time frame (~ 10 y). Kr-85 also belongs to this group of short-lived radionuclides and does not need to be included in the calculations of radionuclide transport in the aqueous phase. However, the fate of Kr-85 in

the case of a gaseous release does need to be considered. Of the actinides considered, some have short half-lives and may conservatively be taken to be in secular equilibrium with other radionuclides in the corresponding decay chain. Table 3-1 shows the nuclides suggested (by the SR-Can team on the basis of the Quantification subsection of Section 3.1) for propagation to migration calculations.

Table 1-3. Important fission and activation products together with half-lives /LBNL 1999/.

Radionuclide	T½ (yrs)	Radionuclide	T½ (yrs)
C-14	5,730	Pd-107	$6.5 \cdot 10^{6}$
Cl-36	$3.01 \cdot 10^{5}$	Ag-108m	418
Co-60	5.27	Cd-113m	14.1
Ni-59	$7.6 \cdot 10^{4}$	Sn-126	$1 \cdot 10^{5}$
Ni-63	100	I-129	$1.57 \cdot 10^{7}$
Se-79	$1.13 \cdot 10^{6}$	Cs-135	$2.3 \cdot 10^{6}$
Kr-85	10.8	Cs-137	30.1
Sr-90	28.8	Sm-151	90
Zr-93	$1.53 \cdot 10^{6}$	Eu-154	8.59
Nb-94	$2.03 \cdot 10^{4}$	Ho-166m	$1.20 \cdot 10^{3}$
Tc-99	$2.11 \cdot 10^{5}$	Ca-41[1]	$1.03 \cdot 10^{5}$

[1] Not identified with the SR 95/SR 97 methodology.

Table 1-4. Important actinides together with half-lives /LBNL 1999/.

4n	T½ (yrs)	4n+1	T½ (yrs)
Cm-244	18.1	Cm-245	8,500
Pu-240	6,560	Am-241	432
U-236	$2.34 \cdot 10^{7}$	Np-237	$2.14 \cdot 10^{6}$
Th-232	$1.40 \cdot 10^{10}$	U-233	$1.59 \cdot 10^{5}$
		Th-229	7,340
4n+2	**T½ (yrs)**	**4n+3**	**T½ (yrs)**
Cm-246/Am-242m	4,730/141	Cm-243/Am-243	29.1/7,370
Pu-242/Cm-242	$3.73 \cdot 10^{5}$/162.8	Pu-239	24,100
U-238/Pu-238	$4.47 \cdot 10^{9}$/87.7	U-235	$7.038 \cdot 10^{8}$
U-234	$2.46 \cdot 10^{5}$	Pa-231	32,800
Th-230	$7.54 \cdot 10^{4}$		
Ra-226	1,600		

2 Approach to data and uncertainty assessment

This chapter outlines the approach to data and uncertainty assessment by listing the set of parameters for which data are to be supplied, and describing the procedures for obtaining expert input and for generating judgements made by the SR-Can team.

2.1 Input data and information flow

In SR-Can, data are needed for quantifying the evolution of the safety functions of the repository and for radionuclide migration calculations leading to dose and risk estimates. As further explained in the **Main report,** where the result of the calculations are presented, these calculations are made with a series of models each calculating the radionuclide flow in a distinct part of the system. Appendix B shows the models used in the analysis in an Assessment Model Flowchart, AMF. The data requirements of these models constitute, in principle, the input data set to be managed in the safety assessment. However, this data report provides data only for a subset of the models. Also, the importance of the various parameters differs markedly. Although data for all the several hundred input parameters must be quality assured, only a limited sub-set are uncertain to an extent important to the safety evaluation, thus requiring a detailed quantification of uncertainty. These data have been identified by sensitivity analyses of calculation results using preliminary input data ranges, often from earlier assessments. A number of calculation end-points regarding both isolation and retardation have been considered and sensitivities of these to input parameter uncertainty has been determined. Preliminary evaluations of calculation end-points and sensitivity analyses were provided in the interim version of the SR-Can Main report /SKB 2004f/, regarding both general evolution and radionuclide dose/risk. Those, and more comprehensive results from later stages of the SR-Can project, have been used to continuously update the list of data, provided in subsection 2.1.3, that required rigorous qualification for the SR-Can assessment.

2.1.1 Models for assessing repository evolution

Some important aspects of the general evolution of the repository near-field are assessed using an integrated near-field evolution model /Hedin 2004/, complemented by more elaborate analyses of specific issues. The integrated model consists of a number of sub-models, see Figure 2-1, each of which mimics a process model that was used in the SR 97 assessment. The integrated model uses the same input data as the process models, meaning that the qualified data can be used for both modelling levels.

Evolution of the far-field is assessed using the general groundwater flow codes, i.e. Connectflow (NAMMU and NAPSAC) /Marsic et al. 2001, 2002/ and DarcyTools /Svensson et al. 2002ab/ and by codes for the analysis of rock mechanics and coupled THM effects i.e. 3DEC /Itasca Consulting Group Inc 2003/ and chemical evolution i.e. PHREEQC /Parkhurst and Appelo 1999/. The input data for these analyses are basically obtained from the SDMs and, with a few exceptions, are not discussed in this report. However, input data to the rock mechanics and THM analyses are provided in Section 6.4.

Also input to codes and analyses used for modelling the climate evolution /**Climate report**/ and the biosphere /Avila et al. 2006, SKB 2006ab/ are not covered in this Data report. Inputs to the analyses not covered in this report are assessed in the modelling reports themselves.

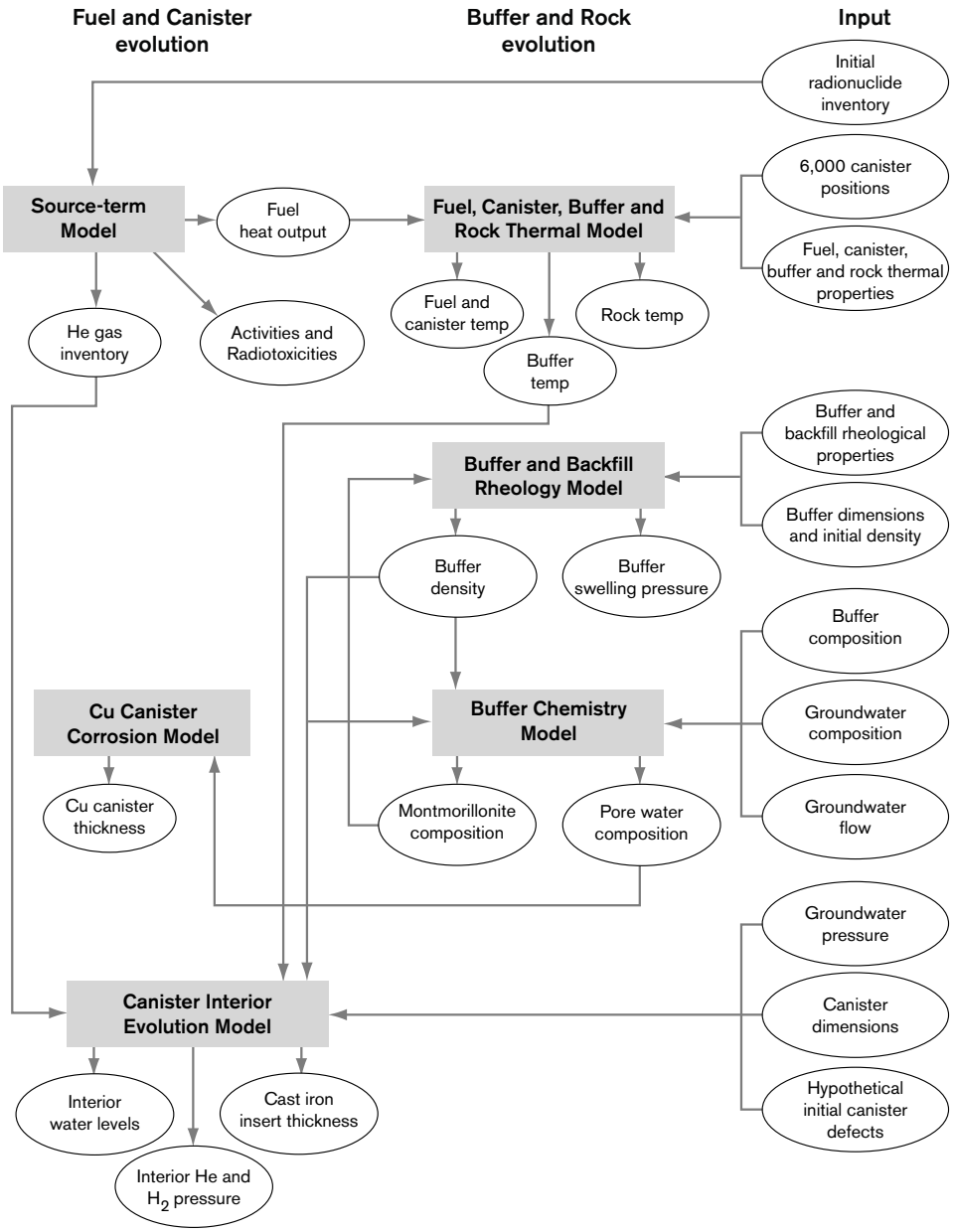

Figure 2-1. *The near-field evolution model with sub-models represented as rectangles; input data and time dependent calculation results as ellipses. Dashed lines represent dependencies, which have not yet been fully implemented.*

In the SR-Can Interim report, data for the assessment of repository evolution were presented directly in tables in Chapter 7 of the Interim main report. In SR-Can, these data are instead provided in this Data report or in other sources, as indicated in the tables (Table 2-1 to Table 2-3) displayed below. Models that require data comprise the following.

- Canister corrosion model; where the time for corroding a canister is calculated, the results of these calculations are presented in the **Main report**. The required data for these models are presented in Table 2-1.
- Thermal model, used for evaluating the thermal evaluation of the repository; the results of these calculations are presented in the **Main report**. The required data are presented in Table 2-2.
- Water saturation of the deposition hole and the effect of rock shear through the deposition hole are calculated using buffer/backfill rheology models. The required data are presented in Table 2-3.

Table 2-1. Canister corrosion sub-model data.

Parameter	Source of Data for SR-Can (and associated chapter in this report if applicable)
Diffusivity of sulphide in buffer	Buffer migration parameters, Section 5.4
Diffusivity of cations in buffer	Buffer migration parameters Section 5.4
Darcy velocity	Flow related migration parameters, subection 6.5.8
Concentration of sulphide in buffer porewater	Corrosion parameters, Section 4.5
Equivalent concentration of sulphide in solid phase	**Initial state report**

Table 2-2. Thermal sub model data for the central case. Site-specific data are taken from the Forsmark site; repository layout data from the D1 version of the site-specific layout at Forsmark. Vacuum is assumed inside the canister.

Parameter	Source of Data for SR-Can
Repository depth	**Initial state report**
Canister spacing	**Initial state report**
Tunnel spacing	**Initial state report**
Canisters per tunnel	**Initial state report**
Initial gap copper/buffer, assumed open	**Initial state report**
Initial gap buffer/rock,	**Initial state report**
Initial canister power, P_0	**Initial state report**
Rock thermal conductivity	Section 6.2 Thermal properties
Rock heat capacity	Section 6.2 Thermal properties
Temperature at repository depth	Section 6.2 Thermal properties
Buffer thermal conductivity	Section 5.1 Thermal properties of buffer
Emissivity of buffer inner surface	Section 5.1 Thermal properties of buffer
Emissivity of copper	Section 4.1 Copper physical data

Table 2-3. Buffer/backfill rheology sub-model data for the central case.

Parameter	Source of Data for SR-Can (and associated chapter in this report)
Initial clay density, ρ	Section 5.3 Density and porosity of buffer and backfill
Groundwater salinity (NaCl)	Section 5.2 Hydraulic and mechanical properties of buffer and backfill
Friction angle buffer/deposition hole, Φ	Section 5.2 Hydraulic and mechanical properties of buffer and backfill
Friction angle backfill/deposition hole	Section 5.2 Hydraulic and mechanical properties of buffer and backfill
Compression modulus of backfill, M	Section 5.2 Hydraulic and mechanical properties of buffer and backfill
Earth pressure coefficient	Section 5.2 Hydraulic and mechanical properties of buffer and backfill

2.1.2 Models for radionuclide migration calculation

Radionuclide migration is studied using a chain of models, which handle radionuclide transport in the near-field, the far-field and the biosphere. These migration models require input from analyses of the state of the barriers and the rock, i.e. the results of the system evolution analyses. The input data used by the different models (the data inventory) and the flow of information between the models are shown in Figure 2-2. Although the models are used in sequence, and radionuclide flow is only passed downstream in the chain of models, different input data may be shared by the different models or derived using the same tools. Figure 2-2 also shows

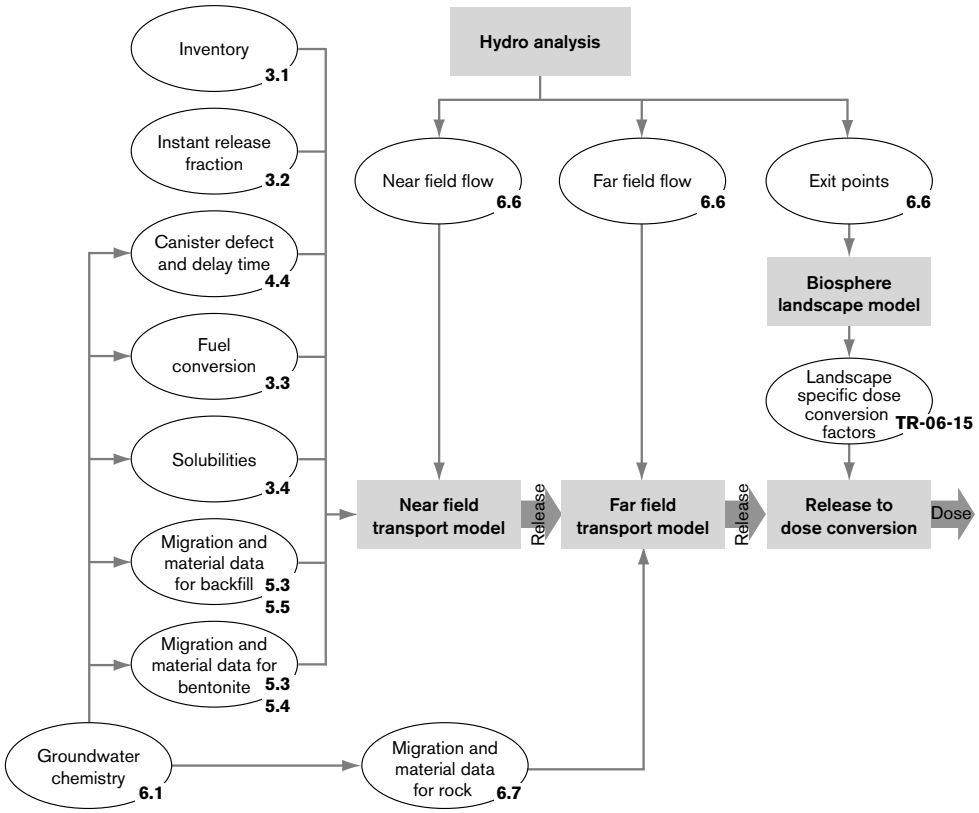

Figure 2-2. *The different radionuclide migration models used in the safety assessment, the input data and the section in the current report in which the input data are presented.*

supporting documentation, either as a reference to a SKB report or to the corresponding section in the present report. The data presented in this report has in turn other supporting documents referred to in each section, but these are not shown in the figure.

The near-field model used in SR-Can is based on the COMP23 model /Romero et al. 1999, Cliffe and Kelly 2004/. In this model, fuel dissolution and radionuclide transport in the near-field are simulated for a canister having a defect that allows water to enter. The canister may not necessarily have this defect initially and the geometry of the defect may evolve over time. The near-field model requires input data on e.g. groundwater composition, radionuclide inventory, fuel conversion data (the fraction of the inventory that is instantly released or later dissolved), solubility limits, geometry and the physical properties of the canister, the buffer and the backfill. Although many of these input data correspond to engineered properties of the barrier system, the dependence on groundwater chemistry (e.g. salinity and pH) will result in site-specific data for most of the near-field parameters. Radionuclide release from the near-field, as calculated by COMP23, occurs by three characteristic transport paths Q1–Q3, Figure 2-3, where:

- Q1, corresponds to a fracture intersecting the deposition hole. In the discrete fracture network model, DFN, used for hydrogeological modelling, several fractures may intersect the deposition hole and these could be located anywhere along the longitudinal axis of the hole. However, to simplify the near-field migration model, the flow rates of all fractures intersecting the deposition hole are assigned to a single fracture. This fracture is placed on the opposite side of the buffer to the canister defect, hence minimising the transport distance and the diffusional transport resistance.
- Q2, corresponds to the excavated damaged zone, EDZ, and is in the hydrogeology model treated as a thin conductive layer located at the bottom of the deposition tunnel. As explained in Section 6.5, the extension of the EDZ in the longitudinal direction depends on the quality control applied during excavation and the excavation method (tunnel boring machine or drill and blast).

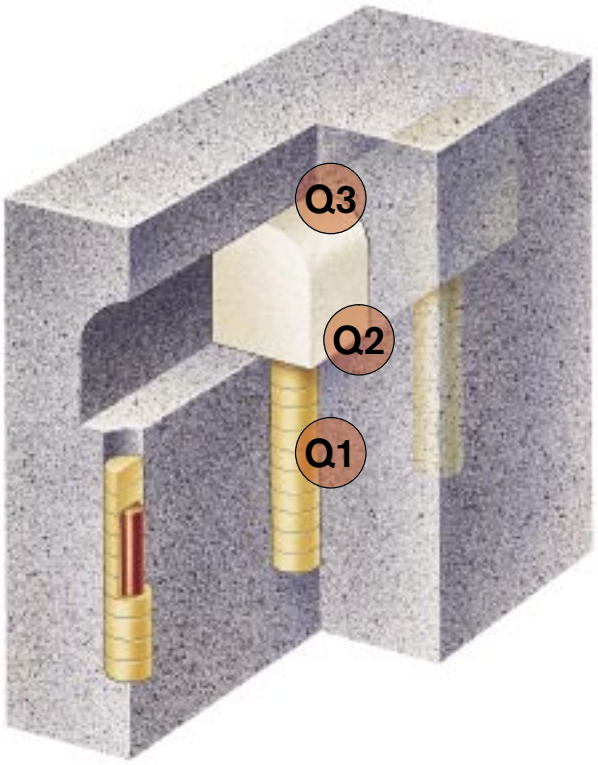

Figure 2-3. *Transport pathways implemented in the near-field model; Q1 represents that to a fracture intersecting the deposition hole located close to a canister defect, Q2 represents release through the EDZ and Q3 represents a larger fracture zone intersecting the deposition tunnel.*

- Q3, corresponds to a larger fracture zone intersecting the deposition tunnel. The deposition tunnel is, in the hydrogeological model, intersected by several fractures and fracture zones with different properties and the location of the Q3 fracture zone is obtained by tracking advectively transported particles released in the centre of the deposition tunnel just over the deposition hole. As the distance between the deposition hole and this fracture zone differs, the longitudinal dimensions of the modelled deposition tunnel may be different for different deposition holes.

The model uses plugs /Kelly and Cliffe 2006/ in order to better estimate the transport resistance between large compartments and fractures or between the canister defect and a larger compartment. These plugs correspond to those used in SR 97 /Lindgren and Lindström 1999/ (except for the case when the deposition hole is affected by spalling when no extra plug resistance is used).

After the particles have left the near-field model through the sinks used to represent these pathways, they are then passed to the geosphere migration code where transport calculations to the biosphere are performed.

Migration in the geosphere is modelled using the FARF31 code /Norman and Kjellbert 1990, Lindgren et al. 2002/. The conceptualisation assumes that the radionuclides migrate by advection and dispersion in the fractured rock, and the radionuclides may also diffuse into and sorb on the surfaces of the rock matrix adjacent to the fracture in which the groundwater flows. The flow properties of the groundwater are calculated by a separate code and the results are passed to the far-field code as input files. The FARF31 model is based on site-specific data that are measured and/or modelled (using site-specific models).

For the biosphere analysis, radionuclide release points given by the hydrological analyses are used together with site-specific data describing the biosphere at the modelled site /Avila et al. 2006, SKB 2006ab/.

The model chain runs either as Fortran 77 programs in the Proper package /Kjellberg 1999abc/ or as Matlab applications in the Pandora package /Jones et al. 2004/. Both codes are based on the same conceptual models for the near-field and the far-field, hence results from the two are very similar. For the biosphere, the Pandora implementation is however more advanced. The biosphere model in Proper, uses equivalent dose factors calculated in a separate code, Tensit /Jones et al. 2005/. For comparison, Pandora may be used to determine such dose factors, as well as being a part of the computational chain in which releases are linked to specific biotopes.

In order to undertake probabilistic risk assessments, these models are run for a large number of realisations using sampled input data from pre-specified distributions. To do this, the probabilistic input data set may either be generated using the Proper probabilistic engine or using a third party application like @Risk /Palisade Corporation 2004/.

2.1.3 Inventory of data needs

In the Interim data report /SKB 2004c/ a preliminary list of the main parameters for which data values were required for the SR-Can assessment calculations was presented. This list was fairly complete with regard to data needed for radionuclide transport calculations, but data needed for assessing the evolution of the repository system, including assessment of the long-term evolution of the function indicators, were generally lacking. These data are now, with some exceptions included in the present Data report. Other data, e.g. data for assessing buffer swelling have also been added. Table 2-4 lists those data that are assessed and described in this report.

Selecting which data to include in the Data report and which not to include is partly a matter of judgement. Generally, data needed by more than one analysis (to ensure consistency) and data of high importance to assessment results are addressed herein, in order to demonstrate that they have been scrutinized according to the assessment procedures presented in Section 2.3. However, there are some potentially important data and associated analyses not covered by this Data report, but instead presented in special SR-Can reports, as summarised below.

- Background, modelling and analyses of climate related processes, such as the development of ice sheets, permafrost, and shore-level displacement, are compiled for both the Forsmark and Laxemar sites in the **Climate report**.
- The biosphere modelling is described and the necessary site data are compiled in /SKB 2006a/ for Forsmark and in /SKB 2006b/ for Laxemar. The underlying dose models for each ecosystem are described in /Avila and Bergström 2006/ and the methodology and results for the calculation of the landscape dose factor values is presented in /Avila et al. 2006/.

All these topics imply extensive modelling calculations and including this information in the Data report was judged to be impractical. The data uncertainty assessment procedures applied to the data described in this report were also, to the extent possible, followed in the special reports.

Furthermore, data presented in the **Site descriptive reports** or in the **Initial state report** are not repeated here – unless it was judged necessary to make additional judgements on these data from a safety assessment point of view. Examples of the latter are rock mass thermal data, characteristics of the discrete fracture network model and evaluation of the impact of the EDZ on rock mass permeability.

Table 2-4. Data covered in this report.

Chapter	Section	Data	Main supporting document
3 Spent fuel data	3.1 Inventory	Radionuclide inventories for BWR and PWR types of fuel.	/Håkansson 2000/ for PWR and BWR
	3.2 Instant release fraction (IRF)	Instant release fractions for the different radionuclides in the analysis.	/Johnson and Tait 1997/ and /Werme et al. 2004/
	3.3 Fuel conversion	Fuel dissolution rate of the spent fuel.	/Werme et al. 2004/
	3.4 Solubilities	Solubilities of different elements used for near-field simulation.	/Duro et al. 2006/
4 Canister data	4.1 Copper physical data	Emissivity of the copper surface (other data from handbooks).	/Roos and Gelin 2003/
	4.2 Initial minimum copper coverage	Initial minimum thickness of the copper shell.	Welding demonstration series /SKB 2006l/
	4.3 Cast iron physical and mechanical data	Emissivities etc, yield strength of the insert.	/Andersson et al. 2005/
	4.4 Delay time and evolving geometry of canister defects	Time between a water pathway being established and the occurrence of a large canister defect.	Text in Data report.
	4.5 Corrosion parameters	Sulphide concentration and cast iron corrosion rate.	Text in Data report.
5 Buffer and backfill data	5.1 Thermal properties of buffer	Buffer thermal conductivity. Emissivity of buffer inner surface.	/Hökmark and Fälth 2003/
	5.2 Hydraulic and mechanical properties of buffer and backfill	Swelling pressure = f(density, salinity). Rheological properties.	Text in Data report
	5.3 Density and porosity of buffer and backfill	Density and porosities for buffer and backfill.	/Johannesson and Nilsson 2006/
	5.4 Migration data for bentonite	Diffusivity, sorption, and porosities.	/Ochs and Talerico 2004/
	5.5 Migration data for backfill	Diffusivity, sorption, and porosities for Friedland and 30/70 bentonite rock.	/Ochs 2006/ for Friedland and text in Data report
6 Geosphere data	6.1 Groundwater composition	Groundwater data.	SDM reports Forsmark and Laxemar and in Data report.
	6.2 Thermal properties	Rock thermal conductivity. Rock heat capacity. Temperature at repository depth.	SDM reports Forsmark and Laxemar and in Data report.
	6.3 Fracture data	Uncertainties in the DFN data.	SDM reports Forsmark and Laxemar and in Data report.
	6.4 Rock mechanics	Stress, rock mechanics properties, THM couplings.	SDM reports Forsmark and Laxemar and in Data report.
	6.5 Hydraulic properties and the EDZ	Hydraulic data.	Site descriptive reports Forsmark and Laxemar and in Data report.
	6.6 Flow related migration parameters	Advective travel times. F-distributions. Peclet numbers and other flow-related data used in the near and far-field simulations.	Text in Data report.
	6.7 Migration properties of the rock (non flow related)	Diffusivities, porosities, and sorption data used in far-field migration simulations.	/Crawford et al. 2006/ and /Liu et al. 2006/.

2.2 Expert input and judgements made by the SR-Can team

All factual information in this report is based on expert input provided in supporting documents. However, all data are not equally important and it would have been inappropriate to require the same precision and detail in processing of all the data. Various sensitivity analyses were used for determining the level of effort appropriate in the assessments of the various types of data.

In some cases, the external expert input require substantial further evaluation by the SR-Can team. In such cases, it has not been considered helpful or appropriate to provide a separate subsection detailing “Expert Input”. Instead, this input is clearly identified through standard referencing.

2.2.1 Instructions to experts

In subject areas where data had the potential to have a large impact on assessment results, specific subject area data assessments were conducted and documented in reports following a predefined outline. These special reports:

- were produced by identified experts,
- followed a fixed outline with instructions to the author on how to address uncertainty, and
- clearly differentiated between input provided by identified experts and input provided by the SR-Can team.

Section 2.3 provides an overall account of these instructions, but for details the reader is referred to the individual subject reports.

2.2.2 Expert input and judgements by SR-Can team in this report

This data report also generally separates expert input from judgements made by the SR-Can team. This is achieved both through clear referencing and by specific subsections entitled “Expert Input” and “Judgement by SR-Can Team”.

The SR-Can team made all the final judgements on which values and ranges to use in the assessment calculations. These judgements were then reviewed by the relevant experts.

2.2.3 Identification of experts

The individuals who originated the expert input are identified in the supporting documents as well as in the SR-Can expert database.

2.3 Assessing input data for different subject areas

The data and uncertainty estimation was made for the various subject areas. The evaluation of uncertainties and the final selection of input data for various conditions are presented in a standard outline. Each subsection summarises input from an expert or experts, usually from a subject-specific data report, and shows the judgements made by the SR-Can team. The outline, as well as the main part of the instructions to the experts, is provided below.

2.3.1 Modelling in SR-Can

Each subject section starts with a brief explanation of how the data to be supplied are used in SR-Can. This information is provided for precisely defining the input data and explaining in what context the data will be used. Motivation for the use of these models in the assessment is provided in the SR-Can report itself, in the process reports – or elsewhere.

The text is usually provided by the SR-Can team and does not involve additional expert input.

2.3.2 Conditions for which data are supplied

In this section of the protocol for data uncertainty evaluation, various "conditions" are listed for which parameter values and uncertainty estimates are needed. "Conditions" refer to boundary conditions, barrier states and other circumstances, which potentially may affect the values of the parameters to be estimated. Alternative "conditions" may arise because of various initial states, evolution within a scenario or conditions under different scenarios.

2.3.3 Sensitivity to assessment results

As appropriate, this section explains what sensitivity analyses have been performed in order to prioritise uncertainty assessments for those parameters and conditions judged to be potentially important to performance (both for overall end-points such as risk and on conditions affecting the state of the system).

Instructions to experts

Whenever sensitivity analyses have been performed, the expert is requested to discuss the following in the supporting document:

- For what ranges of the parameter is the impact on safety assessment significant and are there ranges where the impact is negligible? (For example, an element solubility larger than say 0.1 mole/litre is unlikely to imply any solubility limitation. Consequently, we need not be very precise in estimating such solubilities as long as it is established that the solubility is "high enough").
- Is the impact monotonic, i.e. is there a unidirectional relationship between the parameter value and performance, or is there an "optimal" value, or is the impact dependent in a complicated manner upon the values of other input parameters?
- What precision is needed to have an impact on safety assessment results (this answer may be different for different parameter ranges)?
- Do the answers apply to all applicable conditions – or only to some?
- In answering the above, it was requested that the expert should consider if the cited sensitivity analyses are sufficiently general to provide definitive answers.

The findings are summarised in this Data report.

Judgements by the SR-Can team

In this Data report, the SR-Can team has judged whether the expert input can be supported. When needed, additional judgements are made. In fact, there were many cases were experts did not supply information on sensitivities. In these cases, the SR-Can team has supplied the information.

2.3.4 Conceptual uncertainties

The next section explores conceptual uncertainty.

Instructions to experts

The expert were requested to discuss means of handling conceptual uncertainty in the supporting document by addressing the following set of questions:

- Are there conceptual uncertainties related to the model in which the parameter is used?
- Are there conceptual uncertainties related to models used for deriving the parameter value?
- What alternative conceptual models exist (and what influence might they have on the safety assessment)?
- In light of the previous points, can the conceptual (model) uncertainty be expressed/illustrated as parameter uncertainty in the given model, e.g. by making a bounding assumption or considering the range of different conceptual models that may apply?

The findings are summarised in this Data report.

Judgements by the SR-Can team

In this Data report, the SR-Can team has judged whether the expert input can be supported. This assessment is essentially based on the discussion in the **Process reports**, which focuses on conceptual uncertainty. When needed, additional judgements are made.

2.3.5 Data uncertainty, spatial and temporal variation

The next section concerns spatial and temporal variation and data uncertainties.

Instructions to experts

In the supporting document the experts were requested to address the following types of questions:

- What is known about the spatial variation (scales, variograms, discrete feature statistics etc) of the parameter? Is there any information about the uncertainty in the spatial variability? How is this considered in the parameter and uncertainty estimates?
- What is known about the temporal variability of the parameter? How is this considered in the parameter and uncertainty estimates?
- If the parameter value and uncertainty estimates are drawn from a database, is this site-specific or generic? In the latter case, how does the lack of site-specific data influence the uncertainty?
- Are parameter and uncertainty estimates based on analyses of field/laboratory data? Are there any measurement errors etc and how are they considered in the uncertainty estimates? Are there biases in, or is there poor representativity of, the data and how is this accounted for?
- If data for estimating the parameter have been produced using a model, what uncertainties does this introduce?

The findings are summarised in this Data report.

Judgements by the SR-Can team

In this data report, the SR-Can team judges whether the expert input can be supported. When needed, additional judgements are made.

2.3.6 Correlations

A correct treatment of probabilistic input data requires that any correlations between those data are identified and quantified. The extensive work with the FEP database and the Process reports implies that most functional dependencies between parameters will have been identified – and the important ones implemented in the safety assessment models. Also, the assessment of impacts from various conditions should cover most potential correlations. However, other statistical correlations may exist.

Instructions to experts

In the supporting document experts were requested to address the following questions:

- If the data varies in space or time – is anything known about its autocorrelation structure?
- Is there any other reason (apart from already cited functional relations etc) to suspect correlation between parameters considered as input to SR-Can?

The findings are summarised in this Data report.

Judgements by the SR-Can team

In this Data report the SR-Can team judges whether the expert input can be supported. When needed, additional judgements are made.

2.3.7 Quantification of uncertainty

Finally, the various sources of information are combined into quantified data and uncertainty estimates.

Instructions to experts

Based on their previous assessment, i.e. also considering conceptual uncertainty etc the experts were asked to provide justified uncertainty estimates of the applicable data. Depending on possibilities and assessed importance, the uncertainty estimates were given *either* as a *distribution function*, *subjective percentiles* or as a *range.*

The preferred option was to describe the uncertainty as a *distribution function*, but the distribution had to be justified. For example, for a spatially varying function well described by a given stochastic process, e.g. through a variogram or as realised in a DFN, a potential distribution function would be to state that all realisations of this spatially varying function are equally probable.

Another option is to only provide *subjective percentiles* a_i in the distribution function: $P(x < a_i) = p_i$, i.e. a_i is the parameter value where the subjective probability that the parameter will take a value less than a_i is p_i. If sensitivity analyses show that only part of the range has an impact on the function, less effort may be given to quantification of the distribution of parameter values outside this range. The experts were requested to justify these subjective percentiles.

If distribution functions or subjective percentiles could not be supplied, the uncertainty could instead be described as a *range*. However, the meaning of the range had then to be provided, e.g. does it represent all possible values, all “realistically possible” values or just the more

likely values? Preferably, the expert should have provided two ranges *i*) the range for which it is extremely unlikely that the parameter would lie outside this range and ii) a range for which it is likely that the parameter would lie within it.

Finally, it may also be impossible to express the uncertainty by other means than a selection of alternative data sets.

Furthermore, there are a number of uncertainties that cannot be managed quantitatively in any other rigorous manner from the point of view of demonstrating compliance than by pessimistic assumptions. This was thus allowed, as long as the expert clearly documented this together with the motivation for adopting this approach.

The uncertainty estimates were also required to provide information on correlations. The expert was asked to list other parameters to which the parameter in question may be correlated, and where this correlation is not already taken care of by functional relations in the safety assessment models. An important example was the correlation between different elements (e.g. K_d-values and solubilities) or between different radionuclides (e.g. inventory and LDF:s).

The findings are summarised in this Data report.

Judgements by the SR-Can team

In this Data report, the SR-Can team judges whether the expert input can be supported. In particular, the expert input on uncertainties and correlations may have had to be interpreted into more closed-form mathematical expressions (such as distribution functions), such that it can be used for the assessment calculations. For instance, if a most likely value and an upper and a lower bound were given, a triangular distribution may have been selected by the assessment team. The procedure of assigning distributions (needed by the assessment calculations) to input data based on small data sets includes a degree of subjectivity by the assessment team; for more discussion on this see for instance /Mishra 2002/. It was however shown in the SR-Can Interim main report /SKB 2004f/ that the impact of the use of different distributions had a limited impact on the assessment results. Corresponding work for the SR-Can assessment are shown in the **Main report**.

3 Spent fuel data

The present chapter provides data for the radionuclide inventory in the canister, the fuel dissolution rate and the instant release fractions for different fuel types as well as solubility limits for the given groundwater speciation. All data are provided per canister (or in some cases per tonnes of uranium) and not per fuel element.

3.1 Inventory

The spent fuel that is to be deposited in the deep repository consists of several different waste streams and is presently stored in the Interim storage facility, Clab. The amount of each waste type and the distribution of the total burn-ups for the wastes are described in the **Initial state report**. The majority of the spent fuel origins from boiling water reactors, BWR fuel (estimated 7,200 tonnes at the time for deposition) and pressurized water reactors, PWR fuel (estimated 2,300 tonnes at the time for deposition) in addition to those dominating waste streams, a small amount origins from other sources like mixed-oxide fuel, MOX and research reactor fuel.

By calculating the radionuclide inventory when the fuel is discharged from the reactor for different burn-ups (based on the radiation history of the spent fuel), the inventory at later times that is used for the source term in the radionuclide migration calculations may be determined by considering radioactive decay. Knowledge of the inventory is also needed when predicting the decay power in the canister used to estimate temperatures within the canister and for the repository as a whole. These estimations are however performed outside the SR-Can assessment using other tools and the present design basis is to assemble canisters with a total decay power less than 1,700W /**Initial state report**/. This initial canister power requirement determines (together with the space available in the canister) the fuel composition in each canister.

3.1.1 Modelling in SR-Can

The inventory calculations are made in steps where the first step is to calculate the burn-up of the fuel assemblies in order to find the isotopical composition of the fuel when it is discharged from the reactor. Inventories at later times are then evaluated by considering radioactive decay using ORIGEN-S /ORNL 1996/ which calculates the nuclide content, activity, and decay power from discharged from the reactor until disposed in the repository, which is the input inventory for the radionuclide migration calculations. These inventory descriptions as a function of time are used to describe the source term in the radionuclide migration codes.

3.1.2 Source of information

The present section is based on calculations by Håkansson /Håkansson 2000/ performed within the SR 97 project and no additional calculations of the radionuclide inventory have been performed within the SR-Can project. In that report, the inventories at time for deposition for two different burn-ups (38 MWd thermal output/kg U and 55 MWd thermal output /kg U) of BWR fuel elements and for two different burn-ups (42 MWd thermal output/kg U, 60 MWd thermal output/kg U) of PWR fuel elements were calculated. The calculations were mainly done using the ORNL SCALE 4.3 package based on ORIGEN /ORNL 1996/. Neutron cross sections, gamma cross sections and decay constants were taken from data bases in the SCALE package. The assembly code CASMO /Edenius et al. 1993/ was used for comparison and neutronic verification of the actinide content and the two codes showed corresponding results.

3.1.3 Sensitivity to assessment results

The release from a canister is naturally depending on the composition inside. However, due to solubility limits limiting the concentration inside the canister, as well as fuel dissolution limiting the release rate and instant release, the release for a given time is not necessarily linear to the inventory for all radionuclides /Lindgren and Lindström 1999/.

3.1.4 Conditions for which data are supplied

The calculations by /Håkansson 2000/ were made for the PWR and SVEA-96 BWR fuel. The small amount of mixed-oxide fuel and fuel from heavy water research reactors stored in the Central interim storage facility, Clab /**Initial state report**/ was not considered in that report and is also not regarded in the SR-can assessment.

3.1.5 Conceptual uncertainties

Input from experts

The inventory calculations were performed for fuel burnt under average conditions to an average burn-up. In reality there will be an axially dependent burn-up where the highest exposure will be about 20% higher than the average. For individual fuel pellets this implies that the inventories may differ substantially due to differences in irradiation history. It is however assumed that much of this local variability is averaged out over a fuel element which consist of several tenths of thousands pellets.

Differences in burn-up between different fuel elements as well as the difference between BWR and PWR fuel is also to a great extent evened out on the canister level, as the canister load is controlled by the heat load. In SKB 91 /SKB 1992/ a reference assembly of 8 BWR fuel elements were selected for a reference canister giving rise to a heat load of 950 W at the time of disposal. It was also shown that it was possible to combine fuel elements with different burn-ups and still reach an initial heat load around 1,050 W.

Judgement by the SR-Can team

The SR-Can team notes that there is an axially deviation in the burn-up for single fuel elements. However, due to the averaging over several pellets in the canister as discussed by the experts, this effect is not included in the analysis.

3.1.6 Data uncertainty, spatial and temporal variation

Input from experts

The calculations depend on three types of data:

- decay constants,
- yields,
- cross sections.

The decay constants are the most accurate of these data. The accuracy of half-lives of all important isotopes is generally 0.1% or better. The yields are measured and libraries are then constructed for least square fits for each isotope. This may lead to individual variations, but is considered accurate on the average. The cross section uncertainty is however more complex.

The basic cross section data are measured cross sections and resonance parameters. For stable and long-lived isotopes, the cross sections are well known for all reactor materials, but the uncertainties are larger for the short-lived isotopes. The significance of this uncertainty depends partly on the time frame for which the inventory needs to be calculated. At long term time scales

(>> 100 years which is the primary focus of repository performance assessment) actinides are responsible for the main part of the activity.

Given the lack of information and given the high chance that variability in the fuel pellet level will be evened out already at the fuel element level there does not seem to be a need to address spatial (i.e. from canister to canister) variability in inventory.

Håkansson /Håkansson 2000/ partly studies the impact of the cross-section uncertainty by comparing results from SCALE and CASMO. He concludes that the total uncertainty in actinides may be 20% and the total uncertainty in fission products may be 12%.

Judgement by the SR-Can team

The SR-Can team accepts the uncertainties suggested by the experts and notes that the uncertainties in the actinide inventory will not necessary scale linearly with the risk from the repository both due to the fact that other parameters than the inventory determines the risk of the inventory and, maybe more important, that several fuel elements are stored in one single canister each having an uncertainty described by the experts. The SR-Can team also note that although the general uncertainty in decay constants are small, recent studies have shown that the decay constant for Se-79 used in the calculations are inaccurate. The SR-Can team suggests that the inventory calculations for Se-79 are adjusted in the migration calculations.

3.1.7 Correlations

Input from experts

The inventories are not affected by any other process considered in the calculation chain. According to /Håkansson 2000/ uncertainties arise primarily from uncertainties in the calculation models themselves but also for uncertainties in initial fuel composition, burn-up history and procedures for canister composition. Under the assumptions made, the main uncertainties are associated with the input data used in the calculations. The pure numerical errors involved in the analyses are small.

Judgement by the SR-Can team

The SR-Can team suggest that no correlations are included in the analysis.

3.1.8 Quantification

Input from experts

Håkansson /Håkansson 2000/ presents results from inventory calculations for burn-up of 38 and 55 MWd thermal output for BWR and for 42 and 60 MWd thermal output for PWR. Håkansson /Håkansson 2000/ estimates the total uncertainty in the nuclide inventory to be 20% for actinides and 12% for fission products.

Judgement by the SR-Can team

The uncertainties are mainly connected to uncertainties in burn-up and calculation method. Due to the chain-reactions, inventories of different nuclides are also strongly interrelated. Consequently it may not be appropriate to produce ranges of the uncertainty in the inventory of a specific nuclide. Furthermore, preliminary assessment calculations in SR 97 suggested that variation of inventory has a negligible effect on release calculations since transport is limited by physical and chemical conditions in the repository. This means that it is permissible to discuss impact of inventory uncertainties in a qualitative manner and not to progress these uncertainties further down the calculation chain.

In recent publications, /LBNL 1999/, other half-life's than those used by Håkansson /Håkansson 2000/ have been suggested. Although not stated explicitly, the calculations by Håkansson /Håkansson 2000/ have been performed using a half-life of 127 years and $3.29 \cdot 10^5$ years for Ag-108m and Se-79 respectively (obtained from the tabulated inventories). The more recent studies suggest half-life's of 418 years and $1.13 \cdot 10^6$ years instead /LBNL 1999/. As the inventory description in /Håkansson 2000/ is given in Becquerel, the actual half-life's used by Håkansson /Håkansson 2000/ are hence needed when converting to moles. Moreover, some nuclides (Se-79, Pd-107 and I-129), are not given at the time for deposition (assumed to be 40 years after discharging the fuel elements), the value at 40 years are for these nuclides extrapolated from inventory descriptions at later times. In Appendix A1 the initial inventories given in Becquerel, Table A-1, and moles, Table A-2. Additionally the inventories at 1,000 yrs (when a large defect in the canister is assumed to appear based on argumentations presented in Section 4.4) are presented in Table A-3. In the latter table it is possible to see that the *4n+2* and *4n+3* chain could be simplified to only include nuclides in Table 3-1. These are the nuclides suggested by the SR-Can team to propagate to migration calculations. In addition to the 38 MWd/kg U BWR inventory, /Håkansson 2000/ provides also data for 55 MWd/kg U BWR, 42 MWd/kg U BWR PWR and 60 MWd/kg U BWR. These are however not used in the migration calculations presented in the **Main report** and have not been recalculated to reflect the 1,000 inventories used in the analysis.

Appendix A1 summarises the suggested quantification of inventory.

3.2 Instant release fraction (IRF)

The instant release fraction governs together with the fuel dissolution the release rate of radionuclides from the spent fuel. While actinides and other nuclides embedded in the fuel matrix will be released at the dissolution rate of the UO_2 matrix, a fraction of the nuclides located at the grain boundaries and at the fuel clad gap, will be released much more rapidly (instantaneously, on a repository time scale) /**Fuel and canister process report**/. In addition to the nuclides in the fuel, a part of the inventory presented in Section 3.1, consists of activation products in the metal parts of the fuel assemblies. Since the corrosion rate of the assemblies is high on a repository timescale also the activation products will be assumed to be instantly released /**Fuel and canister process report**/.

For the SR-Can safety assessment a supporting document Werme et al. /Werme et al. 2004/ reviews the available data and is used for the expert input in the following sections. In that document, a deeper description of the processes involved is given while the following sections are aimed at explaining the uncertainty treatment and to supply the data for the calculations. In addition to the report by Werme et al. /Werme et al. 2004/, the corresponding supporting document for SR 97 by Johnson and Tait /Johnson and Tait 1997/ is used as expert documentation. After the publication of the literature review by /Werme et al. 2004/, a third estimate of the instant release fraction was presented as part of the results of the EU-Project Spent Fuel Stability (SFS) by /Johnson et al. 2004/. For fuel relevant for the SR-Can study, /Werme et al. 2004 and Johnson et al. 2004/ are generally in agreement although there are some differences in the judgements. The major difference appears to come from a more pessimistic approach to estimating grain boundary release used by Johnson et al. /Johnson et al. 2004/.

Table 3-1. Radionuclides suggested for propagation to migration calculations.

4n	4n+1	4n+2	4n+3	Single nuclides		
Cm-244	Cm-245	Cm-246	Am-243	Ag-108m	Ho-166m	Se-79
Pu-240	Am-241	Pu-242	Pu-239	C-14	I-129	Sm-151
U-236	Np-237	U-238	U-235	Cl-36	Nb-94	Sn-126
Th-232	U-233	U-234	Pa-231	Ca-41	Ni-59	Sr-90
	Th-229	Th-230		Cs-135	Ni-63	Tc-99
		Ra-226		Cs-137	Pd-107	Zr-93

3.2.1 Modelling in SR-Can

The instant release fraction in combination with the fuel dissolution rate will determine the source term used in the (near-field) radionuclide migration codes COMP23 and Compulink /Romero et al. 1999, Cliffe and Kelly 2004, Vahlund and Hermansson 2006/. The two codes are based on the assumption that a fraction of inventory is released instantaneous while the rest of the inventory is embedded in the fuel and will be released as the UO_2 matrix dissolves. Although the release rate of the radionuclides at the grain boundaries, the fuel clad gap, and in the metal parts will be slightly different /**Fuel and canister process report**/, all radionuclides not embedded in the fuel matrix will be assumed to be released instantaneously. Werme et al. /Werme et al. 2004/ actually emphasise this difference by using the term rapid release fraction instead of instant release. However, in order to avoid confusion, the present report still uses instant release fraction, IRF instead of rapid release fraction.

3.2.2 Sensitivity to assessment results

The concentration of radionuclides inside the canister has for many nuclides an upper limit set by the solubility limit of each element, see Section 3.4. Hence a sensitivity analysis of the IRF and the fuel dissolution rate must be carried out together with the sensitivity discussion for the solubility limit. Based on the near-field migration model it is however possible to make some general assumptions:

1. If the element is not solubility limited, the uncertainty in the concentration inside the canister will be proportional to the uncertainty in the instant release fraction. For some elements for which the solubility limit is expected to be high compared to the amount available inside the canister (which is given by the inventory description) such as I, Cs, C and Se we assume that their release will not be solubility limited.
2. If the element solubility is low (compared to the available amount of each element) and the IRF is high enough for the concentration to reach that level, a precipitate will be formed and the effect of the IRF on the concentration inside the canister is of less importance for the release rate.

3.2.3 Conditions for which data are supplied

The data provided by Werme et al. /Werme et al. 2004/ is based on the present (April 2003) inventory of fuel stored at the Clab interim storage facility. Besides the different waste types, also linear power rating and the burn-up have been considered. Basing the data on the actual inventory is important since the fission gas release to which the instant release fraction is correlated is describe as a function of the burn-up and the linear power rating. Hence corresponding burn-ups as those in the actual fuel should be used when evaluating IRF data from the literature /Vesterlund and Cosetti 1994, Schrire et al. 1997/.

3.2.4 Conceptual uncertainties

Input from experts

A common assumption when determining the instant release fraction is that the release of fission gases and the instant release of other nuclides are correlated. Correlating the fission gas release to the instant release fraction is generally considered as a suitable method to determine the instant release fraction. The majority of the experimental data are available for CANDU fuel and not for the PWR and BWR which are the dominating waste streams in a Swedish repository. However, Werme et al. /Werme et al. 2004/ claims that the CANDU fuel could be used and even be regarded as an extreme case due to the higher linear power rating of the CANDU fuel.

Judgement by the SR-Can team

The SR-Can team accepts the conclusions by Werme et al. /Werme et al. 2004/ that the method of using fission gas release when determining the IRF is a suitable method. The SR-Can team also accepts the conclusion that results from CANDU fuel may be used even for the present waste stream.

3.2.5 Data uncertainty, spatial and temporal variation

Input from experts

The long term variation of the instant release fraction due to athermal diffusion has been studied by Poinssot et al. /Poinssot et al. 2000, 2001, 2002/. Poinssot and co-authors have concluded that the effect of athermal diffusion on the instant release fraction is negligible for the waste streams and burn-ups considered for the SR-Can safety assessment.

Judgement by the SR-Can team

The SR-Can team accepts the conclusions by Werme et al. /Werme et al. 2004/ that the instant release fraction is not time dependant.

3.2.6 Correlations

Input from experts

As shown in a study by /Stroes-Gascoyne et al. 1994/, the release of C-14 could not to be correlated with neither burn-up nor power rating. It was argued by Johnson and Tait /Johnson and Tait 1997/ that this is reasonable since the predominant source for C-14 is nitrogen impurities introduced during the manufacturing process and are not associated with the burn-up history.

The instant release fraction of I-129, Cl-36 and Cs-135 are all proportional to the fission gas release and should hence be correlated.

Judgement by the SR-Can team

Based on the discussions by Werme et al. /Werme et al. 2004/ the SR-Can team suggests nuclides that are assumed to correlate with the fission gas release (Se, Sn, Sr) are correlated.

3.2.7 Quantification

Input from experts

The instant release fractions for C-14, Cl-36, Se-79, Tc-99, Pd-107, Sn-126, I-129 and Cs-135 suggested by Werme et al. /Werme et al. 2004/ are presented in Appendix A2 in Table A-4.

Judgement by the SR-Can team

The instant release fraction proposed by Werme et al. /Werme et al. 2004/ for C-14, Cl-36, Se-79, Tc-99, Pd-107, Sn-126, I-129 and Cs-135 is accepted by the SR-Can team.

Of the nuclides listed in Section 1.9 as important for the safety analysis, the instant release fractions are not given for all by Werme et al. /Werme et al. 2004/. For the activation products in the metal parts, primarily Nb-94, Ni-59 and Ni-61 /Håkansson 2000/ it is assumed that the corrosion rate of the metal part is relatively high. It has therefore been decided by the SR-Can team to use an IRF of 100% for these nuclides which is in line with the SR 97 safety assessment. For actinides and other immobile nuclides embedded in the fuel matrix (like Ho-166m Sm-151) an IRF equal to zero is suggested by the SR-Can team based on discussions by Johnson and Tait

/Johnson and Tait 1997/ and on the **Fuel and canister process report**. For Ag-108m, /Johnson and Tait 1997/ suggest an IRF corresponding to that suggested for I-129 and Cs-135. For Sr-90 Johnson and Tait /Johnson and Tait 1997/ presents pessimistic and realistic values. For Zr-93, an IRF of zero is suggested by Johnson and Tait /Johnson and Tait 1997/ motivated by the fact that although there are Zr-93 present in the fuel cladding, the majority of the Zr-93 inventory is appears as fission products /Håkansson 2000/. Ca-41 are not included in any of the previous studies and is in SR-Can assumed to be instantly released.

As a consequence of a more pessimistic approach of estimating grain boundary release used by Johnson et al. /Johnson et al. 2004/, the best estimate for the instant release fraction coincides with the pessimistic estimate by Werme et al. /Werme et al. 2004/. For Cs-135 and I-129 Werme et al. /Werme et al. 2004/ presents a recommended release fraction and a pessimistic one. The background to this is that Cs-135 and I-129 are the only radionuclides in the set that Werme et al. /Werme et al. 2004/ discuss that have a reasonably well established relationship with fission gas release. The pessimistic values will then refer to the estimated release from fuel with a higher burn-up than the present average. For other nuclides where both pessimistic and realistic values have been presented (Ag-108m and Sr-90), the SR-Can team interprets the pessimistic values are related to high burn-up fuel while the realistic ones are related to low burn-up fuel. Consequently, the realistic values are suggested for the SR-Can analysis.

All suggested data for the instant release fraction are presented in Table A-4.

3.3 Fuel conversion

The fuel dissolution rate is the rate at which the UO_2 matrix is dissolved. While actinides and other nuclides embedded in the fuel matrix will be released at the dissolution rate of the UO_2 matrix, a fraction of the nuclides located at the grain boundaries and at the fuel clad gap, will be released much more rapidly (instantaneously, on a repository time scale) /**Fuel and canister process report**/.In addition to the nuclides in the fuel, a part of the inventory (defined in Section 3.1 of the present report) is activation products appearing in the metal parts of the fuel assemblies. Since the corrosion rate of the assemblies are high on a repository timescale /**Fuel and canister process report**/. also the activation products will be assumed to be a part of those nuclides instantly released.

For the SR-Can safety assessment a supporting document /Werme et al. 2004/ reviews the available data and is used for the expert input in the following sections. In that document, a deeper description of the processes involved is given while the following sections are aimed at explaining the uncertainty treatment and to supply the data for the calculations.

3.3.1 Modelling in SR-Can

The dissolution of the UO_2 matrix starts when there is a hole in the canister which allows for water to enter. Based on available data for the canister defects and the corrosion rate, see Section 4.5, this will occur at least 1,000 years after the canister have been deposited. At that time, many of the shorter lived nuclides has decayed to negligible levels, the initially predominant β- and γ-radiation of the fuel has decayed and the α-radiation is dominating. Furthermore, the near-field have changed from the post-disposal conditions to a near-field that includes canister corrosion products and H_2 both generated by the anaerobic corrosion of the iron insert. Both the H_2 and the corrosion products will lower the dissolution rate.

Measuring the dissolution rate of UO_2 under repository conditions (oxygen free groundwater /**Fuel and canister process report**/.) is generally complicated since only a small amount of oxygen will oxidise the U(IV) to U(VI) which has quite different properties. In experiments, it has been observed that the dissolution rate of Uranium decreases with time, this effect has been attributed to dissolution of U(VI) impurities.

The major assumptions drawn from the studied experiments that have been used for the understanding when developing the SR-Can fuel dissolution model are

1. The solubility of amorphous UO_2 is $6.3 \cdot 10^{-10}$ M (0.15 ppb U). Any experiments that have solution concentrations of U higher than this level must contain U(VI).
2. The presence of reducing agents such as Fe(II) and H_2 in the system is very important for limiting the dissolution of UO_2 and spent fuel. H_2 is more effective than Fe(II) in lowering the U concentration in solution.
3. When experiments are conducted for long enough periods of time, to eliminate artefacts due to sample preparation and to allow the high-energy surface sites to equilibrate with the bulk of the sample, no evidence for any increase in U concentrations in solution or dissolution rate due to alpha radioactivity can be found for samples that contain alpha levels appropriate to the long term disposal condition for spent fuel.
4. Since the solution concentrations for U under the test conditions that are most successful in eliminating oxygen are extremely low, it is not possible to measure the dissolution rate of the samples directly. The best estimate of dissolution rate that can be obtained is by measuring total release from the samples at the end of a long test period and assuming that the release rate is linear. This method will overestimate the long-term release rate since in all cases where testing with H_2 has been conducted, the dissolution rate decreases with exposure time.

Moreover, it is assumed that the actinides are evenly distributed throughout the fuel matrix and will not be available for dissolution as they are exposed to water. Therefore the release of other actinides will be proportional to the uranium dissolution throughout the dissolution period.

3.3.2 Sensitivity to assessment results

The concentration inside the canister has for many nuclides an upper limit set by the solubility limit of each element. Hence a sensitivity analysis of the IRF and the fuel dissolution rate must be carried out together with the sensitivity discussion for the solubility limit. Based on the near-field migration model it is however possible to make some general assumptions:

1. If the element is not solubility limited the concentration inside the canister will be proportional to the instant release fraction. For some elements for which the solubility limit is high compared to the amount available inside the canister (which is given by the inventory description) like I, Cs, C and Se, this can be said to be undisputable.
2. If the element solubility is low (compared to the available amount of each element) and the IRF is high enough for the concentration to reach that level a precipitate will be formed and the effect of the IRF on the concentration inside the canister is of less importance.

3.3.3 Conditions for which data are supplied

The data provided in the literature review by Werme et al. /Werme et al. 2004/ is based on the present (April 2003) inventory of fuel stored at the Clab interim storage facility. Besides the different waste types, also linear power rating and the burn-up have been considered. The experimental data presented in Werme et al. have been obtained in a reducing environment.

Judgement by the SR-Can team

The SR-Can team accepts the conditions suggested by the experts. Based on conservative back of the envelope calculations, the effect of oxygen dissolved in the water is neglected at repository depth.

3.3.4 Conceptual uncertainties

Input from experts

The model is based on empirical data from a number of experiments performed under redox conditions similar to those expected in a repository at the time when water contacts the fuel. The mechanisms that control the fuel dissolution are still not sufficiently understood and there are several hypotheses put forth. There is, however, a general consensus of opinion that the fuel dissolution will be extremely slow under the conditions foreseen in the repository, i.e. in the presence of corroding iron and a hydrogen overpressure.

Judgement by the SR-Can team

The SR-Can team accepts the assessment by the experts.

3.3.5 Data uncertainty, spatial and temporal variation

Input from experts

In the experiments referred to in /Werme et al. 2004/. there are in some cases possible to see that the fuel dissolution rate is decreasing with time. This is however considered to be an experimental artefact due to excess oxygen in the experimental set-up. In the model suggested by Werme et al. /Werme et al. 2004/, the fuel dissolution rate is not dependant on time. Spatial variations have not been considered by Werme et al. /Werme et al. 2004/.

Judgement by the SR-Can team

As the linear burn-up for the fuel stored in the central interim storage is increasing (due to the increased power out take in the power plants) it is not unlikely that deposition tunnels built in the later part of the deposition period will contain fuel with higher burn-up than that deposited in the initial part. However, as neither burn-up nor groundwater composition is regarded as important parameters for the fuel dissolution /Werme et al. 2004/ spatial effects have been disregarded (or at least being assumed to be captured within the uncertainty for the fuel dissolution rate) for the SR-Can safety assessment.

3.3.6 Correlations

Input from experts

No correlations are mentioned in the expert document, based on the assumed fuel dissolution model presented in the **Fuel and canister process report**. The fuel dissolution is not a function of the burn-up and no correlation with the instant release exists.

Judgement by the SR-Can team

No correlation between IRF and fuel dissolution rate or other input parameters are suggested.

3.3.7 Quantification

Input from experts

Based on experiments described by Werme et al. /Werme et al. 2004/, a triangular probability distribution function between 10^{-6} and 10^{-8} with a maximum at 10^{-7} has been suggested.

Judgement by the SR-Can team

The SR-Can team accepts the fuel dissolution rate suggested by the experts. Due to the large magnitude of the suggested data, the SR-Can team proposes triangular distribution in log-space following the methodology suggested by Mishra /Mishra 2002/.

3.4 Solubilities

In the present section solubility limits are presented for the different elements in the assessment. It would be possible to imagine that the radionuclide concentration could be solubility limited within all different parts of the modelled system; in the canister, in the buffer and backfill material and in the rock. Since solubility limits lower the available concentration, disregarding these would generally increase the release rate of radionuclides. Solubility limits are hence only regarded for the near-field.

In contrast to the SR 97 and SR-Can interim safety assessments, where uncertainties in the solubilities were presented, uncertainties in the solubilities are in SR-Can discussed based on uncertainties in groundwater speciation.

One important issue is the sulphide solubility which dictates the corrosion rate of the canister.

3.4.1 Modelling in SR-Can

The solubility calculations in SR-Can have been performed using the computer codes PHREEQC and Medusa using the thermodynamic data base SKB-TDB (/Duro et al. 2005/ which is based on Hummel et al. /Hummel et al. 2002/). The codes are able, based on thermodynamic considerations, to predict the solubility limits for different groundwater speciations. However, in addition to the calculations a certain amount of expert judgement is required to evaluate whether the favourable phases calculated from the thermodynamic database are likely to form or not. However, removing a stable solid phase from the set of possible precipitating phases will increase the calculated radionuclide solubility.

Based on the expert judgement for the given conditions, an Excel spread sheet, which contains a subset of the thermodynamic data base (see Table A-5 in Appendix A3), has been derived in which the given groundwater speciations may be varied.

Based on the water speciation inside the canister, solubility limits are calculated for the different elements using the above mentioned codes. In the case that there are more than one nuclide of the same element, the solubility limit is shared proportionally between the nuclides (the solubility limit for a single nuclide may hence be a function of the amount of all nuclides sharing the solubility) based on the amount available.

3.4.2 Sensitivity to assessment results

Solubility limits puts an upper boundary on the radionuclide concentration inside the canister and is hence for some nuclides (those which concentration reaches the solubility limit) very important for the total release. For other nuclides, like iodine which was the most important radionuclide for early times in the SR-Can interim study /SKB 2004f/, the solubility level is too high to be of any importance in the assessment.

3.4.3 Source of information

The present section is based on expert document by Duro et al. /Duro et al. 2006/.

3.4.4 Conditions for which data are supplied

The solubilities given in /Duro et al. 2006/ are valid for the different groundwater compositions given in the expert document, Duro et al. /Duro et al. 2006/ states clearly that the solubility limits are only valid for the “very-near-field” and cannot be used to predict solubility limits in the far-field or even in some intermediate field where the groundwater composition may be different from that inside the canister. Duro et al. /Duro et al. 2006/ states moreover that the data only are valid for

1. the groundwater compositions used in the solubility assessment;
2. the redox state of the system, especially important for redox sensitive radionuclides
3. the approaches followed to calculate the solubilities.

3.4.5 Conceptual uncertainties

Input from experts

Most of the conceptual uncertainties are related to the choice of models selected to conduct the solubility assessment. In this section we will define "model" as the set of hypothesis enunciated to define our system. Any given model must be exclusively applied once the modeller is aware of which are these hypothesis and has assumed their validity in the system under study. That is, any model must be accompanied with the range of validity and with a list of limitations.

In the expert report by Duro et al. /Duro et al. 2006/ three conceptual uncertainties are listed

1. One of the most relevant uncertainties is lack of information related to the composition of the interacting groundwater. Although this could be seen, a priori as a numerical uncertainty, there is a non trivial conceptual component in it. To deal with this uncertainty, solubility calculations have been performed for a number of different groundwater speciations.
2. Amorphous or less crystalline solid phases have been credited over crystalline phases. This is not necessarily true for high temperatures and long times. This result in more pessimistic estimates.
3. The process of reduction of sulphate to sulphide process has not been considered to be in thermodynamic equilibrium. The reason for assuming this is that this process is slow and has never been observed in any abiotic system below 200°C. Having sulphate reducing bacteria present, will assist this reaction and will have impact on the solubility limit for elements limited by sulphate solids. The rate of sulphate reduction will, however, be limited by the supply of electron donors, most likely methane and hydrogen. Since the concentrations of these are much lower that the sulphate concentration, the sulphate concentration will not be much influenced by the reaction.

To better understand the impact of the different types of uncertainties on the solubility limits /Duro et al. 2006/ have produce a table which lists the different solubility limited elements together with the dominating uncertainty associated with that element, Table A-6.

Judgement by the SR-Can team

It is clear that the conceptual uncertainties define boundaries for which the calculated solubilities are valid.

3.4.6 Data uncertainty, spatial and temporal variation

Input from experts

Duro et al. lists the uncertainty of the groundwater composition as one of the most important factors for numerical uncertainties. Of the factors specifying the groundwater; Eh, pH and the concentrations, Duro et al. /Duro et al. 2006/ lists the concentration of phosphate and the concentration of iron as most important. Lack of data on phosphate concentration (or the fact that the concentration is below the detection limit) is prescribed by Duro et al. to have important impact on the solubility limiting phases and the solubility limits. To reflect this lack of data a zero phosphate concentration has been considered for most of the modelled groundwaters. The uncertainty in the iron concentration will mainly affect elements forming Fe-bearing solid phases, especially Selenium.

Another source for numerical uncertainty is the thermodynamic database used for the calculations of the solubility limiting phases. Duro et al. /Duro et al. 2006/ states that the most important uncertainty associated with the thermodynamic database is the effect of temperature on the stability of aqueous phases and solid compounds. Associated with this are the chosen activity corrections and solvers used in different codes.

Spatial and temporal variation on the longer timescale (> 1,000 yrs) are, by Duro et al. /Duro et al. 2006/ covered in the variation in the groundwater speciations. On a shorter timescale when the residual heat of the fuel element is still large, the conceptual description of the system changes and also the solubility limits.

Duro et al. /Duro et al. 2006/ emphasize that for the calculated cases, the reference temperature has been fixed at 15°C, which is the average expected in groundwater at the repository depth. Due to the presence of the waste, it is foreseen that temperature can reach up to 100°C. This thermal effect can have some effect on the solubility of the radioelements of interest.

Judgement by the SR-Can team

The SR-Can team understands the importance in having as good predictions of the groundwater as possible and are basing the analysis on field data. This data must also be combined with predictions of the groundwater evaluation with time and changes in the groundwater composition as the water passes through the buffer. The uncertainties associated with the increased temperature for earlier times in the analysis are of lesser importance if the defect in the canister occurs for times when the residual heat in the canister is small. This is further discussed in Section 4.4.

3.4.7 Correlations

Input from experts

Correlations are not covered in the expert document.

Judgement by the SR-Can team

In the SR-Can migration calculations, where solubilities are calculated for given groundwater compositions, all solubilities are correlated based on the calculated relations. Since different nuclides are sensitive to different trace element in the groundwater not all nuclides are correlated to each other.

3.4.8 Quantification

Input from experts

In Table A-5 the solubility limiting phases that are assumed to be of importance by the authors of the expert document are presented. Based on these and the thermodynamic database, the experts have provided a Microsoft Excel document which is able to calculate solubilities for the expected range of groundwater.

Judgement by the SR-Can team

The SR-Can team considers the method of basing the analysis and the assessment calculations on the groundwater speciations and uncertainties within to be preferable to the methods used in SR 97. Applicable groundwater compositions are provided in Section 6.1.

4 Canister data

This chapter provides data for the canister to be used in the analysis. Typical reference book data like copper density, thermal conductivity of the copper etc are however not included. The initial section supplies data for determining the thermal development in the canister and in the extension, together with corresponding data for the near-field material given in Chapter 5, for the repository as a whole. In the following sections, data for determining the evolution of a failed canister are provided. These sections include data on the initial copper coverage of the canister shell (the thickness of the canister shell minus the size of the largest expected defect for a full production series). Assuming that a defect in the canister exists, Section 4.4 provides an estimate of the time for a continuous water pathway between the canister insert and the buffer material to be formed. These calculations are based on data on corrosion rates, given in Section 4.5. In contrast to most other chapters in the present report the current makes, with some exceptions, no distinction between expert data and decisions made by the SR-Can team since the data supplied in most cases is SR-Can specific. The data given in some of the sections are based on manufacturing demonstration series, as the work progress these data will be more complete.

4.1 Copper physical data

The present section provides physical data, or more specifically data for the thermal analysis of the canister. While properties like conductivity and heat capacity are relatively well defined for the canister materials (these properties are available in different handbooks) and have an uncertainty of less importance for the assessment, the emissivity of the copper outer shell requires a more detailed analysis which is presented in the present section.

4.1.1 Modelling in SR-Can

Thermal analysis

In order to ensure that the temperature at the canister – buffer interface is below the prescribed, analysis of the thermal development of the repository is performed. For that analysis, information about the residual power of the fuel elements (provided in Chapter 3) and thermal properties like emissivities, thermal conductivity and heat capacity for the canister materials (present section), the engineered system (Chapter 5) and the rock (Chapter 6). In addition, the initial temperature in the repository (Chapter 6) and different geometrical properties of the repository are also required. Depending on the site, different minimum distances between the canisters may be prescribed in order to meet the thermal requirements.

4.1.2 Sensitivity to assessment results

Thermal analysis

In the initial part of the operational phase of the repository before the buffer material is fully saturated there may exist a gap between the canister and the bentonite over which heat is transferred through radiation and conduction. The heat transfer by radiation is linearly dependant on the emissivity and a decrease in the emissivity will lead to a higher thermal resistance over the gap and hence a higher temperature in the canister and at the surface. However, as the total heat transfer from the canister is the sum of the fluxes from radiation and conduction, there will be emissivity values below which a decrease will have no influence on the result as demonstrated by Hökmark and Fälth /Hökmark and Fälth 2003/. Based on the thermal analysis, the necessary distances needed between different canister positions in order to fulfil the temperature requirement may be calculated.

4.1.3 Conditions for which data are supplied and conceptual uncertainties

Thermal analysis

The emissivity of metals is strongly depending on the properties of the surface, which in its turn may be influenced by the manufacturing process degree of oxidisation on the surface etc. The present data /Roos and Gelin 2003/ are based on laboratory measurements on canister lids used in the welding experiments. In addition to the measured data, back calculations from the prototype repository have also been performed.

4.1.4 Data uncertainty, spatial and temporal variation

Presently the data on the emissivity is based on a few measurements on canister lids used in the demonstration series for the canister welds. Pending development of the manufacturing methods for the canister copper shells these emissivity values must clearly be regarded as indications of the emissivities for canisters in series production.

4.1.5 Correlations

Emissivity values should to some extent be correlated for all canisters in the repository based on previous discussion on the dependence on the manufacturing method. However, oxidising layer on the copper shell may yield less correlation between canisters.

4.1.6 Quantification

Input from experts

Laboratory measurements of the emissivity for two different canister lids /Roos and Gelin 2003/ showed an emissivity of 0.1. In another study, Hökmark and Fälth /Hökmark and Fälth 2003/ back calculated the emissivity of the copper canister based on measurements from SKB's prototype repository and obtained an emissivity of 0.3.

Judgement by the SR-Can team

As the manufacturing method has not yet been determined, emissivity values for the future production series can clearly not be determined with high accuracy. However, measurements by /Roos and Gelin 2003/ show emissivity values of 0.1 for representative samples. Hence pending an established manufacturing method for the canisters, the SR-Can team suggest an emissivity of 0.1 to be used for the outer surface of the canister.

4.2 Initial minimum copper coverage

In the KBS-3 concept, the fuel is placed in canisters consisting of a cast iron insert giving the canister its mechanical properties and a copper shell providing corrosion resistance to the insert. After the fuel has been placed in the canister, the canister is sealed and later deposited in the final repository. At SKB's Canister Laboratory, development of the canister production system is conducted in order to establish routines to; produce the copper shell of the canister, to produce the cast iron insert and to seal the canister lid by welding. In the present report, data for the strength of the canister insert is provided in Section 4.3 and data on the initial minimum thickness of the copper shell is provided in the current section. The design thickness of the copper shell of the canister is 50 mm. The corrosion barrier could, if volumetric discontinuities in the copper material occur, be less than that. The discontinuities could occur anywhere in the canister shell, however for the present analysis, defects in the canister welds are judged more likely. If the size of a discontinuity is larger than an acceptance criteria assigned during the development phase, the discontinuity is regarded as a defect.

4.2.1 Modelling in SR-Can

Based on the assumption that the copper shell provides no additional mechanical strength to the canister and only acts as a corrosion barrier, the initial minimum copper coverage is only important when calculating the corrosion resistance of the shell.

Three points in time are of interest for the migration calculations as set up in SR-Can.

1. The time at which a canister is assumed to fail, e.g. due to corrosion, t_{Fail}. Failure times are assessed for several failure mechanisms in the SR-Can main report. Input data for e.g. corrosion calculations are provided in Section 4.5.
2. The time after failure required to establish a continuous water pathway between the fuel in the canister interior and the bentonite buffer, so that radionuclide transport can take place. This time is denoted the delay time and is further discussed in Section 4.4 for the case when the failure takes the form of a small, penetrating hole in the copper shell. The delay time is essentially the time required to fill the canister with water.
3. The time at which all transport resistance in the canister is assumed to be lost, due to corrosion of the cast iron insert and the mechanical consequences of this process resulting in a large failure; t_{Large}, Also t_{Large} is further discussed in Section 4.4 for the case when the initial failure is a small, penetrating hole in the copper shell.

Radionuclide migration calculations are performed from the establishment of a continuous water pathway, i.e. from $t_{Fail} + t_{Large}$.

4.2.2 Source of information

The present section is based on work conducted at the Canister Laboratory until the summer of 2005. Up until then two different methods for welding the canister lid to the body of the canister were developed and in May 2005 one of these, the Friction Stir Welding process, FSW, was chosen as the reference method for the canister lid welds. In the supporting document, /SKB 2006l/, a demonstration series of 20 canister lids welded under production like conditions is reported. After the lids were welded, each weld was examined using the Non Destructive Testing, NDT, methods available at the Canister Laboratory to find defects in the welds. After the non destructive testing, the welds were further analysed using destructive methods to determine the exact size and, for some welds, the material composition in the defects.

The maximum defect sizes obtained for this demonstration series were then used to predict the expected maximum defect size for the total production series using extreme value statistics. This was done by fitting the measured defect sizes to a Generalised Extreme Value distribution (can be seen as a generalisation of the *Gumbel*, *Fréchet* and *Weibull* distributions) using maximum likelihood theory.

4.2.3 Sensitivity to assessment results

Assuming constant conditions (groundwater speciation and transport of corrodants to the shell) which result in a constant corrosion rate, the time for the corrosion barrier to be breached (having zero copper thickness somewhere in the shell) will be inversely proportional to the thickness of the copper shell and if the corrosion rate is high enough, the number of failed canisters during the one million year assessment period will be a function of the initial minimum copper thickness.

However, as shown in previous safety assessments /SKB 1999a, 2004f/ the part of the inventory that are initially released contributes largely to the risk at early times. Since this part of release have been shown to occur over a short time, the risk is not necessarily proportional to the number of failed canisters if the releases occur at different times. Also the fact that different failed canisters may have different release points in the biosphere suggests that the risk from the repository may depend weaker than linearly on the number of failed canisters.

In addition to the different remaining copper ligament of different copper canisters, the time between loss of the corrosion barrier, the time when radionuclides starts to migrate out of the canister and the time when no transport resistance can be attributed to the defect the time when the peak from the initially released nuclides occurs may be different even for canisters having the same initial defect size further reducing the probability for having a linear relation between risk and the remaining copper thickness.

4.2.4 Conditions for which data are supplied

The present data is based on data provided after a demonstration series of the friction stir welding method performed at SKB's Canister Laboratory /SKB 2006l/. For the welding results reported in that supporting document, a full scale (in the dimensions essential for the welds) welding machine has been used and the conditions and results can be regarded to correspond to those expected under production. After welding, non destructive testing, NDT, is performed using radiography and ultrasonic methods to find defects in the welds. Also these methods correspond to those planned to be used in the canister production facility. The data in the supporting document /SKB 2006l/ can hence be regarded as corresponding to production like conditions in a canister production facility.

4.2.5 Conceptual uncertainties

Robustness in the production process

As described in /SKB 2006l/, one requirement on the canister production process is that it should be robust in the sense that the result will be insensitive to variations in the process parameters. To achieve this, factorial design has been used to investigate the effect of the different control parameters on the derived parameters. Based on the results of the factorial experiments, a 'process window' may be defined within which the results (parameters derived from input parameters and finally the welds) are repeatable. In the supporting document /SKB 2006l/, a preliminary acceptance criterion, pending more welding data, has been suggested stating that all welding process parameters should lie within the specified process window.

Model uncertainty

The experts claim that there is a model uncertainty in the Generalised Extreme Value distribution (GEV) model, the model is however regarded to be more pessimistic than other alternative models. To further emphasise the relevance of the GEV model, a preliminary acceptance criterion has been suggested stating that observed discontinuities for welding with process parameters within the process window should not exceed certain (not yet defined) sizes.

4.2.6 Data uncertainty, spatial and temporal variation

The experts report no uncertainties.

Judgement by the SR-Can team

The SR-Can team understands the problem to extrapolate data from limited series, however pending more experimental data the SR-Can team accepts the conclusions based on this dataset.

4.2.7 Correlations

Input from experts

No correlations to other variables are addressed in the supporting document.

Judgement by the SR-Can team

The welding process is not related to any other input data for the assessment calculations, rendering the issue of correlations irrelevant.

4.2.8 Quantification

Input from experts

Based on the results for the demonstration series, the best estimate of the maximum defect size after 4,500 produced is 4.8 mm with 95% confidence limit at 7.8 mm /SKB 2006l/. In addition to the modelled data, measurement errors from the NDT testing are added resulting in an estimate of the maximum defect size of 10 mm.

Judgement by the SR-Can team

According to the statistical analysis performed on the welds in the demonstration series the maximum expected defect size for the 4,500 canister production series will reduce the copper thickness with less than 10 mm. This extrapolation has been performed under the assumption that the welds in the demonstration series are representative to welds performed during canister production. To ensure reproducible welds, a production window has been defined within which all process parameters should be kept. This is formulated in an acceptance criterion, "all welding parameters should be kept within the process window", given in the supporting document /SKB 2006l/. As the demonstration series is limited, it is as yet impossible to estimate any probability for events resulting in this acceptance criterion not being met. In addition to the first acceptance criterion (and the second stated in subsection 4.2.5), a third criterion has been defined for the NDT system stating that no defects larger than 15 mm or, for surface breaching defects, having a radius larger than 20 mm are allowed.

Assigning probabilities for events breaking any of the acceptance criteria is impossible due the limited size of the demonstration series. This may however be performed in the future when more data are available. However, as events breaching both the first and second acceptance criteria are most likely to be independent, the probability for breaching both criteria must be considered to be very small. The remaining cases would hence be an acceptable weld for which the NDT system is not operating according to the specifications or a weld having a non acceptable defect and not detected by the NDT system. For those cases, only the second one is relevant for the assessment.

In order to propagate values to the assessment calculations, the probability for breaking any of the criteria is set to 1% and the remaining case would be:

Table 4-1. Defect distribution.

99% of all canisters have no defect larger than 10 mm.
1% of all canisters have no defect larger than 15 mm.

4.3 Cast iron physical and mechanical data

While the copper shell provides the necessary corrosion barrier for the system, the insert of the canister which is made of cast iron bears the load. The inserts will be made in two different versions, one PWR version capable of hosting four fuel assemblies and one BWR version capable of hosting twelve assemblies. The canister, and hence the load bearing insert, must according the design criteria be able to carry the hydrostatic pressure from the groundwater, the isostatic load of the swelled bentonite (totally 13 MPa) and, during the glacial period, the additional load of an approximately 3,000 m thick ice sheet (30 MPa). In the present section data for assessing the probability for an isostatic collapse of the insert is presented.

4.3.1 Modelling in SR-Can

The SR-Can assessment is based on work reported in /Andersson et al. 2005, Dillström 2005/.

4.3.2 Source of information

The main information for the present section is based on work performed on full scale canister insert manufactured by different foundries /Andersson et al. 2005/. The microstructure of the inserts have been analysed at different position of the canisters and samples for mechanical testing have been taken from the inserts.

The samples have been tested in tension, compression and in three-point bending in order to determine yield stresses and ultimate strength both in compression and tension and fracture toughness. Based on the measured material data, probabilistic simulations of a section of the insert have been performed using the finite element code Ansys /Dillström 2005/. In the probabilistic simulations, not only the material properties were varied but also geometrical properties like outer radius of the inserts and eccentricity of the inserts simulating manufacturing failures.

In addition to the experimental and theoretical work /Andersson et al. 2005, Dillström 2005/, a mock-up of the canister were manufactured and tested in a cold isostatic press to hydrostatic pressures over 100 MPa /Nilsson et al. 2005/. These tests were also compared with Ansys finite element simulations for the mock-up geometries.

4.3.3 Sensitivity to assessment results

An increase in the number of isostatically failed canisters will lead to increased release from the repository. This is, however, of no consequence since the risk of canisters failing from isostatic overpressure can be dismissed (*vide infra*).

4.3.4 Conditions for which data are supplied

The present data is based on three different inserts manufactured at three different Swedish foundries according to SKB specifications and on two pressure tests performed on full diameter, reduced length canisters.

4.3.5 Conceptual uncertainties

Input from experts

The experts report no conceptual uncertainties.

Judgement by the SR-Can team

The SR-Can team accepts the conclusion by the experts.

4.3.6 Data uncertainty, spatial and temporal variation

Input from experts

The data base used for the assessment is limited and some model simplifications are made. The resulting failure probabilities are so low that their significance can be debated. If the resulting failure probability, however, would have been so high as to within the interpretable ranges, this would have shown up in the performed computations. The conclusion from the experts are that there are no uncertainties of any importance for the conclusions drawn.

Judgement by the SR-Can team

The SR-Can team accepts the conclusion by the experts.

4.3.8 Correlations

There are no correlations to other variables in the repository.

4.3.9 Quantification

Input from experts

1. For the baseline case, the probability of failure is insignificant ($\sim 2 \cdot 10^{-9}$). This is the case even though several conservative assumptions have been made both in underlying deterministic analysis and in the probabilistic analysis.
2. The initiation event dominates (over the local collapse event) when the external pressure is below the baseline case ($p = 44$ MPa). The local collapse event dominates when the external pressure is above the baseline case (the two events are equal when $p \approx 47.5$ MPa).
3. The local yielding event is strongly dependent of the assumed external pressure.
4. The analysis of collapse only considers the first local yielding event; total collapse of the insert will occur at a much higher pressure.
5. The resulting probabilities are more dependent on the assumption regarding the eccentricity of the cassette than the assumption regarding outer corner radius of the profiles for steel section cassette. The results indicate that the maximum allowed eccentricity should not be larger than 5 mm.
6. The probability of initiation of crack growth is calculated using a defect distribution where one assumes the existence of one crack-like defect. A simple scaling argument can be applied to consider the number of defects through the thickness.

Judgement by the SR-Can team

The SR-Can team accepts the conclusion by the expert that the probability for failure is insignificant when the canister is isostatically loaded.

4.4 Delay time and evolving geometry of canister defects

Before radionuclides could migrate from a failed canister a continuous water pathway between the spent fuel and the canister exterior needs to be established. Furthermore, the migration will depend on the size of the passage through the copper shell and on the void volume in which radionuclides are dissolved. These geometries also evolve over time. The expert input to this section is an evaluation made by SKB, hence the methodology of distinguishing between expert and the SR-Can team opinions as described in previous chapters have been omitted in the present sections. However, the text is based on various published research projects conducted by SKB which are referred to in the text.

4.4.1 Modelling in SR-Can

The evolution of a failed canister is complex and depends on a number of uncertain factors. Water is likely to intrude into the canister, causing corrosion of the cast iron insert with hydrogen gas generation. The build-up of gas pressure in the canister can be considerable and lead to the suppression of further water entry and also to gas release through the buffer /**Buffer and backfill process report**/. As corrosion proceeds, corrosion products, occupying a larger volume

than the corresponding amount of metallic iron, will exert mechanical pressure on the copper canister, potentially leading to an expansion of the original defect in the copper shell. The corrosion also causes a weakening of the cast iron insert, making the canister more vulnerable to isostatic pressure. This could also lead to expansion of defects.

In the radionuclide transport calculations, the canister interior is pessimistically assumed to possess no transport resistance and no sorbing capacity. Rather, as soon as the canister is filled with water, a continuous pathway between the spent fuel and the canister exterior is assumed and the canister interior is represented as an inert water volume in which radionuclides are dissolved and diffuse freely. Transport resistances or barrier functions of the inner structural parts of the canister and the fuel, including the fuel cladding, are thus disregarded once the transport pathway is established.

Key issues for the transport calculations are therefore reduced to the following:

- After canister failure, when will a continuous water pathway between the spent fuel and the canister exterior be established?
- What is then the size of the passage through the copper shell (the only transport resistance taken into account) and of the void volume in which radionuclides are dissolved?
- How will the defect size and the void volume evolve over time?

The following parameters need to be determined

- Time between failure and onset of radionuclide transport: t_{delay}.
- Time between onset and complete loss of transport resistance in canister t_{large}.
- Eventual size of defect after time t_{large}: r_{large}.

4.4.2 Sensitivity to assessment results

Rank regression coefficients (SRRC) were calculated for the SR-Can Interim base case result /SKB 2004f/. Dominating variables are the ecosystem-specific dose conversion factor for I-129 (EDF I-129), the equivalent flow rate at the deposition hole (Q_{eq1}), the delay time (t_{Delay}), the fuel dissolution rate, the instant release fraction (IRF) and the geosphere transport resistance (F). This is in line with the findings in e.g. the SR 97 assessment.

A base case assumed t_{delay} of 1,000 years, t_{large} Uniform (0–10^5 yrs) and no transport resistance from canister (the latter was implemented by setting r_{large} to an infinite value). As a variant to the base case, various assumptions of the defect were explored, see Figure 4-1. It was concluded that the overall effect of assuming an immediate large defect is small compared to the base case, since the time scales covered in the calculation are longer than the times assumed for the large effect to develop in the base case. Going from a defect radius of 2 mm to a complete loss of transport resistance implies an increase in releases and doses of about an order of magnitude.

In conclusion, it seams that t_{large} and r_{large} are not really important parameters as long as r_{large} is larger than 100 mm and t_{large} is within range assumed for the base case of SR-Can interim.

4.4.3 Conditions for which data are supplied

The evolution of the canister failure will be influenced by external factors like the external mechanical load on the canister and by the thermal conditions. Based on the findings above, no failures are expected during the initial 1,000 years when elevated temperatures will prevail in the repository.

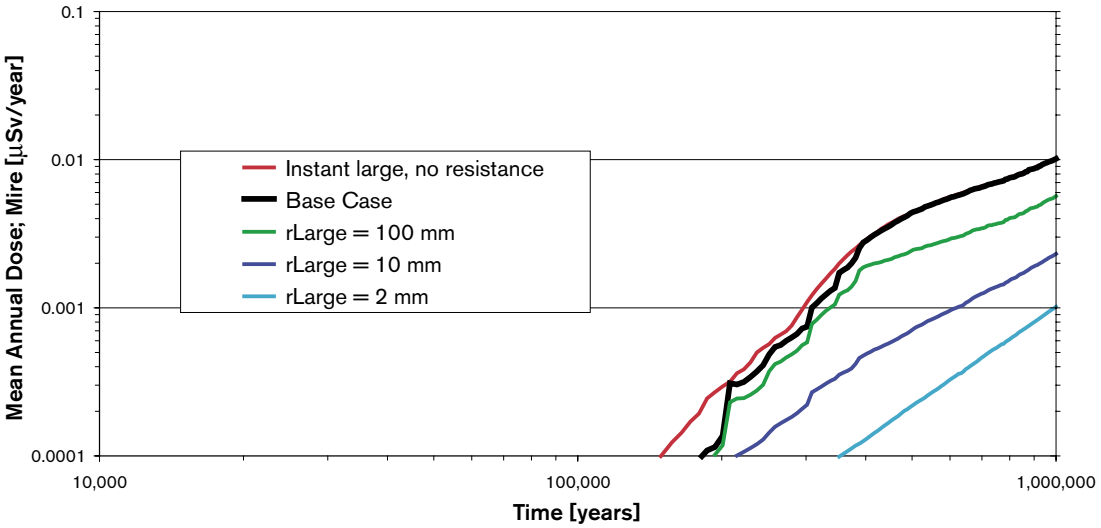

Figure 4-1. *Probabilistic results of calculations with alternative assumptions related to the internal development of failed canisters from the SR-Can interim calculations /SKB 2004f/.*

4.4.4 Conceptual uncertainties

Input from experts

In the SR 97 assessment /SKB 1999a/ the internal evolution was modelled in two separate studies /Bond et al. 1997, Takase et al. 1999/. Uncertainties regarding both understanding of the involved phenomena and data were considerable. The following is a discussion of the problem complex, based on the results of the two SR 97 studies and on some new experimental data.

Once the copper canister has been penetrated, water can intrude. The intrusion rate of water will be determined by the difference between the groundwater pressure and that in the interior of the canister, since the flow resistance of the hole is much smaller than that of the bentonite /Bond et al. 1997, Takase et al. 1999/. At a pressure difference of 4.9 MPa, corresponding to 5 MPa hydrostatic pressure and 0.1 MPa pressure in the canister, the rate of water inflow will be $3 \cdot 10^{-5}$ m^3 per year for a 6 mm diameter hole /Bond et al. 1997/.

In /Smart et al. 2002ab/ a series of different corrosion experiments are reported. Part of the study was to investigate the influence of corrosion products and water chemistry on the corrosion rates. Some of the experimental results are, therefore, not directly applicable to the situation in the repository. The mean corrosion rates were low and generally less than 1 µm per year. In high ionic strength water at pH 7 to 8, the corrosion rate for cast iron was measured as 0.1 µm per year whereas at pH 10.5, the rate was as low as 0.01 µm per year. It is difficult to judge what can be considered as a pessimistic upper bound for the corrosion rate. The measured rates span nearly two orders of magnitude, although most data indicate a rate of less than 0.1 µm per year.

Based on work by Smart et al. /Smart et al. 2002ab/, a realistic rate of anaerobic corrosion of cast iron can be set to be less than 0.1 µm per year, corresponding to a hydrogen production rate of about 0.2 litres/(m^2·year) /Smart et al. 2002ab/. This corresponds to a water consumption of 2.4 g/year, if the corrosion occurs over the full cast iron area (about 14.4 m^2). This can be compared with the water inflow rate of 30 g/year. The galvanic coupling between the cast iron and the copper will have a very limited influence on the corrosion rate. Recent experimental results indicate that the corrosion rate in de-aerated groundwater of iron coupled to copper is close to that of uncoupled iron /Smart et al. 2005/. The corrosion rate will, therefore, be too low to consume all the water that initially enters through corrosion reactions and as a consequence, the corrosion will also take place over the full cast iron surface area since the corrosion rate is the same in water vapour as it is in liquid water /Smart et al. 2002ab/.

It should be pointed out, however, that the annulus between the canister and the insert at the time of the failure of the copper canister will most likely have closed due to the swelling pressure of the bentonite /Knuutila 2001/. In these circumstances, the corrosion will take place over a much reduced area. The creep deformation of the copper shell as a result of the build-up of the bentonite swelling pressure will be further studied and the result may modify the possible scenarios for the development of a failed copper canister.

In the following, four different possibilities for the further evolution are sketched.

Base case: Corrosion in filled annulus ceases, tight insert

There will be a net inflow of water into the annulus. This inflow will decrease with time as the hydrogen counter pressure builds up and finally come to an end when the hydrogen pressure equals the hydrostatic pressure. After that, the corrosion reactions will consume the remaining water inside the annulus and corrosion will continue by water vapour. The area on the surface of the insert that will corrode will be determined by the rate at which the water is consumed, i.e. the corrosion rate, and the rate at which water diffuses into the annulus. The corrosion rate will drop with time as the magnetite layer thickens and its transport resistance increases. After 10,000 to 20,000 years depending on the manufacturing tolerances between the copper canister and the insert, the annulus or part of the annulus will be filled with magnetite. At that time no or very little water will enter the annulus and the subsequent corrosion will be controlled either by the very low supply of water or, alternatively, by the transport of iron to the original hole in the copper shell. In either case, the corrosion will most likely then drop to a very low rate. With this evolution, there will be no release from the canister until the cast iron insert fails. The strength of the insert has been shown experimentally to withstand the extra load during a glaciation and the only conceivable mechanical overload that could cause canister failure would be a massive rock shear movement.

Alternative case I: Corrosion in filled annulus continues, Cu shell expands, bentonite creep relaxation

An alternative evolution would be that, when the annulus is filled with corrosion products, corrosion will not cease but continue at the same rate over at least part of the surface area of the cast iron insert. The growth of the corrosion products will cause the copper canister to expand its radius through creep. The creep ductility of the copper is specified to be at least 10 percent. At a corrosion rate of 0.1 μm/year, this strain would not be reached for about 475,000 years and would require that the whole insert wall thickness had been corroded away. (The corrosion of 0.1 μm of iron produces approximately 0.2 μm of magnetite.) The expansion of the diameter of the copper canister would also lead to an increased bentonite density. The swelling pressure increases very rapidly with the increase in density, see Section 7.7 in SR-Can Interim /SKB 2004f/.

It seems reasonable to assume that the bentonite would “relax” by creeping/extruding into the space above the canister as the canister radius expands, limiting the swelling pressure in the gap between the canister and the rock wall to a value not too far from the original pressure. While this happens, the mechanical strength of the insert is continuously lowered and it will, at some point, fail.

It seems, however, reasonable to assume that sometime during a future glacial period, the canister insert will collapse due to the increased water pressure. Whether this would also result in failure (cracking) of the outer copper shell is not obvious and if such a failure should occur, the size and shape of the resulting hole in the canister would be highly uncertain. A possibility would be the opening of a millimetre wide axial crack over the major part of the canister length.

The above development indicates that there will be no releases until a major glaciation, which occurs in roughly 100,000 year cycles. Then, possibly, a defect of a size that remains to be

determined would occur. It would furthermore be difficult to take credit for any transport resistance from the canister for this defect.

Alternative case II: Corrosion in filled annulus continues, Cu shell expands, bentonite compression

A second alternative evolution would be that the bentonite would not relax through creep the increased swelling pressure due to the expansion of the corrosion products. This evolution is, in fact, in most respects identical to the one described above. The insert's failure would, however, happen earlier and might not even require an ice age for failure within a period of hundred thousand years. Again this evolution indicates no release until the large failure, which might, however, occur earlier than with creep relaxation.

Alternative case III: Corrosion in filled annulus ceases, corrosion continues inside insert

A third alternative evolution would be that although the cast iron in the annulus has ceased to corrode, corrosion is still possible inside the insert, in the fuel deposition channels. This corrosion would be caused by water vapour (see above). The rate is, also in this case, assessed as 0.1 μm/year. The corrosion will lead to a gradual weakening of the insert's mechanical stability until it, most likely under the increased load during an ice age, collapses. The failure would be similar to those described above.

Further development after a large defect

After a larger defect (hole) in the copper canister has developed, the corrosion of the insert will continue at the same rate as previously and the iron in the canister insert will be gradually replaced by magnetite. The copper corrosion will be very limited during this period and its rate will depend on the supply of sulphides from the rock, and the buffer and backfill.

This process will continue for some additional few hundred thousand years after the larger failure developed. The exact time will depend on the volume of iron remaining after the larger failure. During that time, there will be substantial amounts of hydrogen present in the near-field. There will also be relatively small void volumes inside the copper/magnetite canister. It also seems reasonable to assume that the magnetite will extrude into the original crack in the copper canister.

Judgement by the SR-Can team

The SR-Can team accept that it may not be possible to further reduce these uncertainties. In light of the rather limited impact of t_{large} the SR-Can team accepts that t_{large} could be anywhere between 0 and 10^5 years.

4.4.5 Data uncertainty, spatial and temporal variation

Even if the corrosion rate of cast iron is reasonable well known, there are large uncertainties in estimating the time t_{large} as is evident from the discussion above.

4.4.6 Correlations

The oxidation of the cast iron insert is accompanied by the reduction of water. The corrosion rate of the cast iron will, however, to some extent depend on the pH and on substances dissolved in the water. In that respect there is a correlation with water chemistry. This is, however, of negligible importance compared to the uncertainties discussed above.

4.4.7 Quantification

Input from experts

The above sections demonstrate that there are considerable uncertainties regarding the internal evolution of a failed canister. Conceivable outcomes range from situations where the full isolation potential is essentially maintained to those where a water pathway is established within thousands of years and the initially small damaged area expands to a larger region in tens or hundreds of thousands of years. In order to include uncertainties related to the canister evolution in the overall quantification of consequences, the following simplified treatment is adopted:

- The small defect is assumed to be circular and have a radius of 2 mm. This is rather large given the observed distribution of pore sizes from friction stir welding /SKB 2006l/.
- Following failure in the form of a small penetrating defect due to corrosion, it is assumed that at least 1,000 years will elapse before a continuous aqueous transport path between the fuel and the canister exterior is established. This assumption is based on the slow water ingress rate, further decreased by the gradual build-up of an internal counter pressure due to hydrogen gas formation, as well as on the barrier functions of the cast iron insert and of the fuel cladding. Any one of these factors is likely to provide more than 1,000 years of delay.
- The further development is assumed to eventually lead to a large failure of the copper canister, potentially to the extent that the canister offers no transport resistance to radionuclides. Based on the different possibilities for the evolution sketched above, it is assumed that this may occur at any time between 1,000 years and 100,000 years after failure. A uniform distribution of this additional time required for a large failure to develop is therefore assumed. No transport resistance for the canister is assumed when the large defect has developed. This is the most pessimistic case and will be reconsidered in the continuation of the SR-Can project.

Through the above assumptions, the uncertainties related to internal canister evolution are incorporated in the probabilistic calculations. The assumptions are, however, not based on qualified data in the same strict sense as for many other data.

Since both data and conceptual uncertainties are considerable, it is difficult, from a strict compliance calculation point of view, to claim any safety properties of a failed canister, other than an initial delay of radionuclide transport if the original failure is small. A case where all transport resistance from the canister is lost 1,000 years after failure is, therefore, also analysed. This is based on available information at this stage of the analysis and may be reconsidered. Also, the effects of assuming a finite transport resistance after a large failure will be explored in variation cases.

Table 4-2 summaries these suggestions.

Judgement by the SR-Can team

The suggestions made by the SKB expert are accepted by the SR-Can team. Especially, since it is clear from sensitivity studies (see subsection 4.4.2) that the releases would be rather insensitive to the exact choice of t_{delay} and t_{large}, as long as t_{delay} is larger than 1,000 years, and as the suggested value of r_{large} is definitely on the upper bound.

Table 4-2. Suggested values of t_{delay} and related parameters.

Parameter	Value
t_{delay}	1,000 years
r_{small}	2 mm
t_{large}	Triangular (0, 10^5, 10^5) yrs
r_{large}	“infinite”

4.5 Corrosion parameters

The corrosion parameters for the canister are for the corrosion of the copper shell, the pitting factor and the concentration (solubility) of sulphide. The total amount of corrosion during the aerated period will be determined by the amount of oxygen trapped in the repository at the time of closure. The pitting factor will determine the deepest penetration possible during that period.

During the oxygen-free period in the repository, the corrosion rate will be controlled by the transport of sulphide to the canister surface, which is determined by the concentration of sulphide in the groundwater and in the bentonite porewater and the rate of transport through the bentonite buffer.

The corrosion parameter for the canister is for the corrosion of the cast iron insert is the corrosion rate (and as a consequence, the rate of evolution of hydrogen). This parameter will be a controlling factor for the development inside a failed canister.

4.5.1 Modelling in SR-Can

The oxygen entrapped in the deposition tunnels will be consumed by several processes. Microbial activity, reactions with reducing minerals in the backfill and diffusion out of the backfill into the surrounding rock (and there be consumed by microbes and reactions with minerals) will all contribute to consuming the residual oxygen. The oxygen in the deposition hole will either be consumed by corrosion reaction with the copper canister or reactions with minerals in the bentonite buffer. The amount of oxygen reaching the canister will determine the total amount of corrosion, which is expected to be uneven general corrosion with an unevenness around the average corrosion depth of ± 50 μm.

After consumption of all residual oxygen in the repository, the anaerobic corrosion of the copper canister will be determined by the mass transport of corrodants (sulphides) to the canister surface.

After penetration of the other copper canister, anaerobic of the cast iron insert will commence. This corrosion process will be controlled, depending on the access to water by the corrosion rate of the cast iron or the supply of water.

4.5.2 Sensitivity to assessment results

The extent of corrosion and the service life of the canister will depend directly on the availability of corrodants (oxygen and sulphide) and on the assumptions made for the extent of pitting.

4.5.3 Conditions for which data are supplied

The data refer to current conditions in the Swedish bedrock at the sites under investigation and to the current conceptual design of the repository, i.e. SKB-3V.

4.5.4 Conceptual uncertainties

For the copper canister, the rate of general corrosion will be determined by the rate of transport of corrodants to the canister surface and the extent of corrosion will be determined by the amount of transported corrodants. During early period after disposal oxygen will be the corroding agent. Once the oxygen trapped in the repository after sealing is consumed by corrosion reactions, reactions with minerals and through bacterial activity, reducing conditions will be re-established at the repository horizon and transport of sulphide to the canister surface will control the rate and extent of corrosion.

When oxygen is present, pitting corrosion is conceivable. King et al. /King et al. 2001/ discuss the results of a number of corrosion studies that have been performed under conditions that simulate the canister near-field environment. Copper coupons have been exposed to compacted buffer wetted by (initially) aerated saline pore water for extended periods of time (up to 2 years) usually at elevated temperature /Litke et al. 1992, Aaltonen and Varis 1993, Karnland et al. 2000, King et al. 2001/. These experiments simulate the likely environmental conditions soon after emplacement of the canisters and saturation of the buffer material. /King et al. 2001/ concluded that despite the relative aggressiveness of the conditions in these tests, no evidence for pitting is observed. Thus, both Aaltonen and Varis /Aaltonen and Varis 1993/ and Karnland et al. /Karnland et al. 2000/ report no localized corrosion of Cu exposed to compacted clay over periods of up to 2 years. The only instance of non-uniform corrosion reported under such conditions is a so-called under-deposit corrosion reported by Litke et al. /Litke et al. 1992/. In this case the whole surface had been corroded resulting in an uneven general corrosion with variations on corrosion depth of 30 μm for an average corrosion depth of slightly over 40 μm. Based on the experimental data available the most realistic understanding of the pitting during the period when oxygen is present is that it will have the appearance of uneven general corrosion with an unevenness of roughly ± 30 to 50 μm around the average corrosion depth /**Fuel and canister process report**/

In /King et al. 2001/, estimates are made of HS^- concentrations in the groundwaters at Simpevarp and Forsmark at different times after closure of the repository. For Simpevarp, $5 \cdot 10^{-6}$ mol/L was expected immediately after re-saturation and 10,000 years into the future levels in the range 0 to $3 \cdot 10^{-5}$ mol/L were expected. For Forsmark, the corresponding values were 0 to $3 \cdot 10^{-7}$ mol/L and 0 to $3 \cdot 10^{-5}$ mol/L, respectively. In the solubility report to SR-Can a solubility of pyrite of $3 \cdot 10^{-8}$ mol/L is given /Duro et al. 2006/. The sulphide levels at Äspö HRL are in the range less than 10^{-8} mol/L up to 10^{-7} mol/L. Similar values are reported from Forsmark and Laxemar. In view of this a concentration of sulphide of $5 \cdot 10^{-5}$ mol/L can be considered as a very pessimistic upper limit. During reducing conditions only uniform attack by sulphides is to be expected

After the copper shell has been penetrated, water will come into contact with the cast iron insert, which will then start to corrode anaerobically producing hydrogen gas and solid iron corrosion products. The corrosion rate will control the development inside a failed canister. The rate of mild and cast iron corrosion under reducing conditions have been studied extensively by Smart et al. /Smart et al. 2002ab/. Their data indicate that a corrosion rate of 0.1 μm per year will be a realistic assumption. This corresponds to a hydrogen evolution rate of about 0.2 $dm^3/(m^2 \cdot y)$.

4.5.5 Data uncertainty, spatial and temporal variation

See discussion in subsection 4.5.4. For sulphide content there are mainly data uncertainties, while for the pitting corrosion the uncertainties are more of a conceptual nature.

4.5.6 Correlations

The corrosion processes are not directly affected by other processes in the near and far-field. The water flux has a limited influence at lower water flux, while at higher flux the supply of oxidants will be flux independent (See e.g. /SKB 1995/).

4.5.7 Quantification

It follows from 4.5.4 that the data that the experts suggested the following data should be used:

- sulphide concentration: $5 \cdot 10^{-5}$ mol/L,
- cast iron corrosion rate: 0.1 μm/year,

and no pitting corrosion is assumed.

5 Buffer and backfill data

The current chapter provides data for performing the necessary calculations for the buffer development. Both thermally, presented in Section 5.1, hydraulically in 5.2 and for the radionuclide migration calculations where the density and porosity of the buffer and backfill materials are evaluated. In Section 5.3, diffusivities and sorption data for the buffer and backfill, materials are evaluated in Sections 5.4 and 5.5 respectively.

5.1 Thermal properties of buffer

This section provides thermal properties, conductivity for the buffer material. There have been no designated expert report for this part of the analysis produced within the SR-Can project, instead the present section is a collection of data used in previous analyses /Börgesson et al. 1994, Ageskog and Jansson 1999, Hökmark and Fälth 2003/.

The conductivity is, as described in the **Buffer and backfill process report**, depending on the level of saturation, density and mineral composition of the buffer.

5.1.1 Modelling in SR-Can

The thermal properties of the buffer material are used in the thermal analysis for the repository where the temperature at the surface and in the interior of the canister is determined together with the temperature distribution in the bentonite and in the rock. These calculations are in SR-Can assessment performed by assuming isotropic thermal properties of the repository and considering the canister as a point source term /Hedin 2004/.

Thermal properties are also needed for analysis of the hydraulic and mechanical (THM) behaviour of the buffer and backfill material for which data are provided in Section 5.2. These calculations require more detailed data than those used for the bounding calculations for the thermal properties performed in order to determine the temperature distribution around the deposition holes performed using the tools by Hedin /Hedin 2004/ and reported in subsection 9.3.4 in the **Main report**.

5.1.2 Sensitivity to assessment results

For the analysis performed in subsection 9.3.4 in the **Main report,** it is clear that a higher conductivity of the buffer material will ideally lead to a lower temperature inside the canister (provided that the thermal properties of the rock are sufficient). As described in the **Buffer and Backfill process report** and in Section 5.2 of this report, the thermal properties of the buffer and the degree of saturation are coupled. Effects of this are however discussed in Section 5.2.

5.1.3 Conditions for which data are supplied

The present section provides data based on previously performed experiments and literature studies on MX-80 bentonite material /Hökmark and Fälth 2003/. In that study it was concluded that the maximum temperature (at the canister surface) was reached within the first tenths of years.

5.1.4 Conceptual uncertainties

Based on the **Buffer and Backfill** process report the conceptual uncertainties on the buffer thermal properties are judged insignificant by the SR-Can team.

5.1.5 Data uncertainty, spatial and temporal variation

Input from experts

The actual bentonite conductivity will exhibit both temporal and special variations. However, the effective value will lie within a rather narrow range, meaning that bounding estimates may be sufficient /Hökmark and Fälth 2003/.

Judgemen by the SR-Can team

The SR-Can team accepts the conclusions by the experts.

5.1.6 Correlations

No correlations have been reported

5.1.7 Quantification

Input from exterts

The thermal conductivity of the buffer material is a function of both the void ratio, e, and the degree of saturation, Sr. The values used in the modelling of the saturation phase are valid for the initial conditions ($e \sim 0.8$). They are shown in Table 5-4 in the subsequent section where data used in the THM modelling have been presented.

Judgement by the SR-Can team

In addition to the results presented in Section 5.2, Hökmark and Fälth /Hökmark and Fälth 2003/ have used two different bentonite conductivities in their study; 1.0 W/(m·K) and 1.1 W/(m·K) claiming that the latter corresponds to bentonite at a (the initial) saturation of about 80%.

Having fully saturated bentonite would result in a thermal conductivity of 1.2 W/(m·K). In order to not underestimate the temperatures that could arise in the near-field, the SR-Can team have used the lower value suggested by Hökmark and Fälth /Hökmark and Fälth 2003/:

Table 5-1. Thermal conductivity for a buffer at initial saturation.

Buffer thermal conductivity	1.1 W/(m·K)

5.2 Hydraulic and mechanical properties of buffer and backfill

The current section presents hydraulic and mechanical properties used when estimating water saturation time and the effect of rock shear of a deposition hole as a result of earthquake.
No designated expert document have been prepared for the current section hence the distinction between the opinion of the expert and the SR-Can team have been omitted. These calculations are performed using ABAQUS and the current chapter present the input data used by the modeller.

5.2.1 Modelling in SR-Can

The hydraulic and mechanical properties of the buffer and the backfill are included in the material models used for performance analyses in different calculations used for SR-Can. Example of such calculations are:

- Water saturation phase of buffer and backfill (see e.g. /Börgesson and Hernelind 1999, Hökmark 2004, Börgesson et al. 2006/).
- Canister displacement /Börgesson and Hernelind 2006/.
- Rock shear through a deposition hole /Börgesson et al. 2003/.

Since different phenomena are studied and different assumptions used in these calculations the material data may differ. A common simplification is that no account has been taken to the initial radial gaps between the buffer and the rock and canister and the resulting inhomogeneities. The buffer and the backfill are assumed to initially be completely homogeneous with exception of the upwards swelling of the buffer and corresponding compression of the backfill, which has been studied in different occasions (see e.g./Börgesson and Hernelind 2006, Johannesson and Nilsson 2006/)

Slightly different data are needed depending on the code used for the analyses. Since the finite element program ABAQUS has been used for most hydration calculations for SR-Can, the data have been taken from the needs of the ABAQUS analyses. The following data of the buffer are needed in the buffer water saturation analyses for completely coupled thermo-hydro-mechanical analyses:

- Dry density, ρ_d
- Water ratio, w
- Void ratio, e
- Degree of saturation, S_r
- Density of solids, ρ_s
- Density of water, ρ_w
- Thermal conductivity, λ
- Specific heat, c
- Hydraulic conductivity of water saturated material, K
- Parameter δ that controls the influence of the degree of saturation on the hydraulic conductivity according to Equation 5.2.1
- Water retention curve
- Thermal vapour flow diffusivity, D_{Tv}
- Isothermal vapour flow diffusivity (assumed to be zero)
- Porous elasticity
- Poisson ratio
- Friction angle in *p-q* plane
- Cohesion in *p-q* plane
- Dilation angle
- Bulk modulus of water
- Bulk modulus of solids
- Coefficient of thermal volumetric expansion of water
- Coefficient of thermal expansion of solids
- Moisture swelling data

$$K_p = (S_r)^{\delta} K \qquad \text{Equation 5.2.1}$$

where

K_p = hydraulic conductivity of partly saturated soil (m/s)

K = hydraulic conductivity of completely saturated soil (m/s)

δ = parameter (usually between 3 and 10)

The following data are used for 30/70 backfill in the water saturation phase analyses.

- Dry density, ρ_d
- Water ratio, w
- Void ratio, e
- Degree of saturation, S_r
- Density of solids, ρ_s
- Density of water, ρ_w
- Thermal conductivity, λ
- Specific heat, c
- Hydraulic conductivity, K
- Parameter controlling the influence of the degree of saturation on the hydraulic conductivity according to Equation 5.2.1
- Water retention curve
- Thermal vapour flow diffusivity, D_{Tv} (not used since the thermal gradient is low in the backfill)
- Isothermal vapour flow diffusivity (assumed to be zero)
- Modulus of elasticity
- Poisson's ratio
- Bulk modulus of water
- Bulk modulus of solids
- Coefficient of thermal volumetric expansion of water
- Coefficient of thermal expansion of solids

5.2.2 Sensitivity to assessment results

Sensitivity calculations have to some extent been performed concerning the influence of the buffer properties and the rock properties on the wetting rate of the buffer and the backfill.

Influence of buffer properties on the wetting rate of the buffer

Hökmark /Hökmark 2004/ investigated the influence of some parameters in the models of CodeBright on the wetting rate of the buffer under the assumption that the hydraulic conductivity of the rock is high enough to supply the buffer with the required amount of water. The results are summarised in Table 5-2.

Table 5-2. Influence of a variation in buffer properties on the time to full saturation of the annulus between the rock and the canister.

Variation	Range of error or variation	Influence on the wetting rate	Magnitude in applicable range (roughly)	Comment
Retention curve	Factor 2	Strong influence	Proportional to the suction	
Hydraulic conductivity	Factor 4	Strong influence	Proportional	
δ	Factor 2	Small	10%	
D_{Tv}	Factor 10	Moderate		Strong influence on the saturation profile (water redistribution)
Gas confinement		Small		
Thermal conductivity	Factor 2	Small	10%	
Canister power	Factor 1.2	Moderate/strong	50%	Higher temperature yields higher K

The influence is dominated by the retention curve and the hydraulic conductivity. The other variations are small in comparison. The high influence of the canister power is caused by the strong influence on water viscosity and thus hydraulic conductivity.

Influence of backfill properties on the wetting rate of the backfill

The influence of the backfill properties on the rate of backfill wetting has only been investigated in connection with the analysis of the influence of trapped air and in connection with the analysis of the difference between having 30/70 and Fridton /Börgesson et al. 2006/. The following conclusions can be drawn from these calculations:

- Trapped air influences the wetting rate of the backfill 30/70 significantly only when the rock hydraulic conductivity is high since the gas migration rate of the backfill will then rule the water inflow.
- The hydraulic conductivity and the retention curve of the backfill are (as for the buffer) the major regulators of the wetting rate if the water supply from the rock is large enough.

Influence of rock properties

The influence of the rock properties on the wetting rate has been investigated mainly in two reports /Börgesson et al. 2006 and Börgesson and Hernelind 1999/. Both rock modelled as homogeneous porous material with hydraulic properties corresponding to average values and rock with discrete fractures have been investigated. The influence of the rock is complex but some general conclusions are:

- For a fracture free rock the rate of wetting is determined mainly by the rock properties if the hydraulic conductivity of the rock is lower than the hydraulic conductivity of the buffer or backfill and vice versa.
- The water pressure in the boundary (or closest fracture) and the distance to the boundary (or closest fracture) has a clear but limited influence on the wetting rate. The influence is stronger for the backfill than for the buffer.
- The fracture frequency (intersecting the hole or tunnel) is the determining factor if the rock matrix hydraulic conductivity is lower than the hydraulic conductivity of the buffer or backfill.
- The fracture transmissivity seems to be of minor importance for the wetting of the backfill if it is higher than ~ 10^{-10} m^2/s. For the buffer this limit is even lower (< 10^{-11} m^2/s).

It should be noted that the backfill calculations are done with the assumption that no piping takes place. Piping will increase the wetting rate but also introduce other problems.

5.2.3 Conditions for which data are supplied

The data for the THM calculations of the wetting rate of the buffer are taken from measurements done during the last 10–15 years mainly on MX-80 at room temperature and with non-saline water as wetting fluid (see e.g. /Börgesson and Johannesson 1995, Börgesson et al. 1995 and Börgesson and Hernelind 1999/). However, the influence of temperature, water salinity and bentonite type has also been investigated as well as the influence of density, which is very strong.

The data for corresponding calculations of the backfill are taken from measurements done on mainly the following two backfill materials: mixtures of 30% MX-80 bentonite and 70% crushed rock and the natural smectitic clay Fridton (see e.g. /Johannesson et al. 1999, Börgesson and Hernelind 1999 and Johannesson and Börgesson 2002/). The influence of the wetting fluid salinity has been included in the investigations.

Most parameters are derived directly from laboratory tests but some D_{Tv} and δ had to be indirectly evaluated from laboratory tests by modelling the laboratory tests and adapt the parameter value to the results.

5.2.4 Conceptual uncertainties

The THM processes in unsaturated buffer materials are complicated and the conceptual understanding of them not complete. The transport of water can either take place in liquid form or in vapour form. The water transport driven by a hydraulic gradient is solely assumed to take place in liquid form while the transport caused by a temperature gradient is modelled to only take place in vapour form. This is a simplification that has shown to be acceptable for modelling purpose.

The interplay between the suction and the swelling pressure is neither completely understood but tests are ongoing.

Another conceptual uncertainty is the validity of Darcy's law at low hydraulic gradients, but the possible deviation is favourable in the sense that the hydraulic conductivity is reduced.

An important process (especially for the backfill) not taken into account is piping and the remaining effect of piping on the hydraulic properties.

5.2.5 Data uncertainty, spatial and temporal variation

All measured data are associated with uncertainties, the most important ones for the buffer at unsaturated conditions being treated in Table 5-2. Input data for the hydraulic conductivity at full water saturation are primarily the empirical relationships between hydraulic conductivity and density, temperature and pore water composition. The primary aim is to establish that the transport through diffusion is considerably more important than advective transport, meaning that the exact value of the hydraulic conductivity is a secondary concern.

5.2.6 Correlations

The data used in the calculations are strongly correlated to several other parameters. Some examples (see also subsection 5.2.7):

The hydraulic conductivity is a function of the temperature, density and degree of saturation. These correlations are included in the models. The hydraulic conductivity is also strongly correlated to the groundwater chemistry and increases with increasing salt content. This correlation is especially strong in the case of low clay density, which is the case for field compacted backfill materials.

The retention curve is correlated to the temperature (slightly), the density (very strongly) and the external pressure. These relations are not included in ABAQUS but the density dependency has recently been included in Code Bright.

The thermal conductivity is correlated to the density and the degree of saturation. Both these relations are included ABAQUS.

The moisture swelling data are correlated to the initial conditions of the buffer, i.e. the density and the water ratio, and has to be calibrated for each initial condition.

5.2.7 Quantification

Data for the buffer

In this first example only the coupled THM-modelling of the water saturation phase will be included.

Table 5-3 shows the data used for the modelling of the water saturation phase. These data are valid for the ABAQUS calculations. The values and parameter settings may differ slightly from the calculations with CodeBright /Hökmark 2004/.

Table 5-3. Data used for the buffer in the water saturation phase analyses (ABAQUS).

Parameter/variable	Value	Comment
Dry density, ρ_d	1,670 kg/m^3	Initial value of a variable
Water ratio, w	0.17	Initial value of a variable
Void ratio, e	0.77	Derived from ρ_d, w, ρ_s and ρ_w
Degree of saturation, S_r	0.61	Derived from ρ_d, w, ρ_s and ρ_w
Density of solids, ρ_s	2,780 kg/m^3	
Density of water, ρ_w	1,000 kg/m^3	
Thermal conductivity, λ	$f(S_r, e)$	**1)**
Specific heat, c	c = 800/(1+w)+4,200w/(1+w)	
Hydraulic conductivity, K	$f(S_r, e, T)$	**2)**
Water retention curve	$u = f(S_r)$	**3)**
Thermal vapour flow diffusivity, D_{Tv}	$f(S_r, e, T)$	**4)**
Isothermal vapour flow diffusivity	D_{pv} = 0	**4)**
Porous elasticity	κ = 0.2	
Poisson ratio	v = 0.4	
Friction angle in p-q plane	β = 16°	Drucker Prager Plasticity model
Cohesion in p-q plane	d = 100 kPa	Drucker Prager Plasticity model
Dilation angle	ψ = 2°	Drucker Prager Plasticity model
Bulk modulus of water	$B_w = 2.1 \cdot 10^6$ kPa	
Bulk modulus of solids	$B_s = 2.1 \cdot 10^8$ kPa	
Coefficient of thermal volumetric expansion of water	$\alpha_W = 3.0 \cdot 10^{-4}$	
Coefficient of thermal expansion of solids	α_S = 0	
Moisture swelling data	$f(S_r)$	**5)**

1) *Thermal conductivity* of the buffer material is a function of both e and S_r. The values used in the modelling of the saturation phase are valid for the initial conditions (e≈0.8). They are shown in Table 5-4.

Table 5-4. Thermal conductivity λ of the buffer material as a function of the degree of saturation S_r for the void ratio e≈0.8.

S_r	λ W/m,K
0	0.3
0.2	0.3
0.3	0.4
0.4	0.55
0.5	0.75
0.6	0.95
0.7	1.1
0.8	1.2
0.9	1.25
1.0	1.3

2) The *hydraulic conductivity* is at full water saturation a function of the temperature and the void ratio. Table 5-5 shows the values used in the model.

The hydraulic conductivity is also dependant on the degree of saturation. The influence is modelled to be governed by the parameter δ in Equation 5.2.2.

$$K_p = (S_r)^{\delta} K \qquad \text{Equation 5.2.2}$$

where

K_p = hydraulic conductivity of partly saturated soil (m/s)

K = hydraulic conductivity of completely saturated soil (m/s)

δ = parameter (usually between 3 and 10)

For the reference material the standard value

$\delta = 3$

has been found to be satisfactory according to the calibration and validation calculations.

3) The relation between suction and degree of saturation (*water retention curve*) is important for the wetting modelling. The actual relation is also a function of the void ratio and has been adapted to the initial void ratio $e = 0.77$. Figure 5-1 shows the relation derived for the modelling.

Table 5-5. Hydraulic conductivity K at full saturation as a function of void ratio e and temperature T.

T °C	e	K m/s
20	0.4	$0.035 \cdot 10^{-13}$
20	0.6	$0.2 \cdot 10^{-13}$
20	0.8	$0.65 \cdot 10^{-13}$
20	1.0	$1.75 \cdot 10^{-13}$
40	0.4	$0.05 \cdot 10^{-13}$
40	0.6	$0.31 \cdot 10^{-13}$
40	0.8	$1.0 \cdot 10^{-13}$
40	1.0	$2.75 \cdot 10^{-13}$
60	0.4	$0.07 \cdot 10^{-13}$
60	0.6	$0.44 \cdot 10^{-13}$
60	0.8	$1.45 \cdot 10^{-13}$
60	1.0	$3.85 \cdot 10^{-13}$
80	0.4	$0.1 \cdot 10^{-13}$
80	0.6	$0.55 \cdot 10^{-13}$
80	0.8	$1.8 \cdot 10^{-13}$
80	1.0	$4.9 \cdot 10^{-13}$

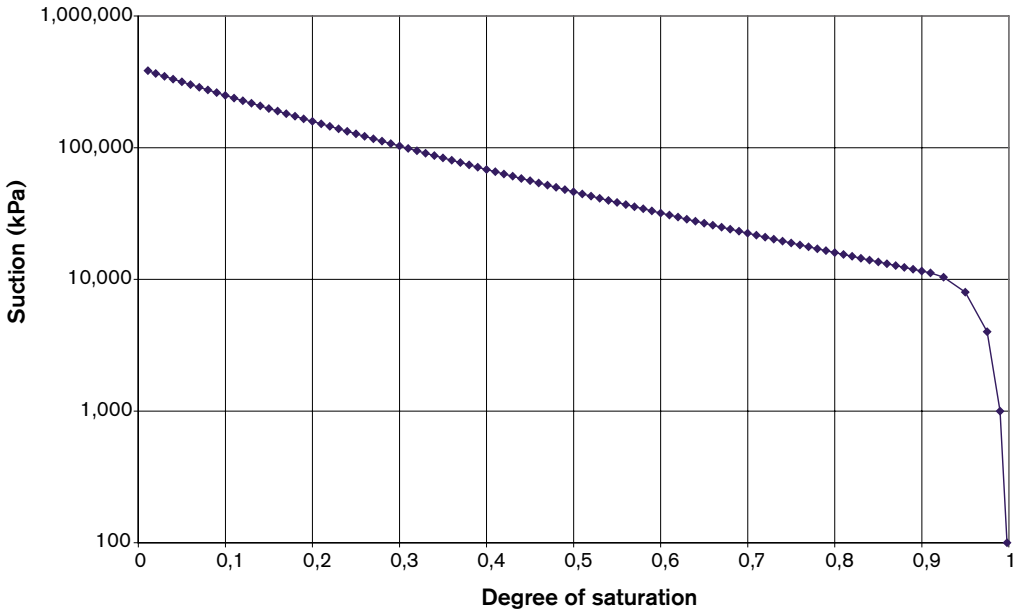

Figure 5-1. *Water retention curve of the buffer at e = 0.77.*

4) The *water vapour flux* is modelled as a diffusion process driven by the temperature gradient and the water vapour pressure gradient (at isothermal conditions) according to Equation 5.2.3:

$$q_v = D_{Tv}\nabla T - D_{pv}\nabla p_v \qquad \text{Equation 5.2.3}$$

where

q_v = vapour flow
D_{Tv} = thermal vapour flow diffusivity
T = temperature
D_{pv} = isothermal vapour flow diffusivity
p_v = vapour pressure

The isothermal vapour flow is neglected and thus $D_{pv} = 0$.

The thermal water vapour diffusivity D_{Tv} is modelled according to equations

$$DTv = DTvb \quad 0.3 \le Sr \le 0.7 \qquad \text{Equation 5.2.4}$$

$$D_{Tv} = D_{Tvb} \cdot \cos^{a}\left(\frac{S_r - 0.7}{0.3} \cdot \frac{\pi}{2}\right) \quad S_r \ge 0.7 \qquad \text{Equation 5.2.5}$$

$$D_{Tv} = D_{Tvb} \cdot \sin^{b}\left(\frac{S_r}{0.3} \cdot \frac{\pi}{2}\right) \quad S_r \le 0.3 \qquad \text{Equation 5.2.6}$$

a and b are factors that regulates the decreased vapour flux at high and low degree of saturation.

D_{Tv} is also depending on the void ratio and the temperature. For the conditions of the reference material the following values have been used

$\boldsymbol{D}_{Tvb} = 0.7 \cdot 10^{-11}$ m²/s,K

$a = 6$
$b = 6$

5) The data for the moisture swelling procedure includes a long list of volumetric strain corrections $\Delta\varepsilon_v$. Table 5-6 shows a selection of values from this table.

Data for the backfill

Two types of backfill materials have been simulated, namely a mixture of 30% bentonite and 70% crushed rock (30/70) and the natural smectitic clay Fridton.

30/70

Table 5-7 shows the data used for the modelling of the water saturation phase with the backfill material 30/70.

Table 5-6. Change in volumetric strain ε_v as a function of the degree of saturation S_r used in the "moisture swelling" procedure (selection of curtailed data).

S_r	$\Delta\varepsilon_v$
0	–0.2
0.1	–0.01
0.2	0.02
0.3	0.03
0.4	0.02
0.5	0.01
0.6	0
0.7	–0.02
0.8	–0.03
0.88	–0.04
0.94	–0.06
0.97	–0.11
0.99	–0.24
1.0	–0.81

Table 5-7. Data used for 30/70 backfill in the coupled THM-modelling of the water saturation phase.

Parameter/variable	Value	Comment
Dry density, ρ_d	1,750 kg/m^3	Initial value of a variable
Water ratio, w	0.12	Initial value of a variable
Void ratio, e	0.57	Derived from ρ_d, w, ρ_s and ρ_w
Degree of saturation, S_r	0.58	Derived from ρ_d, w, ρ_s and ρ_w
Density of solids, ρ_s	2,724 kg/m^3	
Density of water, ρ_w	1,000 kg/m^3	
Thermal conductivity, λ	$f(S_r)$	**6)**
Specific heat, c	1,400 Ws/kg,K	
Hydraulic conductivity, K	$f(S_r)$, $K = 0.5\text{x}10^{-10}$ m/s, δ = 10	Equation 5.2.1
Water retention curve	Table 5.2-6	**7)**
Thermal vapour flow diffusivity, D_{Tv}	$D_{TV} = 0$	
Isothermal vapour flow diffusivity	$D_{pv} = 0$	
Modulus of elasticity	E = 22 MPa	
Poisson ratio	$v = 0.3$	
Bulk modulus of water	$B_w = 2.1\cdot10^6$ kPa	
Bulk modulus of solids	$B_s = 2.1\cdot10^8$ kPa	
Coefficient of thermal volumetric expansion of water	$\alpha_w = 3.0\cdot10^{-4}$	
Coefficient of thermal expansion of solids	$\alpha_s = 0$	

6) The *thermal conductivity* is modelled to be a function of the degree of saturation at $e = 0.57$ according to Equation 5.2.7.

$$\lambda = 1.03+(S_r–0.58)\cdot 1.55 \qquad \text{Equation 5.2.7}$$

where

λ = thermal conductivity (W/m,K)
S_r = degree of saturation

7) The water *retention curve* of 30/70 is determined at $e = 0.57$ (Table 5-8).

Fridton

Table 5-9 shows the data used for the coupled THM-modelling of the water saturation phase with the backfill material Fridton.

Table 5-8. Relation between suction s_w and degree of saturation S_r for 30/70.

S_r	s_w kPa
0.01	400,000
0.28	50,000
0.33	20,000
0.40	12,000
0.43	5,000
0.48	3,000
0.58	1,050
0.67	500
0.77	230
0.87	110
0.92	80
0.97	50
0.995	40
1.0	0

Table 5-9. Data used for Fridton backfill in the water saturation phase analyses.

Parameter/variable	Value	Comment
Dry density, ρ_d	1,590 kg/m^3	Initial value of a variable
Water ratio, w	0.08	Initial value of a variable
Void ratio, e	0.70	Derived from ρ_d, w, ρ_s and ρ_w
Degree of saturation, S_r	0.3	Derived from ρ_d, w, ρ_s and ρ_w
Density of solids, ρ_s	2,625 kg/m^3	
Density of water, ρ_w	1,000 kg/m^3	
Thermal conductivity, λ	$f(S_r)$	**8)**
Specific heat, c	1,400 Ws/kg,K	
Hydraulic conductivity, K	$f(S_r)$, $K = 0.7\text{x}10^{-11}$ m/s, $\delta = 3$	Equation 5.2.1
Water retention curve	Figure 5.2-2	**9)**
Thermal vapour flow diffusivity, D_{Tv}	$D_{TV} = 0$	
Isothermal vapour flow diffusivity	$D_{pV} = 0$	
Modulus of elasticity		No mechanical calculation performed
Poisson's ratio		No mechanical calculation performed
Bulk modulus of water	$B_w = 2.1\cdot 10^6$ kPa	
Bulk modulus of solids	$B_s = 2.1\cdot 10^8$ kPa	
Coefficient of thermal volumetric expansion of water	$\alpha_W = 3.0\cdot 10^{-4}$	
Coefficient of thermal expansion of solids	$\alpha_S = 0$	

8) The *hydraulic conductivity* is modelled to be a function of the degree of saturation at $e = 0.57$ according to Equation 5.2.8.

$$\lambda = 0.57+1.23\cdot(S_r-0.3) \qquad \text{Equation 5.2.8}$$

where

λ = thermal conductivity (W/m,K)

S_r = degree of saturation

9) The *water retention curve* of Fridton for $e = 0.7$ is shown in Figure 5-2. It has been measured for low water contents and theoretically determined from swelling pressure results.

5.3 Density and porosity of buffer and backfill

The density of the buffer and backfill is an important design parameter that is governed by a number of design and safety criteria concerning the hydraulic conductivity, the swelling pressure, and the compressibility of the material. From these criteria, target densities of the saturated buffer and backfill have been formulated. The porosity depends on these target densities and the densities of the buffer and backfill constituents.

5.3.1 Modelling in SR-Can

It is considered in SR-Can that it is not essential to describe the details of the water saturation process in the buffer and backfill. The rational for this is that the buffer and backfill in expected to be fully saturated within a few tens of years. Furthermore, there will likely be an overall inflow of water into the non-saturated material, which will hinder radionuclide transport out of the buffer and backfill. For this reason it is the density and porosity of the saturated material that is of interest for SR-Can modelling. Even if the water saturation process is not modelled, processes in the buffer and backfill that may take place during the saturation, such as erosion and piping, are of interest for SR-Can.

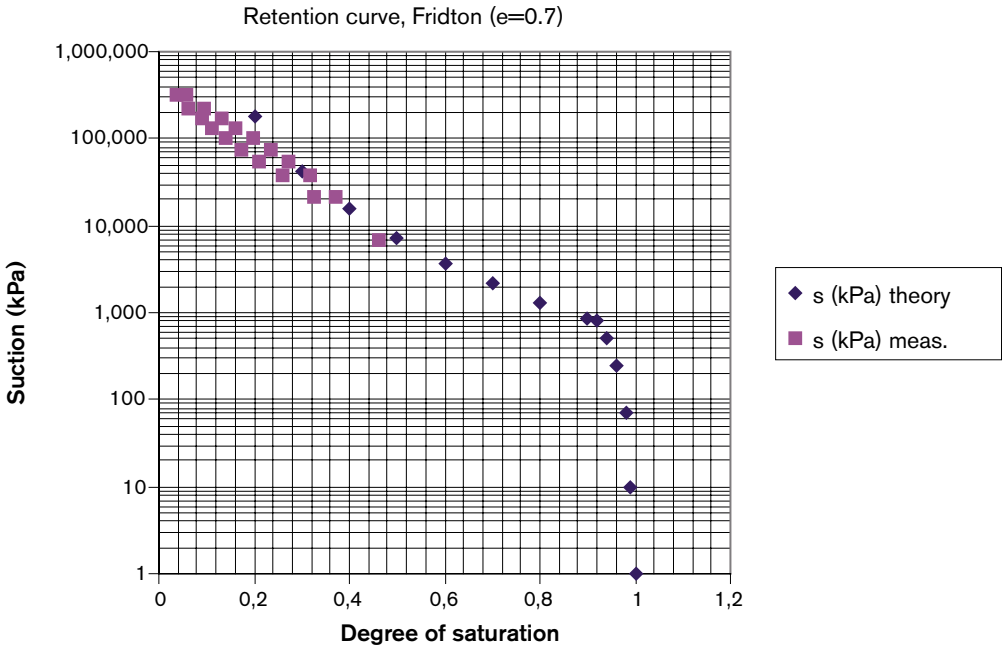

Figure 5-2. *Water retention curve of Fridton. The theoretical relation has been used for the modelling.*

The buffer and backfill will be confined by tunnel walls, deposition holes, and canisters. When the material becomes fully saturated, the buffer and backfill are expected to completely fill the available volume during all conditions. Even if changes in, for example, groundwater chemistry may affect some physical properties of the material, such as the swelling pressure, the density and porosity are not expected to change. Under the prerequisite that buffer and backfill material is not removed from the deposition holes and tunnels, there is no need to model its density and porosity evolution within SR-Can. However, if there are processes that remove or redistribute the material, such as buffer erosion and piping, this must be considered.

5.3.2 Sensitivity to assessment results

The density of the buffer and backfill material may have a significant effect on the assessment results. With decreasing density, the hydraulic conductivity of the material is expected to increase. Furthermore the swelling pressure is expected to decrease. In Figure 5-3, the a) hydraulic conductivity and b) swelling pressure of MX-80 bentonite are plotted vs the dry density of the bentonite. Before obtaining these data, the bentonite was saturated with pore waters of different NaCl concentrations /Johannesson and Nilsson 2006/.

An increase in hydraulic conductivity would directly affect the assessment results, giving rise to a potentially larger radionuclide transport from the engineered barrier to the natural barrier. A substantial decrease in swelling pressure would compromise the mechanically self-healing properties of the buffer and backfill material. If the material looses its self-healing capability, this may lead to channelling effects and potentially result in an increased radionuclide transport to the natural barrier.

A deceased density would also result in an increased porosity, which would generally give rise to less transport resistance for radionuclides in the buffer and backfill.

For the backfill, the compressibility is an important property. Above the canister, about 1.5 m of buffer will be placed in the deposition hole. This buffer material is confined by the canister, the deposition hole, and the overlying backfill. The swelling pressure in the backfill is expected to be substantially lower than in the buffer. For this reason, the compressibility of the backfill must be large enough so that the buffer is not allowed to protrude into the deposition tunnel in such an extent that the buffer density decreases below formulated criteria. If it does, this may give rise to an increase radionuclide transport through the buffer, which could affect assessment results.

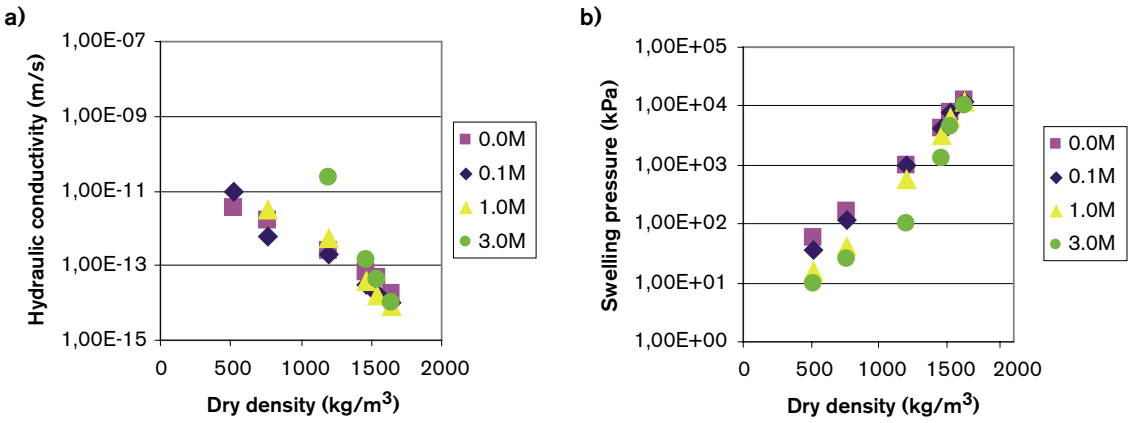

Figure 5-3. *Properties of MX-80 bentonite at different NaCl pore waters. a) Hydraulic conductivity vs dry density. b) Swelling pressure vs dry density. Images from /Johannesson and Nilsson 2006/.*

5.3.3 Sources of information

At present, the engineering solutions for depositing the buffer and backfill material are not chosen. Therefore, there are no hard data on buffer and backfill densities and porosities obtained from experiments using the appropriate engineering solution. Instead, target densities have been postulated. The main documents, where information concerning these target densities can be found, are the **Initial state report** and **Buffer and backfill process report**.

To assess to what extent the postulated target densities and associated variabilities are reasonable, a few documents on experiments using similar engineering solutions as will be finally chosen are of importance.

- In /Johannesson et al. 2000/ the density, void ratio, and degree of saturation are reported for isostatically compacted buffer blocks (MX-80 bentonite) on the scale 1:4.
- In a dedicated data report for the backfill, /Johannesson and Nilsson 2006/ examine how the hydraulic conductivity, swelling pressure and compressibility vary with the density and pore water speciation for a number of backfill materials. Data from recently performed laboratory experiments are given and comparisons with previously performed experiments, reported in /Karnland et al. 2005/, are made.
- In /Gunnarsson et al. 2004/, results from the work made in Phase 1 of the project "Backfilling and Closure of the Deep repository" are reported.

Other supporting publications are:

- A dedicated report series for the buffer and backfill /Pusch 2001, 2003ab/.
- Ochs and Talerico /Ochs and Talerico 2004/ where migration parameters for MX-80 bentonite are assessed.
- Ochs /Ochs 2006/, where migration parameters from Friedland Clay are assessed.

5.3.4 Conditions for which data are supplied

Buffer and backfill material

The buffer materials considered in SR-Can is MX-80 bentonite and Deponite CA-N bentonite. These material are described in e.g. /Pusch 2001, **Initial state report**/.

The backfill materials considered in SR-Can is Friedland Clay or a bentonite/ballast mixture where the bentonite is of buffer quality and the ballast consists of crushed granitic rock with a maximum grain size of a few millimetres. The proposed weight ratio of the bentonite/ballast mixture is 30 wt-% bentonite and 70 wt-% rock /**Initial state report**/. The Friedland Clay and the bentonite/ballast backfills are describe in e.g. /Johannesson and Nilsson 2006, **Initial state report**/.

Pore water speciation

The pore water speciation will not directly affect the density and porosity of the buffer and backfill. However, dissolution and precipitation processes will be affected by the pore water speciation and these processes may slightly affect the density and porosity.

The pore water speciation will affect some physical properties of the buffer and backfill. This can be seen in Figure 5-3 where the salinity of the pore water affects the hydraulic conductivity and swelling pressure at a given density. Generally speaking, higher pore water salinity is expected to lower the transport resistance of the buffer and backfill.

Temperature

The temperature is not expected to significantly affect the density and porosity of the buffer and backfill. The effects from thermal expansion and changes in dissolution/precipitation equilibrium are expected to be minor.

Degree of saturation

For this report, only fully saturated buffer and backfill is of interest. Unsaturated material is described in the **Initial state report**.

Degree of compaction

The density and porosity of the buffer and backfill is governed by the properties of their constituents and on the degree of compaction. Different degrees of compaction have been use in the laboratory to achieve different densities, e.g. /Johannesson et al. 2000/.

5.3.5 Conceptual uncertainties

Even though the fully saturated buffer and backfill is of interest for SR-Can, processes that occur in the saturation phase may give rise to uncertainties.

Presently it is discussed to what extent erosion and piping will affect the buffer and backfill. This is especially important before the system becomes fully saturated, as well as in the wake of a glacial period when non-saline water may reach repository level /**Buffer and backfill process report**/.

Before the buffer and backfill becomes fully saturated, the swelling pressure is significantly reduced compared to the fully saturated state. Since the swelling bentonite is initially a gel, with increasing density over time as water goes deeper into the bentonite, the gel may be too soft to stop water inflow. The results may be piping in the bentonite, formation of a channel and a continuing water flow and erosion of soft bentonite gel /**Buffer and backfill process report**/.

Some of the parameters that govern the target density are affected by the pore water speciation, which in turn is affected by the groundwater speciation (see Figure 5-3). There is a conceptual uncertainty concerning the application conditions during the evolution of the repository. With decreasing groundwater salinity, which may occur in the wake of a glacial period, the risk of buffer and backfill erosion increases.

The compressibility of the backfill material is of importance as the backfill must sufficiently well hinder the buffer from protruding into the deposition tunnel. The buffer may become saturated before the backfill if, for example, water flows into the system from a fracture intersecting the deposition hole but not the deposition tunnel. This may present a problem as the compressibility of the backfill may not be adequate under non-saturated conditions.

For both the buffer and backfill, there are conceptual uncertainties concerning the porosity calculated from the quantities of water and solids the material holds, even at fully saturated conditions. A question is how much of the physical porosity that is available for radionuclide retention. Such considerations are to some extent made in /Ochs and Talerico 2004/.

Judgements by the SR-Can team

There are a number of conceptual uncertainties concerning how the target density is to be obtained. At present, technical solutions for depositing buffer and backfill are still evaluated. Furthermore there are conceptual uncertainties concerning erosion and piping. The buffer and backfill evolution during the saturated phase may have to be looked into, as saturation processes may displace the buffer and backfill material. Buffer and backfill erosion has been identified as potentially troublesome by SKB under certain conditions. This must be further investigated.

5.3.6 Data uncertainties, spatial and temporal variations

Much effort will be made to obtain the right amount of buffer material in the deposition holes, in order to minimise the spatial variability of the buffer density. The buffer will be placed around the canisters as pre-compacted rings. The pile of rings is assumed to have the same height as the canister. Pre-compacted bentonite blocks will be placed on top of the canister.

The degree of compaction of the rings and blocks may be adjusted, based on the geometry of the deposition hole, so that the target density can be achieved. Furthermore, the diameter of the rings and blocks may be adjusted and granular bentonite can be added in the slot between the rock surface and the buffer pile /**Initial state report**/.

When the buffer is saturated, it will fill out the entire deposition hole around the canister and differences in degree of compaction, as well as in density and porosity, will even out. The rational for this is, simply put, that if a unit of buffer has a larger dry density than the adjacent unit, its swelling pressure will be relatively larger when it becomes saturated. The unit will then expand on behalves of the adjacent unit that becomes more compacted until equilibrium is reached.

At the interface between the deposition hole and the deposition tunnel the buffer density may vary. Here the buffer is confined by the backfill. As the swelling pressure of the backfill is expected to be substantially lower than that of the buffer, the buffer will to some extent protrude into the deposition tunnel. As a result, the buffer density of the top layer of the deposition hole is expected to be somewhat lower, compared to the rest the buffer. The thickness of the buffer layer above the canister is around 1.5 m and the density of the buffer in the immediate surroundings of the canister is not expected to be affected.

It has been identified as important to prevent that the buffer comes into contact with groundwater during the deposition phase /**Initial state report**/. When the bentonite is contacted by groundwater it swells and in the deposition phase, such saturation may give rise to problems in achieving the target density. Means to avoid saturation during the deposition phase have been developed /**Initial state report**/.

No large-scale test of placing pre-compacted blocks of backfill in deposition tunnels has been made. The spatial variability within a pre-compacted block has been demonstrated to be small. However, when placing the blocks in the deposition tunnels, there will be a void between the tunnel wall and the blocks. This void must be filled with for example bentonite pellets. This give rises to uncertainty and spatial variability. It has been identified as troublesome /Gunnarsson et al. 2001, 2004/ to achieve a high enough density at the roof of the tunnels. This concern may be valid for all backfill alternatives.

The clay materials of interest for SR-Can, MX-80 bentonite, Deponite CA-N and Friedland Clay, are considered to be sufficiently homogenous to be treated as such for most purposes. The ballast is more heterogeneous, both in mineralogy and grain size.

There is an uncertainty and spatial variability associated with groundwater contacting the backfill during its placement. When groundwater contacts the backfill, it may swell and this complicates obtaining a homogenous backfill and achieving the target density.

As the backfill becomes fully saturated, variations in the compaction degree are likely to even out. For this reason, the spatial variabilities of the porosity and density of fully saturated backfill are likely less that those of dry material.

On a temporal scale, changes in the groundwater system during the evolution of the repository, including the re-saturation of the repository, may cause the buffer and backfill properties to change. This may also induce a spatial variability of the material properties. While major changes of the density and porosity are expected during the saturation phase, due to differences in degree of saturation, only minor changes are expected due to changes in groundwater chemistry.

Unless there is major buffer erosion, the temporal variability of the buffer porosity and density will be minute once the material is fully saturated. Major buffer erosion would require a substantial groundwater flow across the deposition hole. At present the criteria for accepting of rejecting deposition holes, based on the groundwater flow in intersecting fractures, is evaluated. Backfill erosion may occur if the deposition tunnels are intersected by fractures or fracture zones. The concern of buffer and backfill erosion has recently evolved and the matter is discussed within SKB /**Buffer and backfill process report**/.

Judgements by the SR-Can team

At present, technical solutions for depositing buffer and backfill are still evaluated. Until an appropriate solution is chosen, only approximate estimates of densities and porosities, with their associated variabilities, can be delivered. At this stage it appears to be reasonable to achieve the target density of the buffer material with adequate precision. There are concerns regarding how to prevent groundwater from contacting the bentonite in the deposition phase and to what extent the buffer will protrude into the deposition tunnel as it becomes saturated. It is judged that the measures taken to achieve the target density are sufficient, as long as significant protrusion of buffer into the deposition tunnel can be prevented.

In the large-scale backfilling investigation in the Äspö Hard Rock Laboratory /Gunnarsson et al. 2001/ it was shown that it is possible to deposit the backfill in such a manner that it becomes fairly homogenously distributed. Problems were identified associated with the backfill density at the roof of the tunnel. It is judged that it should be possible to find an engineering solution that can assure sufficiently small backfill density variability. However, such an engineering solution must handle filling the gap between the backfill and tunnel roof adequately.

It is judged that the temporal variability of buffer and backfill density and porosity is small, once the material is fully saturated. One may object to this judgment if one considers buffer erosion, predominantly in the wake of a glacial period, to be a major concern. It is recognised by the SR-Can team that presently this issue is not fully understood and more studies are required.

5.3.7 Correlations

For the buffer and backfill, the porosity ε (–) is correlated to the dry density ρ_d (kg/m^3) and density of the solid material ρ_s (kg/m^3) according to:

$$\varepsilon = 1 - \frac{\rho_d}{\rho_s} \qquad \text{Equation 5.3.1}$$

For the fully saturated backfill the porosity is correlated to the saturated density ρ_{sat} (kg/m^3), the density of the solid material, and the pore water density ρ_w (kg/m^3) according to:

$$\varepsilon = \frac{\rho_{sat} - \rho_s}{\rho_w - \rho_s} \qquad \text{Equation 5.3.2}$$

If the material is only partly saturated, none of the equations above should be used. The degree of saturation S_r (–) refers to the volumetric fraction of the total void that is water filled. If assuming that the mass of the gas filled void is insignificant:

$$\varepsilon = \frac{\rho_{sat} - \rho_s}{S_r \rho_w - \rho_s} \qquad \text{Equation 5.3.3}$$

In many reports the void ratio e (–) is reported. This is the volumetric ratio of the water and solids in the material.

$$e = \frac{S_r\, \varepsilon}{1 - \varepsilon} \qquad \text{Equation 5.3.4}$$

Judgements by the SR-Can team

The SR-Can team has nothing to add regarding correlations.

5.3.8 Quantification

Input from the experts

Buffer

According to the **Initial state report** the density targeted for the saturated buffer is 2,000 ± 50 kg/m^3. By using ρ_s = 2,780 kg/m^3 and ρ_w = 1,000 kg/m^3 /**Initial state report**/ in Equation 5.3.2, the porosity becomes 0.44 ± 0.03.

It has been demonstrated that high densities can be achieved by isostatic compaction of bentonite blocks in /Johannesson et al. 2000/. Here a density of 2,059 ± 4 kg/m^3 was obtained. In this investigation the blocks were not fully saturated and one could expect that as they become fully saturated, the density will increase.

The values given for the pre-compacted rings and blocks of bentonite in the **Initial state report** are:

Blocks: ρ_d = 1,655 kg/m^3, S_r = 70%, e = 0.680

Rings: ρ_d = 1,754 kg/m^3, S_r = 81%, e = 0.585

By applying Equations 5.3.1–5.3.4, these values would correspond to the following saturated densities and porosities:

Blocks: ρ_{sat} = 2,145 kg/m^3, ε = 0.49

Rings: ρ_{sat} = 2,174 kg/m^3, ε = 0.42

When obtaining these values, it was assumed that the bentonite blocks and rings are confined and that no change in volume occurs when the buffer becomes saturated. However, as there will be a void between the pile of buffer and the rock surface of the deposition hole, the saturated densities shown above are expected to decrease. As measures are taken to obtain the exact amount of buffer material required in the deposition hole, it is thought that the targeted density 2,000 ± 50 kg/m^3 can be achieved.

Backfill

The following three backfill concepts that are analysed in SR-Can:

- The deposition tunnel is filled with pre-compacted blocks of Friedland Clay.
- The deposition tunnel is filled with pre-compacted blocks of a bentonite/ballast mixture.
- The deposition tunnel is filled with a bentonite/ballast mixture that subsequently is compacted in situ.

In the **Initial state report** it is stressed that neither the backfill material nor the backfill method has been chosen yet. This severely complicates the task of selecting appropriate data concerning backfill density and porosity for use in SR-Can modelling. In the **Initial state report**, data are given that reflect the current development of the proposed backfilling concepts.

The spatial variability of the density and porosity of the backfill depends much upon the engineering solution chosen when filling the deposition tunnels. Until experiments are made using the appropriate engineering solution, the spatial variability of the density and porosity cannot be assessed. However, if the magnitude of the variability is requested, one could base this on experience from the large-scale backfilling investigation in the Äspö Hard Rock Laboratory, using bentonite/ballast backfill /Gunnarsson et al. 2001/. As discussed in subsection 5.3.6 of this present report, by analysing data from /Gunnarsson et al. 2001/, a standard deviation of the dry density of ± 80 kg/m^3 was obtained. If assuming a ρ_s of 2.7·10^3 kg/m^3, this would result in a standard deviation for the porosity of about 3%.

Pre-compacted blocks Friedland Clay: In this concept the cross-section of the tunnel is assumed to be filled to 78% with pre-compacted blocks, 20% with pellets, and 2% is void. The following values are given for the blocks and pellets /**Initial state report**/:

Blocks: ρ_d = 2,000 kg/m^3, S_r = 93%, e = 0.35

Pellets: ρ_d = 1,100 kg/m^3, S_r = 19%, e = 1.45

If assuming that density and porosity differences even out as the backfill becomes fully saturated, ρ_{sat} becomes $2.19 \cdot 10^3$ kg/m^3 and ε becomes 0.41. These numbers are obtained by calculating the quantities of solid material and porosity of the individual components. The final porosity is obtained by weighting the porosity of the components. When obtaining the fully saturated density, it is assumed that the porosity is completely water filled with water of the density 1,000 kg/m^3 and that backfill completely fills the deposition tunnels.

Pre-compacted blocks bentonite/ballast: In this concept the cross-section of the tunnel is assumed to be filled to 78% with pre-compacted blocks, 20% with pellets, and 2% is void. The following values are given for the blocks and pellets /**Initial state report**/:

Blocks: ρ_d = 2,190 kg/m^3, S_r = 81%, e = 0.23

Pellets: ρ_d = 1,100 kg/m^3, S_r = 19%, e = 1.45

If assuming that density and porosity differences even out as the backfill becomes fully saturated, ρ_{sat} becomes $2.30 \cdot 10^3$ kg/m^3 and ε becomes 0.37.

Judgements made by SR-Can team

For the buffer, it seems reasonable that the target density can be achieved, as measures are taken to deposit the exact amount of bentonite required in each deposition hole. A prerequisite for achieving the target density is that a significant amount of buffer is not displaced in the saturation process, or the subsequent evolution of the repository. It should be doable to hinder significant buffer erosion associated with an inflow of water in fractures intersecting the deposition hole. One way of doing this is to adjust the criterion concerning the allowed water flow (or hydraulic conductivity, transitivity, etc) in fractures intersecting the deposition holes. Limiting the magnitude of inflow into the deposition hole also limits the risk that the buffer becomes saturated before the backfill. If this still happens, one may have problems with buffer protruding into the deposition tunnel, where non-saturated backfill may not meet the compressibility criterion.

For the three suggested backfilling concepts, the technical solution how to achieve the target densities has not yet been chosen. Before this is done, the densities and porosities given in this report can only be seen as approximate data that reflect the present development of the proposed backfilling concepts.

It is judged that the magnitude of backfill density variability can be approximated from the large-scale backfilling investigation performed /Gunnarsson et al. 2001/. The rational for this is that in /Gunnarsson et al. 2001/ it was shown that a low density variability could be obtained. Based on this it is judged by the SR-Can team that the density variability is not a significant concern for reaching the target density.

5.4 Migration data for bentonite

This section concerns migration data for the bentonite buffer, or more specifically sorption distribution coefficients, diffusivities, and porosities. The data evaluation is based on a designated expert report /Ochs and Talerico 2004/. The alternatives for the buffer material are MX-80 bentonite and Deponite CA-N.

Migration properties of the bentonite buffer may be site sensitive, depending mainly on the groundwater speciation of the site.

5.4.1 Modelling in SR-Can

Radionuclide migration

As shown in the **Buffer and backfill process report**, radionuclide migration through the compacted bentonite buffer is predominantly a diffusive transport which may be modelled using Fick's laws. In the buffer, radionuclides are (to different degree) also assumed to sorb to the buffer material, which will influence the migration. Sorption of radionuclides in the near-field may be modelled using a linear relation (justified by a low radionuclide concentration) between sorbed species and solute concentrations, with the sorption distribution coefficient K_d (m^3/kg) as the proportionality coefficient.

Radionuclide migration through the bentonite buffer is in the near-field transport simulation code COMP23 /Romero et al. 1999, Cliffe and Kelly 2004/ modelled as a diffusive transport through the microporous network of the buffer, in combination with sorption of radionuclides to the buffer material. The modelling parameters used to describe these processes are the effective diffusivity D_e (m^2/s), the porosity ε (–), and the sorption distribution coefficient K_d. The magnitudes of these parameters depend on physical properties of the buffer, like the dry density ρ_d (kg/m^3), on the porewater speciation, and on the migrating species. From the entities listed above, an apparent diffusivity D_a (m^2/s) may be derived /Ochs and Talerico 2004/.

$$D_a = \frac{D_e}{\varepsilon + K_d \rho_d} \qquad \text{Equation 5.4.1}$$

As many of the parameters controlling radionuclide transport through the buffer will be site-specific, conversion procedures of experimental data derived at other conditions may be necessary.

The diffusion-available porosity used in the calculations is for most nuclides equal to the porosity of the buffer material. However, for anions, a lower porosity than that of the bentonite is used due to interactions with the negatively charged pore walls /**Buffer and backfill process report**/.

5.4.2 Sensitivity to assessment results

Based on analyses in SR 97 /Lindgren and Lindström 1999, SKB 1999ab/, and subsequent sensitivity analyses, the buffer migration data generally affect calculated dose or risk in the following way. The release of a nuclide, escaping from a defect canister, from the near-field depends on the half-life of the nuclide and the migration time through the buffer. For species having short half-lives compared to their migration times through the buffer, uncertainties in the migration data will be of less importance, as the species will have decayed to low levels before reaching the far-field. For species having half-lives comparable to the migration time or longer, such as iodide, only a fraction will have decayed as the species reach the far-field. Therefore, uncertainties in migration and sorption parameters directly affect the calculated release to the far-field. It should be mentioned that as the storage capacity of the buffer becomes utilised, the migration times for the species through the buffer generally decrease.

If the total migration time in the near-field and far-field is short or comparable to the half-life of the species, uncertainties in the migration data of the buffer directly affect the dose or risk. In general, the impacts of K_d, ε, and D_e are monotonic. Low K_d- and ε-values and high D_e-values tend to increase the release /Ochs and Talerico 2004/. As the storage capacity of the buffer becomes utilised, the impact of K_d and ε diminish and the impact becomes, at steady state conditions, proportional to D_e.

In conclusion, this means that for some species, the values of migration data in the buffer may affect the release linearly. This should be considered when assessing the precision in the uncertainty estimates.

5.4.3 Source of information

A designated data report on migration parameters in the buffer has been prepared /Ochs and Talerico 2004/. Details about sources of information and how they were used are found there.

In /Ochs and Talerico 2004/, the derivation of distribution coefficients and diffusion parameters for the specified conditions is generally based on element-specific batch sorption data and diffusion parameters for tritiated water, HTO. This is considered as significantly more reliable than a possible attempt of deriving K_d-values based on data for compacted bentonite.

In case of diffusion parameters, the situation is relatively straightforward as most diffusion studies available to date for bentonite have been carried out at relatively high degrees of compaction. In /Ochs and Talerico 2004/ the reference density for MX-80 bentonite is 1,590 kg/m^3 and while few data found correspond directly to the reference density, many diffusion studies have been carried out using bentonite with a density of 1,590 ± 500 kg/m^3.

The situation is more difficult for the derivation of K_d-values for compacted bentonite. Practically all sorption measurements are carried out in dilute suspensions. Due to experimental difficulties, no reliable sorption measurements in compacted material are available. Moreover, it is extremely difficult to obtain pore solution from compacted bentonite, and the representativeness of extracted solutions is questionable. This situation requires the application of sorption data from batch experiments to compacted material; i.e. a transfer of data from low to very high solid/water ratios. In /Ochs and Talerico 2004/ it is suggested that K_d in principle is independent of the solid/water ratio and that no reduction of sorption-available surface area takes place upon compaction.

To check the consistency of the proposed methodology of obtaining apparent diffusivities, /Ochs and Talerico 2004/ have compared the data, wherever possible, with independent D_a-values obtained in compacted bentonite. Special considerations concerning the effective diffusivity have been made for anions and Cs. This is due to the interaction of these species with the electrical double layer.

The data sources considered in /Ochs and Talerico 2004/ as basis for selecting diffusion parameters and distribution coefficients for compacted MX-80 bentonite and Deponite CA-N in contact with specific groundwater types fulfil two requirements:

- They correspond to, or allow the derivation of, parameters applicable to the compacted state.
- They correspond to, or allow the derivation of, parameters applicable to the relevant geochemical conditions. In particular, this includes the porewater composition corresponding to the compacted state.

The main databases used for the derivation of the buffer migration parameters are listed below. The full reference list can be found in /Ochs and Talerico 2004/.

A recent Nagra report on selected K_d-values for MX-80 /Bradbury and Baeyens 2003/, and original data sources cited therein.

- SKB reports on K_d, D_e, and D_a /Yu and Neretnieks 1997/ and groundwater /Laaksoharju et al. 1998/, and original data sources cited therein.
- JNC reports mainly written by Sato and co-workers on diffusion in Kunigel-V1 and Kunipia-F bentonites as a function of dry density.

5.4.4 Conditions for which data are supplied

Backfill density and composition

Ochs and Talerico /Ochs and Talerico 2004/ consider the buffer material to be MX-80 bentonite. The results obtained on MX-80 bentonite are transferable to Deponite CA-N. A reference dry density of 1,590 kg/m^3 and a porosity of 0.43 are used. When obtaining the porosity, a dry density is used in /Ochs and Talerico 2004/ that deviates somewhat from the dry density used in the **Buffer and backfill process report**. The deviation is of minor significance. The dry density corresponds to a bulk density for saturated bentonite of 2,000 ± 50 kg/m^3 /**Initial state report**/. No other density was evaluated in the supporting document but /Ochs and Talerico 2004/ state that there is clear evidence that the porewater composition and therefore, radionuclide sorption, is not significantly influenced by limited variations in buffer density. The bentonite composition considered is given in /Ochs and Talerico 2004/. For some cases, the following variations in bentonite composition were considered:

- Bentonite converted completely to the Ca-form.
- Bentonite completely depleted of soluble impurities (NaCl, KCl, gypsum).

Groundwater

The migration parameters, especially K_d, depend on the groundwater composition. In /Ochs and Talerico 2004/ K_d-values are tabulated for three different porewaters corresponding to two different groundwater types within a reasonable range in terms of salinity and pH. As the reference groundwater, a slightly saline water based on /Laaksoharju et al. 1998/ is used, see Table A-9. An alternative groundwater with higher salinity is also used. The compositions of these two groundwater types are tabulated in Table A-9. No K_d-values that correspond to a non-saline groundwater are tabulated in /Ochs and Talerico 2004/.

Porewater

The speciation of the bentonite porewater, corresponding to the reference density of the buffer, forms the central element for the evaluation of migration parameters, in particular K_d /Ochs and Talerico 2004/. The pore solution in compacted bentonite is practically inaccessible for chemical analysis. Therefore, porewater compositions were evaluated by using thermodynamic models. The results of these model calculations are dependent on the composition of the bentonite and the geochemical boundary conditions, but also on the chosen modelling approach.

Variations in the calculated porewater compositions result from variability in:

- the incoming groundwater composition,
- whether CO_2 gas is allowed to leave and enter the compacted buffer; i.e. whether pCO_2 in the bentonite buffer is the result of groundwater-bentonite reactions (closed system) or whether pCO_2 in the bentonite buffer is imposed by the CO_2 level in the host rock (open system),
- the bentonite composition.

The calculated porewater composition obtained, using the reference and alternative groundwater and an open system with respect to CO_2 gas, is described in Table A-10 of the present report. Other calculated porewater compositions are described in /Ochs and Talerico 2004/.

5.4.5 Conceptual uncertainties

Input from experts

Ochs and Talerico /Ochs and Talerico 2004/ identify a number of conceptual uncertainties both in the data derivation process and in the underlying databases and models.

- Conceptual uncertainties are introduced when interpreting experimental data into recommended diffusion and sorption values. Several related conceptual uncertainties exist regarding the interpretation of, and self consistency among, batch K_d-values and diffusivities of sorbing radionuclides on one hand, and of diffusivities and diffusion-available porosities of anions and certain mobile cations, such as Cs, on the other hand. In the case of diffusion coefficients, uncertainties correspond to the experimental error as well as to any uncertainty introduced in the required modelling for raw data reduction.
- Conceptual uncertainties are introduced when converting suggested data obtained at a specific set of conditions through models or estimation procedures into data applicable at conditions relevant for safety assessments.
- If there are significant uncertainties associated with the application conditions themselves, it is critical to take the conditional nature of the relevant migration parameters into account. K_d-values in particular are highly conditional and need to be derived for each specified set of (expected) conditions. In /Ochs and Talerico 2004/, variability of geochemical conditions was addressed by deriving K_d-values separately for several sets of possible geochemical conditions.

There are some open questions regarding the fundamental, underlying chemistry of radionuclides in aqueous solutions. This is also acknowledged in recent TDB (thermodynamic database) compilations e.g. /Hummel et al. 2002/. For example, the importance of actinide(III)-silicate, mixed actinide(IV)-OH-CO_3 and Ni-CO_3 complexes is not established to date. There are also uncertainties regarding the solution speciation of many of the less well researched elements, such as Nb, Zr, etc.

There are significant scientific shortcomings regarding the derivation of the porewater composition in compacted bentonite and its evolution over time under repository conditions. Since the porewater composition of compacted bentonite cannot be determined experimentally with any certainty for the present purpose, it is calculated using thermodynamic surface chemical models. Several published models are available for this purpose, and while they are based on the same principles, they differ in a number of details regarding e.g. the treatment of specific surface chemical equilibrium. These differences are, however, small in comparison to other uncertainties according to /Ochs and Talerico 2004/.

There are questions regarding the effects of the electrical double layers in the pore space on e.g. the amount of “free” water, water activity, etc that are clearly beyond the present scientific understanding.

Judgements made by SR-Can team

The judgements made by Ochs and Talerico /Ochs and Talerico 2004/ are accepted by SR-Can team.

5.4.6 Data uncertainty, spatial and temporal variation

Input from experts

According to /Ochs and Talerico 2004/ the following applies concerning spatial variability, temporal variation and data uncertainty:

On the scale of a typical buffer, bentonite can be considered as homogeneous. Therefore, spatial variation and its related uncertainty, is not considered relevant for the bentonite buffer. Uncertainties of K_d-values correspond to experimental errors and uncertainties in diffusion data correspond to experimental errors as well as to uncertainties introduced by the models used when extracting raw data.

- Temporal variation becomes important when the evolution of buffer and porewater is being considered. The evolution of buffer and porewater compositions over time has to be assessed through models. The corresponding uncertainties can be viewed as extensions of the uncertainty introduced by variable groundwater chemistry.

The sorption and diffusion data, as well as the various models underlying the present data selection, are generic and therefore, not site-specific. However, the extracted buffer migration parameters will be site-sensitive to the extent that they are derived based on site-specific conditions. Of particular importance are groundwater composition, including redox conditions, and pCO_2 imposed by the host rock formation.

The selected data are valid for 25°C. An increase to 50°C is expected to lead to a twofold increase of D_e. Based on the data available to date, it is not possible to assess the influence of temperature on K_d with any certainty. However, no significant effect is expected for an interval of ca. 10–50°C. No effect on porosity is expected for this temperature range.

Judgements made by SR-Can team

The judgements made by Ochs and Talerico /Ochs and Talerico 2004/ are generally accepted by SR-Can team. The following considerations are made.

- As bentonite is considered as homogenous, uncertainties in K_d-values correspond to experimental errors according to /Ochs and Talerico 2004/. It can be questioned whether all bentonite used in a repository can be considered as a homogenous mass. However, the SR-Can team judge that it is acceptable to view bentonite as homogenous with the underlying assumption that the variation and uncertainty imposed on migration properties by the natural variation of the buffer are small in comparison to those imposed by other issues.
- In /Ochs and Talerico 2004/ it is stated that uncertainties associated with diffusion coefficients are introduced by both experimental errors and by the modelling required for raw data reduction. However, uncertainties associated with distribution coefficients are introduced by experimental errors only, with the underlying assumption that no models are used when evaluating sorption data. This is not entirely true. Even in batch sorption experiments, migration processes may have to be modelled. Alternatively, one assumes that the system is in equilibrium. This may give rise to uncertainties in the raw data that are not associated with experimental errors. There may also be methodological issues, associated with experimental set-up, data reduction, etc, giving rise to uncertainties. For example, what error is induced when transferring data from batch experiments to compacted bentonite? Even if there are many possible sources of uncertainty, the SR-Can team judge that /Ochs and Talerico 2004/ have identified the major ones.

5.4.7 Correlations

Input from experts

In /Ochs and Talerico 2004/ correlations within the buffer migration data is assessed. They conclude the following:

Following their chemical characteristics, the radionuclides considered can be organised into groups (correlation groups) of elements and oxidation states whose migration behaviour will generally show a similar response to variations in porewater composition caused by variations in groundwater composition, bentonite evolution, etc. Moreover, elements handled via chemical analogies correlate with the respective analogues. Overall, the following grouping is used,

where analogies are also indicated (X/Y: both elements were treated identically in the data derivation; X(Y): X was derived based on analogy with Y)

1. Alkaline and alkaline earth elements: Cs, Ra/Sr.
2. Other di-valent elements (Pb, Ni).
3. Tri-valent elements: Am, Cm(Am), PuIII(Am), Sm/Ho/Ce(Eu).
4. Tetra-valent elements and Zr: Th, UIV(Th), PuIV(Th), NpIV(Th), TcIV(Th), Zr(Th), Sn(Th).
5. Penta-valent elements: NpV, PuV(NpV).
6. Hexa-valent elements: UVI, PuVI(UVI).
7. Non-sorbing anions: $Cl^-/I^-/TcO_4^-/SeO_4^{2-}/HSe^-$/simple organic anions
   - Some elements are not known well enough to assess correlations (Pa, Nb, Pd, Ag).
   - The weakly sorbing anions SeO_3^{2-} and carbonate will not correlate. Carbonate is proposed to be handled via isotope exchange.
   - Gases: Rn, CH_4.

Furthermore Ochs and Talerico /Ochs and Talerico 2004/ assess that:

- Redox-sensitive radionuclides will take on higher oxidation states if oxidising conditions are considered, generally leading to lower K_d-values. An exception is Se(-II→IV).
- A lower porewater pH (within the range considered) will decrease the K_d of most radionuclides (actinides, lanthanides, transition elements, heavy metals) in a similar way. Exceptions are penta-and hexavalent actinides that form oxo-cations: U(VI), Np(V), Pu(VI/V).
- An increase in major cation concentration will lower K_d-values for alkaline and alkaline earth elements.
- A lower density of the buffer will lead to higher D_e- and D_a-values.

Judgements by the SR-Can team

The judgements made by Ochs and Talerico /Ochs and Talerico 2004/ are generally accepted by SR-Can team. The following consideration is made.

It is suggested to use correlation groups 1–7, as used in /Ochs and Talerico 2004/, when assigning input K_d-values, for the radionuclide retention modelling, based on the suggested probability distribution functions (Appendix A4). From a transport point of view, species within the same correlation group can thus be lumped together when probabilistic data are generated. However, if doing this it must also be justified in terms of half-lives and decay chains.

5.4.8 Quantification

Input from experts

The data selection procedure applied by Ochs and Talerico /Ochs and Talerico 2004/ rely strongly on sorption data obtained in batch experiments. No element-specific D_e-values were derived for reactive elements. Instead, the selected D_e-value for HTO was relied upon. D_e-values for anions and Cs were selected to take into account the electrostatic potential in bentonite pores. Data derivation and assessment of uncertainties were carried out in four main steps.

- *Step 1*: All conditions considered were defined and the bentonite porewater composition corresponding to the reference density was calculated. The uncertainties associated with the boundary conditions were addressed by carrying out the derivation of migration parameters for several self-consistent bentonite/porewater systems.
- *Step 2:* Effective diffusivities and diffusion-available porosities for the specified reference density were derived. Uncertainties relating to the influence of conditions on diffusion relevant bentonite characteristics were assumed to be included in the uncertainties of the underlying experimental measurements, which already cover different conditions.
  a) D_e-values and associated uncertainties were selected for HTO, to be used together with the entire physical porosity for all conditions and for all elements, except non-sorbing anions and Cs.
  b) D_e-values and associated uncertainties were selected for all non-sorbing anions (Cl^-, I^-, TcO_4^-, SeO_4^{2-}, HSe^-, simple organic anions) to be used for all conditions together with the selected anion diffusion-available porosity.
  c) A D_e-value was selected for Cs, to be used together with the entire physical porosity.
- *Step 3:* Derivation of K_d-values for each element by a) a selection of source data and quantification of their experimental uncertainty and by b) conversion of source data to the selected reference conditions and quantification of the additional uncertainties introduced in this process.

When selecting source data, high priority was given to systematic data obtained on MX-80 bentonite. According to Ochs and Talerico /Ochs and Talerico 2004/ the uncertainty introduced in extrapolating sorption data from source to the present application (safety assessment) conditions can be significantly higher than experimental uncertainties and will increase with the extend of extrapolation. It is further proposed that this holds for any extrapolation method, i.e. both thermodynamic model applications as well as semi-quantitative estimations. Therefore, systematic data obtained on MX-80 bentonite in solutions that closely match the present application conditions /Bradbury and Baeyens 2003/ were preferred over thermodynamic sorption models that had been calibrated in the absence of key chemical parameters.

The conversion of source data to the selected reference conditions was carried out in /Ochs and Talerico 2004/ by the introduction of conversion factors (*CF*). The derivation of K_d-values corresponding to the desired conditions in compacted bentonite from experimental data almost invariably involves an extrapolation step. Where possible, this extrapolation was done with the help of an appropriate thermodynamic sorption model. Where such a model was not available, semi-quantitative conversion procedures were applied. The basic approach of the conversion procedure was taken from /Bradbury and Baeyens 2003/. The actual conversion factors were in all cases calculated specifically for the present source data sets and application conditions. To scale selected K_d-values obtained for bentonites or clays other than MX-80 to the MX-80 application conditions, a conversion factor *CF-CEC* based on the respective CEC-values was applied:

$$\text{CF-CEC} = \text{CEC (application)}/\text{CEC (data source)} \qquad \text{Equation 5.4.2}$$

In this relation, *CEC* is used as a measure for total site density, based on the reasonable assumption that the density of surface complexation (edge) sites is proportional to the *CEC*. Where possible, data sources were selected that allowed the selection of K_d-values at the pH-values corresponding to the application conditions. Where this was not possible, scaling to the appropriate application pH could in many cases be made on the basis of additional data for the same radionuclide. In such cases, scaling to the application pH was done using the conversion factor *CF-pH* defined below:

$$\text{CF-pH} = K_d \text{ (pH data source)}/K_d \text{ (pH application)} \qquad \text{Equation 5.4.3}$$

The presence of dissolved ligands can have a significant influence on radionuclide sorption. Therefore, scaling of K_d to application conditions should be carried out in all cases where the source data correspond to a solution composition different from that of MX-80 porewater.

The conversion factor CF-spec takes into account differences in the competition for the radionuclide by those dissolved ligands present in the different solutions that are not already covered by *CF-pH*:

$$CF\text{-}spec = F_{sorb}\ (application)/F_{sorb}\ (data\ source) \qquad \text{Equation 5.4.4}$$

where

$$F_{sorb} = (RN_{tot} - RN_{cmp})/RN_{tot} \qquad \text{Equation 5.4.5}$$

with RN_{tot} as the total dissolved concentration of a given radionuclide, and RN_{cmp} as the total concentration of all dissolved radionuclide complexes evaluated as being competitive with regard to sorption. In /Ochs and Talerico 2004/, care has been taken so that *CF-pH* and *CF-spec* do not account for the same effect. Therefore, variants of CF-spec, mainly handling carbonate complexation effects, are introduced. This is described in /Ochs and Talerico 2004/. Generally, the overall conversion factor *CF-total* that was used when scaling the selected K_d-values was obtained according to:

$$CF\text{-}total = CF\text{-}CEC \cdot CF\text{-}pH \cdot CF\text{-}spec \qquad \text{Equation 5.4.5}$$

The numerical value for the conversion factors used for each individual species can be found in /Ochs and Talerico 2004/. The magnitudes of the uncertainties introduced when transferring the source data to the recommended K_d-values for the application condition are discussed in /Ochs and Talerico 2004/

- *Step 4:* Calculation of D_a-values for the specified reference density based on the results from step 2 and 3, and comparison with independent experimental data. Final assessment of overall consistency and uncertainty.

In providing migration data and uncertainty estimates for the various conditions, /Ochs and Talerico 2004/ generally provide a median value and a lower and upper limit in logarithmic scale. The likelihood for any data to fall within the recommended ranges is expressed verbally, i.e. based on expert judgment by the authors. This is supported by consistency checks using independent data and a traceable and extensive documentation of data derivation in appendices. The uncertainties are evaluated in a way that makes it generally very likely that the indicated limits encompass all possible values. For each element, this is supported with illustrations and consistency checks using diffusion data to facilitate an independent interpretation by the user of the report, where required.

Resulting estimates for D_e-, ε- and K_d-values for the SR-Can base case conditions are provided in Table A-11. Resulting estimates for D_e, ε and K_d for other explored conditions can be found in /Ochs and Talerico 2004/

Judgements made by the SR-Can team

The judgements made by Ochs and Talerico /Ochs and Talerico 2004/ are generally accepted by SR-Can team. For the selection of data to the assessment calculations the following additional considerations are made by the SR-Can team:

According to the discussion by Ochs and Talerico /Ochs and Talerico 2004/ and in the **Buffer and backfill process report**, the external impact on the migration parameters in the buffer is essentially through groundwater composition (including assumptions of the redox conditions) and assumptions of CO_2 interactions with the host rock. It is judged by the SR-Can team that the assumption of an open system with respect to CO_2 interactions is reasonable. In /Ochs and Talerico 2004/, D_e-values are assumed to be unaffected by the groundwater salinity. Furthermore, K_d values corresponding to "saline" and "highly saline" groundwaters, as specified in Table A-9, are tabulated. However, no K_d-values corresponding to non-saline groundwater are given. In the SR 97 safety assessment, the K_d-values corresponding to non-saline groundwater were all equal or higher than those corresponding to saline groundwater /Andersson 1999/.

Based on this, it is judged that the K_d-values given for the reference groundwater in /Ochs and Talerico 2004/ can, conservatively, be used also for the non-saline groundwater. D_e- and K_d-values are tabulated in Appendix A4 of the present report. In Appendix A4 it is noted what species that should be correlated with each others.

The ranges (lower to upper) provided for the given conditions are evaluated in a way that makes it generally very likely that the indicated limits encompass all possible values. In order to convert these values to probability distributions, a triangular distribution (lower, mode, upper) is suggested. In SR-Can, values outside these ranges are considered as "hypothetical" or "what-if".

Migration parameters are also used in assessments of buffer evolution. These analyses primarily concern other elements, e.g. sulphide, but consistency with radionuclide migration parameters is still needed. Since no reliable data is available for the diffusion of sulphide in bentonite, the selected value for HTO from /Ochs and Talerico 2004/ will be used in SR-Can. This is probably conservative since sulphide most likely will be present in an anionic form.

The K_d-values for the species Ag and carbonate deserve special comments. No K_d value is given by the experts for carbonate in Table A-11 and Table A-12 as the sorption mechanism is proposed to be ion exchange. Sorption due to ion exchange is at present very difficult to quantify. If a value is needed in calculations, the SR-Can team cautiously recommend to treat carbonate as non-sorbing ($K_d = 0$). This is conservative in some, but not necessarily in all, cases. However, it is judged to be acceptable as carbonate has not been identified as troublesome in e.g. SR 97 /Lindgren and Lindström 1999/.

Furthermore, in Table A-11 and Table A-12 the central and lower K_d values of Ag are zero while the upper value is either 4.4 or 15 m^3/kg. This presents a problem when making a distribution in log-space. For this reason, a lower K_d-value of $2.7 \cdot 10^{-5}$ m^3/kg can be used for the distribution. This value is 10% of the storage capacity of the buffer due to the porosity, using the porosity 0.43 and dry density 1,590 kg/m^3. A triangular distribution in log-space between $2.7 \cdot 10^{-5}$ m^3/kg and the upper K_d-value is recommended.

5.5 Migration data for backfill

This section concerns migration data for the backfill, or more specifically sorption distribution coefficients, diffusivities, and porosities. In SR-Can, the backfill only concerns the deposition tunnels and not the ramp or shafts. Two backfill concepts will be analysed in SR-Can. In both concepts the entire tunnels are backfilled with blocks of the backfill material. The gaps between the rock and the blocks are filled with pellets of the same material. In one main concept, Friedland Clay constitutes the backfill and in the other main concept, a mixture of bentonite of buffer quality (MX80 or Deponit CA-N) and crushed rock with a weight ratio of 3/7 constitutes the backfill /**Buffer and backfill process report**/.

Migration of solutes through the backfill depends on several parameters. Some of these parameters are closely related to the groundwater flow, i.e. are "flow related". This section evaluates sorption and diffusion properties of the backfill material, whereas the flow related parameters are discussed in Section 5.2 of the present report.

The data evaluation for the bentonite/ballast concept is based on designated expert reports on migration properties of the buffer /Ochs and Talerico 2004/ and of the rock /Crawford et al. 2006, Liu et al. 2006/. The data evaluation for the Friedland Clay concept is based on a designated expert report /Ochs 2006/. Migration properties of the backfill may be site-specific, depending mainly on the groundwater speciation of the site.

5.5.1 Modelling in SR-Can

As shown in the **Buffer and backfill process report**, radionuclide migration through the backfill may occur both by advection and diffusion. In the backfill, radionuclides are to different degrees assumed to sorb to the buffer material, which will influence the migration. Sorption of radionuclides in the backfill may be modelled using a linear relation (justified by a low radionuclide concentration) between sorbed species and solute concentrations, with the sorption distribution coefficient K_d (m^3/kg) as the proportionality coefficient /**Buffer and backfill process report**/.

Radionuclide migration in the backfill is in the near-field transport simulation code COMP23 /Romero et al. 1999, Cliffe and Kelly 2004/ modelled as a diffusive and advective transport through the porous network in combination with sorption of radionuclides. The modelling parameters that are not flow related, used to describe these processes, are the effective diffusivity D_e (m^2/s), the porosity ε (–), and the sorption distribution coefficient K_d (m^3/kg). The magnitudes of these entities depend on physical properties of the backfill, like the dry density ρ_d (kg/m^3) and the weight ratio of bentonite and crushed rock, on the porewater speciation, and on the migrating species. From the entities listed above, an apparent diffusivity D_a (m^2/s) may be derived /Ochs and Talerico 2004/.

$$D_a = \frac{D_e}{\varepsilon + K_d \rho_d} \qquad \text{Equation 5.5.1}$$

As many of the parameters controlling radionuclide transport through the backfill will be site-specific, conversion procedures of experimental data derived at other conditions may be necessary.

5.5.2 Sensitivity to assessment results

In SR 97 /Lindgren and Lindström 1999/, a number of exit paths are assumed for radionuclides escaping from a defect canister. Some of these exit paths do not involve the backfill and for these cases, the assessment results are more or less insensitive to the migration data of the backfill. In cases where the radionuclides pass through the backfill, the migration data may directly affect the assessment results, depending on the half-lives of the species.

Species with short half-lives may have decayed to low levels before reaching the backfill or may decay to low levels in the backfill. If the migration time from the canister to the far-field is long in relation to the half-lives of the species, uncertainties in migration data of the backfill will be of lesser importance. If the migration time is short or comparable to the half-lives of the species, the migration parameter will directly affect the release to the far-field.

If the total migration time in the near-field and far-field is short or comparable to the half-life of the species, uncertainties in the migration data of the backfill may directly affect the release. In general, the impacts of K_d and ε are monotonic. Low K_d- and ε-values tend to increase the release /Ochs and Talerico 2004/. In case of a diffusive flow through the backfill, high D_e-values tend to increase the release. In case of an advective flow and if there is channelling in the backfill, e.g. close to the roof of the tunnel where the hydraulic conductivity may be relatively high /**Buffer and backfill process report**/, high D_e-values may decrease the release.

Since retention in the backfill is attributed to both the bentonite and the rock in the bentonite/ ballast concept, uncertainties in migration properties of the bentonite as well of the rock apply for the backfill. If investigating the porosities, effective diffusivities, and sorption partitioning coefficients for granitic rock and MX-80 bentonite (appendices A.4 and A.10) one can see that the retention parameters for the bentonite in general are orders of magnitude larger that those of the rock. Thus the crushed rock may contribute to only a small fraction of the retention capacity of the backfill and uncertainties derived from the rock may be of minor importance.

In conclusion, for some species and for some pathways, the values of the migration data in the backfill may affect calculated risk linearly. This should be considered when assessing the precision in the uncertainty estimates.

5.5.3 Sources of information

For the bentonite/ballast concept, designated expert reports on the migration properties of the bentonite /Ochs and Talerico 2004/ and of the rock /Crawford et al. 2006, Liu et al. 2006/ have been prepared. For the Friedland Clay concept, a dedicated data report on migration properties of the backfill has been prepared /Ochs 2006/. In addition, the **Buffer and backfill process report** and the **Initial state report** were used as supporting documents. Details about sources of information and how they were used are found in the respective report.

A short description of the sources of information of /Ochs and Talerico 2004/ is found in Section 5.4.3 of the present report. Short descriptions of the sources of information of /Crawford et al. 2006, Liu et al. 2006/ are found in subsection 6.7.3 of the present report.

Concerning the Friedland Clay concept, no diffusion data at all are available for Friedland Clay /Ochs 2006/. Therefore, data from /Ochs and Talerico 2004/ were scaled to the reference density of Friedland Clay.

Where possible, K_d-values were evaluated for the specific porewater composition and solid/water ratio representative for Friedland Clay compacted to the reference density. Where experimental data of sufficient quality were available for clay materials with mineralogy similar to that of Friedland Clay, these were preferred over data for bentonites or pure montmorillonite. On the other hand, sorption data for illite were typically not given first priority, as Friedland Clay does not contain a significant fraction of this mineral. The sources of information, generally taken from the open literature, are described in /Ochs 2006/.

Where experimental data or sorption models of sufficient quality were not available, the reference K_d selected in /Ochs and Talerico 2004/ was scaled for the sorption capacity of Friedland Clay. The data derivation in /Ochs and Talerico 2004/ was done for MX-80 bentonite and in comparison to MX-80, Friedland Clay contains a lower proportion of expandable clays and has a significantly lower CEC.

While diffusion parameters may be derived directly for compacted clay, K_d-values from batch experiments had to be converted to compact clay conditions. This was done by fully taking into account the dependency of K_d on the calculated, expected in situ porewater composition of the compacted clay.

5.5.4 Conditions for which data are supplied

Backfill density and composition

In /Ochs and Talerico 2004/, the density of the clay material has been identified as an important condition affecting the investigated migration properties. The bentonite investigated in /Ochs and Talerico 2004/ was MX-80 bentonite at the reference dry density of 1,590 kg/m^3 with a corresponding porosity of 0.43. The density corresponds well with that of the bentonite in the bentonite/ballast backfill, where the dry clay density is 1,559 kg/m^3 /**Initial state report**/.

For the Friedland Clay concept investigated in /Ochs 2006/, the reference dry density was 1,780 kg/m^3 with the corresponding porosity of 0.36. No other density was evaluated but according to /Ochs and Talerico 2004/ there is clear evidence that the porewater composition and, therefore, radionuclide sorption, is not significantly influenced by limited variations in buffer density. Diffusivities and porosities were scaled to apply to the density of interest.

The migration properties of clay are affected by the clay composition. For the MX-80 bentonite, the following variations in bentonite composition were considered /Ochs and Talerico 2004/:

- Bentonite converted completely to the Ca-form.

- Bentonite completely depleted of soluble impurities (NaCl, KCl, gypsum).

For the bentonite/ballast concept, the weight ratio between rock and bentonite is of interest. For both concepts, the backfill is considered as homogenous on a larger scale and no channelling is expected to occur.

Groundwater

For both backfill concepts, containing either MX-80 bentonite or Friedland Clay, the reference groundwater used, see Table A-9, is slightly saline /Laaksoharju et al. 1998/. For the MX-80 bentonite, an alternative groundwater with higher salinity was also used. The compositions of these two groundwater types are tabulated in Appendix A4. No K_d-values that correspond to a non-saline groundwater are tabulated in /Ochs and Talerico 2004/ or /Ochs 2006/.

For the rock in the backfill consisting of a bentonite/ballast mixture, a groundwater with the salinity ≥ 500 mg Cl^-/l and pH between 7–9 was used at oxidizing or reducing conditions Furthermore a non-saline groundwater with the salinity < 500 mg Cl^-/l and pH between 7–9 was used at oxidizing or reducing conditions. As there are no K_d-values tabulated in /Ochs and Talerico 2004/ that correspond to non-saline groundwater, for the bentonite/ballast backfill K_d-values are only reported for saline conditions.

Porewater

The speciation of the bentonite or clay porewater, corresponding to the reference density, forms the central element for the evaluation of migration parameters, in particular K_d /Ochs and Talerico 2004/. The pore solution in compacted bentonite is practically inaccessible for chemical analysis. Therefore, porewater compositions were evaluated by using thermodynamic models. The results of these model calculations are dependent on the composition of the bentonite and the geochemical boundary conditions, but also on the chosen modelling approach.

Variations in the calculated porewater compositions result from variability in:

- the incoming groundwater composition,
- whether CO_2 gas is allowed to leave and enter the compacted backfill; i.e. whether pCO_2 in the backfill is the result of groundwater-clay reactions (closed system) or whether pCO_2 in the backfill is imposed by the CO_2 level in the host rock (open system),
- the backfill composition.

The calculated reference porewater composition obtained for MX-80 bentonite, using the reference groundwater and an open system with respect to CO_2 gas, is described in Table A-10 of the present report. Other calculated porewater compositions are described in /Ochs and Talerico 2004/. The calculated reference porewater composition was obtained for Friedland Clay by using a reference groundwater and dissolved carbonate corresponding to a pCO_2 of $10^{-2.6}$ atm. imposed by the host rock formation.

For the rock, the porewater composition was assumed not to deviate significantly from that of the groundwater /Liu et al. 2006/.

5.5.5 Conceptual uncertainties

Input from experts

Conceptual uncertainties concerning the migration properties of the MX-80 bentonite are described in subsection 5.4.5 of this report. Conceptual uncertainties concerning the migration properties of the rock are described in subsection 6.7.5 of this report.

In the bentonite/ballast concept, additional conceptual uncertainties arise when scaling the retention properties of the backfill from those of the bentonite and rock.

The conceptual uncertainties concerning Friedland Clay are according to /Ochs 2006/ very similar to those discussed in /Ochs and Talerico 2004/ and described in Section 5.4.5 of the present report. However, an additional uncertainty arises when transferring data from MX-80 bentonite to a clay based backfill /**Buffer and backfill process report**/.

Judgements by the SR-Can team

The judgements made by the experts, relevant for the backfill, are generally accepted by SR-Can team. An additional consideration is made:

In the bentonite/ballast concept, a scaling of the migration properties of the backfill from those of the bentonite and rock can be proposed. However, it is not clear along what paths the transport will occur. Will the transport be evenly distributed in the backfill or will there be channelling effects, enabling the radionuclides to encounter more or less bentonite than expected from the bentonite/rock weight ratio? Furthermore, it is likely that the availability of mineral surfaces, as well as the pore volume, in the bentonite and in the crushed rock differ. One could question to what extent the bentonite/ballast backfill can be considered as homogenous. The homogeneity of the bentonite/ballast backfill is discussed in Section 5.3 of this present report and based on this discussion it is judged that this is not a major uncertainty by the SR-Can team.

5.5.6 Data uncertainty, spatial and temporal variation

Input from experts

The data uncertainty, spatial and temporal variation of the migration properties of the MX-80 bentonite are described in subsection 5.4.6 of this report. The data uncertainty, spatial and temporal variation of the migration properties of the rock are described in subsection 6.7.6 of this report.

The data uncertainty, spatial and temporal variation of the migration properties of the Friedland Clay are, according to /Ochs 2006/, very similar to those for the MX-80 bentonite discussed in /Ochs and Talerico 2004/ and described in subsection 5.4.6 of this report. However, an additional uncertainty arises when transferring data from MX-80 bentonite to a clay based backfill /**Buffer and backfill process report**/.

In the bentonite/ballast concept, uncertainties arise when scaling the migration properties of the backfill from those of the bentonite and rock.

Judgement by the SR-Can team

The judgements made by the experts are accepted by the SR-Can team.

5.5.7 Correlations

Input from experts

Correlations concerning the migration properties of the MX-80 bentonite are described in subsection 5.4.7 of this report. Correlations concerning the migration properties of the rock are described in subsection 6.7.7 of this report.

According to Ochs /Ochs 2006/, the effective diffusivity of HTO in Friedland Clay correlates to the density of the clay in the same way as for MX-80 and Kunigel-VI bentonites. The correlations described in /Ochs and Talerico 2004/ and in subsection 5.4.7 of this report also apply for Friedland Clay.

Judgement by the SR Can team

The judgements made by the experts are accepted by the SR-Can team.

5.5.8 Quantification

Input from experts

For the bentonite/ballast concept, migration data are needed for both the bentonite and the rock. Quantification of migration data of the MX-80 bentonite and rock is described in subsections 5.4.8 and 6.7.8 of this of this report, respectively. Furthermore, migration data for the backfill need to be scaled from those data. The designated expert reports /Ochs and Talerico 2004, Crawford et al. 2006, Liu et al. 2006/ give no guidance on how to perform the scaling.

In the **Initial state report**, an initial physical porosity of the pre-compacted bentonite/ballast blocks of 0.23 is given. No diffusion available porosities are given. As there is no clear guidance from the expert on the subject how to scale the migration parameters for the bentonite/ballast backfill, a discussion on how to perform the scaling is given by the SR-Can team below.

For the Friedland Clay concept, the quantification was carried out in the same why as for MX-80 bentonite described in /Ochs and Talerico 2004/ and in subsection 5.4.8 in this report. Very few, if any, experimental data obtained on Friedland Clay were available and therefore, the data were obtained by transferring data obtained on MX-80 bentonite or other clays. For a dry density of 1,780 kg/m^3, a diffusion-available porosity of 0.36 is proposed for all elements, except for anions where a porosity of 0.14 is proposed. The recommended distribution coefficients and effective diffusivities are found in Appendix A5 of the present report.

Input from the SR-Can team

As there is no clear guidance from the expert on how to scale the migration parameters for the bentonite/ballast backfill, a discussion on this subject is given below.

Concerning sorption distribution coefficients, it is suggested in /Crawford et al. 2006/ that for rock, K_d-values can be scaled by using the N_2-BET surface area. Such a scaling could be transferred to the backfill, with the prerequisite that all mineral surfaces in the rock and bentonite are equally available. This prerequisite is not unreasonable as the scale of the crushed rock, where the maximum grain size is on the order of 5 mm /**Buffer and backfill process report**/, is very small relative to the scale of the flow paths.

In /Crawford et al. 2006/, a generic N_2-BET surface area for intact granitic rock of 100 m^2/kg is suggested. In /Ochs and Talerico 2004/, a N_2-BET surface area of compacted MX-80 bentonite of 2,000 m^2/kg is given. If assuming that all mineral surfaces are equally available and that such a scaling suggested in /Crawford et al. 2006/ is reasonable for the bentonite/rock mixture, scaled K_d-values for the backfill can be obtained. With a bentonite/rock weight ratio (w_b/w_r) of 3/7, the distribution coefficient of the backfill, $K_{d,bf}$ (m^3/kg), could be calculated by:

$$K_{d,bf} = K_{d,b} \times \frac{w_r \times N_2\text{-}BET_r + w_b \times N_2\text{-}BET_b}{(w_r + w_b) N_2\text{-}BET_b} \qquad \text{Equation 5.5.2}$$

where N_2-BET_r and N_2-BET_b is the surface area for the rock and bentonite respectively. Furthermore, $K_{d,b}$ is the sorption partitioning coefficient for the bentonite. If inserting the values stated above:

$$K_{d,bf} = K_{d,b} \times \frac{7 \times 100 + 3 \times 2000}{(7+3) \times 2000} = K_{d,b} \times 0.335 \qquad \text{Equation 5.5.3}$$

This approach gives similar K_d-values as the most conservative approach, where the rock matrix is considered as inaccessible and only sorption in the bentonite is considered:

$$K_{d,bf} = \frac{w_b \times K_{d,b}}{w_r + w_b} = 0.3 \times K_{d,b} \qquad \text{Equation 5.5.4}$$

This conservative approach may seam appealing, as there is no prerequisite that the mineral surfaces in the rock are as available as the mineral surfaces in the bentonite. If the bentonite is considered as homogenous and no channelling is expected in the bentonite, Equation 5.5.4 gives the lowest boundary for the K_d-value of the backfill. In SR 97 /e.g. Lindgren and Lindström 1999/ a direct scaling of the K_d-values based on the bentonite/rock weight ratio was made:

$$K_{d,bf} = \frac{w_r \times K_{d,r} + w_b \times K_{d,b}}{w_r + w_b} \qquad \text{Equation 5.5.5}$$

In general, K_d-values for the bentonite are much larger than those for rock. In such a case, the K_d-values for the backfill obtained by Equation 5.5.5 will not differ significantly from those obtained Equation 5.5.4. However, in some cases the reported K_d-value is similar for rock as for bentonite, or even larger, and in these cases the conservative approach of Equation 5.5.4 may be over-conservative. As for Equation 5.5.2, a prerequisite for Equation 5.5.5 is that all mineral surfaces are equally available.

The effective diffusivity of bentonite is on the order of 10^{-10} m^2/s while the effective diffusivity of rock is on the order of 10^{-14} m^2/s. Therefore, the diffusive transport in the rock is negligible in comparison. When scaling the effective diffusivity, the bentonite/rock volume ratio must be used. If using a rock density of $2.7 \cdot 10^3$ kg/m^3 /Lindgren and Lindström 1999/ and a clay density of $1.6 \cdot 10^3$ kg/m^3 /**Initial state report**/, the bentonite/rock volume ratio V_b/V_r becomes 0.42/0.58 and the effective diffusivity for the backfill can be scaled according to:

$$D_{e,bf} = \frac{V_b \times D_{e,b}}{V_r + V_b} = 0.42 \times D_{e,b} \qquad \text{Equation 5.5.6}$$

where the indexes are the same as for Equation 5.5.2. It is suggested by the SR-Can team that the central, lower and upper D_e-values given in /Ochs and Talerico 2004/ is scaled using Equation 5.5.6.

As the physical porosity of the pre-compacted bentonite/ballast blocks, a central value of 0.23 is given /**Initial state report**/. The upper and lower values 0.21 and 0.26 are given. No value for the diffusion-available porosity is given.

Based on /Ochs and Talerico 2004/ it is suggested by the SR-Can team to used the physical porosity of the bentonite/ballast backfill as the diffusion available porosity for all species except for anions. The upper and lower values for the physical porosity are used as lower and upper values of the diffusion-available porosity.

For anions, the diffusion-available porosity 0.092 is obtained by reducing the physical porosity by a factor of 2.5, as in /Ochs and Talerico 2004/. For upper and lower values, the central value of the physical porosity is reduced by a factor of 1.8 and 3.5, respectively, based on /Ochs and Talerico 2004/.

Judgement by the SR-Can team

The judgements made by /Ochs and Talerico 2004, Ochs 2006, Liu et al. 2006, Crawford et al. 2006/ are generally accepted by the SR-Can team. Specific comments on /Liu et al. 2006/ and /Crawford et al. 2006/ are found in subsection 6.7.8, and on /Ochs and Talerico 2004/ in this report.

Comments concerning the Friedland Clay concept

In /Ochs 2006/ K_d-values are only tabulated for a saline reference groundwater. Some additional uncertainties of the K_d-values are given for different groundwater types. However, there is no clear guidance how these additional uncertainties are evaluated and variation due to different changes in groundwater (such as high or low salinity, high or low pH, open or closed carbonate system) seems to have been lumped together. This tends to increase the data ranges.

No central values have been given for groundwater types other than the saline reference groundwater specified in Table A-9. Transferring these K_d-values to non-saline groundwater could be done in a conservative manner. However, care should be taken when transferring the K_d-values to higher salinities groundwater. For the buffer, /Ochs and Talerico 2004/, have reduced K_d-values for highly saline groundwater with a factor of up to 5 in comparison to those for saline groundwater. Therefore, it is recommended by the SR-Can team to use a reduction factor of 5 when transferring the K_d-values for Friedland Clay to groundwaters with high salinities.

No central value was given for Ag(I). This value was set to 0 by the SR-Can team.

No upper and lower values for the porosity was given in /Ochs 2006/, except for the case of anions. For cations, the uncertainty in the backfill porosity given in Section 5.3 may be used. However as the term $K_d\rho_d$ in Equation 5.5.1 dominates over the porosity the impact of porosity variations on the apparent diffusivity is limited.

Comments concerning the Bentonite/ballast concept

The scaling methods described by Equations 5.5.5 and 5.5.6 are recommended for K_d-values and effective diffusivities, respectively. The rational for this is that the scale of the crushed rock pieces is very small relative to the scale of the flow paths. For the effective diffusivity, the capacity in the rock is considered as negligible in comparison. Upper and lower values should be scales in the same way as the central value. Species deemed important in /Ochs and Talerico 2004/ for the buffer are deemed important for the bentonite/ballast backfill. Where no K_d-value is availably for either the rock or the MX80 bentonite, the K_d for this medium is set to zero by the SR-Can Team (but only in this particular calculation).

A slightly saline groundwater is used as reference water (see Table A-9). As an alternative groundwater a groundwater with a higher salinity is used. Transferring these K_d-values to non-saline groundwater from slightly saline groundwater could be done in a conservative manner.

No central value was given for Ag(I). This value was set to 0 by the SR-Can team. The fact that the central and lower K_d values of Ag are zero while the upper value is 4.40 m^3/kg presents a problem when making a distribution in log-space. For this reason, a lower K_d-value of $2.0 \cdot 10^{-5}$ m^3/kg can be used for the distribution. This value is 10% of the storage capacity of the backfill due to the porosity, using the porosity 0.36 and dry density 1,780 kg/m^3. A triangular distribution in log-space between $2.0 \cdot 10^{-5}$ m^3/kg and the upper K_d-value is recommended.

Comments concerning both concepts

The ranges (lower to upper) provided in Appendix A5 for the given conditions are evaluated in a way that makes it generally very likely that the indicated limits encompass all reasonably possible values. In order to convert these values to probability distributions, a triangular distribution (lower, mode, upper) is suggested. In SR-Can, values outside these ranges are considered as “hypothetical” or “what-if”. When the *Kd*-values for species correlate, this correlation is noted in Appendix A5.

6 Geosphere data

The present chapter presents data for the geosphere, some of the data, such as properties of the excavation damaged zone EDZ, are part of the system commonly referred to as the near-field (or the engineered system) but most data can be regarded as far-field data. This chapter also provides future groundwater data for the studied sites for different distinct times. The groundwater data is also of importance in previous chapter since, in some cases, the provided data are only valid for certain groundwater speciations. The groundwater speciation used has therefore been compared with that given in Section 6.1. This section also provides data of the groundwater flow and the discrete fracture network data necessary to perform these calculations.

This chapter contains to a larger extent than previous chapters information obtained in SKB's site characterisation program. For most sections, data from the **Site descriptive reports**, /**Forsmark, Simpevarp and Laxemar**/ has been the main reference and supporting document. In the site description, information is given for specific drill holes, rock domains and deformation zones. A brief information of the sites is presented in Section 1.8 of the present document.

In some sections where the data is strongly SR-Can specific no distinction between Expert and SR-Can team decisions have been made. All information in those sections may therefore be regarded as SR-Can team decisions.

6.1 Groundwater composition

This section discusses the groundwater compositions during a glaciation cycle. The data is largely based on the results from groundwater flow models and on the groundwater samples and chemical analysis for the **Site descriptive report, /Forsmark and Laxemar/**.

6.1.1 Modelling in SR-Can

The compositions of groundwaters in SR-Can are evaluated using different methodologies depending on the time period involved.

For the period extending from the operation phase to the end of the initial temperate domain (i.e. the first few thousand years) groundwater compositions are modelled through advection, mixing and chemical reactions with fracture filling minerals. The modelling of the transport of solutes in groundwater through advection and mixing during this period is performed in a detailed scale with the hydrodynamic models and parameters described later in Section 6.5. These calculations produce the spatial and temporal distribution of salt and reference groundwaters, which are then used as input to calculations that include reactions with some fracture filling minerals such as calcite, silica and iron(III) hydroxides which are abundant and equilibrate quickly with circulating groundwaters. The result of this modelling is an estimate of the groundwater detailed composition. The consequences during the operation phase from grouting and stray materials are evaluated in a generic way. Chemical reactions have been modelled with the PHREEQC and PHAST codes /Parkhurst and Appelo 1999, Parkhurst et al. 2004/.

For the remaining of the reference glacial cycle the hydrodynamic modelling is non-site-specific, and the focus in SR-Can has been to estimate the reactions between fracture filling minerals and intruding glacial melt waters.

6.1.2 Source of information

The main source of information is the hydrogeological modelling performed for Forsmark and Laxemar within the site description modelling /**Site descriptive report, Forsmark and Laxemar**/, described later in Section 6.5. The results of geochemical evaluations are given in the background report on groundwater chemistry over a glacial cycle /Auqué Sanz et al. 2006/

Chemical reaction data

The majority of chemical *equilibrium* reaction data, including dissolution and precipitation of minerals, are provided with the PHREEQC and PHAST codes /Parkhurst and Appelo 1999, Parkhurst et al. 2004/. The database in the file "wateq4f.dat" distributed with these two programs has been used in the SR-Can calculations. Small changes concerning the solubility constants for FeS and alumino silicates were introduced, as described in /Auqué Sanz et al. 2006/. There should be no inconsistencies between these equilibrium data and those used elsewhere within SR-Can, e.g. for radionuclide solubilities. Reactions not considered here concern chemical elements of no interest for the groundwater compositions (e.g. Pb or Am) and the reactions that affect groundwater components, such as CO_3^{2-} or SO_4^{2-}, are the same in all databases.

Parameters to evaluate *rates* of reactions have been used in a few cases and their values and data sources are provided in the corresponding reports whenever they are used.

Compositions of Reference Waters

Mixing calculations, based on the results of hydrodynamic transport models, have used the following reference waters: deep brine, glacial, marine, and superficial groundwater of recent meteoric origin. The compositions of these waters are discussed in /Auqué Sanz et al. 2006/.

Rock and fracture mineral geochemistry

Calculations involving reactions of dissolution and precipitation of minerals assume the presence of these solids in the rock or in fracture fillings. Their reducing capacity is especially important when modelling the consumption of dissolved oxygen in inflowing melt water under a glacier. The available information is compiled in /Drake et al. 2006/.

6.1.3 Sensitivity of the assessment results on groundwater data

Groundwater compositions affect the chemical conditions in the radionuclide solubility calculations for a breached canister, and furthermore they affect indirectly the results of radionuclide transport calculations through the choice of retention parameters. Groundwater chemistry may also affect buffer and backfill stability and canister corrosion. These influences are described in the corresponding sections of this report.

6.1.4 Conditions for which data are supplied

Groundwater compositions are provided for the Laxemar and Forsmark sites, from the excavation and operation phases to the end of the first glacial cycle.

The data have been estimated using as input the results from hydrological simulations which in turn are conditioned to a given hydrogeological model, the past historical evolution of the site, etc (compare with Section 6.5).

The impacts from the thermal load of the repository and from the temperature decrease during cold periods of a glacial cycle on calculated groundwater compositions are expected to be small and have not been evaluated in SR-Can.

6.1.5 Conceptual uncertainties

The groundwater compositions have been estimated using as input the results from hydrological simulations. The processes of groundwater flow and salt transport are well understood processes, see the discussion in subsection 6.5.5. In this section only uncertainties associated with chemical reactions will be explored.

Input from experts

According to /Auqué Sanz et al. 2006/ the concept of mixing is useful in describing the observed variability of groundwaters observed within the site investigations. Furthermore, hydrological simulations indicate that groundwaters at a given spatial location and time may be described by mixing proportions of reference waters. However, chemical interactions along the paths followed by these reference waters before they reach the mixing point may have obliterated their original composition. For example, one of the reference waters is rain water, and when participating as a mixture component in a groundwater at 400 m depth, it is to be expected that the rain water composition has suffered substantial changes, such as depletion of O_2 and CO_2, through water-rock reactions. In part this may be corrected for when choosing reference waters, in this case superficial groundwaters of meteoric origin, representing rain water that has reacted slightly.

The chemical reactions included in the evaluation of groundwater compositions have several types of uncertainties:

1. The effects of salinity (ionic strength) on chemical equilibrium reactions may be evaluated using different models. The simple model included in PHREEQC has been used /Parkhurst and Appelo 1999/.
2. Temperature effects on chemical reactions due to the thermal load of the repository and cooling through a glacial cycle are expected to be small and they have been neglected. Pressure effects on chemical reactions due to the formation of an ice sheet are also expected to be small and they have also been neglected.
3. The choice of minerals assumed to be in equilibrium with the groundwater mixtures is perhaps the major source of uncertainty. This set of minerals will influence the concentrations of some components, such as H^+, Fe(II) and HCO_3^-, while it will leave unaffected other components such as Cl^-. Given the large spatial domain and the long time span of the evaluations, the set of minerals has been kept constant and relatively simple. Calcite is in general assumed to be in equilibrium as it is widespread in fractures and it has fast rates of dissolution and precipitation. This mineral has a large effect on the results concerning pH and alkalinity.
4. The consequences of microbial reactions on groundwater compositions are in general difficult to evaluate. Although sulphate reduction has as a rule been allowed in the PHREEQC calculations, other processes have not been explicitly modelled.

Calculations of the penetration of oxygen-rich glacial melt waters rely either on reactions with fracture fillings or on matrix diffusion and dissolution of rock minerals containing Fe(II). Models dealing with fracture filling minerals rely strongly on the availability of reducing minerals along the flow path, while rock-matrix models are sensible to assumptions concerning the dissolution of rock components in the matrix pore waters.

Judgement by the SR-Can team

The uncertainties vary substantially between groundwater components. Major ions are well described by mixing and there is little associated conceptual uncertainty.

Acidity (pH) and alkalinity (HCO_3^-) are more dependent on the choice of minerals assumed to react under the equilibrium condition. The assumption of equilibrium with calcite ($CaCO_3$) is well substantiated although slight deviations have been observed, e.g. at Stripa (SKB's underground laboratory prior to Äspö HRL).

Calculated redox conditions and Fe(II) will depend largely on the set of minerals assumed to be in equilibrium with the groundwater mixtures. The chosen set of redox minerals in the calculations is such that the calculated Eh values are in qualitative agreement with measurements at the sites.

There are still some uncertainties concerning the extent of microbial sulphate reduction and its impact on groundwater sulphide levels.

For the models of oxygen consumption during the infiltration of glacial melt waters, the data uncertainties (e.g. the reducing capacity of the fracture minerals) appear to be more important than the conceptual uncertainties.

6.1.6 Data uncertainty, spatial and temporal variation

The groundwater compositions have been estimated using as input the results from hydrological simulations. The associated uncertainty is strongly related to the hydrological parameters and to the assumed properties of the fracture network, compare with subsection 6.5.6. In this section only data uncertainties associated with chemical reactions will be explored.

Input from experts

The description of the reference waters used in mixing calculations originates from several groundwater sampling and analyses obtained during the site investigations and elsewhere, as well as from knowledge concerning the recent evolution of the sites. There is some limited uncertainty in the composition of Littorina sea water.

Only few groundwaters have been satisfactorily sampled and analysed in Forsmark and Laxemar at repository level or larger depths. These groundwaters have been used to calibrate the hydrogeological models in the Site descriptions. Although the spatial uncertainty is substantial, especially for the deeper groundwaters, the good agreement between the results of the calibrated hydrogeological models and the sampled groundwaters gives confidence in the mixing proportions of reference waters.

Chemical equilibrium constants and the equivalent thermodynamic data are used when evaluating the effect of chemical reactions on groundwater compositions. The database in the file "wateq4f.dat" provided with the PHREEQC and PHAST codes has been used /Parkhurst and Appelo 1999/.

There are large uncertainties concerning rock and fracture filling mineralogy /Drake et al. 2006/. This is due in part to the natural spatial variability, and to the fact that the finer fracture minerals might have been washed away or destroyed during drilling. Furthermore data is lacking on the redox characteristics of the rocks and fracture fillings.

Judgement by the SR-Can team

The SR-Can team agrees in that the effects of uncertainties in the input data are in general small compared with the conceptual uncertainties. The uncertainty in the reducing capacity of the rock and fracture minerals will only be important if it turns out to be below a certain threshold and can therefore become exhausted. The available evidence suggests however that the reducing capacity has been sufficient to withstand all intrusions of glacial melt waters in the past.

6.1.7 Correlations

Input from experts

According to /Auqué Sanz et al. 2006/, the concentrations of groundwater components that are mainly controlled by mixing are highly correlated. This is seen in the groundwaters sampled both in the Laxemar and Forsmark areas, see for example the correlation between calcium and chloride in Figure 7.2-19 on p.169 in the Hydrogeochemical evaluation for Simpevarp /SKB 2004b/ and in Figure 2-7 on p.276 in the Hydrogeochemical evaluation for Forsmark /SKB 2005a/. Plots displaying the variation of concentrations with depth in the granitic rocks considered here show seldom so clear trends /e.g. Figure 4-8 on p.170 of SKB 2005a/ because the hydraulic conditions of the different fractures influence the mixing between reference waters.

The correlations between groundwater components are used in the process of evaluating the site data, and in obtaining reference water compositions involved in mixing models. Other trends may be used to infer chemical reactions, for example by plotting the data in stability diagrams /see Appendix D, p. 319 in SKB 2005a/.

Chemical reactions will also generate correlations between groundwater parameters. For example equilibrium with an Fe(III) oxyhydroxide /Grenthe et al. 1992/ according to:

$Fe(OH)_3(s) + 3\ H^+ + e^- \leftrightarrow Fe^{2+} + 3\ H_2O$

produces values for the redox potential that are strongly correlated to pH.

Judgement by the SR Can team

The groundwater compositions obtained by using mixing and chemical reaction models necessarily show strong correlations between the chemical components. These correlations have to be taken into account when using the groundwater compositions.

6.1.8 Quantification

Input from experts

The results are presented in a background report /Auqué Sanz et al. 2006/. For the temperate period after repository closure the data are presented for several time steps as tables containing the spatial coordinates and the calculated chemical properties of the groundwaters at that particular point in time and space. The chemical properties include TDS (total dissolved solids), pH, Eh (redox potential), as well as the total concentrations of important chemical elements, such as chloride, calcium, etc. The special coordinates selected constitute thee slices of the hydrogeological regional model for each site. One slice is at repository depth, and the other two are vertical planes approximately perpendicular and parallel to the main direction of the coast line at the sites. Further details are given in the background report.

For the glaciation periods, the results from hydrogeological calculations are used to produce groundwater salinities. Qualitative results are also presented from the results of O_2 depletion models.

Judgement by the SR Can team

The data presented in the cited reports are judged to be sufficient to describe the variability of groundwater compositions and its evolution with time.

In order to perform radionuclide migration calculations, redox data are also needed. Table A-7 present radionuclide redox speciation based on the suggested groundwaters and on the solubility calculations presented in Section 3.4.

6.2 Thermal properties

In the present section, thermal properties, i.e. rock thermal conductivity and rock heat capacity, as well as the temperature at repository depth that are needed for evaluating repository evolution are presented. No special SR-Can expert document have been prepared for these data, instead, quantities are assessed from Chapter 7 of the **Site descriptive reports**. These latter inputs have been authored by the SKB Site Modelling expert on thermal properties.

6.2.1 Modelling in SR-Can

Thermal modelling in SR-Can is performed using a semi-analytical model /Hedin 2004/, based on the methods of /Hökmark and Fälth 2003/ where the temperature in the fuel, the cast iron insert, the copper canister, the buffer and the host rock is determined based on canister spacing, thermal properties of the canister, the buffer, and geosphere. The following geosphere specific properties and conditions are used as input data in SR-Can thermal calculations:

- Spatial distribution of thermal conductivity (W/(m·K)).
- Spatial distribution of heat capacity (MJ/(m³·K)).
- Initial temperature at repository depth (°C).
- Regional heat flow (mW/m^2) and temperature gradient (°C/km).

The thermal properties are also used to assess the overall thermal evolution of the repository and is thus input in assessment of thermo-hydro-mechanical (THM) analyses /Hökmark et al. 2006/ and for assessing the long term thermal evolution caused by potential climate evolution. The thermo-mechanical parameters, i.e. the coefficient of thermal expansion, is discussed together with the other mechanical input in Section 6.4.

6.2.2 Sensitivity to assessment results

The peak canister and buffer temperatures are quite sensitive to the thermal conductivity and initial temperature, as demonstrated in the Interim main report /SKB 2004f, Section 7.3/. The peak value is reached after a few years (in the order of 10 years or less) implying that the thermal pulse has not migrated very far when the peak temperatures are reached. Thus, it is the local value of thermal conductivity in the vicinity of each canister, and the canister separation distance, that will determine these peak temperatures. The impact of the heat capacity is judged comparatively small, as noted by /Hökmark and Fälth 2003, subsection 5.2.2/, since a quasi-equilibrium soon establishes between the heat output and the thermal gradients in the near-field.

For the larger scale temperature calculations there will be a considerable averaging of the local variability of thermal conductivity. For such calculations it would most likely be appropriate to apply average values of the thermal conductivity.

6.2.3 Source of information

Site-specific thermal properties of the bedrock are provided in Chapter 7 of the **Site descriptive reports** and from supporting thermal modelling reports by /Sundberg et al. 2005a/ for Forsmark and by /Sundberg et al. 2006/ for Laxemar.

The thermal properties essentially depend on the lithology, i.e. the distribution of rock types, see Section 1.8. In the Site descriptive model, the lithology is described by rock domains, which are defined based on composition, grain size, homogeneity, and style and inferred degree of ductile deformation. The distribution and nomenclature of these rock domains are defined in the geology chapter of the respective site descriptions and are also, in short, in Section 1.8 of the present report. For Forsmark, thermal properties are provided for rock domains RFM029 and RFM012. For Laxemar thermal properties are provided for rock domains RSMA, RSMBA, RSMD, RSME and RSMM.

6.2.4 Conditions for which data are supplied

Data for the thermal properties of the bedrock provided in the two Site descriptive reports concern the situation as it appears today. However, these properties directly depend on the distribution of rock types and the mineral composition of the rock types and are thus not expected to change in the future.

6.2.5 Conceptual uncertainties

The Site descriptive reports only discuss uncertainties connected to the actual data. However, as further discussed in the **Geosphere process report** there are essentially no conceptual uncertainties related to heat transport.

Judgement by the SR-Can team

Based on discussions in the **Geosphere process report**, the SR-Can team does not consider it necessary to include any conceptual uncertainty in the estimated thermal data for SR-Can assessment calculations. Furthermore, in the many in situ experimental programmes in rock masses involving heaters inserted in the rock and measuring the temperature at various points away from the heater, see e.g. /Sundberg et al. 2005c/, it has been found that the heat distribution is mainly uniform and not significantly affected by fractures in the rock mass. This is despite the fact that fractures affect most of the other rock properties and valid even if advection with the groundwater flow may have some limited impact on the heat flow. This implies that the intact rock properties can indeed be used for the rock mass properties.

6.2.6 Data uncertainty, spatial and temporal variation

Input from the Site descriptive model report

There are several uncertainties to consider when estimating thermal data. Most of these uncertainties concern thermal conductivity. The origin of these uncertainties are essentially the same for both sites and is further discussed in Chapter 7 of the **Site descriptive reports**.

Thermal conductivity

There is some, but limited, uncertainty in the measured thermal conductivities which are primarily obtained from laboratory measurements on core samples. Both a direct measurement method, TPS (Transient Plane Source), and an indirect method estimating the conductivity based on the mineral composition, SCA (Self Consistent Approximation), have been used.

- The uncertainty in TPS measurements is low and may be quantified. The accuracy of TPS measurements is better than 5% and the repetitiveness is better than 2% according to the manufacturer of the measurement equipment /Sundberg 2002/. However, this uncertainty refers to the measurement volume (which is approximately 10 cm^3) and not to the volume of the sample since only a subvolume of the sample is subject to measurement. If the TPS measurement is supposed to represent the sample scale (which is approximately 0.1 dm^3) the uncertainties will be larger and depend on small-scale heterogeneity of the rock. There is also a possible bias introduced since there are some minor deviations between results from different laboratories.
- The uncertainty associated with SCA data is significantly larger than for TPS data. For SCA data there are three important sources of uncertainty; (1) determination of the volume fraction of each mineral in the sample (2) representative values of thermal conductivity of the different minerals and (3) (partial) alterations of minerals makes mineral identification and quantification more difficult. Also when comparing TPS and SCA data, there is an uncertainty due to the fact that the modal analysis is not performed for the whole volume of the TPS sample where only the surface of the sample is analysed.

There is a potential underestimation (which would result in a bias) in thermal conductivity data since the *stress dependence has not been assessed* as the measurements are made on stress released samples. However, the effect is assumed to be low since the samples are water saturated before measurement. The thermal conductivity of water is generally lower than the rock, but much higher than it would be for the gas (air) in the void spaces of an unsaturated sample.

It can also be questioned whether samples selected for TPS measurements are *representative* for the rock types they are sampled from since the samples are not taken with the purpose of statistically representing the rock mass. Similarly, the question of representativeness applies for the calculated values based on modal analyses (SCA method). The problem with representativity is potentially more severe at the Laxemar subarea where there are few data from rock domains RSME and RSMM and no representative boreholes. Altered rock has not been analysed, and it is thought that altered rock (red-staining) has higher thermal conductivities than unaltered rock.

At the Laxemar subarea, the *spatial variability* of thermal conductivities of the Ävrö granite is estimated using a correlation between density loggings and thermal conductivity. Although these data are important since they provide high spatial resolution of the variation they are also uncertain. There are potential errors in the density data. /Sundberg et al. 2006/ suggest that potential random errors due to noise might, for some of the boreholes, be as high as 50–60 kg/m^3. There is also a potential bias in the values calculated from density measurement. This would be the case if the observed density versus thermal conductivity relationship did not accurately represent the rock volume in the Laxemar subarea. Also the density versus thermal conductivity relation is uncertain although demonstrated. There are only few data confirming the relation for samples with low thermal conductivities.

Measurements of samples from Forsmark have suggested the *thermal properties to be anisotropic*. The interpretation is however uncertain and the resulting anisotropy might be overestimated in the small scale. There is an uncertainty in the anisotropy measurements since the used heat capacity values have not been measured separately. When upscaling the anisotropy it would depend on foliation or lineation of rock types and in larger (domain) scale. The effective anisotropy would also depend on the frequency and orientation of subordinate rock types occurring as dykes of significant extension and with different thermal characteristics. No evaluation of the extent of such anisotropic occurrence was made in the Forsmark Site descriptive model. There are also some geophysical indications of anisotropy the Laxemar subarea, but this is not verified with actual thermal property measurements.

The *upscaling methodology is uncertain*. The thermal conductivity is measured on very small scale (0.1 dm^3) samples. At this scale there is substantial variation between samples as the mineral composition may vary strongly between different samples. This variability would be averaged out if considering the larger scale that would be important for determining heat transport in the rock. However, as noted in the Site descriptive reports, there is also significant variation of rock types in the larger scale at both sites. Thus, upscaling the thermal data requires consideration of the spatial distribution of the rock types in the rock domains. As further explained, different upscaling approaches are applied to arrive at a reasonable value of the thermal conductivity variability at the 0.75 m scale. There are still uncertainties in this approach as:

- Models of the spatial variability within the occurring rock types of the Forsmark area have not been developed. The spatial variability is only considered in the domain modelling. Spatial variability within the domain is handled in the domain modelling approaches but there are uncertainties in spatial variability within rock type.
- The upscaling depends on the structure, orientation and size distribution of the secondary rock types, and not only in their relative proportions. There is little information on this in the Site descriptive reports.

- Preliminary studies /Sundberg et al. 2005c/ suggest that the spatial variability at a scale less than 1 m is insignificant for the heat transfer. However, there are still uncertainties in this analysis, and the appropriate scale may be larger. Here, the uncertainty is handled by selecting a sufficiently small scale, 0.75 m scale, in order not to underestimate the variability.

Nevertheless, the uncertainty in thermal conductivity has been quantified as ranges, for different scales, although better understanding of the upscaling could possibly allow further variance reduction at the larger scales.

Finally, there is uncertainty in *statistical assumptions*. In Forsmark, the thermal data suggest a bimodal distribution which has been considered when providing the confidence intervals calculated for each domain /Sundberg et al. 2005a/. Thereby the confidence intervals are unevenly distributed around the mean value. This is an uncertain assumption and as long as knowledge of spatial variability is insufficient, it is not possible to check the validity of this assumption. The rock type models have been considered as normal distributions although data is somewhat skewed. This results in a too small change of the mean value for the domain when the scale increases. The effect is however insignificant compared to the other uncertainties. This issue is even more pronounced at Laxemar. The distributions of thermal conductivities at domain level cannot be shown to be normal. This is most likely due to the fact that the rock domains consist of rock types of different thermal properties. Therefore, estimations of lower tail 0.5 and 2.5 percentiles based on the revised standard deviations cannot be calculated using parametric methods. To estimate lower tail percentiles for the revised standard deviations, a correction, based on these observed differences, is made to the corresponding percentiles estimated from the modelled distributions of the base approach. The correction method is further described in the Thermal modelling report for Laxemar /Sundberg et al. 2006/.

Heat capacity

According to the **Site descriptive reports** the representativeness of the measured values (TPS data) could be questioned at both sites. The samples are relatively few and focused on certain parts of the rock volume. Furthermore, no direct laboratory measurements of heat capacity have been performed. Instead, heat capacity has been determined through conductivity and diffusivity measurements performed with the TPS method. This may also introduce a bias.

In situ temperature

Both at Forsmark and Laxemar, temperature loggings from different boreholes show a variation in temperature at specified depth **Site descriptive reports, /Forsmark and Laxemar**/. The difference implies an uncertainty in temperature loggings and even small uncertainties may influence the design of the repository. Possible sources of uncertainty are errors timing of the logging after drilling (drilling adds to temperature disturbance), water movements along the boreholes, uncertainty in the temperature logging or in the measured inclination of the boreholes.

Judgement made by the SR-Can team

There are evidently various sources of uncertainty affecting the estimates of thermal conductivity, where the most important uncertainty concerns the upscaling. However, there is an elaborate attempt to quantify the uncertainty and spatial variability in thermal conductivity. These uncertainty estimates are judged appropriate for SR-Can.

6.2.7 Correlations

Input from the Site descriptive model report

The most important aspect of correlation of thermal properties is related to the spatial correlation as this would affect the up-scaling of thermal properties measured at core samples. The Site model /**Site descriptive report, Forsmark and Laxemar**/ accounts for this upscaling by applying various approaches and considering the spatial variability of the rock at various scales. In a base approach, the spatial variability is estimated from assuming a correlation between thermal conductivity and detailed density loggings along boreholes. Upscaling is performed by calculating geometric means for different scales on this data. To estimate the spatial variability within the dominating rock types for which density loggings are unavailable or for rock types when the correlation between density and thermal conductivity would not apply, it is assumed that the variance caused by spatial variability within these rock types is identical to spatial variability within rock type where density data apply. In a third approach, variograms based on density logging data are used to estimate the small scale variance and in a fourth approach the spatial variability within the dominant rock type is estimated based on TPS measurements or density loggings and then the measurement data are classified in spatial groups depending on their location, and the geometric mean is calculated for each group.

The uncertainties have been discussed in subsection 6.2.6.

The thermal conductivity and the heat capacity have slight temperature dependence. The dependence is larger for the heat capacity. These dependencies are estimated in the **Site descriptive reports**.

Chapter 12 of the **Site descriptive reports** also assesses the consistency between disciplines. It concludes that the thermal property assignment is generally consistent with the geological description. However, it is noted that foliation at Forsmark could impact anisotropy in thermal properties. At Forsmark there are also indications of anisotropy in the thermal data, but the anisotropy is not yet fully assessed.

Judgement by the SR-Can team

It is judged that the identified correlations are handled satisfactory in the data analyses of the Site descriptive reports. The noted consistency between the thermal model and the geological description enhances confidence, although further analyses of anisotropy would possibly reduce the uncertainty in the thermal data.

6.2.8 Quantification

Input from Site Model report

Subsection 7.3.4 of the **Site descriptive report, Forsmark** summaries the modelled thermal properties and conditions of the Forsmark area. Subsection 7.3.4 of the **Site descriptive report, Laxemar** summaries the modelled thermal properties and conditions of the Laxemar subarea.

In situ temperature – Forsmark

As further explained in Chapter 7 of the **Site descriptive report, Forsmark** the in situ temperature, or rather the temperature of the borehole fluid, has been measured in five boreholes. The mean of all temperature loggings is a mean of the in situ temperature at 400, 500 and 600 m depth are estimated to be 10.6, 11.7 and 12.8°C, respectively, see Table 7-11 of the **Site descriptive report, Forsmark**.

There is an uncertainty in the temperature logging results due to disturbance from the drilling and water movements along the boreholes. Even if the measured difference in temperature is relatively small for a specified depth, the influence on the design of a repository may be important. The uncertainty is quantified as a range.

In situ temperature – Laxemar

As further explained in Chapter 7 of the **Site descriptive report, Laxemar**, the in situ temperature and gradient profiles have been measured by fluid temperature logging in five boreholes. The mean of all temperature loggings over a specific depth interval provided as a mean of the in situ temperature at 400, 500 and 600 m depth are estimated to be 12.1, 13.8 and 15.5°C, respectively, see Table 7-10 of the **Site descriptive report, Laxemar**. The filtered temperature seems to be almost linear with depth.

There are potential errors in the loggings since there is a difference in temperature for the same borehole logged on different occasions. This is probably due to disturbance from the drilling and water movements along the boreholes. Although this difference in temperature is relatively small for a specified depth, the influence on the design of a repository may be important. The uncertainty is quantified as a range. For more detail, see the thermal modelling report for Laxemar /Sundberg et al. 2006/.

Thermal transport properties – Forsmark

As further explained in Chapter 7 of the **Site descriptive report, Forsmark** the thermal conductivity at canister scale is modelled using different modelling approaches. Results indicate that the mean thermal conductivity is 3.55 W/(m·K) in rock domain RFM029 and 3.46 W/(m·K) in rock domain RFM012, see Table A-21 in Appendix A6. The standard deviation varies according to the scale considered, and for the canister scale it is expected to range from 0.22 to 0.28 W/(m·K). The lower confidence limit, taking account of the spatial variation at the canister scale, is 2.9 W/(m K) both in rock domain RFM029 and in rock domain RFM012. There is a temperature dependence with a decrease in thermal conductivity of about 10 percent per 100°C increase in temperature for the dominant rock types.

There is less variation in heat capacity with a mean values of 2.17 MJ/(m³·K) and a standard deviation of about 0.19 MJ/(m³·K), see Table 7-15 of the **Site descriptive report, Forsmark**.

Thermal transport properties – Laxemar

As further explained in Chapter 7 of **Site descriptive report, Laxemar**, the thermal conductivity at canister scale is modelled using various approaches. Table A-22 lists resulting distributions of thermal conductivity for the various rock domains. The ranges essentially represent spatial variability between different canister positions, although there is also an uncertainty contribution. It should also be noted that the thermal conductivity decreases slightly at higher temperatures, 1–5% per 100°C temperature increase.

The distributions of thermal conductivities at domain level cannot be shown to be normal. This is most likely due to the fact that the rock domains consist of rock types of different thermal properties. Therefore, estimations of lower tail 0.5 and 2.5 percentiles based on the revised standard deviations, cannot be calculated using parametric methods. To estimate lower tail percentiles for the revised standard deviations, a correction, based on these observed differences, is made to the corresponding percentiles estimated from the modelled distributions of the base approach. The correction method is further described in /Sundberg et al. 2006/.

The resulting values are suggested to be reasonable approximations of the respective percentiles for the 0.8 m scale, see Table A-22. It should be mentioned that uncertainties associated with estimation of percentiles becomes larger at the extreme ends of the distributions. Because no scaling up has been performed for rock domains RSME and RSMM, the lower tails percentiles estimated from realisations based on Monte Carlo simulation are conservatively low for larger scales. By taking into account the effect of upscaling observed in the other domains, which on average is about 0.2 W/(m·K) for the 0.8 m scale, corrected lower 0.5 and 2.5 percentiles can be approximated for these domains, Table 7-17. These approximations are uncertain.

Results of modelling of heat capacity on domain level, presented in Table 7-15 of the **Site descriptive report, Laxemar** for four domains indicate a small range (2.23–2.29 MJ/(m^3·K) at 20°C) in mean heat capacity and a low standard deviation (0.13 MJ/(m^3·K)).The heat capacity increases by approximately 25% per 100°C for the dominating rock types.

As also noted in the **Site descriptive report, Laxemar** the modelled thermal properties are uncertain due to potentially poor representativity of the data, uncertainty in the density logging method and uncertainties in the scaling. There are few data from rock domains RSME and RSMM. There is also altered rock visible as "red-staining" that mainly occurs along and around fractures and interpreted deformation zones. The red-staining of the wall rock around many fractures and deformation zones corresponds to hydrothermal alteration/oxidation, which has resulted in alteration of plagioclase to albite and *K*-feldspar, decomposition of biotite to chlorite and oxidation of Fe(II) to form hematite, mainly present as micrograins in secondary *K*-feldspar and albite in plagioclase pseudomorphs giving the red colour. This means that the thermal conductivity of this altered rock may be higher than in the unaltered rock, but this has not been analysed in version 1.2. Thermal conductivity of Ävrö granite from density logging is uncertain although the validity in using density to calculate thermal conductivity in Ävrö granite is demonstrated. There are, however, few samples with data for low thermal conductivities. There are uncertainties in the large-scale variations within domains with medium or low presence of Ävrö granite since there only a small number of boreholes are used to characterise these domains and since the three-dimensional geometry of most of the rock domains is uncertain. The uncertainty and spatial variability are nevertheless estimated, see e.g. Table A-21, but more representative data would improve the confidence in these estimates.

Judgement made by the SR-Can team

For SR-Can the upscaled mean values and standard deviations provided in the Site descriptive model reports and cited above are judged appropriate, despite the noted and un-quantified uncertainty stemming from potential bias in samples and from the anisotropy. Attempts have been made not to underestimate the uncertainty and the adopted averaging scale of 0.75 m is pessimistically low. However, some additional considerations are necessary before the data can be directly used in the safety assessment:

- Calculation of peak canister and buffer temperatures essentially only depend on the thermal properties at the deposition hole scale, see /Sundberg et al. 2005c/. This means that only thermal properties in the rock domains where the repository is located need to be considered in this calculation; rock domain RFM029 in Forsmark and domains RSMA, RSMBA, RSMD, RSME and RSMM for Laxemar.
- In order not to overestimate the thermal transport for the peak canister temperature calculations (i.e. underestimate the peak temperature) it seems appropriate to apply the thermal conductivity at elevated temperature, i.e. the values for 80°C. For Forsmark values are given for 20°C, i.e. the thermal conductivity should be reduced by 6 percent, i.e. by 0.21 W/(m·K). For Laxemar it is suggested to reduce the thermal conductivity by 2%, which would correspond to a reduction by 0.05 W/(m·K).
- The site reports notes that the distributions of thermal conductivities at domain level cannot be shown to be normal. Nevertheless, for SR-Can a normal distribution is judged appropriate for Forsmark, but not for Laxemar, since a normal approximation there would lead to a subset of canister positions with unrealistically low thermal conductivity. At Laxemar it is instead suggested to use a truncated normal distribution with the lowest value set to the 0.5 percentile now given by Table A-22. More accurate distributions may be needed for SR-Site, but the current level of uncertainty quantification is judged to appropriately reflect the potential spatial variability and uncertainty at the sites. It should also be noted that the uncertainty essentially represents *spatial variability* between deposition holes, although embedded is also the uncertainty in the upscaling, as discussed in subsection 6.2.6. This should be considered when calculating peak canister temperature.

- For temperature calculations in repository scale, the noted spatial variation in thermal conductivity will be averaged out, and is rather insignificant to results. The reduction of thermal conductivity with temperature will not be so important either. Such calculations can use the mean values given by Table A-21 and Table A-22.

Table A-23 suggest values for SR-Can thermal calculations.

6.3 Fracture data

In the present section, fracture data are presented. No designated expert document following the SR-Can data report template, as described in Section 2.3, has been produced. Consequently no distinction have been made in the text between expert opinions and those of the SR-Can team.

Fractures in rock are described by means of Discrete Fracture Networks models (DFN models), see /see e.g. Munier 2004 for details/ for details, which are summarised in the **Site descriptive reports** and detailed in supporting model reports /Hermanson et al. 2005 for Laxemar, La Pointe et al. 2005 for Forsmark/. The DFN models that are, essentially, assemblies of various statistical distributions, are synthesised in the SKB model database, SIMONE, which also provides means of handling subsequent model revisions.

To ease communication, some terms commonly referred to in the present section is initially defined. The terminology stems from Munier /Munier 2004/ to which the reader is kindly asked to address should further details be required.

Fractures are rarely randomly oriented in the bedrock. Commonly, one or several dominating orientations occur, hereafter called *fracture sets* (see for example /Ståhle 2001/ for terminology). The orientations can be described by an orientation distribution. The most commonly used is the Fisher distribution which describes the distribution of vectors that are symmetrically distributed about the mean vector as Fisher /Fisher 1953, Fisher et al. 1987/ :

$$f(\theta) = \frac{\kappa \cdot \sin\theta \cdot e^{\kappa \cos\theta}}{e^{\kappa} - e^{-\kappa}}, \quad 0 \le \theta \le \pi \qquad \text{Equation 6.3.1}$$

in which θ is the angle of divergence from the resultant vector and κ is a concentration parameter. As κ increases, the poles get increasingly centred around their mean direction.

Fracture sizes are described in terms of radii distributions. The power-law distribution has become the one most commonly used to describe fracture sizes in the Site descriptive modelling reports and essential to the assumption of "tectonic continuum" (see subsection 6.3.5). The probability density function of a power-law distribution can be expressed as /Evans et al. 2000/:

$$f(x) = \frac{k\, x_{\min}^{k}}{x^{k+1}} \qquad \begin{matrix} k > 0 \\ x_{\min} > 0 \\ x_{\min} \le x < \infty \end{matrix} \qquad \text{Equation 6.3.2}$$

where $x_{\min}$ is the location parameter (smallest value of *x)*, and *k* the shape parameter.

For the purpose of describing fracture radii, SKB recommends the use of r_0 for the location parameter and k_r for the shape parameter /e.g. Munier 2004/.

Fracture intensities can be expressed in a multitude of ways. SKB has, however, adopted the terminology of Dershowitz /Dershowitz 1995/ which denotes the various notions of intensity as follows:

P_{10} = Fracture frequency along a one-dimensional sampling space, e.g. the centreline of a borehole, expressed as fractures per meter (m^{-1}).

P_{20} = Number of fractures on a two dimensional sampling space, e.g. an outcrop.

P_{21} = Fracture frequency on a two dimensional sampling space, e.g. an outcrop, expressed as trace length per square meter (m/m^2).

P_{30} = Number of fractures in a three dimensional sampling space, e.g. a rock volume.

P_{32} = Fracture frequency in a three dimensional sampling space, e.g. a rock volume, expressed as fracture area per cubic meter (m^2/m^3).

6.3.1 Modelling in SR-Can

DFN models are used within SR-Can to simulate fracture arrays for estimating the intersection probabilities of fractures with canisters and canister positions. These computations steer the degree of utilisation and hence governs the required repository volume. The method to compute intersection probabilities is presented in /Hedin 2005/ though it has been slightly revised since.

DFN models are also essential input to the hydrogeological modelling. However, this aspect of the modelling is assessed in Section 6.5 and will not be discussed further here.

6.3.2 Impact on assessment results

The intersection probability is, briefly, a function of orientations, sizes and intensities of the fractures in relation to the geometry and size of the canister. The impact of these properties is discussed below.

Fracture orientations

Analyses in /Hedin 2005/ show that the assessment results are essentially insensitive to the fracture orientations having used the univariate Fisher distribution. Though *strongly* elliptical spreads around the mean pole, for which e.g. the Bingham distribution might be used, may considerably alter the intersection probabilities, only faint ellipticity of the sets have been published in the Site descriptive modelling reports. These reports present the Univariate Fisher distribution as alternative orientation models and parameters for such are synthesised in Table A-24 in Appendix A7. Due to the reasoning above, and computational convenience, SR-Can make use of the Univariate Fisher distribution.

Area normalisation

Outcrops constitute a very small portion of the area to be modelled. Hence, unsampled areas need to be adjusted for to obtain a coverage over the model area. The manner in which the fracture intensity scales with area can, according to /Hermanson et al. 2005/, be quantified by the Mass Dimension of the fracture traces. When the Mass Dimension of the traces has a value of 2.0, the intensity, expressed as the number of fractures per unit area, scales proportionately (linearly) to area, and the spatial pattern of traces can be characterized by a Poissonian density function which inherently has no spatial correlation among the fractures. If the area of the outcrop is doubled, the number of fractures are also doubled. If, however, the mass dimension is different from 2.0, then intensity scaling of fractures is better described by a fractal model. In a fractal model, intensity varies according to:

$$N(r) = \rho \cdot r^{Dmass}$$

where ρ is a constant, termed the prefactor, r is the radius of a circle defining an area, Dm is the Mass Fractal dimension, and $N(r)$ is the number of fracture traces (partial or entire) contained within the circle of radius r. The reader is kindly referred to e.g. /Hermanson et al. 2005/ for a detailed discussion on this matter.

The procedure of area normalisation governs the trace-length distribution which in term steers the probability of intersection between a fracture and a canister as described in the next section.

Fracture sizes and intensities

Unlike fracture orientation statistics, the form and parameters of the distributions of fracture radii both have a significant influence on canister intersection rates. Essentially, this regards to fractures in the size range 50 - 250 m. This is, perhaps, mostly accentuated for the power-law distribution and its location and shape parameters r_0 and k_r respectively. The shape parameter, k_r, is defined as a range in the Laxemar model report /La Pointe et al. 2005/ but as an uncertainty envelope (see subsection 6.3.8 for explanation) in the Forsmark model report /La Pointe et al. 2005/.

The location parameter, r_0, has not been given any physical meaning, that is, r_0 does not represent the smallest fracture in the *population*. It represents a truncation limit, chosen for practical or engineering purposes, and thus represents the smallest fracture in the *model*, given a particular (truncated) intensity, P_{32}, and a particular k_r.

The impact on assessment is such that larger values of k_r results in fewer canister intersections, everything else held constant. Larger values of r_0 tend to increase intersection probability, everything else held constant.

The largest uncertainty in this context is that there was virtually no data, at the time of analysis, regarding the fracture size of interest, $50 < r < 250$ m. The size distribution for this range of fracture radii was in the Site descriptive models deduced by interpolation between outcrop traces and deformation zone traces and using area normalisation as described in previous section.

As the parameters of the size distributions and intensities are dependent upon one another, the parameters r_0, k_r and P_{32} (truncated) should be treated as triplets. It is therefore not possible to invoke uncertainty in only one of these parameters, e.g. the range given for k_r, without properly adjusting the other two, e.g. r_0 and P_{32} (the relation is quite intricate and the reader is kindly referred to /Hermanson et al. 2005/ for details).

Computed intersection probabilities are sensitive to the intensity, P_{32} of various fracture sets, in particular the intensity in the size range $50 < r < 250$ m. The impact on assessment is such that larger values of P_{32} increase intersection probability, everything else held constant.

Spatial structure

Intersection probabilities are, under certain conditions, sensitive to the spatial structure of the fractures. The impact on assessment is such that a choice of a Poissonian structure, i.e. randomly located fractures in 3D space, tends to increase the amount of affected canisters as compared to a fractal clustering structure, everything else held constant. This because pronounced (fractal) clustering will tend to let fractures intersect relatively fewer canister positions, as compared to a Poissonian spatial arrangement, and more so the more pronounced the clustering. That is, a canister position is considered discriminated regardless of how many discriminating fractures intersect. Both the Forsmark and Laxemar DFN model reports /La Pointe et al. 2005/ argue for a faint fractal correlation structure, which for all practical purposes can be approximated by a Poissonian structure for computational convenience. However, the uncertainty of the estimated fractal dimensions was not expressed in such a way that they can be readily incorporated into the computations of canister intersections /Hedin 2005/. It is possible that a computationally defendable range of fractal dimensions could host values reflecting more pronounced clustering and hence would have an impact on the intersection computations.

6.3.3 Source of information

The DFN models are presented in separate modelling reports /Hermanson et al. 2005 for Laxemar, La Pointe et al. 2005 for Forsmark/ and syntheses of relevant tables are made public in the model database SIMONE. An overview of the DFN models is also presented in the Site descriptive model reports /SKB 2005a, 2006k/.

It should be noted that these sources supplies the basic input to the DFN models used in SR-Can, but provide insufficient information regarding uncertainties. SKB's own expert, who is also part of the SR-Can modelling team, has appended the uncertainty information appropriate for the SR-Can needs. For this reason, the heading "Input from experts" is not used in this section of the report. However, we here make it clear, using standard referencing methods, when we use input from La Pointe et al. /La Pointe et al. 2005/ and Hermanson et al. /Hermanson et al. 2005/ or other experts in the peer-reviewed scientific literature.

6.3.4 Conditions for which data are supplied

DFN parameters are to be supplied by the site descriptions for defined rock domain within the site description model volumes. The DFN parameters, the intensity in particular, are dependent on the size (volume) of the domain due to the scaling properties. The intensities of the DFN models must be adjusted for significant changes of domain or model volumes according to procedures in /La Pointe et al. 2005/.

Possible changes of the fracturing, e.g. due to construction, thermal load or climate related mechanical loads, are not assessed here. These potential changes are assessed as a part of the scenario analysis within SR-Can.

6.3.5 Conceptual uncertainties

Judgement by the SR-Can team

Tectonic continuum

In both the Forsmark and Laxemar site descriptive models, a basic assumption is that fractures on outcrop constitute the smaller, size-censored, portion of a population of much larger fractures. It is motivated by also assuming that the same geological and mechanical processes have created the fractures of the identified orientation sets, at various scales. The authors /La Pointe et al. 2005/ argue that while similar orientations could occur even if the two fracture sets were not part of the same parent population, they consider it as less probable. By assuming that outcrop fracture patterns thus are a smaller-scale expression of regional features, the size calculation for deformation zone-related sets was based upon fitting a power-law curve to the combined data set of deformation zone and area-normalised outcrop fracture trace lengths. Though this approach yielded acceptable results in verification exercises in the Forsmark and Simpevarp site descriptive models, the Laxemar Site description failed to produce a unique match between the size and intensity models for some of the defined sets. The assumption of tectonic continua also influences the spatial structure (see subsection 6.3.6).

The data used for the construction of the size models consisted of meter- to ten meter-scale fracture traces, and traces of kilometre-scale deformation zones. Deformation zones may well be composed predominantly of secondary or anatomizing faults, while the traces in outcrop appear to consist of, with some exceptions, individual joints. There was no data available on fractures between these two scales, although the existence or lack thereof would fundamentally change both the hydrological model and the risk associated with future earthquakes.

The current models have assumed that this tectonic continuum exists and the SR-Can team judge this to be a reasonable assumption in the light of numerous theoretical works /Allègre et al. 1982, Turcotte 1986, 1990/ and field evidence /Barton et al. 1985, Bour et al. 2002/ in support. However, the subhorisontal fracture set constitutes a special problem and is therefore discussed separately below.

Horizontal fracture sets

The size distribution of subhorisontal fractures is very difficult to assess, as the only source of information is outcrops, which present a bias towards subvertical fractures. There is also a conceptual uncertainty for this set, as its relation to other tectonic features is unknown, and the current method for calculating the size of the fractures assumes that it is not related to any other tectonic feature. That is, unlike the vertical fractures, there are no equivalent data sets for horizontal deformation zones available for the DFN model on which to anchor the size distribution even if the tectonic continuum assumption were true. The size distribution of subhorisontal fractures thus constitutes one of the largest uncertainties in the DFN model and at the same time, the most difficult to resolve.

According to authors /La Pointe et al. 2005/ analyses of the mineral filling in the different fracture orientation sets do not show mineralogical or morphological differences with the vertical sets. The authors therefore conclude that it seems more likely than not that these horizontal fractures do extend in size to hundreds or even thousands of meters. Accordingly, the DFN model for Forsmark made use of the Powerlaw size distribution to represent the sub-horisontal set. However, in the Laxemar DFN, the choice of size model for the gently dipping fracture set (set *S_d*, Table A-28) was the Exponential distribution. The mean radius proposed (0.25 m) hardly produce any larger fractures in a regional model in contrast to their discussion on genesis. As large horizontal deformation zones are absent from the nearby Äspö HRL it appears reasonable to use the exponential distribution while awaiting more data from forthcoming Laxemar boreholes.

Fracture shape

Fractures have, in both the Forsmark and Laxemar site descriptive models, been conceptualized as planar, circular discs possessing no thickness. The authors /La Pointe et al. 2005/ argue that while the fractures in the rock are probably neither circular nor planar, there is not sufficient data to mathematically characterize deviations from these two idealizations. In outcrop, the deviations from planarity do not appear to be large, according to the authors. Additionally, the authors argue that there are also mechanical reasons to suppose that the actual fracture shapes may tend towards being equant, as the mechanical layering present in sedimentary rocks which promotes non-equant fracture shape is far less well-developed in the crystalline rocks for Laxemar and Forsmark.

Due to sampling difficulties, there is very little empirical data on fracture shapes as this would require a complete dismantling of the rock mass under study. Yet, a few studies of *faults*, /e.g. Rippon 1985, Walsh and Watterson 1988/ indicate elliptical shapes with a major axis parallel to the direction of slip, and an axial length ratio of 2:1 to 3:1. On the other hand, studies of *joints* /e.g. Aydin and Johnson 1978/ indicate that a circular shape is a reasonable assumption. Site investigations have not produced sufficiently firm kinematic evidence to address the ellipticity of fractures.

Modelling efforts usually require some degree of idealisations, either to purify the problem under study or for computational convenience. Naturally, a great deal of the fundamental work on discrete fracture modelling /e.g. Baecher et al. 1977, Barton 1978, Dershowitz et al. 1979, Long et al. 1985/ and stereology /e.g. Warburton 1980, Berkowitz and Adler 1998, Darcel et al. 2003/ relies on the assumption of disc shaped fractures.

The methods used for DFN modelling within SKB are based on the stochastic generation of fractures, using tools and algorithms based upon the work cited above. Considering the huge amount of fractures generated and the uncertainty in the direction and relative size of the major axis, we believe that fracture shapes can be simplified to circular discs, as a statistical average, for use within SR-Can. We do, however, recognise that this lack of data causes an uncertainty that should be addressed in future safety assessments by e.g. analyses of the sensitivity of intersection statistics to variations in fracture ellipticity.

A fracture commonly undulates in 3-dimensions so that its strike and dip varies in different locations on its surface /Newman and Mitra 1993/. It is also known that the undulation of fracture surfaces varies in amplitude with direction. Such variation in its local orientation occurs on many scales and can be considerable. For instance, the amplitude of undulation parallel to the shear vector is at least 10 times less than in a perpendicular direction /Power et al. 1987, Power and Tullis 1991/. Using a fractal approach, a number of studies /e.g. Okubo and Aki 1987, Hirata 1989, Chilès and Delfiner 1999/ report fractal dimensions that would correspond to an amplitude of 2–15% of the fracture diameter. In most DFN applications, fractures are simplified to planar discs as the use of self-affine surfaces is simply not computationally feasible. Yet, in view of relatively small deviations from the idealisation, the assumption of planarity ought to be reasonable as an average in the modelled fracture networks.

In addition to large scale undulation as reasoned above, fractures display small scale roughness /e.g. Power et al. 1987, Vermilye and Scholz 1995/ that governs the aperture (or width if sealed) along the surface. In DFN modelling, fractures are assumed having a constant aperture, either by applying a constant aperture attribute to the simulated fracture or, to the cost of computation time, simulating constant width by simplifying fractures to thin cylinders, to represent average aperture or width. Though we believe these are reasonable assumptions for the purpose of SR-Can modelling, the stochastic nature of this roughness results in an uncertainty in the current classification of fractures into open and sealed respectively.

Orientations and radii assumed independent of position

Fractures have, in both the Forsmark and Laxemar site descriptive models, been assumed to have orientations and radii that were independent of position. The authors argue that since existing outcrop data is insufficient for making detailed studies of fracture size throughout the regions of interest, they assumed that sizes might vary by subarea and rock domain, but that within each domain and subarea, sizes are assumed homogeneous. A similar reasoning was applied to assume orientations being independent of location.

Underlying the power-law assumption of fracture sizes and the fractal correlation structure of the fracture networks is the notion of self-similarity, i.e. fractal fracture pattern. Not only does this *require* a tectonic continuum, as discussed above, but also, in fact, dependence between orientation, size, and location. That is, to be able to form larger scale structures, smaller fractures are required to cluster into zones, i.e. a correlation between size, location, and orientation is inherent in the basic assumption.

Nevertheless, the simplification of fracture zones from being, essentially, tabular clusters of smaller fractures to single object is, in our opinion, defendable both from pragmatic and scientific point of view. However, for this to be justified, the transition zone /Munier and Hökmark 2004/, in some literature referred to as damage zone, must be included in the computation of thickness of the zone.

Current DFN models use single hole interpretations (see method description MB 810.003 for definitions) to extract fracture data in the rock between deformation zones. The methodology of single hole interpretation as currently pursued, includes a much larger portion of the rock than the core when defining boundaries of the zone, thereby essentially including the macroscopically fractured part of the transition zone. We therefore believe that fractures in the rock blocks bounded by zones and their transition zones, can be confidently assumed to have orientations and radii independent of position. Yet, there are indications in the data that points, rather firmly, towards changes in orientation of fracture sets with depth. Not only do the sets rotate, they also display changes in intensity. Neither of the site descriptive models provide any quantification for these depth dependences. Nevertheless, the variability in fracture orientation within each defined domain is quantified in terms of concentrations around the mean orientations and we believe this geometrical uncertainty has been adequately treated, given the data available at the time of modelling.

Linking of traces

According to the authors /La Pointe et al. 2005/, the linked length of a deformation zone trace, or fracture trace in outcrop, is in the site descriptions judged to be an accurate and appropriate measure of the structure's trace length for the purpose of deriving the radius distribution of geologic structures. This assumption contains three parts: that the segments that have been linked constitute separated section of a single structure, that the linked length is a sufficiently accurate measure of the structure's linear size, and that it is the appropriate measure for computing size statistics. The authors argue that although the size model depends on the lengths of the deformation zone traces and the way structure segments are linked, the uncertainty can be bracketed and quantified. The potential uncertainties in trace lengths at the outcrop scale are manifested (along with other uncertainties) as the variance among area-normalized frequency values for the outcrops.

We believe that the process of linking fracture traces and lineaments is an analogue to concatenating tabular fracture swarms or clusters into zones and the rational behind this procedure is essentially the same: The links are genetically related and the linked lineaments judged to be the surface expression of single feature despite sporadic gaps in the geophysical data. The SR-Can team agrees with the authors of the Site descriptive models and find the underlying assumptions reasonable.

The physical meaning of r_0

The estimation of r_0 (see subsection 6.3.2) has been treated differently within the framework of the **Site descriptive reports**. In the Hydro-DFN /Follin et al. 2005, 2006, Hartley et al. 2005ab/, the location parameter has been set to the smallest measurable fracture size i.e. either the borehole radius or the censoring set by outcrop mapping policy, depending on application. In the Geo-DFN /La Pointe et al. 2005/, the location parameter was obtained by inference.

Ideally, r_0 ought to be set to the smallest radius in the fracture population. This entity is, however, unknown and there are no data to support assessment of any particular size of r_0 but it ought to be in the order of mm or microns. Implementation of such small fractures is simply not computationally possible, and, in fact, quite unnecessary. The pragmatic approach is to set r_0 to the smallest size of the sample, or any other size argued for by engineering considerations, and adjust the intensity accordingly. The ConnectFlow application /e.g. Hartley et al. 2005a/ made use of the smallest trace measured on outcrop, 0.5 m, as it was truncated to by fracture sampling policy. The DarcyTools application made use of the core radius, 0.038 m.

6.3.6 Data uncertainty, spatial and temporal variation

Judgement by the SR-Can team

Lineaments represents deformation zones

The procedure of lineament interpretation is, by design, tuned towards identifying possible deformation zones, other geological structures filtered out. However, interpretation uncertainty yields lineament maps containing structures with varying degree of confidence in existence, see /Johansson 2005/ for discussion. It is therefore possible that some lineaments used for analysis are not in fact deformation zones.

In both the Laxemar and Forsmark DFN, in addition of using the lineament map as a basis for intensity and size estimations, an alternative DFN, made use of the high and low confidence deformation zone that was presented in the Site descriptions. However, for the Laxemar DFN, the Simpevarp 1.2 model was used as the Laxemar 1.2 deformation zone model was developed simultaneously with the Laxemar DFN 1.2 model and was not available for analysis.

The SR-Can team has judged the deformation zone models reasonable. The uncertainties associated to the subhorisontal set, especially for the Laxemar site description, could have been more explicitly expressed to facilitate sensitivity analyses in SR-Can. However, the **Site descriptive report, Forsmark** reported an alternative model to the base case, called "base case variant" in which the size of four dominant gently dipping zones is different. The alternative models presented for both sites differ mainly in the intensity of deformation zones.

Truncation and censoring of fracture traces

The smallest fractures that can break a borehole equals the borehole radius. The smallest fracture trace that is mapped on outcrop is limited by mapping policy: 0.5 m in area mapping and 0.2 m in scanline mapping.

The authors of the Laxemar DFN claim that the addition of "smaller" fractures (i.e. more fractures with a measured trace length below the outcrop truncation threshold of 0.5 m) does not affect the match of the produced DFN to the data. According to the authors, it exacerbates the issue of the higher fracture intensities observed in outcrop (P_{21}) when compared to borehole data, and creates a more difficult environment to successfully match the power-law relation fracture set sizes and intensities. The issue of r_0 was discussed earlier and will not be repeated here.

The largest fracture that can be detected on outcrop is limited by the outcrop size. As consequence thereof, there is a lack of data in the size range (traces) 30 – ca. 1,000 m. This lack of data has been highlighted in both the Laxemar and Forsmark DFN.

The reasonably good fit to power-law size distributions, a consequence of the assumption of tectonic continuum and fractal scaling, make the SR-Can team confident in that the intensity of fractures in the critical size range for earthquake analyses ($50 < r < 250$ m) can be adequately addressed. Theoretical analyses and field work elsewhere have demonstrated the existence of these intermediately sized structures. Using the interpolation between small-scale and large-scale structures to estimate the intensity of fractures in the data gap, thereby assuming that they exist, will thus yield a cautious estimate for the intended use in SR-Can.

Spatial structure

Analyses of spatial structure of fractures was in both the Forsmark and Laxemar Site Descriptions restricted to a fractal approach of which the Poissonian structure constitutes a special case. The spatial model was determined through the calculation of the mass dimension of the number of fractures per unit area (P_{20}) for outcrop trace data, and the number of fractures per unit length (P_{10}) for borehole data. The regressions were tested for statistical significance and expressed in terms of standard deviations of the error. The adopted spatial model also steers the area normalisation procedure.

In the Forsmark DFN model /La Pointe et al. 2005/ the mass fractal analysis showed a slight departure in the spatial model from Poissonian towards a slightly fractal spatial pattern. The authors argue that the conceptual uncertainty as to whether to specify the spatial model as Poissonian or slightly fractal will slightly impact the size calculations in a minor way, although the treatment of size uncertainty probably overshadows the impact, including the possibility to estimate the mass fractal dimension. Based on this reasoning, the authors conclude that the spatial model is best described by the simpler, Poissonian model for all modelled domains and all model scales.

For the Laxemar DFN model /La Pointe et al. 2005/ the authors conclude that the spatial model is best described by a fractal model for discretisation scales up to 30 m, and by a Poissonian model for discretisation scales between 30 and 100 m. The data could not be analysed for even larger discretisation scales, e.g. repository scale, but the authors judged that a Poissonian model would be defendable.

Though we note that the different spatial structures proposed for different discretisation volumes are in conflict to the assumption of tectonic continuum, the SR-Can team accepts the arguments brought forward by the authors and intend to use the Euclidian scaling and the DFN parameters stemming there from, for the purposes of SR-Can. However, the Laxemar model did not report any Poissonian DFN parameters for one of the local fracture sets, *S_f*, and SR-Can intends to use two alternatives by either omitting the set or using the parameters corresponding to the fractal spatial structure.

Area normalisation

The area normalisation (scaling) is a procedure to relate the number of fractures of a given trace length measured over an area, to the number of fractures of the same size class measured over an area of a different size, i.e. a procedure for fracture intensity scaling. Area normalisation enables combining deformation zone traces with outcrop fracture traces so that the shape parameter of the power-law distribution, k_t, may be computed for all scales. The procedure makes use of the mass dimension deduced from the analysis of spatial structure.

In the Forsmark DFN model /La Pointe et al. 2005/, the authors demonstrate a slight departure in the spatial model from Poissonian towards a slightly fractal spatial pattern (see section Spatial structure). This will slightly impact the number of fractures in the larger scale models which extrapolate the P_{32} from small scales, like outcrops, to entire model regions. Depending upon whether the mass dimension is slightly below or above 2.0, the large scale model will overestimate or underestimate, respectively, the number of fractures that would be inferred from the Poissonian spatial model. However, the uncertainty inherent in the P_{32} intensity for the small domain has, according to the authors, probably a far greater impact than the scaling uncertainty. Therefore, a Euclidian scaling model was recommended for Forsmark.

For the Laxemar DFN model /La Pointe et al. 2005/ the authors conclude that the spatial model is best described by a fractal model for discretisation scales up to 30 m, and by a Poissonian model for discretisation scales between 30 and 100 m. The spatial variability in intensity is very large and the upscaling of intensity problematic as a consequence thereof. Fracture set intensities based solely on outcrop two-dimensional fracture trace intensity (P_{21}) tend to produce higher estimations of three-dimensional fracture intensity (P_{32}) than do boreholes, although in general, boreholes do not indicate that fracturing has been enhanced by surficial stress-relief mechanisms. As a result of the outcrop uncertainty, the authors conclude /La Pointe et al. 2005/ that it is not yet possible to produce a size and intensity model for all three regional power-law scaling fracture sets that simultaneously fit both borehole and outcrop data.

Having accepted the argumentation for the use of a Poissonian spatial structure of fractures beyond deformation zones, the natural consequence for SR-Can is to also accept the Euclidian area normalisation. This can be justified by the fractal dimensions which, on average, lie very close to 2 (see e.g. /La Pointe et al. 2005/ for details).

6.3.7 Correlations

Judgement by the SR-Can team

The linking of traces and the radii being independent on location, were discussed in subsection 6.3.5. The spatial structure of fractures was discussed in subsection 6.3.6.

Correlation between intensity and depth

In both the Forsmark and the Laxemar site description models, the authors claim not being able to demonstrate any dependence of fracture intensity with depth regardless of whether they were classified as open or sealed. Yet hydraulic information indicates a clear variability in intensity of hydraulically active fractures with depth, which ought to be reflected somehow in the Geo-DFN.

It is possible that future site modelling will resolve this issue by the use of additional domains, as the resolution and density of SI data increases. For instance, in the Forsmark site description, the zone ZFMNE00A2 has been used as divider within the rock domain RFM029 for both Hydro-DFN and the validation case of the Geo-DFN to account for the obvious difference in intensity between near surface rock and rock at repository level. The SR-Can team will, nevertheless, in the absence of such higher resolution Geo-DFN models, accept the general remark that no correlation with depth can be demonstrated.

6.3.8 Quantification

With support from the reasoning in subsections 6.3.1–6.3.7, we here briefly summarise the DFN-parameters to be used in SR-Can for computation of the intersection probabilities between canisters and fractures.

Fracture orientations

The orientation distribution has been shown to have a minor impact on the canister/fracture intersection probabilities /Hedin 2005/. Additionally, many of the analysed fracture sets did not pass formal K-S goodness–of-fit tests regardless of tested distribution. Moreover, the ellipticity of the fracture poles is faint. For computational convenience, we therefore intend to use the Univariate Fisher orientation model as presented in Table A-27 and Table A-29 for Forsmark and Laxemar respectively.

Size and intensity

Neither of the site descriptive models provided any uncertainties in the size models such that they could be incorporated into SR-Can without additional simulations. That is, uncertainties were quantified for some parameters, such as the shape factor k_r, and variabilities were given for P_{32}. However, as the size parameters are coupled to intensity and triplets P_{32}-k_r-r_0 were only provided for the best estimate, SR-Can can only make of the use triplets provided in Table A-24 and Table A-28.

The size model recommended by the authors for the fracture set *S_d* in Laxemar is, based on significance tests, exponential (Table A-28). Such a distribution does, with the mean value proposed, hardly produce any large fractures in the model volume. This is in direct conflict with the reported deformation zone model of the site description /**Site descriptive report, Laxemar**/ which includes a fairly large gently dipping zone (ZSMNW928A). Given the fairly reasonable assumption that some gently dipping zones might still remain undetected, paired with the relatively weak statistical significance of all tested size distributions (25%, 56% and 27% for the log-normal, exponential and power law distributions respectively) SR-Can intends to use the power law distribution as an alternative to the exponential. The size model for domain A in the Laxemar sub area is shown in Table A-28.

Spatial structure

Both sites display a faint fractal spatial structure. Following the recommendations by the authors of the Site descriptive models, the spatial structure can for all practical purposes be simplified to a Poissonian structure for the purposes of SR-Can.

6.4 Rock mechanics

This section present rock mechanics properties, as wells as the stress conditions, needed for analysing the potential for rock mechanics evolution and coupled THM effects. No special SR-Can expert document has been prepared for these data, instead the needed quantities are assessed from the **Site descriptive reports** and the version D1 repository layout /SKB 2004a/.

These latter inputs have been authored by the SKB Site Modelling expert on rock mechanics properties. The data presented are given per rock domain, a brief description of these are given in Section 1.8. Furthermore, the rock mechanics modelling conducted for SR-Can is presented in a separate modelling report /Hökmark et al. 2006/. That report also assesses the input data used for the modelling.

6.4.1 Modelling in SR-Can

The rock mechanics modelling explicitly conducted for SR-Can is done using the extensively tested 3DEC code /Itasca Consulting Group Inc 2003/. 3DEC is a distinct element code, particularly developed to analyse the mechanical and thermo-mechanical behaviour of jointed media such as fractured rock. The results of the modelling are presented in a separate modelling report /Hökmark et al. 2006/. The objective of the modelling is to estimate the disturbance caused by mechanical and thermo-mechanical processes on the hydraulic conditions in the near-field and in the far-field, and to estimate the risk for spalling in the walls of the deposition holes during excavation and the thermal period.

The thermo-mechanical near-field 3DEC analyses /Hökmark et al. 2006/ are based on input data determined during different stages of the site descriptive modelling work and on general layout and design guide-lines /SKB 2004a/. Most of the data are direct picks from the **Site descriptive reports, Forsmark and Simpevarp**. The fracture geometry, however, is generic and without links to the site models. There are separate 3DEC near-field models for Forsmark site conditions and for Simpevarp site conditions. As far as rock mechanics input data is concerned, the Simpevarp model is judged to be reasonably representative also of the Laxemar subarea, i.e. the predominant rock type is Ävrö granite in both subareas. However, the results of additional Laxemar 3DEC models would have to take into account specific Laxemar layout considerations, for instance tunnel directions. The 3DEC models are analysed with respect to effects of excavation, effects of the development of pore pressure and buffer swelling pressure, effects of the thermal load (Simpevarp and Forsmark) and of glaciation/deglaciation (Forsmark).

6.4.2 Sensitivity to assessment results

General

The main results of the 3DEC analyses are:

- upper bound estimates of mechanically induced changes of the transmissivity of fractures that intersect the near-field, as well as fractures in the far-field, due to excavation, thermal effects and effects of ice load. These upper bound estimates are based on results from the 3DEC models giving the largest impacts,
- estimates of the scope and extent of fracturing around deposition holes and based on this a qualitative assessment of the potential hydraulic impact of this fracturing.

Values of intact rock and rock mass deformability parameters do typically vary within tens of percents rather than within orders of magnitude. Because of this, the upper bound estimates of transmissivity changes and the spalling risk estimates are not very sensitive to input data variations within the ranges suggested by the probability distributions given in the site descriptions for these parameters. Fracture strength parameter values and in situ stresses are potentially more important.

Stress

The site reports provide uncertainty intervals for the stress data. At present there has not been any systematic check for sensitivity to stress assumptions. Comparison between the 3DEC results obtained for the different sites/stress domains gives an approximate picture of the sensitivity to stress variations. The high-stress Forsmark model gave the largest fracture shear

displacements. The low-stress Simpevarp and Laxemar stress domain *II* model (presented in the Site descriptive report) did not give shear displacements sufficiently large that the fracture transmissivity would change (according to the experimental data used to evaluate the modelling results). On the other hand, transmissivity changes induced by normal stress variations were at maximum in the low-stress Simpevarp stress domain *II* model. For the bounding and general estimates of the effects on transmissivity, the net effect of in situ stress variations between the Forsmark mean values and the Simpevarp stress domain *II* mean values are unimportant.

Fracture geometry

All analyses were conducted using schematic fracture geometry with a small number of fractures located in a region of potential importance in hydro-models. The fracture orientations were selected to give a high sensitivity to mechanical disturbances. Yet, the possibility that other fracture geometries could have given different results cannot be excluded.

Fracture strength

The fracture strength is treated schematically in the site descriptive reports, with common values for all joint sets and all rock domains. The 3DEC results were checked with additional analyses using the minimum and maximum values of fracture friction given in the Forsmark site description. The minimum value of friction did not give more slip on the particular fracture that gave the largest slip in the base case analysis, i.e. using the mean value of the Forsmark site descriptive report. This means that the upper bound estimate of effects on fracture transmissivities would not change, or be sensitive to fracture strength reductions. The maximum friction gave approximately half the slip on all fractures. Strength variations appeared to have insignificant effects on transmissivity changes related to normal stress variations.

Fracture shear stiffness and fracture normal stiffness

In the 3DEC model mean values are used throughout without sensitivity tests, while the site models give standard deviations, corresponding to about 40% of the mean values. Variations within these ranges are not judged important to any of the results.

6.4.3 Conditions for which data are supplied

The data supplied from the sites do all regard present-day conditions. None of the geosphere property data used as input in the thermo-mechanical models is sensitive to changes in temperature, or is in any way likely to change over time. Initial stresses are based on the present-day knowledge of the site conditions. The thermal load, i.e. the deposition geometry, is conditioned to the rock mass heat conductivity according to current design guide-lines /D1 layout, SKB 2004a/.

The representation of the glacial load is derived from preliminary, not yet published, results from ice/crust/mantle Abaqus finite element calculations of the stress evolution at repository depth during a glacial cycle based on Lambeck's ice model. A set of simplified analyses with a less detailed ice model is presented by /Lund 2005/. The finite element model includes assumptions regarding the properties of the viscous mantle and the elastic crust. Should the results of the finite element simulations be modified significantly, the input to the near-field models may have to be modified accordingly.

6.4.4 Conceptual uncertainties

Input from SR-Can rock mechanics modelling team

According to /Hökmark et al. 2006/ there are no major conceptual uncertainties associated with the description of the rock mass, or the thermo-mechanical laws assumed to apply. There is some conceptual uncertainty associated with the changes in fracture transmissivity that will accompany the mechanical evolution. Fracture shear displacements may increase or decrease the transmissivity of individual fractures, depending e.g. on the magnitude of the displacement, the fracture roughness, the fracture filling (if any), and the fracture normal stress. Shear displacements calculated in the 3DEC models take place under much higher normal stresses, tens of MPa, than those generally applied in hydro-mechanical tests on rock fractures. Trends can be established from test results, for instance that high normal stresses limit or inhibit possible shear-induced transmissivity increases, but there are no clear and generally applicable relations between displacement and transmissivity changes. This uncertainty is not judged to invalidate any of the conclusions or the upper bound estimates of fracture transmissivity changes.

It is possible to convert realisations of DFN models to 3DEC input. However, it is not possible to analyse numerous 3DEC models in a statistically meaningful way. The 3DEC fracture geometry was selected particularly to capture the behaviour of fractures at specific positions and with specific orientations. This means that the fracture network characteristics are not captured.

Judgement by the SR-Can team

The SR-Can team accepts the expert input.

6.4.5 Data uncertainty, spatial and temporal variation

Input from the Site descriptive reports

The rock mechanics data obtained from the Site report model tables used as input to the 3DEC models has a degree of uncertainty which is described, or quantified, by standard deviation values given in these tables. The confidence in these uncertainty ranges are also discussed in the Site descriptive reports:

- At Forsmark the rock stress magnitudes and their spatial distributions are uncertain, since measured stresses are at the upper limit of applicability of the measurement methods. Furthermore, all the stress measurement methods suffer from different kinds of uncertainties that often derive from the assumptions behind the processing technique. These uncertainties are considered in the stress estimation, as further discussed in subsection 6.4.5 of the **Site descriptive report, Forsmark**.
- Rock mechanics properties at Forsmark are obtained by means of internationally established standard methods and procedures (e.g. ISRM suggested methods) and the uncertainty is considered to be represented by the scatter of the experimental results. Moreover, it is also assumed that the rock samples are representative of the intact rock inside each rock domain. There is also confidence in the data since they compare well with old data from the final repository for radioactive operational waste, SFR, located just northeast of the candidate area.
- At Laxemar, both data and stress modelling results suggest that the Laxemar subarea could be divided into two different stress domain (*I* and *II*), where stress domain *II* has lower stresses **/Site descriptive report, Laxemar/**. An uncertainty range is given for these two stress domains. The reasons for uncertainty in the stress model are several. Firstly, the accuracy of the measurements themselves is limited. Secondly, the amount of data is not large, from a statistical viewpoint, and the fitted linear stress model functions have an inherent uncertainty due to this fact. Thirdly, the assumptions made regarding the stress domains and the need to extrapolate the available measurement results over large volumes also contribute to the uncertainty. The value selected for the total uncertainty thus encompasses different contributions and is based on an expert judgement for each contribution.

- Rock mechanics properties at Laxemar are also obtained by means of internationally established standard methods and procedures (e.g. ISRM suggested methods). To describe the uncertainty in the estimations, an estimated span was selected based on the statistical analysis of the data sample (the 95% confidence values around the mean). However, as further discussed in the **Site descriptive report, Laxemar** the rock mechanics properties for intact rock of rock type Quartz monzodiorite and the Ävrö granite in the southern part of Laxemar subarea are possibly biased, since only laboratory tests from the Simpevarp subarea and northern Laxemar are available. The Ävrö granite in southern Laxemar is expected to have lower quartz content than the available samples of Ävrö granite, and the quartz content may affect the mechanical properties. This uncertainty cannot be quantified until representative data from the potential repository volume become available.

The 3DEC near-field models /Hökmark et al. 2006/ do not include spatial variations of any rock mechanics properties. The site descriptive models /**Site descriptive report, Forsmark**/ do not include any such variations other than alternative parameter values given for the properties of deterministic deformation zones. This means that the 3DEC model results are valid for the competent rock mass parts of the sites.

There are no temporal variations in any rock mechanics properties.

Judgement by the SR-Can team

The SR-Can team judges the data uncertainty description to be sufficient for the purpose of SR-Can. However, it is also noted that the confidence in the stress levels from Forsmark is limited due to few data and that the rock mechanics data from Laxemar is limited by the fact that there are few data from the potential rock volume. This means that conclusions reached based on currently available data must be regarded as preliminary.

6.4.6 Correlations

Input from SR-Can rock mechanics modelling team

According to /Hökmark et al. 2006/ there are no known or suspected correlations among the rock mechanics properties that could have any impact on the results of the rock mechanics modelling.

Judgement by the SR-Can team

The SR-Can team accepts the expert input.

6.4.7 Quantification

Input from SR-Can rock mechanics modelling team

The data used in the 3DEC analyses are given in Table A-36 to Table A-38 in Appendix A10. The list below describes the data and the way it was determined.

- *Rock mass elastic properties (Young's modulus and Poisson ratio, Table A-36)*: For the Forsmark model the mean values given for rock domain RFM012 were used /**Site descriptive report, Forsmark**/. For the Simpevarp models the values given for rock domain A were used /**Site descriptive report, Simpevarp**/.
- *Intact rock elastic properties. (Young's modulus and Poisson ratio, Table A-36):* For the Forsmark model the mean values given for the dominating rock type in Domain RFM012, *granite to granodiorite,* were used. For the Simpevarp models the values given for the dominating rock type in rock domain *A*; Ävrö granite, were used.

- *Rock mass density:* A generic value, identical for both sites was used (2,600 kg/m^3). The vertical stress/depth relations for the Forsmark site /**Site descriptive report, Forsmark**/ and for Stress domain *I* in Simpevarp /SKB 2005d/ suggest that the density should be 2,700 kg/m^3 and 2,850 kg/m^3, respectively, i.e. 6 or 7% larger. The density of the dominating rock type at the Forsmark site, granite to granodiorite, varies between 2,640 kg/m^3 and 2,660 kg/m^3. None of the rock types at the Forsmark site has a density larger than 2,825 kg/m^3, other than diorite, quarts diorite and gabbro /Sundberg et al. 2005a/. Direct measurement of Ävrö granite density gives values between 2,640 and 2,815 kg/m^3 /Sundberg et al. 2005b/. Underestimating the density has no influence on the mechanical 3DEC results, since gravity is not included. It will have some impact on the rock heat capacity values (see below).
- *Fracture shear stiffness and fracture normal stiffness:* Mean values given for fractures in Forsmark and Simpevarp in the **Site descriptive reports, Forsmark and Simpevarp** were used in the Forsmark and Simpevarp models respectively, Table A-36. In the site models, there are no differences between fractures belonging to different fracture sets or different domains within the sites. In the 3DEC model, mean values are used throughout without sensitivity tests, while the site models give standard deviations, corresponding to about 40% of the mean values. Variations within these ranges are not important to any of the results.
- *Fracture friction and cohesion:* Data given for the mean peak friction angle and the mean peak cohesion in the site descriptive reports were translated into parameter values of a Mohr-Coulomb plasticity model, common to the Forsmark and Simpevarp 3DEC models (Appendix A8, Table A-36). The fracture strength data from the two sites do not differ sufficiently to justify the use of different fracture material models. The peak friction angle for Forsmark fractures is 34° and for Simpevarp fractures 32° /**Site descriptive report, Forsmark and Simpevarp**/. The site reports give standard deviations of 3° and 4°, respectively. Min-max ranges are 27°–40° for Forsmark and 24°–40° for Simpevarp. The Forsmark 3DEC model was analysed for two additional assumptions: friction angle = 27° and friction angle = 45°.
- *Fracture dilation:* The value of the fracture dilation angle, 10°, was obtained from early work on Ävrö granite fractures /Olsson 1998/. The Forsmark site descriptive report include dilation angles that bound the value used in the 3DEC models. In the **Site descriptive report, Simpevarp** there are no dilation values.
- *Fracture geometry:* The 3DEC models have generic orientations and positions of a small number of fractures selected to capture the behaviour of fractures of potential importance to near-field permeability conditions. The fractures are the same in the Forsmark and Simpevarp models, Table A-37. There are no links to any of the site DFN models.
- *Rock mass thermal conductivity:* (Same as intact rock thermal conductivity.) The 3DEC models were established prior to the appearance of the Forsmark and Simpevarp thermal site descriptions /Sundberg et al. 2005ab/. The values used in the 3DEC models, Table A-36, were based on pilot layout versions /Brantberger 2004, Glamheden 2004/ in which the canister spacing (8 m in the Simpevarp 3DEC model and 6 m in the Forsmark 3DEC model) was conditioned to preliminary estimates of relevant heat conductivity values. These data have been kept in 3DEC models, although the thermal site models have been updated such that the RFM012 domain mean value is 3.46 W/(m·K) rather than 3.65 W/(m·K) /Sundberg et al. 2005a/ and the RSMA01 value is 2.80 W/(m·K) rather than 2.61 W/(m·K) /Sundberg et al. 2005b/. The values accord approximately, but not exactly, with the mean values given for the dominating rock types in Forsmark and Simpevarp /Sundberg et al. 2005ab/. The sensitivity of the maximum canister temperature to rock thermal conductivity variations is examined in /Hökmark and Fälth 2003/. An overestimate by 0.19 W/(m·K), as for the Forsmark model, means a 2°C under-prediction of that temperature.

- *Rock mass thermal diffusivity:* 3DEC diffusivities, Table A-36, are calculated from generic values of density (2,600 kg/m^3, see above) and specific heat (800 J/(kg·K)). These values correspond to a volumetric heat capacity of 2.08 MJ/m^3, while the RFM012 and RSMA01 mean values are 2.15 MJ/m^3 and 2.23 MJ/m^3, respectively /Sundberg et al. 2005ab/. The importance of this difference is modest: For the Forsmark model, the 3DEC temperature will be estimated by between 1 and 1.5°C. In addition, the values used here are within one standard deviation for both sites (0.12 MJ/m^3 for Simpevarp and 0.15 MJ/m^3 for Forsmark /Sundberg et al. 2005ab/).
- *Intact rock thermal conductivity and diffusivity:* There is no distinction between intact rock and rock mass as regards thermal properties in the 3DEC models.
- *Rock mass thermal volumetric expansion coefficient:* (intact rock thermal expansion coefficient). For the Forsmark 3DEC models, the value given for *granite to granodiorite* in v1.2 of the Site description was used. For the Simpevarp model, the value used in the 3DEC model is about 3% higher than the mean value finally established for *Ävrö granite* in the v1.2 Site descriptive report for the Simpevarp subarea, Table A-36.
- *Initial, pre-mining stress magnitudes:* For the Forsmark 3DEC model, the values given in draft versions the 1.2 Site description were used, Table A-38. The value used for the minor horizontal stress at 500 m depth (18 MPa) differs from the one given in the final version (31.5 MPa). There are additional results from Forsmark 3DEC models analyzed using the updated, final version stress field at 400 m depth. For the Simpevarp subarea there is one 3DEC model for Stress Domain *I* and another for Stress Domain *II*. In both Simpevarp models the stress states given in the site reports are used throughout.
- *Initial stress orientation:* For all stress states given in the site reports, one of the principal stresses is exactly vertical. Therefore the relevant input to the 3DEC models is the relative orientations of the major horizontal stress and the tunnel axis, Table A-38. These relative orientations were based on information obtained from pilot layout versions /Brantberger, 2004, Glamheden 2004/.

Numerical values are found in Table A-36 to Table A-38 along with a list of notes with additional comments.

In addition to the regular rock mechanics data and repository layout data, there are stress data derived from numerical, yet unpublished, FEM studies of ice/crust/mantle interactions, similar to those presented by /Lund 2005/, but with a more detailed representation of the ice load. These stress data are presented by /Hökmark et al. 2006/. A selection of results corresponding to the conditions at 800 km distance from the NW edge of the ice were used as boundary conditions of the 3DEC Forsmark model for simulation of a glacial cycle.

Judgement by the SR-Can team

The SR-Can team judges the data uncertainty quantification to be sufficient for the purpose of SR-Can. However, it is also noted that the confidence in the stress levels from Forsmark is limited due to few data and that the rock mechanics data from Laxemar is limited by the fact that there are few data from the potential rock volume. This means that conclusions reached based on currently available data must be regarded as preliminary.

6.5 Hydraulic properties and the EDZ

Groundwater flow modelling provides some key entities for the subsequent radionuclide transport calculations in the SKB safety assessment model chain. The primary input to the flow modelling is the hydraulic properties of the bedrock. These are assessed in the Site descriptive models. Furthermore, the impact on these properties from the tunnel and its construction, i.e. the potential for development of an Excavation Damaged Zone (EDZ) needs also be considered.

6.5.1 Modelling in SR-Can

Groundwater Flow Modelling

As further described in the **Geosphere process report**, the following groundwater flow modelling is performed in SR-Can:

Excavation/operation period: During the excavation and operation period of the repository, the system is characterised by the tunnels being at atmospheric pressure. Also, the re-saturation phase of the repository is included in this period, when the back-filled tunnels go from zero to full saturation. Simulations of the excavation and operation period are performed using the code DarcyTools /Svensson 2004, Svensson et al. 2004ab/. Fully saturated groundwater flow with a free groundwater surface is used. DarcyTools can also handle unsaturated groundwater flow above the groundwater table in a simplified manner. Additional simulations of near-surface effects may be done using the hydrogeological modelling tool MIKE-SHE /DHI 2004/. The objective with these latter studies is primarily to assess the interaction between the surface hydrological and deep groundwater systems.

Initial Temperate period: The modelling of the temperate period is well exemplified in the SR-Can Interim hydrogeological simulations /Hartley et al. 2004/. Here, the simulation of an approximately 10,000 year long period, extending from after repository re-saturation up till the initiation of the next permafrost-glaciation event, is undertaken. The shore-line displacement is included in the model as a transient boundary condition. The backfilled tunnels are explicitly included in the models that are based on a nesting of different scales (from regional to canister) using a mixture of continuum and discrete fracture network representations of the rock mass. The ConnectFlow code /Serco Assurance 2005/ is used for these simulations.

Permafrost: The main objective of the permafrost simulations is to assess the groundwater flow pattern during a period when the upper part o the geosphere may be frozen and thus restricted to flow. A second objective is to study the possible movement of salt, due to salt exclusion during freezing, from beneath the permafrost layer to greater depths. Both the depth of the salt front and corresponding transport times are of interest.

Glaciation: The simulation of groundwater flow during a glaciation cycle aims at establishing groundwater flow patterns during the glaciation build-up and retreat. A large super-regional domain needs to be considered for these simulations. Input from an ice-sheet model provides boundary conditions in terms of glacial melt rates.

Required input and model concepts

The required property input for this modelling is the geometry and spatial distribution of the hydraulic properties of the deformation zones and the fractures of the bedrock. Depending on scale, the geometry and properties of these features are provided “deterministically” or “statistically” as a hydraulic Discrete Fracture Network (DFN). However, these basic descriptions need to be adapted to describe the hydraulic properties of the rock mass. As further explained by /Hartley et al. 2005a/, SR-Can adopts a modelling methodology where the rock mass could be represented by either a pure DFN representation in model volumes close to the repository, an Equivalent Continuous Porous Medium (ECPM) model with heterogeneous properties based on the use of the underlying discrete fracture network (DFN) concept, or by a pure porous medium representation model with large scale average hydraulic properties. (In the Site model this latter representation is denoted a multi-component Continuous Porous Medium model – CPM).

These different descriptions are based on the hydrogeological model determined as a part of the site description and documented in the Site descriptive reports /Hartley et al. 2005a, **Site descriptive report, Forsmark**/ for Forsmark and /Hartley et al. 2006b, **Site descriptive report, Laxemar**/ for Laxemar. The numerical flow models (ConnectFlow and Darcy Tools) used to derive these descriptions, have the capability to explicitly model a network of connected

fractures where each fracture is given a size location and orientation. This forms a network of fractures in which the water can flow. Large and conductive deformation zones, denoted hydraulic conductor domains (HCD), with known locations and properties are modelled deterministically. The fractures in the rock mass, which can be divided into different Hydraulic Rock Domains (HRD), are modelled stochastically based in the geological DFN-model, see Section 6.3, but given hydraulic properties by calibration against flow and transmissivity data obtained from interpretations of hydraulic tests in boreholes. The latter are data obtained by PFL (Posiva Flow Log) and PSS (Pipe String System) test. PFL tests measure flow in individual fractures and PSS in a packed off section, typically 5 m long.

The number of open fractures seen in cores and boreholes are used to calibrate the (flowing) fracture density in the DFN model. The DFN model uses the above data to generate a fracture network and imposes hydraulic boundary conditions based on topographic and other information. Flow in the DFN model is calculated. The flow rate distribution in the fractures in the model is compared to the observations in boreholes. As it cannot be expected that the observed and modelled distributions agree directly, model parameters are adjusted until a good agreement is obtained. One parameter that can be adjusted is the density of open fractures in the network, the so called P_{32} (for definition, see definition in Section 6.3). Other parameters that are adjusted relate to the length distribution of the fractures, which influences the connectivity of the network and the relation between length and transmissivity of the fractures which influences the spread and persistence of flow rates in the network. Often it is found that no drastic parameter adjustments must be made but also that several possible parameter combinations give similar and acceptable agreement. An example of measured and simulated flow rate distributions and flowing fracture frequencies is shown in Figure 6-1.

As will be further discussed in Section 6.6, the DFN model contains the flow related information needed for solute transport calculations. The advective travel time, t_w (yrs) in a fracture is given by the groundwater flow in the fracture, the migration path and the fracture aperture, whereas the more important transport resistance in the fracture, the so-called F-factor (yrs/m), is given by the migration path and the flow. Upscaled migration properties can thus be obtained by particle tracking in the DFN-model. In particular, and very importantly, a DFN model inherently contains information on the so called Flow Wetted Surface, FWS, which is the surface over

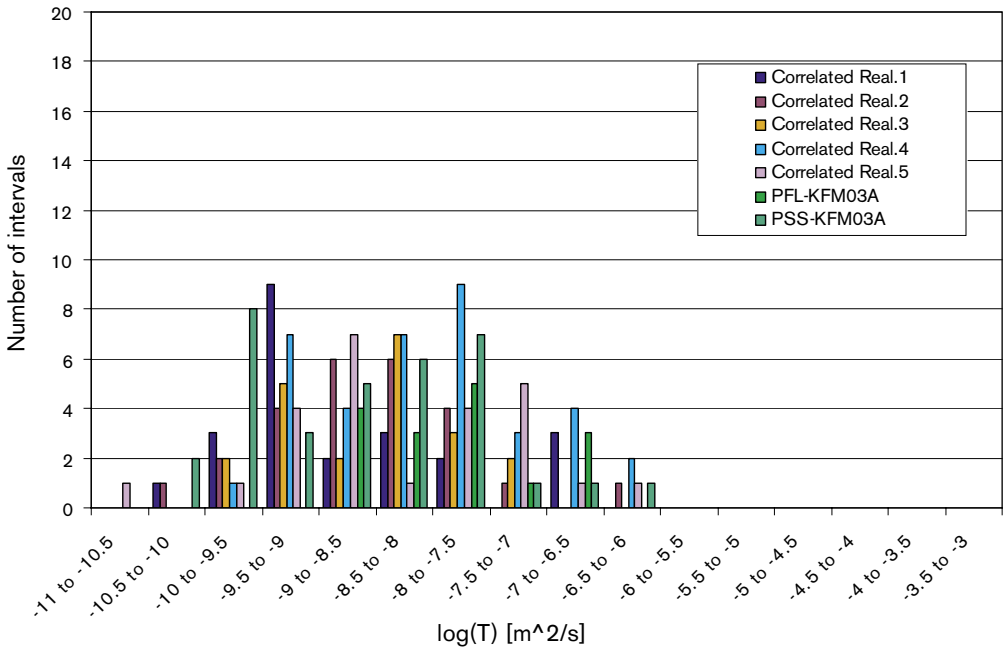

Figure 6-1. *Example of calibrated fit between DFN-model and hydraulic data measured in a borehole.*

which solutes are exchanged between the flowing water and the stagnant water in the rock matrix. This fundamentally influences the radionuclide retardation, should nuclides leak, and also influences how other solutes such as salts intrude or are washed out of the network. The pore volume of the water is much larger than that of the flowing fractures and dominates the migration of solutes. The salt distribution observed in the water in the boreholes and that in the rock matrix can be used to further validate the DFN model by comparisons with observations of chemical composition of the water at different locations. Adjustments can be made on for example the depth influence on the density and hydraulic properties of the fractures in the network.

In a regional scale, the DFN models will have to contain many millions to hundreds of millions of individual fractures to cover the entire rock volume to be modelled. In large scale applications, this is not possible to handle with present day computer systems. Instead an ECPM-model is applied, which need to be simplified but in such a way that sufficiently well mimic the properties of the DFN model. This is done by transforming the DFN model properties of a larger rock volume that contains many fractures to an equivalent porous medium block. This can e.g. be a cube with 100 m sides. The properties of ECPM blocks are fitted to results from DFN models covering the same size block. The hydraulic properties, even directional, are then used to model the large region but using much fewer blocks than fractures. Furthermore the blocks are assigned the average FWS expressed as a specific flow wetted surface a_R, (m^2 surface/m^3 of rock). The value could either be taken as the average surface of the DFN covering the same volume or just be assessed separately. This is further discussed in Section 6.6.

An even more simplified representation is to describe the rock as a porous medium with constant properties over large volumes. This concept is applied in the Forsmark site report /Hartley et al. 2005a, **Site descriptive report, Forsmark**/ and is there called the *CPM-model*. The hydraulic conductivity of the CPM-model is obtained by averaging the hydraulic conductivities obtained from the multi-packer injection test data for 100 m long testing intervals, using the Pipe String System (PSS) testing equipment. This approach will not directly provide a value of the flow wetted surface per volume of rock a_R. Instead it must be assessed from other information, such as the frequency of flowing fractures along boreholes. This is further discussed in Section 6.6.

The Excavated Damaged Zone

With the adopted modelling approach, also the effect of the Excavation Damaged Zone (EDZ) needs to be included in this description as a (potential) change in the DFN properties close to the tunnel and not as a specific input to the near-field migration codes – as was the case in SR 97 /SKB 1999ab/. The EDZ is defined as "*the part of the rock mass closest to the underground opening that has suffered irreversible deformation where shearing of existing fractures as well as propagation and/or development of new fractures has occurred*" /Bäckblom et al. 2004/, and in Safety assessment, the concern is on the *remaining impact*, i.e. after resaturation, on the hydraulic properties (see above) from the tunnelling. The EDZ basically originates from:

- excavation damage (i.e. from the blasting or from a Tunnel Boring Machine, TBM, if this is used) and
- the changes of the stress field and associated fracture dilation effects resulting from the changed stress boundary conditions compared to the undisturbed situation.

The hydraulic modelling will also require initial and boundary conditions. These are, however, not discussed in the Data report, but in the assessment and modelling reports.

Furthermore, and as will be discussed below, the hydraulic properties are in principle stress dependent. However, assessing the consequences of future stress changes lies outside the scope of the Data report. These effects will be discussed in the **Main report**, being part of the assessment of future evolution.

6.5.2 Sensitivity to assessment results

Groundwater flow directly affects near-field release and far-field retention. The latter is essentially proportional to the groundwater flow. SR 97 /SKB 1999ab/ as well as subsequent sensitivity studies /Hedin 2002/ demonstrate that transport resistance in particular has a large impact on retention and thus on resulting risk and dose – in case there is a release.

In the Forsmark site description /**Site descriptive report, Forsmark**/ several different variant cases were analysed with respect to groundwater flow paths from a repository. The analyses were performed in a regional scale. It was found that many of the variants considered had a relatively small effect on safety assessment performance measures and exit locations. However, some cases were highlighted as ones that should be retained in SR-Can either because they suggested sensitivity in the results or that they were of sufficient interest that they needed to be demonstrated in the safety assessment. The parameter that proved to have a clear effect on resulting flow paths were the transmissivity/length distribution. Among the other cases of interest are the variant Geo-DFN (using a different fracture length distribution) and the Alternative Case (AC) geological model.

Some variants of the regional flow model were analysed in Laxemar /Hartley et al. 2006b, SKB 2006k/. Also these analyses show that the flow in the repository region is quite insensitive to the regional groundwater flow. Due to the topographic elevation, most of the Laxemar release-area is beneath a recharge area. The discharge areas are located close to the shoreline and in a few valleys onshore. Particle tracks show that most released particles exit inside, or very close to, the local scale model area, including the two release areas. The exit locations are located close to the shoreline and in the valleys with lower topographic elevation in the area.

The overall hydraulic conductivity also affects the impacts of the open repository. A low conductivity implies low inflows, but may also imply relatively longer resaturation times.

The importance of the EDZ, being limited to a portion of rock around the tunnel, is less pronounced. It would only have an impact if it results in a continuous flowing pathway allowing for more effective migration from the deposition hole to highly flowing fractures. Minor changes of transmissivity of individual fractures are not likely to have any impact at all.

6.5.3 Source of information

Initial hydraulic properties of deformation zones and remaining rock mass

Data for the initial geometry and hydraulic properties of deformation zones and remaining rock mass of the bedrock are provided from the applicable Site descriptive models as described in the corresponding Site descriptive reports /Hartley et al. 2005a and the **Site descriptive report, Forsmark**/ for Forsmark and /Hartley et al. 2006b and **Site descriptive report, Laxemar**/ for Laxemar using procedures already outlined in subsection 6.5.1 of this present report. The hydraulics properties are assessed in Chapter 8 in the reports mentioned above.

Impact from the EDZ

The possibility that the damage done to the rock during excavation will result in zones of increased axial permeability has long been considered. The question has been addressed in topical overviews, e.g. /Winberg 1991/ and more recently /Tsang et al. 2005 / as well as in various conceptual studies /Pusch 1990, Pusch and Stanfors 1992/. The ZEDEX experiment conducted at the Äspö HRL was specifically designed to compare drill and blast damage with damage found in a nearby and parallel tunnel excavated with a tunnel boring machine /Emsley et al. 1997/. For the safety analysis, the issue is to estimate the dimensions of the EDZ and assign it with relevant hydraulic properties. More recently, SKB has conducted EDZ studies in connection to the excavation of the TASQ tunnel at the Äspö HRL /Olsson et al. 2004/.

SR-Can hydraulic analyses

The hydraulic data, including the EDZ, have subsequently been addressed in hydraulic analyses, /Hartley et al. 2006a/ for Forsmark and /Hartley et al. 2006b/ for Laxemar, designed for Safety assessment needs. These analyses constitute the main part of the groundwater flow calculations conducted within the framework of SR-Can. The sections below partly forms the rationale for the analyses undertaken.

6.5.4 Conditions for which data are supplied

Data for the initial geometry and hydraulic properties of deformation zones and remaining rock mass of the bedrock provided in the Site descriptive models concern the situation as it appears today. Changes in rock mechanics or chemistry may alter these properties but the impacts are generally small apart from possibly the following conditions:

- impacts from construction of the repository and its operation (the EDZ and its evolution up to closure),
- impacts from the thermal load,
- impacts from major future mechanical loads such as earthquakes and glaciations.

However, only the impact of the EDZ is assessed here. The other impacts are part of the SR-Can scenario analysis and are to be analysed in the **Main report**.

6.5.5 Conceptual uncertainties

Input from the Site descriptive model report(s)

The process groundwater flow is well understood as noted in Section 3.1 of the **Geosphere process report**. The conceptual hydrogeological model of the rock, outlined in Section 8.3 of the Site descriptive model reports, is that the flow is confined to the connected fractures and deformation zones, whereas the rock matrix is essentially impervious to fluid flow.

Uncertainty arises due to uncertainties in the geometry and connectivity of the network of fractures and deformation zones and due to uncertainty in the spatial distribution of the hydraulic properties of these features. For these reasons various alternative descriptions are suggested and tested in the site descriptive modelling – generally these include (see Table 12-1 of the **Site descriptive reports**):

- Alternative geometry of the deformation zones
- Alternative property distribution in the deformation zones
- Alternative DFN representations in different sub domains of the site
- Alternative hydrogeological properties of the DFN including different assumptions on size transmissivity relations and channelling inside fractures

The impact from varying salinity and temperature (buoyancy and viscosity effects) are well understood and can easily be modelled. However, sometimes the impact of these processes is neglected for simplicity.

- While the basic conceptual model of flow being confined to the fracture and deformation zone network is unchallenged, there are various ways of representing this in a computer model. As already discussed in subsection 6.5.1, SR-Can adopts a modelling methodology that maintains the three alternative model concepts (DFN, ECPM, and CPM) that were developed in the site modelling. However, for practical reasons the pure DFN representation is confined to the model volumes close to the repository. These volumes are then surrounded either by a CPM or ECPM representation further out.

While all these representations should produce the same overall groundwater flow, they could possibly differ a lot in how this flow would be distributed in the rock mass and how much fracture surface the water will contact.

Input from assessing the EDZ impact

As further discussed in the **Geosphere process report**, the stress changes caused by the excavation technique and the stress changes resulting from the removal of the rock itself may cause fracturing of the intact rock, and deformation (movement) of the existing fractures. These alterations may affect the hydraulic properties of the rock in the affected zone, especially if new paths are formed. Due to the complex geometries involved, the situation can only partly be assessed using modelling. Field experiments are needed to substantiate general claims.

Judgement by the SR-Can team

As also stated in the **Geosphere process report** there are essentially no conceptual uncertainties on the process level regarding the hydraulic properties. Uncertainty arises due to uncertainties in the geometry and connectivity of the network of fractures and deformation zones and due to uncertainty in the spatial distribution of the hydraulic properties of these features. These uncertainties need to be explored by formulating alternative hypotheses as being made within the Site descriptive modelling /**Site descriptive report, Forsmark and Laxemar**/. The sufficiency of the assessed alternatives, with respect to the purposes of SR-Can, will be discussed when assessing the quantification of the uncertainty, i.e. in subsection 6.5.8.

While the basic conceptual model of flow being confined to the fracture and deformation zone network is unchallenged, the various ways of representing this in a computer model, i.e. by the ECPM, CPM, nested ECPM/DFN or nested CPM/DFN descriptions, would result in different resolution of the flow field. Basically, the nested DFN approaches should be closest to the "real" system, but the practical limitations of handling discrete fracture models, as well as the data needs, warrant exploration of the importance of the assessment model. The alternatives analysed by /Hartley et al. 2006a/ are judged to sufficiently illustrate this aspect. However, although there are major uncertainties in the different models and modelling approaches, robustness will be increased (possibly achieved) by calibrations of all models to PSS and PFL measurements. Furthermore, the *T*-distribution and conductive fracture frequencies can give 1st order estimates of *F*-factors for DFN modelling and a_R for ECPM and CPM modelling as shown in Section 6.6.

6.5.6 Data uncertainty, spatial and temporal variation

Hydraulic properties of the rock – expert input

As further explained in Chapter 8 of the **Site descriptive reports** the conceptual hydrogeological model of the site implies that only fractures and fracture zones could conduct water, although the rock matrix may be connected to the flow system by diffusion. In the model, the conductive features are divided between Hydraulic Conductor Domains (HCD), which essentially coincide with the deformation zones in the geological model, and the Hydraulic Rock Domains (HRDs) representing the rock mass between the HCDs. The hydraulic properties of the HRDs are modelled as discrete fracture network models, with the geometry taken from the geological discrete fracture network model, but with added hydraulic properties. The models are calibrated against existing hydrogeological borehole data, although it is clear that different conceptual models could be calibrated to the same data.

Data uncertainties of the HCD in Forsmark

The HCDs in the hydrogeological model are based on the regional-scale deformation zones of the Forsmark regional-scale structural model /Chapter 5 of **Site descriptive report, Forsmark**/. A majority (27) of the 44 deformation zones are hydraulically tested and attributed transmissivity values that are regarded as high confidence information. The estimation of the hydraulic

thicknesses of the deformation zones is based on the interpretation of the geological thicknesses of the base case model deformation zones.

A significant observation is made by correlating deformation zone transmissivity to deformation zone dip and depth, see Figure 6-2. The correlation analysis indicates that gently dipping deformation zones generally have greater transmissivities than steeply ones at comparative depths and both gently and steeply dipping deformation zones have much greater transmissivities close to ground surface than at depth.

Although data plotted in Figure 6-2 suggests simple depth dependent trends, it also shows quite a large variation between different deformation zones. Apart from zones being different, this could also be an indication of the spatial variability within individual zones, although estimates of the latter would require multiple measurements in the same zone.

The uncertainty in geometry and connectivity of deformation zones motivated the formulation of alternative deformation zone models, see the Site description Forsmark /Chapter 5 of **Site descriptive report, Forsmark**/. Three alternative deformation zone geometries are suggested as follows:

- Base Case (BC): containing only high confidence deformation zones.
- Variant Case (VC): is similar to the BC model except a few large sub-horizontal zones are extended beyond the Eckarfjärden deformation zone.
- Alternative Case (AC): contains the deformation zones included in the BC model with the addition of many regional-scale lineaments, based on lineament and comparison studies, which are potential hydraulic conductors but of lower confidence.

These uncertainties also imply uncertainty as to how these modelled structures relate to structures of hydrogeological significance. Apart from the uncertainty in the geological model, this uncertainty is due to lack of hydrogeological data testing whether there is a hydraulic contact between the rock inside the candidate area and rock outside, e.g. through gently dipping deformation zones.

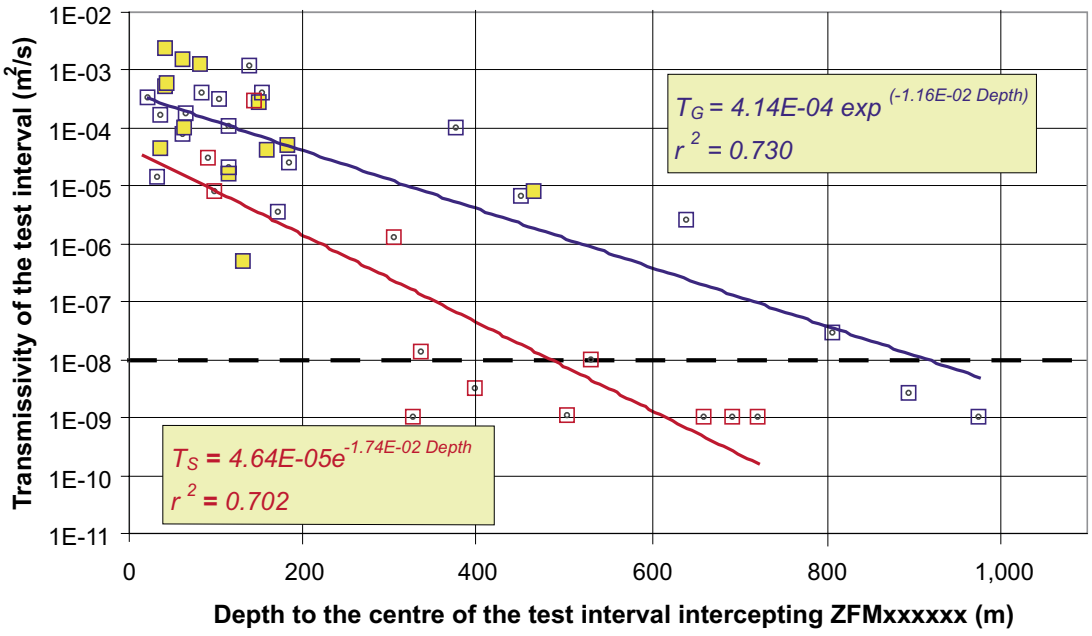

Figure 6-2. *Modelled (lines) and observed (squares) depth dependence of transmissivity in deformation zones. Red squares indicate steeply dipping deformation zones and blue gently dipping. Blue squares with a yellow infilling refer to the hydraulic test interpretations associated with the deformation zone ZFMNE00A2.*

The transmissivity distribution and its spatial variability in deformation zones outside the candidate area are also uncertain, since there are few, if any, hydraulic measurements in these zones. This uncertainty could potentially affect the estimated strength of the hydraulic contact between the rock inside the candidate area and rock outside.

Partly, the impact of these uncertainties are already explored as a part of the site modelling, by analysing the sensitivity to the transmissivity distribution in the regional groundwater flow modelling and by testing two alternative models for deformation zones in the regional domain /Chapter 8 of **Site descriptive report, Forsmark**/. It is there concluded that the flow inside the target area is essentially insensitive to the regional uncertainties treated, whereas the spatial variability of the transmissivity for the zones inside the target area would have an impact on the detailed flow in this area. This spatial variability of the HCDs inside the target area would eventually need to be handled.

Data uncertainties of the HRD in Forsmark

The hydraulic properties of the rock mass are described by means of a hydraulic discrete fracture network model (hydrogeology DFN). The analyses were made by two different modelling teams /Follin et al. 2005/ and /Hartley et al. 2005a/. Both teams reached very similar conclusion, although their resulting description show slight differences due to the uncertainty and ambiguity of interpreting the data. As further discussed in Chapter 8 and Chapter 12 of the Forsmark site descriptive model /**Site descriptive report, Forsmark**/ there are several related uncertainties in the hydraulic properties of the rock mass between the modelled deformation zones. This concerns *division into volumes* of different hydraulic properties, the *connectivity* of the discrete fracture network (DFN), the *transmissivity* distribution in these fractures, *anisotropy,* and the *spatial variability in the fractures*.

As discussed in Chapter 8 of the **Site descriptive report, Forsmark**, the hydraulic data from the boreholes strongly suggest that the rock mass, inside rock domain RFM029, should be divided into volumes of different hydraulic properties, see Figure 6-3. Noteworthy is the volume below deformation zone ZFMNE00A2 below about the –360 m level (denoted Volume *D* or *G* by the different modelling teams), where there are essentially no measured hydraulic responses in the data. However, since there are few boreholes, the exact division of the different volumes remains to be defined. In particular, it should be noted that although it is likely that most of the repository panels according to the layout would lie within model volume *D* (or *G*) it cannot be excluded that some parts will be in the more permeable volume *B* (or *F*).

Table 6-1 presents the basic fracture frequency data outside the deformation zones used in the analysis carried out by /Follin et al. 2005/. N_{CAL} is the number of potentially flowing Open and Partly Open fractures in each borehole (Volume) to be matched in the modelling process and N_{PFL} is the number of flow anomalies in the connected network of flowing features above the lower measurement limit of the Posiva Flow Log method (PFL). T_{PFLmin} is the smallest transmissivity value measured and may be considered as an estimate of the lower measurement limit T_{lim}. As noted in the Site description for Forsmark /Chapter 8 of **Site descriptive report, Forsmark**/, the lower measurement limit of the PFL method is not a threshold with a fixed magnitude but varies in space depending on the in situ borehole conditions.

The frequency of potentially flowing Open and Partly Open borehole fractures P_{10CAL} varies an order of magnitude between Volumes *A–D*. In comparison, the P_{10} value of the geological DFN, 67 fractures per hundred metres, falls between the P_{10CAL} values shown in Table 6-1. Between Volume *C* and Volume *D*, the P_{10PFL} value varies by more than two orders of magnitude. The value of P_{10PFL} in each Volume is at least an order of magnitude lower than the corresponding value of P_{10CAL}, indicating that most fractures identified as “Open” or “Partly Open” are either tight or conducted very little water. This also shows the need to calibrate the hydraulic DFN models against the hydraulic data, as is done, rather than accepting the frequency of “open fractures” as input to this modelling.

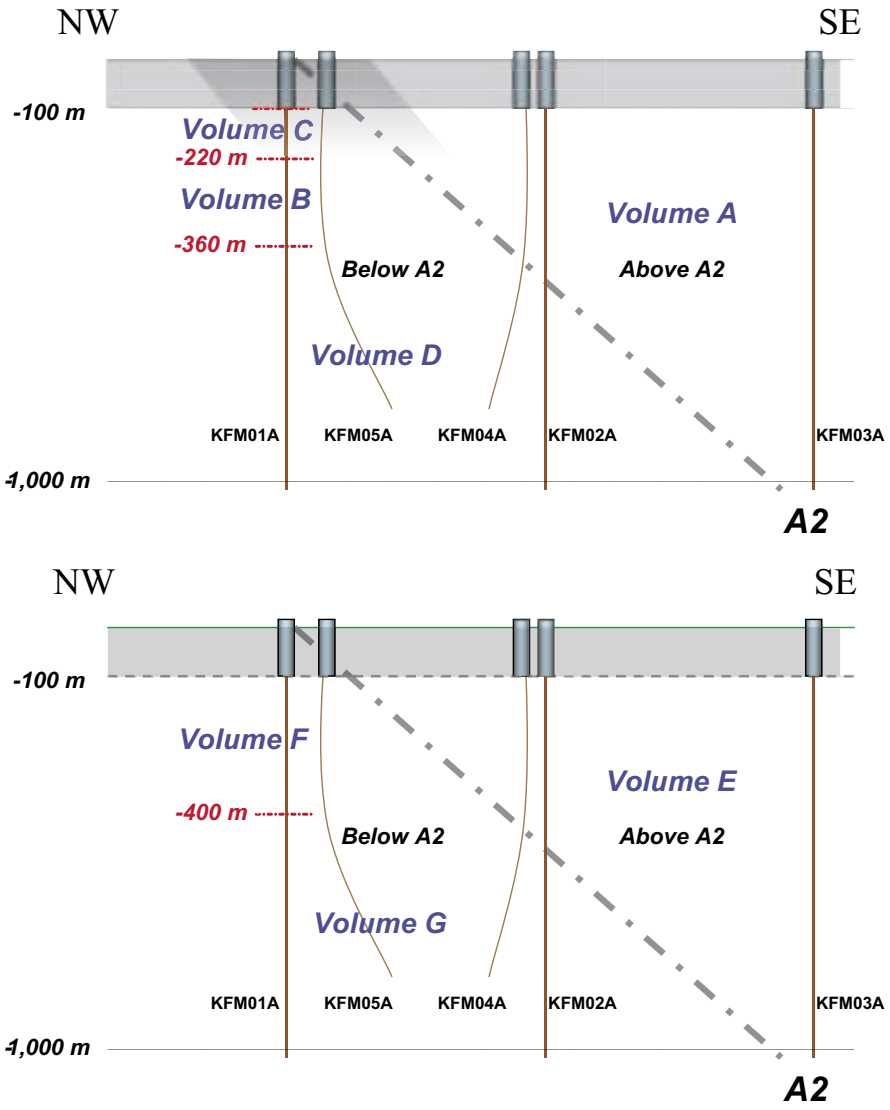

Figure 6-3. *Schematic cross-sections through the tectonic lens illustrating the division of the rock domain RFM029 into smaller volumes by two modelling teams. The upper model was treated by /Follin et al. 2005/ and the lower by /Hartley at al. 2005a/. The difference between the two cross-sections concerns the division of Volume F into volumes B and C mainly. Thus, Volumes A and E may be considered equivalent as may Volumes D and G, respectively. Volume C is the most conductive, whereas Volume D (G) has almost no measurable inflows according to the data available for the Forsmark site descriptive model.*

Table 6-1. Basic hydraulic data measured by the Posiva Flow Log (PFL). Measurements made in sections belonging to HRD's are excludes /Table 8-8 in *Site descriptive report, Forsmark*/. Volume notation refer to /Follin et al. 2005/ but note that Volume *B* is essentially the same as volume F and volume D essentially the same as volume G in /Hartley et al. 2005a/.

Borehole	Volume	Interval (m)	N_{CAL}	P_{10CAL} (/100m)	N_{PFL}	P_{10PFL} (/100 m)	T_{PFLmin} (m^2/s)	T_{PFLmax} (m^2/s)
KFM03A	A	106–994	248	27.9	24	2.7	$1.09 \cdot 10^{-9}$	$3.46 \cdot 10^{-7}$
KFM01A	B	222–363	210	149	11	7.8	$2.71 \cdot 10^{-10}$	$2.22 \cdot 10^{-9}$
KFM01A	C	103–222	304	255	23	19.3	$2.47 \cdot 10^{-10}$	$5.35 \cdot 10^{-8}$
KFM01A	D	367–956	134	22.8	0	< 0.170	$3.62 \cdot 10^{-10}$	$< 3.94 \cdot 10^{-10}$

The hydraulic analysis of the borehole data involves simulations with the DFN models in order to match the flow data measured in the boreholes. However, given the uncertainties in the DFN model, see Section 6.3, and the scarcity of observed transmissive features in the boreholes, the hydraulic DFN analysis should rather be seen as indicative, where various alternative models are explored.

As already discussed, there is an uncertainty in the intensity of fractures in the size range 100–1,000 m. This is an important issue to be resolved by the geologists. This causes uncertainty in the connectivity of the fracture network, which also affects the assignment of transmissivity distributions to the fractures and the resulting block scale hydraulic conductivities. As assessed in subsection 8.4.2 of Site description for Forsmark /**Site descriptive report, Forsmark**/ the different volumes may be modelled as percolating networks of discrete features, however with quite different hydrogeological DFN properties depending on the assumptions of the intensity of larger fractures in the DFN model. In the low percolating networks it is necessary to set the transmissivity higher in order to match the total measured transmissivity in the different boreholes.

Of special interest is volume *D* (or *G*). In this volume there is no recorded transmissivity from the hydraulic tests. Depending on the assumptions made on the fracturing, alternative interpretations are possible ranging from a non-percolating fracture network to a poorly percolating fracture network with transmissivities that are low and below the lower measurement limit of the hydraulic test equipment. In the case of a non-percolating fracture network, the flow and advective transport would essentially only take place in the deterministically modelled deformation zones, possibly with the addition of a very low hydraulic conductivity of the rock matrix itself. These two alternatives are schematically outlined in Figure 6-4.

The main assumption is to fully correlate fracture size and transmissivity, setting $log(T) = b \cdot log(a \cdot r)$, where r is the fracture radius. However, alternative models, with no correlation, $log(T) = N(\mu,\sigma)$, or with some correlation, $log(T) = b \cdot log(a \cdot r) + N(\mu,\sigma)$, are also applied to the data. These alternatives results in quite different block properties and are possibly less realistic, but cannot be excluded at this point. Concerning the three transmissivity models /Hartley et al. 2005a/ concluded that Volume *E* and Volume *F* have essentially the same properties. The best match was obtained for the correlated transmissivity model but further fits were produced for the uncorrelated and semi-correlated transmissivity models as well. Table A-39 summarises the parameter values suggested for the uncorrelated, correlated and semi-correlated transmissivity models in Volumes *E*–*G*. From the table it can be noted that the correlated model suggest that a 100 m size fracture has about the same transmissivity (i.e. about 10^{-7} m^2/s) in all volumes, but the intensity of such fractures is more than a factor of 10 less in volume *G*,

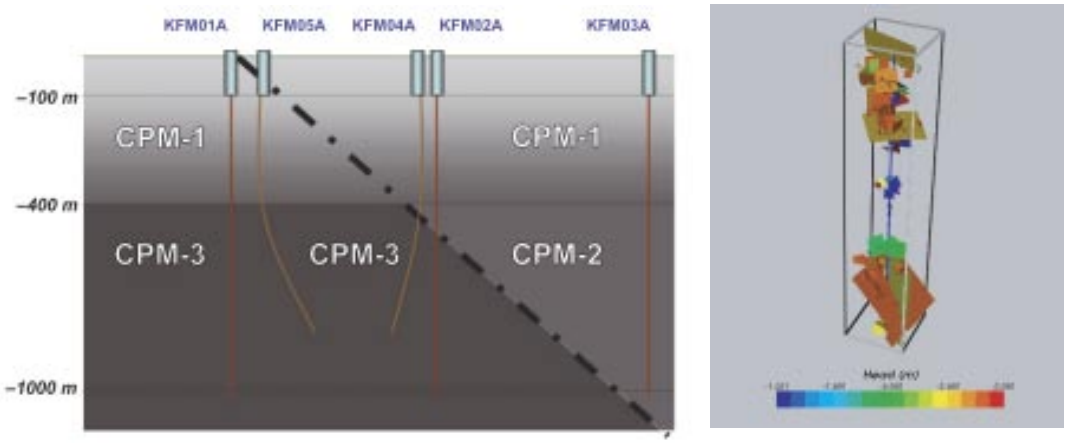

Figure 6-4. *There are different means of describing the low permeability of the deeper rock volumes ranging from a low permeability porous medium CPM (left) to a poorly connected fracture network (right). Both these representations could be made to match the hydraulic data.*

see Table 6-1. For the uncorrelated case the median fracture transmissivity is higher, $3 \cdot 10^{-7}$ m^2/s, but the majority of fractures are much shorter than 100 m.

In apparent contrast to Table A-39, Follin et al. /Follin et al. 2005/ suggested a much lower transmissivity of the fractures in Volume *B* and in Volume D. In their analysis a 100 m fracture in volume *B* and Volume *D* would have a transmissivity in the range 10^{-9} m^2/s to 10^{-8} m^2/s (see Figure 8-41 of the Forsmark Site description /**Site descriptive report, Forsmark**/). This is most likely due to the fact that volume *B* does not include the upper part (Volume *C*) which is much more conductive.

In the Site description for Forsmark it is also concluded that the hydrogeological DFN analyses of Volumes *D* and *G* are especially uncertain, as there are no flow anomalies in KFM01A. Follin et al. /Follin et al. 2005/ concluded that Volume *D* becomes non-connected or very poorly connected depending on the used DFN reference size parameter $X_{r(l)}$, however, with all flow below the lower measurement limit. This finding goes well with the sensitivity test conducted by /Hartley et al. 2005a/, which suggests that this HRD is close to the percolation threshold.

Whether fractures of different orientations have different transmissivity distributions (i.e. anisotropy) has been analysed by both teams. They only suggest moderate anisotropy, but since there are few data this issue is still uncertain.

Finally, there is likely to be a spatial variability of the transmissivity in the plane of each fracture. This will cause channelling and could also have an impact on the connectivity analysis. This uncertainty is not resolved in the site modelling, but is left for further analysis within safety assessment.

Overall, the uncertainty in the hydraulic properties of the rock mass in the target area is at least partly quantified, and especially by considering alternative models of fracture network connectivity, and fracture transmissivity distribution. The uncertainty in the different volumes can at this point be represented by considering a range of properties for each of the different volumes.

Data uncertainties of the HCD in Laxemar

The deterministic deformation zones in the geological model of Laxemar /**Site descriptive report**, **Laxemar**/, are all assumed to be HCDs in the hydrogeological model. Hydraulic tests confirm that the deformation zones usually are more conductive than the surrounding rock. As further discussed in the **Site descriptive report, Laxemar**, the measured hydraulic conductivity of the deformation zones, assessed by dividing the zone transmissivity by the zone thickness, is about an order of magnitude larger than the hydraulic conductivity of the rock mass where test sections intersected by deformations zones are excluded. However, some HCDs in the current model may have low transmissivity (and hydraulic conductivity). Furthermore, many of the deformation zones are not tested hydraulically.

To estimate the properties of the HCDs in the hydrogeological model, generally results from transient pumping or injection tests have been used. If there is a hydraulic test section in a borehole covering the entire length of what the responsible geologist considers to be the zone, the corresponding test results have been used, instead of summing up the transmissivities for shorter test sections over this zone. With this description, the deformation zone is described as a single feature, whereas in reality it is made up of many small fractures contributing to a complex flow path pattern.

Table 8-9 of the **Site descriptive report, Laxemar** presents the transmissivity data evaluated for the HCDs. Such test data exists for about two thirds of the high confidence zones and for a few of the medium confidence zones in the local model volume, but there are few instances with more than one measurement from the same zone. HCDs with no hydraulic tests have been assigned the geometric mean value ($1.2 \cdot 10^{-5}$ m^2/s) for all HCDs and with an assumed geological thickness of 20 m. It can be observed that this mean value of T is higher than that measured at the intercepts of many of the high confidence deformation zones. Furthermore, many of the low

confidence zones in the local model area have shorter trace length on the surface compared to the high and medium confidence deformation zones. Consequently, it not unlikely that many of the low confidence zones would be less transmissive than the high and medium confidence deformation zones, i.e. that the current model grossly exaggerates the transmissivity of many of the deformation zones.

The data also possibly suggest a decreasing transmissivity with depth as indicated by Figure 6-5. Different depth trend curves are fitted to the data. As can be seen in the figure the confidence limits for mean $Log_{10}(T)$ is wide for all thee depth intervals, demonstrating that the inferred depth trend of the transmissivity is very uncertain due to sparse data for the deformation zones.

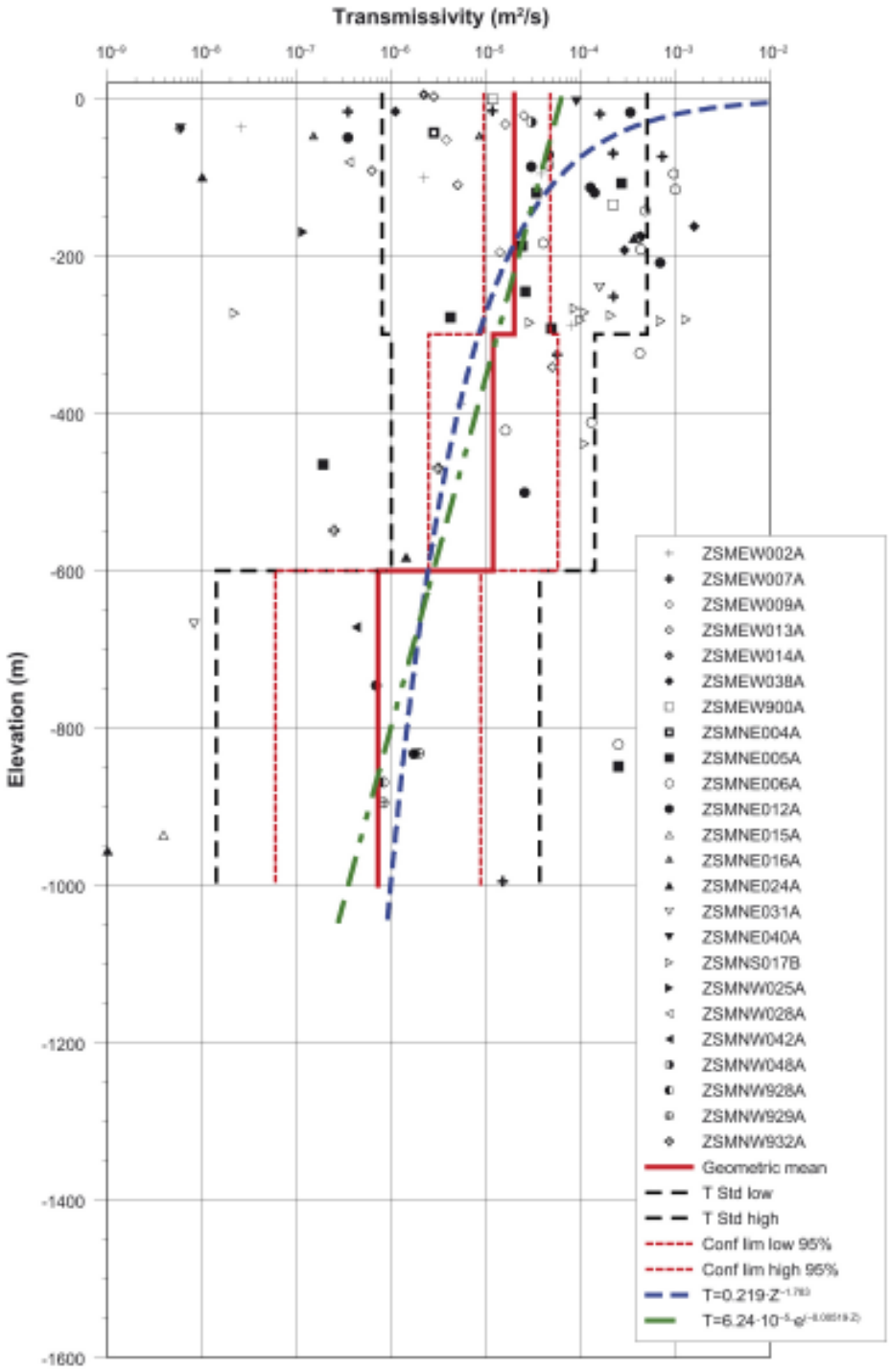

Figure 6-5. *Possible depth trend of the transmissivity in HCDs /Site descriptive report, Laxemar/.*

Furthermore, there are few measurements from the same deformation zones, so the differences in *T*-values could be coincidental. Apart from zones being different, this could also be an indication of the spatial variability within individual zones, although estimates of the latter would require multiple measurements in the same zone.

The geometry and connectivity of the deformation zones is uncertain. There are only few interference tests in the Laxemar subarea. In principle, this uncertainty affects transport paths and the integrated evaluation in conjunction with hydrogeochemistry, but the actual importance is tested by analysing cases with and without the low confidence zones.

Spatial variability of transmissivity in the deformation zones is uncertain. Only a few deformation zones have been subjected to more than one flow test. Nevertheless, the combined data from many zones suggest a depth trend, in which transmissivity decreases with depth. The overall depth trend is used as the basic model. The spatial variability is estimated based on the overall spatial variability in data as measured in different zones, but the main case analysed in the flow simulations assumes no spatial variability apart from the depth trend. Alternative cases with different transmissivity distributions are also formulated.

Data uncertainties of the HRD in Laxemar

In assessing the hydraulic properties of the rock mass, the data were first explored and used to develop an overall conceptual model of the distribution of hydraulic properties in the subarea. As discussed in Chapter 8 of the **Site descriptive report, Laxemar**, the hydraulic data from the boreholes suggest that the rock mass at the Laxemar subarea has a depth dependent conductivity, but the interpretation is uncertain.

Table 6-2 presents some basic fracture frequency data outside the deformation zones. N_{PFL} is the number of flow anomalies in the connected network of flowing features above the lower measurement limit of the Posiva Flow Log method (PFL) and P_{10PFL} (m^{-1}) is the frequency of such features along the borehole section. The table also provides the mean and standard deviation of $log_{10}(T)$ (m^2/s) for the different borehole sections. As noted in the Laxemar site description /**Site descriptive report**, **Laxemar**/ in Chapter 8, the lower measurement limit of the PFL method is not a threshold with a fixed magnitude but varies in space, in and between boreholes, depending on the in situ borehole conditions. However, P_{10PFL} may still be regarded as a good measure of the frequency of fractures with a transmissivity of 10^{-9} m^2/s or larger.

As can be seen from the table, P_{10PFL} decreases by about a factor of 6 below –300, in KLX02, but only by a factor of 2 to 3 in KLX03 and by a factor of 2 in KLX04. There is less change in the mean transmissivity with depth, but there is a factor of about 3 lower mean transmissivity in KLX03 than in KLX04. These data indicate that the hydraulic characteristics may depend on depth and on rock domain, but also illustrate the strong spatial variation of the hydraulic properties. There is standard deviation of about one order of magnitude. The noted difference between the boreholes may not be valid.

Figure 6-6 shows results of 100 m injection test data from the Laxemar subarea, where data representing the deterministically interpreted deformation zones are excluded. Two depth trend functions, a power law and an exponential model, were fitted to the mean values. There seem to be a slight decrease in hydraulic conductivity with depth, but one should also observe that there are rather few observations in the elevation intervals 100 m to 300 m in the Laxemar subarea, and some of the data may be directly or indirectly affected by the proximity of deformation zones. In any case, it seems that there is a zone close to the surface with higher hydraulic conductivity. This zone of increased hydraulic conductivity reaches down to 300 m to 400 m depth in both KLX02 and KLX04, but may be shallower, 100 m to 300 m, in other boreholes.

Table 6-2. Basic hydraulic data measured by the Posiva Flow Log (PFL) at the Laxemar subarea. Measurements made in sections belonging to HRDs are excluded /Based on Table 8-7 SKB 2006k/.

Borehole	Upper elevation limit (m)	Lower elevation limit (m)	N_{PFL}	P_{10PFL} (m^{-1})	Lower meas. limit Log_{10} T (m^2/s)	Mean $Log_{10}(T)$ (m^2/s)	Std $Log_{10}(T)$ (m^2/s)
KLX02	–186	–300	32	0.31	–10 to –8.3	–7.23	0.95
	–300	–700	21	0.052	–10 to –8.3	–7.93	0.75
	–700	–1,372	21	0.043	–10 to –8.3	–7.77	0.89
KLX03	–79	–300	25	0.11	–9.8 to –8.2	–7.81	1.05
	–300	–700	15	0.038	–9.8 to–8.2	–7.87	0.70
	–700	–944	3	0.017	–9.8 to –8.2	–7.44	0.94
KLX04	–75	–300	44	0.20	–9.6 to –8.7	–7.01	0.85
	–300	–700	51	0.13	–9.6 to –8.7	–7.34	0.77
	–700	–957	1	0.0063	–9.6 to –8.7	–	–

There is also a potential difference in mean hydraulic conductivity between rock types. granite, medium- to coarse-grained and granite and fine grained granite are the most permeable. Ävrö granite has a lower hydraulic conductivity. The lowest hydraulic conductivity is found in the more basic rock types. For this reason the hydraulic description distinguishes HRDs with different properties. Within the Laxemar subarea these HRDs relate to the geological Rock Domains in the following way:

- HRD(A) : Rock domains RSMA and RSMBA within the Laxemar subarea.
- HRD(D,E,M) : Rock domains RSMD, RSME and RSMM within the Laxemar subarea.

Additional HRDs are suggested outside the Laxemar subarea.

Using this overall description, the hydraulic properties of the rock mass are described by means of a hydraulic discrete fracture network model (Hydro-DFN). The analyses were mainly made by /Hartley et al. 2006b/. In addition /Follin et al. 2006/ studied the key assumptions in the methodology in the underlying geological DFN model and addressed how these propagate into the hydraulic DFN modelling. The following boreholes have defined the properties of the HRDs:

- KLX04: HRD(A).
- KLX03: HRD(D,E,M).

The hydraulic analysis of the borehole data involved simulations with the DFN models in order to match the flow data measured in the boreholes. The main assumption was to fully correlate fracture size and transmissivity, setting $log(T) = b \cdot log(a \cdot r)$, where r is the fracture radius. However, alternative models, with no correlation, $log(T) = N(\mu,\sigma)$*, or with some correlation, $log(T) = b \cdot log(a \cdot r) + N(\mu,\sigma)$, are also applied to the data. These alternatives results in quite different block properties and cannot be excluded at this time. The resulting hydraulic DFN models for defined HRDs of the Laxemar subarea are illustrated in Figure 6-7.

A variant of the Hydro DFN base case, *Hydro-DFN regional case*, was made during the calibration of the regional model, cf Section 8.5 of the /**Site descriptive report, Laxemar**/. For the regional modelling reference case, the underlying hydraulic DFN model was initially based on the Hydro DFN base case with a semi-correlated T model. However, during the regional modelling studies, modifications were made to the hydraulic DFN prescription to achieve a better calibration against borehole hydrogeochemistry. The use of homogeneous

* $N(\mu,\sigma)$ is the normal distribution with mean μ and standard deviation σ.

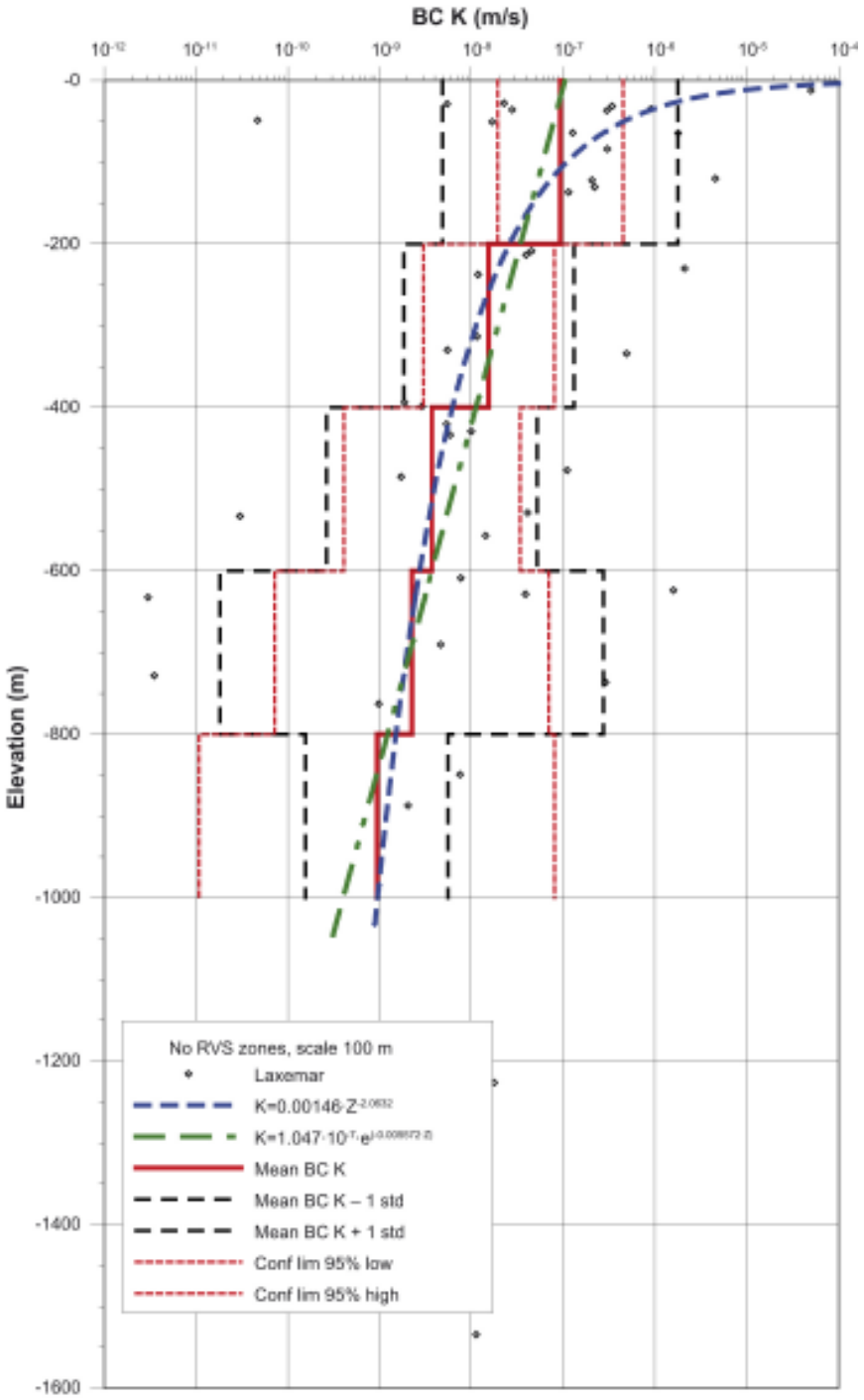

Figure 6-6. *Depth trend of the hydraulic conductivity in HRDs. Test scale 100 m. Data, statistics and depth trends based on data from the Laxemar subarea alone. Data representing deterministically interpreted deformation zones are excluded. Based on Boreholes HLX01–09, –32, KLX01–KLX06 (in KLX05 and KLX06, only data from WLP measurements are included). BC = Best choice value /Figure 8-21, SKB 2006k/.*

models for hydraulic conductivity using depth dependency trends based on the PSS data all resulted in a poor match against the hydrogeochemical data. For such models, a calibration could only be achieved using a hydraulic conductivity in the deep rock more than an order of magnitude less than measured values. Using the Hydro-DFN base case gave interval conductivities consistent with the hydraulic injection test data (PSS) 100 m interval data, and when anisotropy was introduced by reducing the transmissivity in the subvertical fracture sets *Set_A* and *Set_B*, a reasonable match with hydrogeochemistry was obtained.

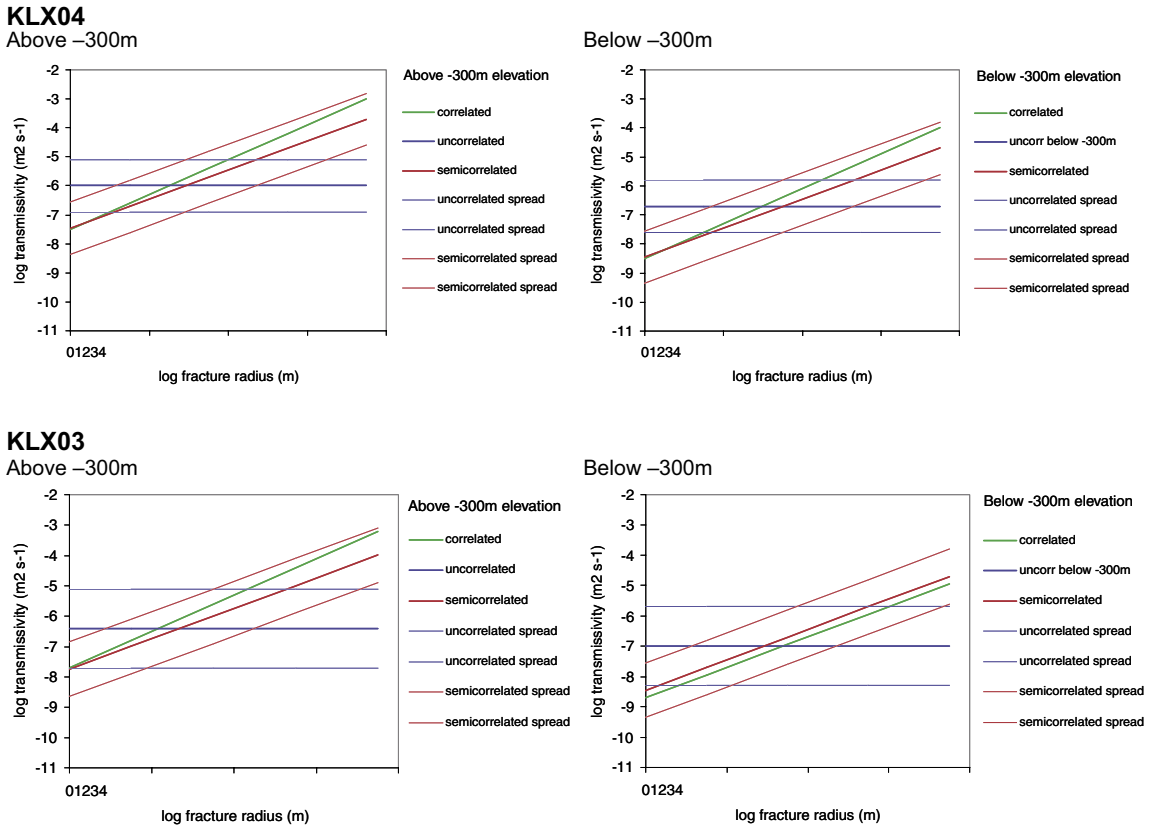

Figure 6-7. *Transmissivity model relationships for KLX04 and KLX03, above and below –300 m.*

Some important conclusions from the results of the hydraulic DFN modelling are given in the **Site descriptive report, Laxemar**:

- At least in borehole KLX04 there are a number of high transmissivity sections and high flow rates that cannot be described by the model. This can to some extent be related to the definition of what parts of the borehole (KLX04) should be considered as being in a deformation zone (where the transmissivities are summed up to represent one feature). Possibly some flow anomalies near the defined deformation zones should be considered to be part of those deformation zones. However, this may not be the sole explanation, and needs be the subject of continued analysis in future modelling.
- If the input fracture intensity (P_{32}) is adjusted, all three transmissivity models parameter settings can be fitted such that the model simulations generate flow rate distributions similar to the ones measured. However, the semi-correlated model seems to provide somewhat better match than the other transmissivity models.
- The noted variability in transmissivity between boreholes and the relatively few boreholes actually investigated, implies uncertainty when extrapolating the statistics of a single borehole to larger volume (rock domain). This needs to be better explored.
- The PFL data can be correlated to individual fractures. These data give some indication that the subvertical sets *Set_A* and *Set_B* have a 0.5 to 1.0 orders of magnitude lower transmissivity than *Set_C* and *Set_d*. This concept was also successfully tried in the *Hydro DFN regional case*. However, at the moment these results are only to be regarded as indicative, being based on analysis of KLX04 data alone. Also, it should be understood that the importance of anisotropy may have been underestimated in opting for a simplified hydraulic DFN model with the same transmissivity relationships for all fracture sets.

Input from the EDZ assessment

The ZEDEX experiment /Emsley et al. 1997/ was conducted particularly to examine the integrated effects of disturbances caused by stress redistribution and direct excavation damage, while the currently used EDZ definition regards only direct damage. (As already noted, assessing the consequences of future stress changes lies outside the scope of the Data report. These effects will be discussed in the **Main report**, being part of the assessment of future evolution.) Two nearby and parallel tunnels were used for the study. One of the tunnels (Drill and Blast, D&B) was excavated with different drill and blast techniques, while the other one (TBM) was excavated mechanically with a tunnel boring machine. As expected the depth of the damage was found to be much less in the TBM tunnel (about 0.03 m) than in the D&B tunnel (0.3 m – 0.8 m) /Emsley et al. 1997/. Also the nature of the damage was different in the two tunnels. In the TBM tunnel there was modest induced micro-fracturing, while there was evidence of induced macro-cracks in the D&B tunnel.

The evaluation of the ZEDEX experiment did not include direct measurements of the axial conductivity of the damaged zone, meaning that there is still a lack of knowledge when it comes to the question of assigning relevant values in hydro models to be used in the safety analysis. Local permeability increases were found, but these could not be shown to represent values relevant along a continuous zone of connected fractures. However, it may also be noted that the ZEDEX experiment was conducted with tunnels going in a specific direction relative to the maximum principal stress and hence the information derived is potentially orientationally specific.

The TASQ tunnel at Äspö HRL was excavated specifically to accommodate the Äspö Pillar Stability Experiment. This experiment required well-defined conditions in the floor region with a minimum of excavation damage. The D&B technique used for the excavation included a number of procedures to limit the extent of the EDZ /Olsson et al. 2004/. Excavation with top and bench separately, for instance, meant that smaller specific charges could be used for the floor contour holes. The extent of the EDZ was studied by sawing several slots in the tunnel wall, see Figure 6-8.

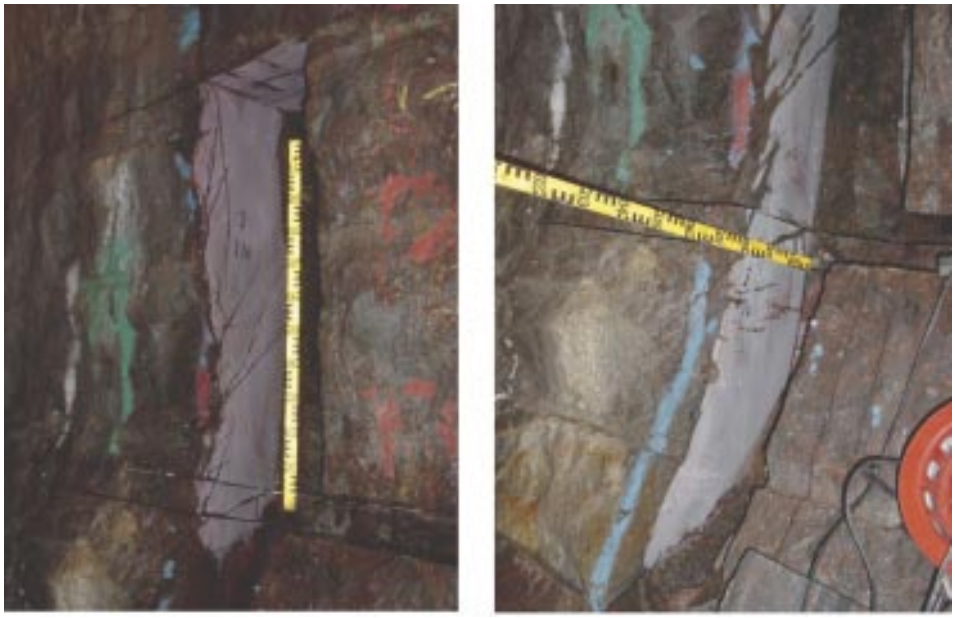

Figure 6-8. *Example of EDZ as observed by sawing a slot in the tunnel wall after excavating the TASQ tunnel at the Äspö HRL.*

Several conclusions were drawn including:

- To excavate with top heading and bench gives significantly lower damage in the floor compared to ZEDEX experiences, even less than in the roof and walls. However, further development in blast design is needed to enable similar results in terms of a small EDZ in the floor without excavation of a separate bench.
- For the "average" tunnel construction, based on current Swedish practice, the observed excavation damage is similar to that observed in the ZEDEX D&B tunnel eight years ago.
- The look-out angle and the distribution of specific charge along each round causes a discontinuous EDZ along the tunnel. It is therefore concluded that the impact of the EDZ on hydraulic conductivity along the tunnel is very small, because it is manageable through D&B design and QA control during excavation.
- The reasons for local significant larger extension of the EDZ are well understood. They are most likely manageable in a systematic QA program during excavation. To implement quality plans in the common organisation for a tunnelling project may require special care and training.

Other rock mechanics impact on the hydraulic properties of the rock are analysed in a special report /Hökmark et al. 2006/. The rock mechanics input to these analyses are discussed in Section 6.4 of this report. The evaluations of the findings lie outside the scope of the Data report. They are assessed directly in the SR-Can Main Scenario.

Judgement by the SR-Can team

The descriptions of data uncertainty and variability as provided in the reports cited above are judged adequate. As mentioned above, the limited number of boreholes and small amounts of data available for Laxemar 1.2 do not firmly allow dividing the volume into hydraulic rock domains with different and depth dependent hydraulic properties. However, new data, which have become available after data freeze Laxemar 1.2, strongly support both the depth dependence and that the rock domains in southern Laxemar, Figure 6-9, have significantly lower hydraulic conductivity than in northern Laxemar, Figure 6-10. Figure 6-11 shows locations of the boreholes and the surface expression of the rock domains. These new data show a higher degree of lithological homogeneity and also distinctly lower hydraulic conductivity in the depth interval 300–700 m, cf new data from boreholes KLX05, KLX10A, KLX11A, and KLX12A in Figure 6-9. It should also be noted that many of the boreholes in northern Laxemar (KLX06, KLX07, and KLX08) are strongly affected by their proximity to the deformation zones EW007A and EW002A. Consequently, it is highly likely that the hydraulic conductivity of the Laxemar area is much lower than indicated by the hydrogeological model derived for Laxemar version 1.2.

The following can also be noted:

- Describing the deformation zones as single features, whereas in reality they are made up of many small fractures contributing to a complex flow path pattern, would result in pessimistically low values of the transport resistance, see Section 6.6, since no single migration path would have the high value represented by the sum of transmissivities of the paths in zone. Using the detailed hydraulic data could result in a more realistic, and less pessimistic, description of the zone, but this approach would arguably be more difficult to defend in light of the limited amount of detailed data from different locations in the same zone.
- There are substantial uncertainties and judgements involved in the hydrogeological DFN-modelling. However, as will be further discussed in Section 6.6, the basic hydraulic data, based on the PFL-log and displayed in Table 6-1 and Table 6-2, can be used to provide more robust estimates of the flow related migration parameters.

- Given the uncertainties of the hydraulic properties of the rock mass in the potential repository volumes of the Laxemar subarea, the hydraulic DFN analysis should be seen as indicative only. More data from the rock mass of the potential repository volume are needed before it is meaningful to more elaborately try to bound the uncertainties and spatial variability of the rock mass hydraulic properties of the Laxemar subarea. Such data will also be acquired during the concluding part of the site investigation at Laxemar. In fact, data obtained after data freeze 1.2 contain much more information from the potential repository volumes. Furthermore, these data show much more favourable hydraulic characteristics than what is presently imbedded in the hydraulic flow models derived from the version 1.2 site description. This means that the current flow models might be unduly biased and they do not fully capture the actual variability of the hydraulic properties. For these reasons, it is only recommended to carry out a limited set of analyses of the Laxemar site in SR-Can. It is not judged meaningful to explore different variants.
- Given the experimental evidence it is reasonable to assume that the EDZ, if it all develops, is limited to a narrow zone (a few tens of cm) close to the tunnel and it would not form a continuous path, unless there were a significant fracture set present sub-parallel to the tunnel axis to which the blast-induced and stress-induced cracks could be connected. Possibilities for more extensive fracturing would only be connected to poor engineering and QA practices.

Evidently, the data uncertainties require analyses of different cases, i.e. cannot be captured in single distributions. It is therefore necessary to formulate a set of cases exploring the significance, for the Safety assessment applications, of the different issues discussed above. The formulation of such cases will be further discussed in subsection 6.5.8.

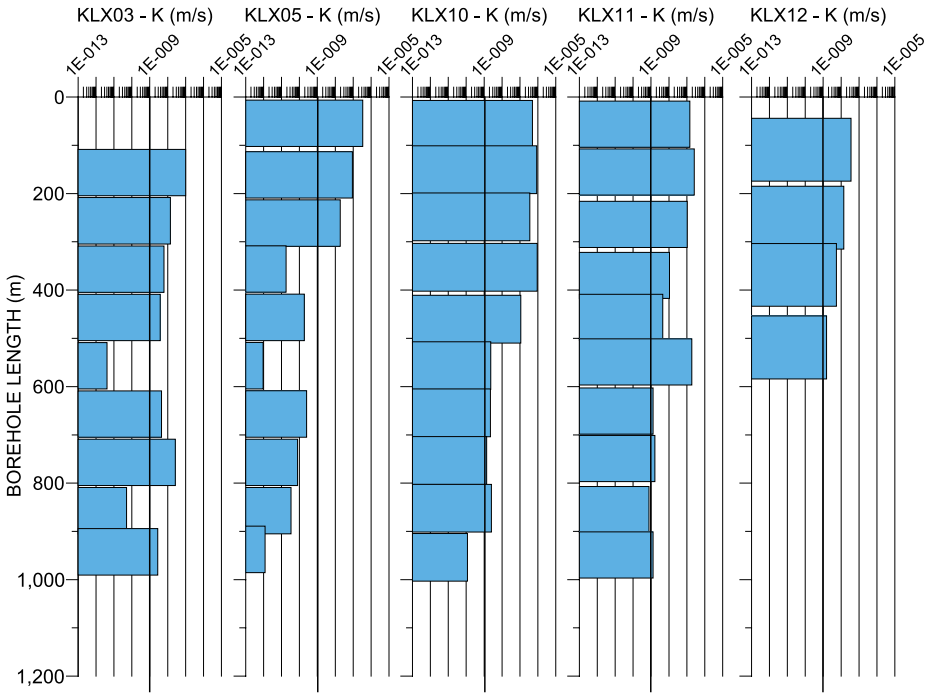

Figure 6-9. *Laxemar South – Hydraulic conductivity at a 100 m test scale. Results from injection tests (PSS) in KLX03 and KLX05. Preliminary results from WLP tests during drilling in KLX10, KLX11 and KLX12, see Figure 6-11 for location of the boreholes.*

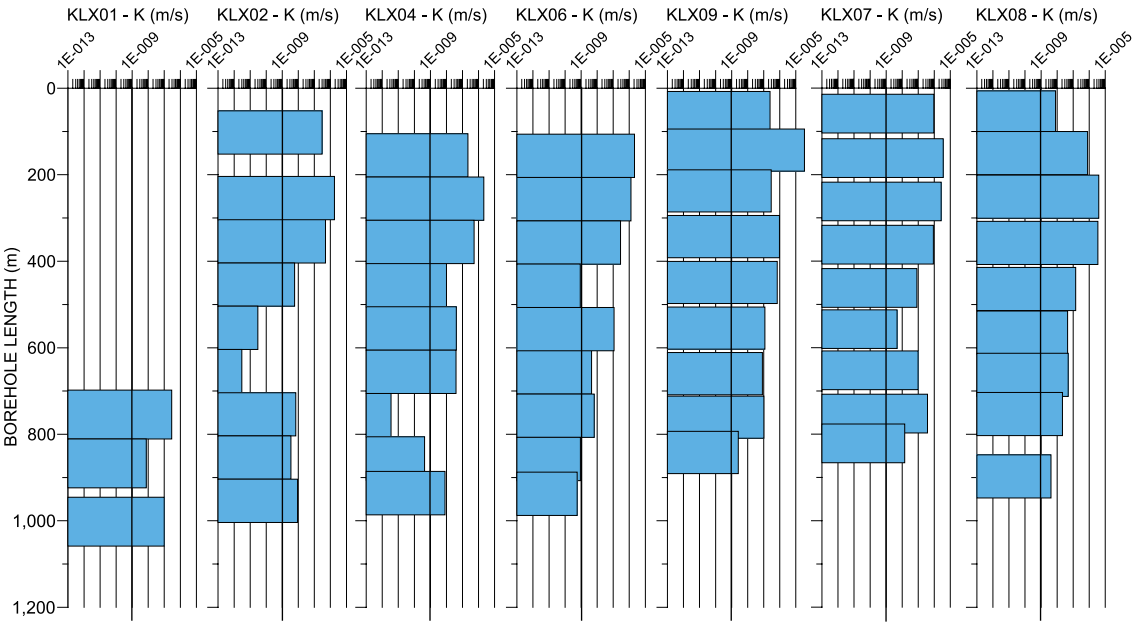

Figure 6-10. *Laxemar North – Hydraulic conductivity at a 100 m test scale. Results from injection tests (PSS) in KLX02, KLX04, KLX06 and KLX07. Preliminary results from WLP tests during drilling in KLX08 and KLX09. Old test methodology employed in KLX01. Depth is given as borehole length. (See Figure 6-11 for location of the boreholes).*

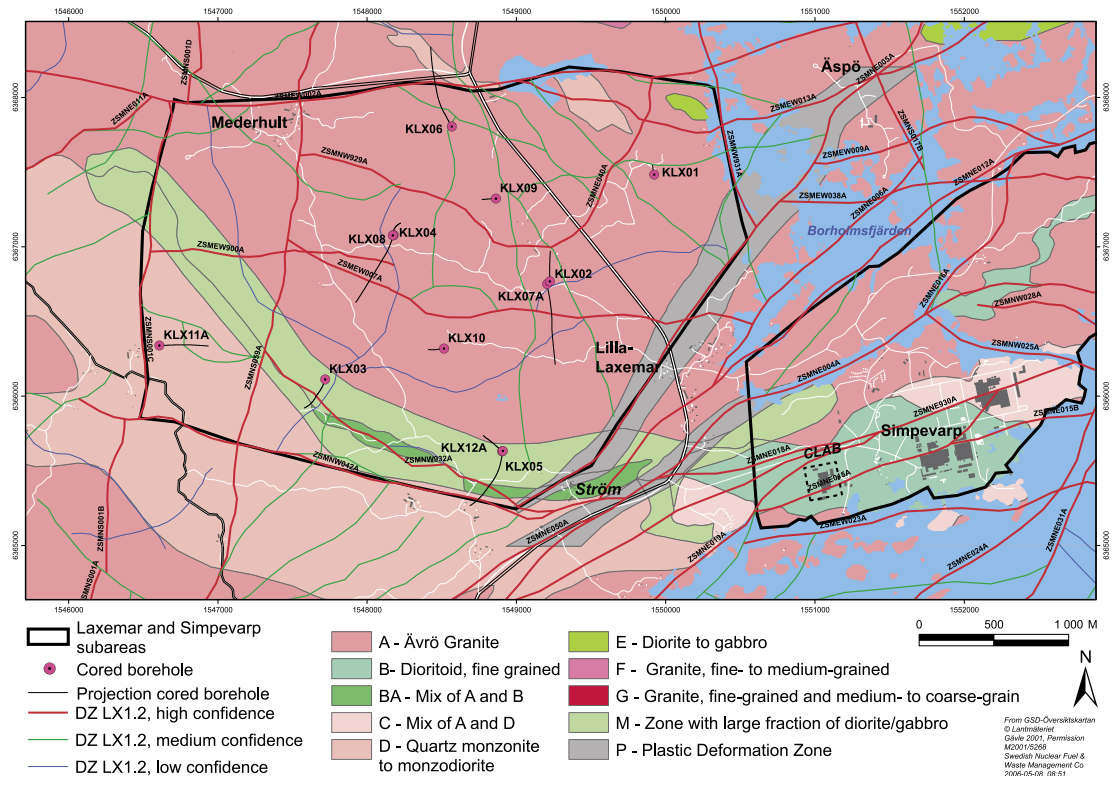

Figure 6-11. *Location of cored boreholes in the Laxemar subarea draped on a combined rock domain and deformation zone model (model version Laxemar 1.2). It should be noted that rock domains D, E, and M are more abundant at potential repository depth.*

6.5.7 Correlations

Input from the Site descriptive model report(s)

The statistical discrete fracture network, with its connection to the "deterministic deformation zones", is intended to capture the spatial correlation of the hydraulic properties. However, there is also a question whether fracture transmissivity is correlated to fracture size.

In the Site descriptive models the main assumption is to fully correlate fracture size and transmissivity, setting $log(T) = b \cdot log(a \cdot r)$, where r is the fracture radius. However, alternative models, with no correlation, $log(T) = N(\mu,\sigma)$, or with some correlation, $log(T) = b \cdot log(a \cdot r) + N(\mu,\sigma)$, are also applied to the data. All these alternatives could be fitted to the hydraulic test data, but they results in quite different block properties.

Possibly, the alternative with full, or at least much, correlation between size and transmissivity is easier to fit to the field data. This alternative also has theoretical support. A larger fracture can deform much more. However, there is not sufficient reason to omit the other alternatives at this point.

Chapter 12 of the **Site descriptive report, Forsmark and Laxemar** also assesses the consistency between disciplines. As can be seen from Table A4-7 in Appendix 4 of these reports, many disciplines should inform the hydrogeological modelling and most of this input is considered.

Specific considerations for Forsmark

Bedrock geology provides the geometrical framework in terms of rock domains, deformation zones and DFN geometry for the hydrogeological models. This input is certainly used. However, the DFN is close to the percolation threshold and, especially below the deformation zone ZFMNE00A2, the hydraulic conceptual model could be questioned /Chapter 8 of **Site descriptive report, Forsmark**/. Possibly, only the deformation zones are hydraulically interesting. Also, the potential differences in deformation zone pattern and fracturing within rock domain RFM029 (NW vs SE) are possibly not fully assessed and the analysis is concentrated on rock domain RFM029 and has not assessed variation in other rock domains (there are few data for these domains).

Stress orientation, i.e. a rock mechanics input, is expected to affect hydraulic anisotropy. Above the deformation zone ZFMNE00A2 there is clear hydraulic anisotropy. Only three fracture sets are conductive. There the sub-horizontal set is the most conductive and orthogonal to the minimum principal stress ($\sigma_3 = \sigma_v$). At depth, i.e. below the deformation zone ZFMNE00A2, the lack of hydraulic conductive features is reasonable in relation to the elevated stress situation, although no formal analysis has been undertaken.

Temperature affects water density and viscosity. This impact is considered and judged unimportant.

There is a strong coupling between hydrogeology and hydrogeochemistry, since it is suggested that mixing is the main process for groundwater evolution. Furthermore, density differences, created by varying salinity, affect the flow regime. These couplings are considered in the modelling work. Present-day salinity and water type distribution are "calibration targets" for simulation and the hydrogeologic modelling considers density effects. However, it is not always trivial to match the hydrogeological model to the chemical data, and vice versa. For example, it was not possible to fully match the rather high salinity in some of the boreholes. The chemical data could be rather insensitive to key aspects of the hydrogeological model (i.e. the flow characteristics in the repository volume), but very sensitive to other aspects – like the details of the near-surface hydrogeology or the initial conditions at the time of the past glaciation. Further enhancement of the interaction is warranted, but it is also important to understand the limitations in achieving full integration.

The regional simulations of past groundwater evolution involve modelling of salt migration. The migration properties should be consistent with assessed migration properties of the transport model. Such a test is made, but it is also concluded that the migration of salt is not very sensitive to migration properties of the rock matrix, including the migration distance in the matrix.

There are also interactions with the surface system. The identification of water types and boundary conditions in the near-surface hydrogeochemistry provides input to the surface water type considered in the modelling. Also, surface hydrology and near-surface hydrogeology as well as topography and the description of the Quaternary deposits provide input to the formulation of the top boundary conditions. All these interactions are considered in the modelling, although simplifications are made.

Specific considerations for Laxemar

The **Site descriptive report, Laxemar** makes very similar observations concerning the interdisciplinary consistency of the hydrogeological model.

Bedrock geology provides the geometrical framework in terms of rock domains, Deformation zones and DFN-geometry for the hydrogeological models. Most of this input is considered. Potentially, a more detailed property description could be used for assessing the variability within the deformation zones, but an updated zone characterisation (e.g. ductile/brittle) is needed before such data could be used for classifying zones into different transmissivity classes.

Stress orientation, i.e. a rock mechanics input, is expected to affect hydraulic anisotropy. There is an attempt to assess anisotropy from the borehole data (using the detailed PFL-data), but the issue is not yet fully resolved. However, since strong anisotropy and correlation with the stress field is found at Äspö HRL – this hypothesis is retained despite unclear evidence in data from the Simpevarp and Laxemar subareas.

Temperature affects water density and viscosity. In version Simpevarp 1.2, the impact was assessed in the regional hydrogeological modelling. The impact is insignificant.

There is a strong coupling between hydrogeology and hydrogeochemistry, since it is suggested that advection with the groundwater flow is a main process for groundwater evolution. Furthermore, density differences created by varying salinity affect the flow regime. These couplings are considered in the modelling work and there is a general agreement between the hydrogeological and hydrogeochemical descriptions. However, a detailed match between the two disciplines have not yet been obtained, as already discussed, and further assessment of this issue is expected in coming versions of the site description.

It should also be noted that mixing is not the only important process controlling the groundwater composition, especially for less conservative species than chlorine. Other parameters, like redox, pH, sulphate, and carbonate, are controlled by local and/or global geochemical reactions. These species, however, would not affect the flow. Model predictions of the depth of the redox front have not yet been made.

The regional simulations of past groundwater evolution involves modelling of salt migration. The migration properties should be consistent with assessed migration properties of the transport model and the models can fairly match total dissolved solids (TDS) in boreholes for the present situation by adjusting flow and matrix parameters, but clearly there are uncertainties in the parameterisation of the models and the issue will be further assessed in the coming site model reports.

Surface hydrology, near surface hydrogeology and oceanography provide the upper boundary conditions, although a simplified description is used in the deep rock model. Topography and the description of the overburden provide input to the description of the bedrock surface.

Judgement by the SR-Can team

The spatial correlation provided by the Site descriptive modelling should of course be maintained in the safety assessment calculations, e.g. by noting that individual realisations of the hydraulic DFN represents spatial variability, whereas uncertainty is captured by multiple realisations.

As already concluded in the respective Site reports, /e.g. Table 12-1 of **Site descriptive reports, Forsmark, Simpevarp and Laxemar**/, the alternatives with different correlation between fracture transmissivity and size need to be retained for further analysis in the Safety assessment. This needs to be reflected in selecting cases for hydraulic analysis within SR-Can.

The regional flow modelling made in support of the Forsmark Site description was not able to match the observed rather high salinity levels in the upper part of the bedrock. This is currently believed to be due to the very high transmissive parts of the upper bedrock, not fully represented in the version 1.2 models and this hypothesis will be explored in the ongoing modelling work connected to the complete site investigation, and should be resolved in time for SR-Site. However, this issue is judged to have limited impact on the flow distribution in the repository level.

The significance of the EDZ is likely to be much related to the actual discrete fracture network, to the stress situation and to the local rock mechanics properties. The EDZ will manifest itself mainly as a transmissivity increase due to depth of failure in spalling studies and because of existing (i.e. modelled) fractures in the vicinity of the tunnels.

6.5.8 Quantification

The various issues affecting the prediction of the hydraulic properties of the two sites have been briefly discussed in the previous sections. It is also concluded that these uncertainties are difficult to capture in terms of a single statistical distribution.

Cases explored for Forsmark – input from experts

Hartley et al. have explored the data analysis and site modelling as documented in the Site description and the modelling reports /Follin et al. 2005, Hartley et al. 2005a/. By assessing the main assumptions and identified uncertainties in the site modelling, /Hartley et al. 2006a/ defines set of different calculation cases, which should capture the main uncertainty space. These different issues and the parameter variation used to explore it are summarised in Table A-30 and further discussed in the following. A complete listing of the cases explored by Hartley et al. /Hartley et al. 2006a/ is given in Table A-31 to Table A-33.

The uncertainty stemming from the alternative deformation zone models was essentially explored already in the Site descriptive modelling work /**Site description, Forsmark**/. There it was concluded that the all three alternatives resulted in very similar flow fields inside the target volume. However, Hartley et al. /Hartley et al. 2006a/ decided to use the AC geological model as the SR-Can base case. The site modelling suggested flow paths were not sensitive to the choice of structural model. However, this conclusion was based on only performing particle tracking for the present-day groundwater flow which is governed mainly by the deformation zones due to the proximity of the shoreline, and these deformation zones are very similar for all three geological models. At future times when the shoreline retreats then the lineaments to the north in the AC model tend to shorten path lines compared to the BC model.

The uncertainty stemming from different descriptions of the rock mass between the deformation zones are expressed in several different possibilities:

- The most realistic case according to /Hartley et al. 2006a/ is to describe the rock mass as a heterogeneous DFN, with different properties in the various volumes indicated in Figure 6-3. The very poorly connected fracture network in Volume G, defined as the area in RFM029/017 below z = –350 m and zone ZFMNE00A2, is described either as DFN network with very low fracture density or a DFN network with lower transmissivity in the individual fractures.
- A conceptually different way of representing the low permeability region in Volume *G* would be to describe the rock mass as a very low permeability porous medium intersected by the much more transmissive deformation zones, i.e. the CPM-model suggested by /Follin et al. 2005/.
- In the Site descriptive modelling, Hartley et al. /Hartley et al. 2005a/ selected a hydrogeology DFN model defined for Volume *E*, see Figure 6-3, throughout the tectonic lens. This is a conservative assumption since the repository area is inside Volume *G*, which is thought to have lower fracture intensity based on boreholes KFM01A and KFM05A. However, the extrapolation of fracture properties over the large volume of the repository is uncertain, and so it is important to consider a more pessimistic case where fracture properties are more like those seen in KFM03A, which has some flow at all depths.
- As already discussed in Section 6.5, Hartley et al. /Hartley et al. 2006a/ presents alternatives to the main assumption to fully correlate fracture size and transmissivity. These alternatives are no correlation, or with some correlation.
- A couple of variants are formulated to explore the importance of the various ways of representing the hydraulic properties of the rock mass in a computer model, i.e. by the ECPM, nested ECPM/DFN or nested CPM/DFN descriptions. All these variants aim to represent the heterogeneity of the discrete fracture network, i.e. they are not conceptually different from the base case.
- A base case and an alternative case for representing the EDZ is analyzed.

The findings from these different cases are discussed in Section 6.6.

Cases explored for Laxemar

Hartley et al. /Hartley et al. 2006b/ have explored the data analysis and site modelling as documented in the **Site descriptive report, Laxemar** and the modelling reports /Hartley et al. 2006c/. By assessing the main assumptions and identified uncertainties in the site modelling, /Hartley et al. 2006b/ defines set of different calculation cases based on the uncertainty discussion in the Site description.

As for Forsmark Hartley et al. /Hartley et al. 2006b/ first carried out a set of transient, regional scale analyses. The simulations start 8,000 BC and continues to 20,000 AD for the Reference case. During the simulated time, the model is subjected to a shore level displacement and changes in the salinity in the Baltic Sea. At chosen release times particles are released from locations based on a repository layout. No repository is included in this model. Path-line calculations are performed under steady state conditions resulting in ensemble statistics for performance measures such as travel time, initial Darcy velocity, *F*-factors and path lengths. In addition, exit locations are obtained to indicate where possible discharge areas are located. The simulations used the reference case of the Site description, and thus adopts an ECPM derived from the semi-correlated hydraulic DFN-model. In addition, several variant cases were analysed considering, depth dependence, anisotropy and different initial conditions, see Table A-34.

It was found, that the highest flows and the lowest *F*-factor and times, i.e. least favourable performance measures, are found between 2,000 BC and 1,000 BC. This time frame coincides with

that the coastline is just above or near above the starting positions. It was found that the results are sensitive to increase in the anisotropy. Cases with stochastic properties in the deformation zones gave a spread in the results. Some performance measures in the simulations were worse than in the Reference case whereas the opposite could also be found. As the higher standard deviation set was used, unrealistically salinity profiles are found. The correlated concept resulted in slightly worse performance measures than the Reference case. Not surprisingly, the case with removed deformation zones gave improved performance measures. In the cases where the full set of deformation zones is used about 3% of the starting positions start within the HCD, but a clear effect could be observed by removing these low confidence zones.

As for Forsmark, the direct input to the SR-Can analyses is provided by detailed repository-scale modelling. Generally, the approach is to use a repository-scale DFN model to represent in detail the pathways around the deposition holes, and if this is of insufficient volume to capture the full flow-path to the surface, then the path is continued in a larger regional-scale DFN model, i.e. in this case all performance measures are calculated directly by the DFN-model. In the repository-scale DFN model a fully nested porous medium sub-model is used to represent the porous materials used to backfill the deposition holes (bentonite) and tunnel system (mixed bentonite and crushed rock or Friedland Clay). The repository is represented explicitly down to a resolution of a metre or less, and so the model domain must be limited for practical reasons. This means that the individual repository-scale model domains may not capture the entire length of all flow paths. Therefore, once a particle reaches the boundary of the repository-scale model, the path line is continued in the regional-scale DFN model.

The reference case repository scale model is similar to the reference case of the regional scale model, i.e. a DFN-model with semi-correlated *T* versus size. A slight simplification was made in that the small volumes of rock domains HRD(B,C) and HRD(A2) were incorporated into HRD(A) and HRD(D,E,M). Neither of these two domains is intersected by the repository. The following cases were analysed with the repository scale model:

- Reference case, with a Semi-correlated hydraulic DFN-model.
- Enhanced EDZ case, based on the Reference case, but with a 10 times enhanced EDZ ($3 \cdot 10^{-7}$ m/s).
- Enhanced Tunnel case, based on the Reference case, but with 100 times higher hydraulic conductivity in tunnel backfill (10^{-8} m/s).
- Cubic law transport aperture, based on the reference case, but with cubic law transport aperture.
- Anisotropy case, based on Reference case, but with transmissivity for *Set_C* 10 times higher.
- Correlated *T*-case, based on Reference case, but with Correlated T versus size hydraulic DFN-model.

A full reference to the cases is given in Table A-35. The findings from these different cases are discussed in Section 6.6. Input from EDZ assessment

The expert input regarding the quantification of the EDZ is already given in subsection 6.5.6.

Judgements made by the SR-Can team

Hydraulic properties – Forsmark

The different variant cases as defined by Hartley et al. /Hartley et al. 2006a/ and summarised in Table A-31 to Table A-33, are judged essentially sufficient for capturing the uncertainty relating to migration through the rock. Given the hydraulic assessment in the site descriptive modelling of Forsmark, the site data strongly suggest that the rock has very low permeability at depth below zone ZFMNE00A2, see Figure 6-3. However, depending on the assumptions made on the fracturing, alternative interpretations are possible, see Figure 6-4, ranging from a

non-percolating fracture network to a poorly percolating fracture network with transmissivities that are low and below the lower measurement limit of the hydraulic test equipment. In the case of a non-percolating fracture network, the flow and advective transport would essentially only take place in the deterministically modelled deformation zones, possibly with the addition of a very low hydraulic conductivity of the rock matrix itself. This means that:

- The alternative case deformation zone model (AC) is judged to be sufficiently conservative to be used as a base case, and sensitivity studies could made about it.
- A realistic base case for the rock mass is to assume the volume *G* Hydro-DFN in the repository volume. This could be represented by setting the fracture intensity a factor of 2 lower than in Volume *E* or by reducing the *T*-values in model volume *G* as suggested by Hartley et al. /Hartley et al. 2006a/. It should be noted, that while these representations results in no, or very few, intersections between conductive fractures and borehole, see Figure 6-4, there is still a chance that the model volume contains some undetected high transmissivity paths. At the current level of site understanding the existence of such paths could not be excluded.
- A conceptually different way of representing the low permeability region in Volume *G* would be to describe the rock mass as a very low permeability porous medium intersected by the much more transmissive deformation zones. This could approximately be captured by the CPM-model, being one of the alternatives treated by Follin et al. /Follin et al. 2005/. In this conceptualisation there are no possibilities for high transmissivity paths outside the already modelled deformation zones, see Figure 6-4. Eventually, it may be found that this is indeed the most reasonable description of the low permeability rock, but currently the existence of the "stochastic" high transmissive paths cannot be fully out ruled. Furthermore, the CPM model is not correct in the volumes above volume *G*. There it is quite clear that the flow takes place in fractures and a not in a homogeneous porous medium. Compared to the current DFN model, the CPM model would overemphasize the connectivity in the lateral plane. On the other hand, Follin et al. /Follin et al. 2005/ also suggest that there might be a significant horizontal anisotropy, currently not captured in the DFN model. Nevertheless, the CPM description would be a good indication of the potential excellent retention properties of the rock at the potential repository level at Forsmark. But, for all the reasons given, it should only be seen as an alternative to the realistic case suggested above. Some of these issues may anyway be better resolved after the complete site investigation of the Forsmark site.
- In order to explore the uncertainty in the actual extent of the low permeability volume it is necessary to explore with Volume *E* properties throughout the model domain. This would bound the possibilities of flow variation stemming from this uncertainty.
- The uncertainty stemming from the alternative models for correlation between fracture size and conductivity should be assessed by setting the fully correlated case as the realistic base case, but to also the explore semi-correlated T versus size case. In contrast, the fully uncorrelated T versus size case is judged unrealistic, see further discussion in subsection 6.6.8.
- As already concluded in subsection 6.5.5, the basic conceptual model of flow being confined to the fracture and deformation zone network is unchallenged, but there are various ways of representing the heterogeneous flow field, i.e. by the ECPM, nested ECPM/DFN, or nested CPM/DFN descriptions. Basically, the nested DFN approaches should be closest to the "real" system, but the practical limitations of handling discrete fracture models, as well as the data needs, warrants exploration of the importance of the assessment model. The alternatives analysed by Hartley et al. /Hartley et al. 2006a/ are judged to sufficiently illustrate this aspect.

It should be noted that it is likely that many of these variants would produce very similar results and would thus not need further propagation in the safety analyses. However, such an assessment can only be made against the specific migration end-points, as defined in Section 6.6. The discussion on which variants actually needs to be retained thus has to be postponed to that section. Given the various assumptions involved in the hydrogeological discrete fracture network analysis, the implications for this on radionuclide migration also have to be carefully considered.

Based on the experiences from the EDZ, as discussed in subsection 6.5.6, it is reasonable to assume that the EDZ, if it at all develops, is limited to a narrow zone (a few tens of cm) close to the tunnel and it would not form a continuous path. Possibilities for more extensive fracturing would only be connected to poor engineering and QA practices. Such conditions could certainly be avoided, but for the purposes of SR-Can it would be of interest to explore the importance of the EDZ and the importance of controlling its impact. For this reason two different cases are formulated.

- The expected conditions would be that the tunnel excavation work is performed with the intent of limiting the EDZ and with application of the necessary QA. In this case, the EDZ would be limited and discontinuous. The hydraulic conductivity parallel to the axis of the tunnel will be enhanced by about half an order of magnitude over a thickness of 0.3 m, but due to the drill and blast techniques used the EDZ will occur in 5 m sections with intact breaks of 0.5 m in-between.
- A limiting case is to assume conventional and drill-and-blast of the tunnel, without applying any special QA procedures for controlling the EDZ. This may possibly create a continuous damaged zone in the tunnel bottom. The resulting hydraulic conductivity of this zone is pessimistically increased by two orders of magnitude, i.e. a value much higher than the surrounding rock mass.

Hydraulic properties –Laxemar

As already noted, Laxemar data obtained after data freeze 1.2 contain much more information from the potential repository volumes. Furthermore, these data show much more favourable hydraulic characteristics than what is presently imbedded in the hydraulic flow models derived from the version 1.2 site description. This means that the current flow models might be unduly biased and they do not fully capture the actual variability of the hydraulic properties.

For these reasons, it is only recommended to carry out a limited set of analyses of the Laxemar site in SR-Can and it is not judged meaningful to explore different variants. Consequently only the base case of /Hartley et al. 2006b/, i.e. repository scale hydro-DFN with semi-correlated T versus size needs to be propagated to the following SR-Can analyses. However, the findings of the other cases explored will be discussed in Section 6.6.

Distance between flow paths

The migration analysis need also consider the distance between flow fractures in the rock, see Section 6.6. This distance can be directly estimated from the measured frequency of flow paths in the hydraulic data as shown in Table 6-1 for Forsmark and Table 6-2 for Laxemar. If flow paths occur randomly (a Poisson process) the spacing will be exponentially distributed with a mean given by $1/P_{10PFL}$. This would give a mean vertical fracture spacing of 12.8 m in Volume B (P_{10PFL} = 0.078 m^{-1}) and 600 m in Volume D (P_{10PFL} = 0.0017 m^{-1}). In Laxemar the corresponding values would be 7.7 m in HRD(A) (P_{10PFL} = 0.13 m^{-1}) and 26 m in HRD(D,E,M) (P_{10PFL} = 0.038 m^{-1}). Furthermore, Hartley et al. /Hartley et al. 2006a, Table 2-10 and Hartley et al. 2006b, Table 2-12/ estimated the distances between the flowing fractures in the numerical DFN analyses. These analyses show distances of the some order of magnitude as above results, which is not surprising given that the DFN-model is based on the PFL-data.

However, due to the uncertainty and variability in these numbers and the fact that small separation would imply less retention in the modelling, the SR-Can team do not recommended to use this different numbers directly. It is instead suggested to use 10 m, without further uncertainty, as a typical spacing between hydraulically conductive fractures for all sites.

6.6 Flow related migration parameters

An important part of the parameters controlling the radionuclide migration is related to the amount and distribution of the groundwater flow. The values of these flow related migration parameters are essentially obtained by simulation, using the basic data and description as provided in the applicable **Site descriptive reports**.

6.6.1 Modelling in SR-Can

The radionuclide transport calculations, see subsection 2.1.2, are performed using two different computer codes, the near-field code COMP23/Compulink /Romero et al. 1999, Cliffe and Kelly, 2004, Vahlund and Hermansson 2006/, and the far-field code FARF31 /Norman and Kjellbert 1990, Elert et al. 2004/. The codes use the following flow-related migration parameters:

COMP23:

- Equivalent flow rates Q_{eq1}, Q_{eq2} and Q_{eq3} (m^3/yr) for three possible transport paths, namely one for fractures intersecting a deposition hole (the Q1 path), one for the EDZ (the Q2 path), and one for a fracture intersecting the tunnel (the Q3 path), see subsection 2.1.2. The equivalent flow rates are derived from the Darcy velocity (specific flow rate) q (m/yr). Details are given below.

FARF31:

- Transport resistance, the so-called F-factor (yrs/m).
- Advective travel time, t_w (yrs).
- Peclet number, Pe (1).

The transport resistance and advective travel time are integrated parameters along flow paths obtained through particle tracking. The transport resistance, advective travel time and Peclet number are direct input parameters for FARF31. Internally, FARF31 uses the flow-wetted surface per volume of water, a_w, for each path line defined as $a_w = F/t_w$.

It is further noted that the exit coordinates of the flow paths are used within the biosphere modelling.

Below, all parameters are discussed and chosen distributions and values are motivated. However, the Peclet number /Norman and Kjellbert 1990/, which relates to dispersive and advective transport mechanisms along the individual flow paths through a dimensionless ratio, is not further dealt with. Instead, it is suggested that a single value of 10 is used (central value in previous assessments). The motivation is twofold:

- Large scale dispersion is handled through multiple flow paths in the groundwater flow models. Dispersion along individual flow paths has a minor effect on breakthrough characteristics. The more important effect of channelling is handled through a reduction of the F-factor, see below.
- Since dispersion is more of a model concept than a strict process, it is hard to motivate shapes of distributions.

6.6.2 Sensitivity to assessment results

Sensitivity analyses of the parameters discussed in this report were made in SR 97 /Lindgren and Lindström 1999, SKB 1999a/, and to a limited extent also in the SR-Can Interim main report /SKB 2004f/.

In SR 97 it was shown that the flow related parameters that mostly affect radionuclide retention in the geosphere are q and F. For the Darcy velocity (flux) it was shown that low values may result in the boundary layer between the buffer and rock being the limiting factor for doses; conversely, for higher fluxes other resistances control the dose.

For the transport resistance, it was shown that a value larger than 10^4 years/m for most nuclides provides adequate retention. The impact is monotonous, but not linear, for both these parameters; a higher F and lower q always yield lower doses and associated risks.

The advective travel time is mainly of interest for non-sorbing nuclides. However, a long advective travel time is beneficial only for short-lived, non-sorbing nuclides. Thus, the release of long-lived nuclides such as iodide are, even in a short term perspective, effectively un-affected by the advective travel time.

Varying the Peclet number within the range used in the SR 97 assessment did not influence the breakthrough of radionuclides in any significant manner. This is an important observation, since it is difficult to estimate this parameter from field or any other evidence.

6.6.3 Source of information

The flow related migration properties are assessed by groundwater simulation and subsequent particle tracking carried out by Hartley et al. /Hartley et al. 2006a/ for Forsmark and Hartley et al. /Hartley et al. 2006b/ for Laxemar. The input to these analyses in turn, build on the hydraulic data assessed from the site investigations /**Site descriptive report, Forsmark and Laxemar**/, and an assessment of Excavation Damaged Zone (EDZ), as further discussed in Section 6.5.

The major objective of the SR-Can hydrogeological modelling is to compute groundwater flow paths from each deposition hole to the surface. The approach taken is to track particles moving with the advective flow velocity from release points around the deposition holes until they reach the top surface or model boundaries. In doing this, two key issues that have to be addressed are how to do this when multiple scales and/or different conceptualisations of models are being used, and how to deal with the transient evolution of the flow-field.

Nesting of scales and model concepts

Three types of concepts are used to model the hydraulic properties of the system:

- Discrete Fracture Network (DFN) models, which explicitly represent fractures within the rock mass and calculate flows through the individual fractures and between fractures at intersections.
- Equivalent Continuous Porous Medium (ECPM) models with heterogeneous properties based on the use of an underlying discrete fracture network (DFN) concept. Based on these DFN models, it is possible to generate equivalent continuous porous medium (ECPM) models by converting the flow properties of blocks of the fracture network into the equivalent properties for a porous medium block of the same size. Hydraulic conductivity, porosity, and flow-wetted surface can be obtained in this manner. Both the codes Connectflow and DarcyTools have this functionality. How this is done in practice is discussed in subsection 6.6.8 below.
- Multi-component Continuous Porous Medium (CPM) models, with homogenous properties. In this case, the hydraulic properties are based on data derived for large volumes (e.g. from the Pipe String System, PSS, long interval data). In the CPM application, information on porosity and flow-wetted surface is not obtained directly from the model but needs to be based on independent information. How this is done in practice is discussed in subsection 6.6.8 below.

These concepts are discussed in more detail in Section 6.5. Several different methods of nesting scales and types of models have been applied. Below the main types of analyses conducted for Forsmark and Laxemar are summarized:

Forsmark

- Regional scale models using the ECPM and CPM concept, with limited resolution of the flow field. The regional-scale model grid used in the SR-Can study of Forsmark is nearly identical to the model used in Forsmark site description, i.e. a 100 m element-size regional model of about 15 km (SW-NE) × 11 km (NW-SE) with a 50 m element-size embedded grid covering the key areas including the potential repository area and the five cored boreholes KFM01A–KFM05A.
- A detailed local-repository scale model that models the repository explicitly as a CPM surrounded by a DFN model with fractures down to a scale of order 2 m to resolve the release of particles from a canister and then advected through surrounding rock. However, this type of model has to be limited in size, so it may not necessarily be able to capture flow paths all the way to the surface of the model.
- A multi-component CPM model with homogeneous properties within the various components of the bedrock, and a CPM representation of the tunnels in the same way as for the DFN/CPM model above.
- A local scale DFN model is nested within a regional scale ECPM model with the repository modelled as equivalent fractures with appropriate properties. In this case, it is only possible to include fractures down to order 6 m. This means it is possible to track particles through the regional domain, but some retention in small fractures around the repository is possibly lost. Hence, this type of model can be used to compliment the other models in quantifying the sensitivities to the approximations necessary for practical reasons.

The local-repository scale DFN/CPM representation is judged to be most realistic. The other options are used for sensitivity analyses.

In terms of the hydraulic properties, the repository is represented implicitly in the regional-scale modelling since the grid resolution only goes down to 50 m, while in the local-repository scale the tunnels and EDZ are modelled explicitly, i.e. one or more finite-elements are used to represent each deposition hole and the tunnel sections and EDZ in between.

The deposition tunnels are defined by a start and an end point for each tunnel. The start point of each deposition tunnel is geometrically connected to the main tunnels. The main tunnels, transport tunnels and the ramp are defined by smaller parts all connected to each other to form a hydraulically connected system. The shafts are two vertical features that should have a diameter of 3 m but are here represented as square sections with the equivalent cross-section area. Neither the deposition holes nor EDZ are represented in the regional-scale continuum models. The hydraulic parameter values assigned to the repository at Forsmark are given in Table 2-2 of /Hartley et al. 2006a/. All different parts of the tunnel and ramp system are assigned the same values.

In the local-repository scale models the EDZ is modelled explicitly. In the continuum models the EDZ is modelled by a layer of elements below the base of the tunnel, whereas in the nested DFN/CPM models it is represented as an equivalent fracture beneath the tunnel. The EDZ ‘fracture’ is subdivided into 6 m sections to improve discretisation, and is assumed to be continuous as a conservative approximation. Table 2-4 of /Hartley et al. 2006a/ gives the properties used in the EDZ at Forsmark. An example of how the tunnels are modelled in the nested DFN/CPM model is shown in Figure 6-12. Finally, in the regional-scale nested ECPM/DFN, both the tunnel system and EDZ are represented by equivalent fractures. The EDZ ‘fracture’ and tunnel ‘fractures’ are orthogonal to give a hydraulic connection between the tunnels and EDZ. Similarly, the sections of tunnels, ramps and shafts are all linked to ensure they are hydraulically connected.

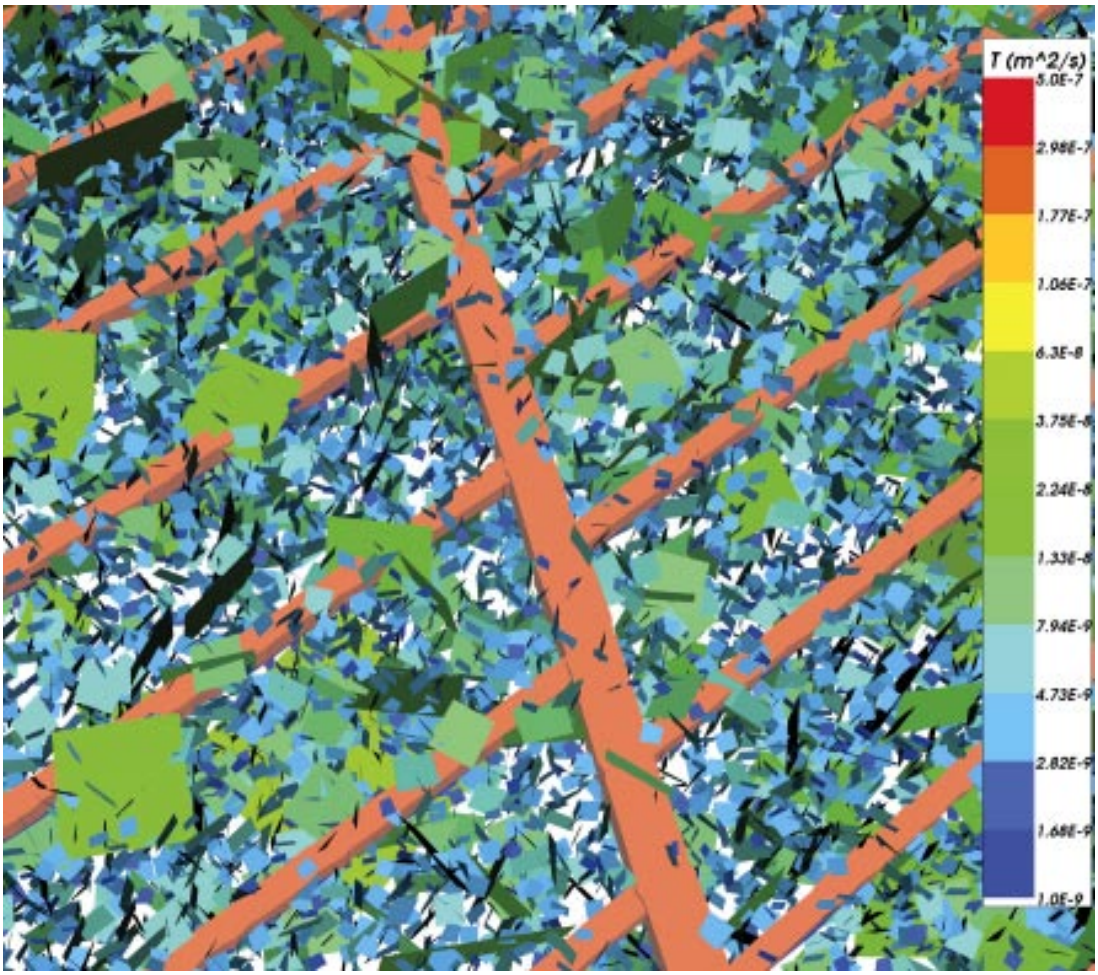

Figure 6-12. *An example of a combined DFN/CPM ConnectFlow model using a CPM sub-model of deposition and access tunnels nested within a DFN sub-model. Some fractures have been removed to reveal the tunnels. The interface between the two sub-models is on the boundary of the CPM model /Hartley et al. 2006a/.*

Laxemar

For the Laxemar application, see /Hartley et al. 2006b/, only a DFN description of the rock is used. This is implemented as a pure DFN model on local-repository scale, and as an up-scaled ECPM model on regional scale. Also here, the repository tunnels are included using a continuum representation. The continuum model of the repository is formally nested within the explicit DFN model on local-repository scale, and the local-repository scale DFN model adopts boundary conditions from the up-scaled ECPM model on regional scale. Thus, the nesting procedure is identical to the procedure used for Forsmark; however, only a limited set of different models for each scale is adopted.

Also the treatment of the tunnel and EDZ on different scales is identical to the treatment in the Forsmark case.

Deriving the input to migration analyses – performance measures

To provide input to safety assessment calculations, tables of performance measures are produced.

Continuum models

In a continuum model these are defined as:

1. Travel-time, $t_r = \sum_l \frac{\phi \delta l}{q}$ where δl is a step in distance along the path, for example through one finite-element, φ is the kinematic porosity, and q the Darcy velocity.
2. Initial Darcy velocity at the release point (Canister flux), $U_r = U_{0,r}$.
3. Path length, $L_r = \sum_l \delta l$.
4. F-factor, $F_r = \sum_l \frac{a_r \delta l}{q}$ where a_r is the fracture surface area per unit volume.

The subscript "*r*" indicates that the performance measure is calculated in the rock. That is, they only represent cumulative performance measures for those parts of paths within the rock and exclude parts of flow paths that pass through the EDZ or tunnel backfill. Performance measures are calculated for legs of paths within the EDZ and tunnels, but these are computed as separate performance measures for each path and distinguish by a *EDZ* or *T* subscript, respectively. It is noted that path length not is a direct input to the radionuclide transport calculations, but is provided as additional information.

Q equivalent release into fractured rock for the nested model (Q1)

Path Q1 considers release of radionuclides into the fractured rock surrounding the deposition hole. For a continuum model the Darcy velocity, U_0, is calculated at the initial point. The equivalent groundwater flow rate for Q_{eq1} can be written as:

$$Q_{eq1} = 4 w_c \sqrt{\frac{D_w U_{r0} L \varepsilon_r}{\pi}} \qquad \text{Equation 6.6.1}$$

where:

D_w is the diffusivity in water, (m²/y),
L is the half circumference of the deposition hole, (m),
U_{r0} is the initial Darcy velocity adjacent to the canister (m/y),
ε_r is the kinematic porosity of the rock adjacent to the deposition hole (–),
w_c is the canister height (m).

For the Forsmark application, D_w is set to 0.0316 m²/y, L is 2.8 m, w_c is set to 5 m, and ε_r is $5 \cdot 10^{-6}$ in the bedrock, though it could have higher vales if the canister is located within a deformation zone in the Alternative Case geological model. All other values are determined in the CPM flow simulations.

For conditions with a spalling zone, see Section 6.4 for a description of the phenomenon, an additional component to the equivalent flow rate needs to be considered /Neretnieks 2006/. This component is estimated as

$$Q_{eqDZ} = 1.13 \sqrt{\frac{D_p q W_{zone} L_{zone} \varepsilon_{zone}}{d_{zone}}} \qquad \text{Equation 6.6.2}$$

where

d_{zone} Thickness of damaged zone, (m),
D_p Pore diffusion coefficient, (m²/s),
L_{zone} Length of damaged zone, (m),
q Flow rate, (m³/s),
Q_{eqDZ} Equivalent flow rate in zone, (m³/s),

W_{zone} Width of damaged zone, (m),

ε_{zone} Porosity of zone, (–)

and q is estimated as the Darcy velocity multiplied with the capture area, i.e. $q = U_{r0} \cdot A$ where the area is 12.8 m^2 /Neretnieks 2006/. Values for the porosity and geometry of the spalled zone are also given in /Neretnieks 2006/.

Q equivalent release into the EDZ (Q2)

Path Q2 considers the release of radionuclides into the EDZ. Here the particles are released within finite-elements used to represent the EDZ that surrounds the top of the deposition hole. The equivalent groundwater flow-rate, Q_{eq2}, can be written as:

$$Q_{eq2} = 4 w_E \sqrt{\frac{D_w L \varepsilon_E U_{E0}}{\pi}} \qquad \text{Equation 6.6.3}$$

where:

L is the half circumference of the deposition hole (m),

U_{E0} is the initial Darcy velocity in the EDZ (m^3/yr),

ε_E is the EDZ porosity (1),

w_E is the EDZ thickness (m).

For the Forsmark application, L is set to 2.8 m, w_E is set to 2.0 m, and ε_E is set to 10^{-4}. All other values are determined in the CPM flow simulations.

Q equivalent release from the tunnel (Q3)

Path Q3 considers the release of radionuclides into a fracture that intersects the tunnel. It is assumed that diffusive equilibrium of radionuclides is achieved in the tunnel backfill and advection takes place into fractures surrounding the tunnel. Hence, an equivalent flow-rate, $Q_{eq3,}$ is required for advective flow from the tunnel into a fracture zone that intersects it. The equivalent groundwater flow-rate, Q_{eq3} is calculated from the Darcy velocity in the tunnel assuming the Darcy velocity in the fracture zone is of similar order of magnitude to that in the tunnel (by conservation of mass). The equivalent groundwater flow-rate, $Q_{eq3,}$ can be written as:

$$Q_{eq3} = 4 w_z \sqrt{\frac{D_w L_z \varepsilon_r U_{T0}}{\pi}} \qquad \text{Equation 6.6.4}$$

where:

L_z is the length of the fracture zone intersection with the tunnel (m),

U_{T0} is the initial Darcy velocity in the tunnel (m/y),

ε_r is the porosity of the fracture zone (1),

w_z is the fracture zone thickness (m).

For the Forsmark application, L_z is set to 7 m, and ε_r is set to $5 \cdot 10^{-6}$, w_z is set to 2.5 m. All other values are determined in the CPM flow simulations.

It is observed that the equation above assumes no flow in the backfill. When there is flow in the backfill, an additional advective component needs to be added to Q_{eq3} given by

$$Q_{eq3,adv} = \frac{L_{tunnel-fracture}}{t_{tunnel-fracture}} \varepsilon_{tunnel} A_{tunnel} \qquad \text{Equation 6.6.5}$$

where

$L_{tunnel\text{-}fracture}$, $t_{tunnel\text{-}fracture}$, ε_{tunnel} and A_{tunnel} are the length and advective travel time in the tunnel from the top of the deposition hole to the fracture intersecting the tunnel, the porosity of the back-filled tunnel, and the cross-sectional area of the tunnel, respectively.

Discrete fracture network models (DFN)

In a DFN model the PM definitions are the following:

1. Travel-time (y), $t_r = \sum_f \frac{e_{t,f} w_f \delta l}{Q_f}$, where δl (m) is a step in distance along the path, between a pair of fracture intersections, $e_{t,f}$ (m) is the fracture transport aperture, w_f (m) is the flow width between the pair of intersections, and Q_f (m^3/y) is the flux between the pair of intersections in the fracture.
2. Initial Darcy velocity (m/y) at the release point (Canister flux), $U_r = \frac{1}{w_c} \sum_f \frac{Q_f}{\sqrt{a_f}}$, where the sum is over fractures intersecting a deposition hole, a_f is the area of the fracture (m^2) and w_c (m) is the height of the deposition hole.
3. Path-length (m), $L_r = \sum_f \delta l$.
4. F-quotient (y/m), $F_r = \sum_f \frac{2 w_f \delta l}{Q_f} = \sum_f \frac{2 t_{rf}}{e_{tf}}$, t_{rf} (y) is the travel time in a fracture along the path.

It is noted that Darcy velocity and path-length not are used in the radionuclide transport codes but are calculated as performance measures that can be compared across different model applications.

Q equivalent release into fractured rock for the nested model (Q1)

Path Q1 considers release of radionuclides into the fractured rock surrounding the deposition hole, and hence the particle starts within a fracture that intersects the wall of the deposition hole. Several fractures may intersect the canister. For reasons of making a conservative assumption, the flux into all fractures that intersect the canister and contribute to advective flow away from the canister are included in the calculation of Q_{eq}. That is, an effective flow-rate is calculated for all fractures that cut a deposition hole and are connected to at least one other fracture. These effective flow-rates are summed for the deposition hole to give the total Q_{eq}. The equivalent groundwater flow rate for Q_{eq1} can be written as:

$$Q_{eq1} = \sum_f \left(2 \frac{Q_f}{\sqrt{a_f}} \sqrt{\frac{4 D_w t_{wf}}{\pi}} \right), \text{ where } t_{wf} = \frac{L_f \cdot e_{tf}}{Q_f / \sqrt{a_f}}. \qquad \text{Equation 6.6.6(a,b)}$$

If there are several fractures intersecting a single deposition hole, then a conservative approach to calculate the equivalent groundwater flow-rate requires the flow to be summed across all the fractures. Hence, the equivalent Darcy velocity, U_{r1}, for all fractures intersecting the deposition hole is:

$$U_{r1} = \frac{1}{w_c} \sum_f \frac{Q_f}{\sqrt{a_f}} \qquad \text{Equation 6.6.7}$$

where:

D_w is the diffusivity in water, (m^2/y),
t_{wf} is the time the water is in contact with the deposition hole within each fracture, (y),
L_f is the length of the fracture intersection with the wall of the deposition hole, (m),
U_{r1} is the average initial Darcy velocity in the fracture system averaged over the rock volume adjacent to the canister (water flux) (m/y),
Q_f is the volumetric flux in the fracture adjacent to the deposition hole (m^3/y),
e_{tf} is the transport aperture adjacent to the deposition hole (m),
a_f is the area of the fracture plane intersecting the hole (m^2),
w_c is the canister height (m).

Here, D_w is set to 0.0316 m²/y, and w_c is set to 5 m for both the Forsmark and Laxemar applications. All other values were determined in the DFN flow simulations. The transport apertures are related to the transmissivity of the fractures cutting through the deposition hole using a functional relationship, see subsection 6.6.6 below for further details.

For conditions with a spalling zone, see Section 6.4 for a description of the phenomenon, an additional component to the equivalent flow rate needs to be considered /Neretnieks 2006/. This component is estimated as

$$Q_{eqDZ} = 1.13\sqrt{\frac{D_p q W_{zone} L_{zone} \varepsilon_{zone} f}{d_{zone}}} \qquad \text{Equation 6.6.8}$$

where the definitions are the same as given above for the CPM case with the addition

f Fraction of zone where water effectively flows, (–)

and in this case q is estimated as $q = U_{r1} \cdot w_c \cdot min\ [2L_{zone}, L_{fracture}]$ where $L_{fracture}$ is the length of the fracture intersecting the spalled zone. Values for spalling parameters are given in /Neretnieks 2006/.

Q equivalent release into the EDZ (Q2)

Path Q2 considers the release of radionuclides into the EDZ. Here the particles are released within a fracture used to represent the EDZ that surrounds the top of the deposition hole. The equivalent groundwater flow-rate, Q_{eq2}, is calculated from the flow in the EDZ fractures that cut a deposition hole and are connected to at least one other fracture. These effective flow-rates are summed for the deposition hole to give the total Q_{eq}. The equivalent groundwater flow-rate, Q_{eq2}, can be written as:

$$Q_{eq2} = 2\sqrt{\frac{4 D_w L w_E \varepsilon_E \left(Q_E / \sqrt{a_E}\right)}{\pi}}. \qquad \text{Equation 6.6.9}$$

The equivalent Darcy velocity, U_{r2}, for flow in the EDZ is:

$$U_{r2} = \frac{Q_E}{w_E \sqrt{a_E}} \qquad \text{Equation 6.6.10}$$

where:

L is the half circumference of the deposition hole, (m),

U_{r2} is the average initial Darcy velocity in the EDZ fracture averaged over the fracture cross-sectional area (m/y),

Q_E is the volumetric flux in the EDZ fracture between each deposition hole (m³/yr),

ε_E is the EDZ porosity (m),

a_E is the horizontal area of the EDZ between each deposition hole (m²),

w_E is the EDZ thickness (m).

Here, L_E is set to 2.8 m, w_E is set to 0.3 m, and ε_E is set to 10^{-4} for both the Forsmark and Laxemar applications. All other values were determined in the DFN flow simulations.

Q equivalent release from the tunnel (Q3)

Path Q3 considers the release of radionuclides into a fracture that intersects the tunnel. It is assumed that diffusive equilibrium of radionuclides is achieved in the tunnel backfill and advection takes place into fractures surrounding the tunnel. Hence, an equivalent flow-rate, Q_{eq3}, is required for advective flow in the first fracture encountered along the path after a particle is released in the tunnel backfill above the deposition hole. The equivalent groundwater flow-rate,

Qeq_3 is calculated from the flow-rate in the first fracture the particle enters after leaving the tunnel. The equivalent groundwater flow-rate, Q_{eq3}, can be written as:

$$Q_{eq3} = 2\sqrt{\frac{4D_w L_f e_{tf} \left(Q_f / \sqrt{a_f}\right)}{\pi}}. \qquad \text{Equation 6.6.11}$$

The equivalent Darcy velocity, U_{r3}, for flow in the EDZ is:

$$U_{r3} = \frac{Q_f}{w_T \sqrt{a_f}} \qquad \text{Equation 6.6.12}$$

where:

L_f is the length of the fracture intersection with the wall of the tunnel (m),

U_{r3} is the average initial Darcy velocity in the fracture averaged over the fracture cross-sectional area (m/y),

Q_f is the volumetric flux in the fracture adjacent to the tunnel (m^3/y),

w_T is the fracture width intersecting the tunnel (m),

a_f is the area of the fracture plane intersecting the tunnel (m^2),

e_{tf} is the transport aperture of the fracture intersecting the tunnel (m).

Here, L_f is set to 7 m and w_f is set to 2.5 m for both the Forsmark and Laxemar applications. All other values are determined in the DFN flow simulations. The transport apertures are related to the transmissivity of the fractures cutting through the deposition hole using a functional relationship, see subsection 6.6.6 below for further details.

It is observed that the equation above assumes no flow in the backfill. When there is flow in the backfill, an additional advective component needs to be added to Q_{eq3} given by

$$Q_{eq3,adv} = \frac{L_{tunnel-fracture}}{t_{tunnel-fracture}} \varepsilon_{tunnel} A_{tunnel} \qquad \text{Equation 6.6.13}$$

where

$L_{tunnel\text{-}fracture}$, $t_{tunnel\text{-}fracture}$, ε_{tunnel} and A_{tunnel} are the length and advective travel time in the tunnel from the top of the deposition hole to the fracture intersecting the tunnel, the porosity of the back-filled tunnel, and the cross-sectional area of the tunnel, respectively.

In order to study each of these paths, the detailed repository-scale models have to represent the deposition holes, tunnels and EDZ explicitly, and flow paths have to be computed for a release at three appropriate positions around each canister. Hence, the performance measures are calculated for three paths for each canister. It is possible that the three particles may follow very similar trajectories, such that T_r, L_r and F_r for the three starting positions are similar, but U_r, U_{EDZ} and U_T will vary. Further for each path, the performance measures are calculated for portions of the path spent in the rock, tunnels, and EDZ separately. Because $a_r = 0$ in the tunnel and EDZ, F_{EDZ} and F_T are zero, and therefore only T_{EDZ}, L_{EDZ}, t_t and L_t are calculated. Clearly a_r in the EDZ (and possibly in the tunnel) is non-zero in reality. However, we do not include retention in EDZ and tunnel as retention mechanisms, and hence a_r is assumed to be zero since there is no need to quantify this retention.

The results from the particle tracking are used to produce ensemble statistics for the performance measures, as well as locating the discharge areas. In Forsmark /Hartley et al. 2006a/, the ensemble is over the set of 6,824 particle start locations, one for each canister.

Apart from the work done on the repository layout by Design, no further attempt is made to avoid starting particles in either deterministic fracture zones or high transmissivity stochastic fractures in the DFN or ECPM models. In reality such features are likely to be avoided during repository construction, and hence the model may tend to see particles start in a wider range

of possible fracture transmissivities than might be encountered in reality. However, when radionuclide transport calculations are performed, possible starting locations in deformation zones are sorted away.

6.6.4 Conditions for which data are supplied

The hydraulic analyses of Hartley et al. /Hartley et al. 2006a/ and Hartley et al. /Hartley et al. 2006b/ concern the situation as it appears today and the potential evolution during a temperate climatic period. This means that the flow analyses consider the changing boundary conditions resulting from shore line displacement and projected changes in the salinity of the sea. The analyses consider the presence of a repository and the potential impact of an EDZ. The analyses intend to capture the important conceptual and data uncertainties related to the flow related migration parameters. Considering the uncertainties in the hydraulic input data, a large set of variants are analysed as is further described in Section 6.5.

6.6.5 Conceptual uncertainties

The conceptual uncertainties relating to the flow field and the hydraulic properties of the rock mass have already been discussed in subsection 6.5.5. These uncertainties are propagated into the quantification of the flow-related transport properties. Specifically, if the continuum representation of the rock mass is a more appropriate description of reality, higher transport resistances are obtained, see discussion below for further quantification.

6.6.6 Data uncertainty, spatial and temporal variation

The conceptual uncertainties relating to the flow field and the hydraulic properties of the rock mass have already been discussed in subsection 6.5.6. These uncertainties resulted in the formulation of a set of variants for further analysis, see Table A-30 in Appendix A8. The implication of these uncertainties on flow-related transport issues are captured through the results obtained from the performed variants. Below, other uncertainty aspects, not directly captured through the variants, are explored in more detail.

Internal fracture variability

In the DFN models used, fractures are assumed homogeneous. In reality, fractures have spatially variable apertures resulting in possible channelling effects. The calculated transport resistance, F, is thus associated with some uncertainty since the internal aperture variability is not resolved. This uncertainty is dealt with by dividing the resulting F-values by a factor of ten. Supporting analyses by Painter /Painter 2006a/ where internal fracture variability within a fracture network has been analyzed explicitly indicate that a factor of ten is conservative for realistic fracture variability. It is shown that most of the channelling in fact stems from the geometrical effects of the fracture network. It is also clear that channelling effects can not result in F-factors approaching zero. This stems from the fact that flow path widths approaching zero are associated with increasing volumes of surrounding stagnant water. This stagnant water, accessible through diffusion from the mobile water, will effectively increase the area available for diffusion into the matrix. Thus, a lower bound for the F-factor exists where it does not make sense to decrease values more. However, such a limit is not invoked in SR-Can, and thus some of the adopted F-values may become unrealistically low using the factor ten approach. Related to the issue of channelling is the notion of “wormholes”; i.e. the presence of long range, narrow, preferential flow paths. It is observed that such long range preferential flow paths are created in the DFN models when a positive fracture transmissivity-length correlation is invoked. Thus, long range flow paths are present in the models, and the additional effect of channelling within the fracture plane is conservatively handled through the reduction of the area with a factor ten.

Finally, it is emphasized that the use of the factor ten is based on a more solid foundation, and appears more conservative, relative to the use of the same factor in previous safety assessment applications due to the insight gained by the analysis of /Painter 2006a/. However, it is also noted that the procedure adopted here may be subject to change in the future, if and when the methodology by /Painter 2006a/ is applied to site-specific data on internal fracture variability.

Engineered Damaged Zone (EDZ)

The EDZ is handled in a conservative manner since the whole EDZ is modelled as continuous even though empirical evidence indicates that the damaged zone rather takes place in discrete intervals with intact, unmodified rock in between, see Section 6.5. This simplification magnifies the influence of the EDZ on the flow pattern, and is thus conservative from a safety assessment perspective. However, the implementation also implies an uncertainty in the resulting true flow field since the effect is magnified.

Varying spatial resolution along flow paths

The nesting issue, see also subsection 6.6.3, arises because the local-repository scale models are very detailed around the repository but have a limited spatial extent both laterally and vertically (however, the Forsmark and Laxemar local-repository scale models extend all the way up to the soil layers). The solution is to track particles from the release points to the outer boundary of the local-repository scale model, and then restart the particle tracking in the corresponding regional scale model. Performance measures, such as travel-time, are calculated as the cumulative travel time along both legs of the path. The same approach is used for both nested CPM models and DFN models, although for the DFN model this means starting the particle in the corresponding ECPM regional scale model.

Temporal variation

Fixed velocity-fields, or snapshots in time, from selected times in the future are used for the particle tracking simulations. This is mainly because flow-related transport parameters obtained from particle tracks in a transient velocity-field are not compatible with the streamline based formulation of radionuclide transport used in the code FARF31 /Norman and Kjellbert 1990/. Furthermore, flow-related transport parameters obtained from a transient velocity field would be sensitive to the release time, kinematic porosity and retardation of each radionuclides by sorption or rock matrix diffusion, which makes it difficult to interpret the results and quantify the various uncertainties. Hence, most transport calculations are based on fixed flow-fields at several selected times, between 2,020 AD and 9,000 AD for the Forsmark application, and between 8,000 BC and 20,000 AD for the Laxemar application.

For cases where the shoreline is retreating away from the site, such that major discharge areas is getting further away with time, the snapshot in time method is expected to be a conservative approximation. Moreover, the influence of deformation zones and discrete fractures will cause flow paths to be predominantly vertical even in such time evolving flow fields /Hartley et al. 2006a/.

For SR-Site, additional geosphere transport modelling is planned using codes where transport in transient flow fields can be handled. Both stand-alone tools such as CHAN3D /Moreno et al. 2006/ and next-generation transport codes within the SKB model chain /Painter 2006b/ can handle transient flow.

Assumed transmissivity-aperture relationship

In the DFN simulations, a functional relationship between transmissivity and aperture is assumed. The relation used is $e_t = 0.46T^{0.5}$ where e_t is aperture and T transmissivity. The basis for the relationship is empirical evidence from Äspö /Dershowitz et al. 2003/. An alternative to this relationship is the cubic law, where $T \sim e_t^3$. For a parallel plate, the cubic law is the formally

correct relationship between aperture and transmissivity; however, in real heterogeneous fractures the empirical model has been shown to possess good predictive qualities. The choice of relationship is thus associated with some uncertainty. Using the cubic law, where aperture is proportional to transmissivity to the 1/3 power, results in a more narrow aperture distribution for a given transmissivity distribution. Specifically, for the largest *T*-values relevant, smaller aperture values will be obtained relative to the empirical relationship.

For transport of solutes, the difference in calculated apertures will result in changed advective travel times, but not in changed *F*-factors, see subsection 6.6.3. This advective effect is negligible when transport of radionuclides subject to matrix diffusion are considered. However, the aperture is also used in the calculation of the equivalent flow rate for paths Q1 and Q3, see subsection 6.6.3. Here, more narrow aperture distributions will result in also more narrow distributions for the equivalent flow rates. The flow rates of most interest are the high ones; since high flow rates are obtained for high transmissivities, an accompanying lowering of the calculated aperture will result in lower overall flow rates relative to the empirical transmissivity-aperture model. Thus, the assumed empirical model is conservative in a safety assessment context. The possible effect of internal aperture variability on the equivalent flow rates has been addressed in /Liu and Neretnieks 2005/. The results show that including aperture heterogeneity results in lower equivalent flow rates. Thus, neglecting aperture heterogeneity is conservative concerning the equivalent flow rates.

6.6.7 Correlations

All flow-related transport parameters vary in space. The Darcy velocity values are point values, whereas the *F*-factor and advective travel time are Lagrangian quantities integrated along path lines. However, the values at the end of the path lines can be represented as point values with Univariate distributions.

The auto-correlation is not an issue of interest, but rather the Univariate distribution of each parameter, and the cross-correlation between the parameters. A clear cross-correlation is seen between travel time and *F*-factor (in fact, a functional relationship can be approximated as $F = a_w \cdot t_w$ where a_w is the flow-wetted surface per volume of water), whereas the correlation between Darcy velocity and *F* (or t_w) is weaker in a discrete fracture network, see Figure 6-13.

Due to the correlations, triplets of values are sampled (i.e. corresponding values of q, t_w and F for the same canister location) for further transport calculations. When separate pathways Q1, Q2 and Q3 are considered, three pairs of triplets for the same canister location are sampled.

6.6.8 Quantification

Below some of the key results from the simulations by Hartley et al. /Hartley et al. 2006a/ and Hartley et al. /Hartley et al. 2006b/ are summarised. Simulations are performed on both regional and local-repository scales. In the regional scale analysis, transient simulations covering a large number of variants are performed. The variants judged most important from a safety assessment context (in terms of consequence or associated uncertainties) are propagated to the local-repository scale analysis. Here, only a sub-set of the variants are analyzed, and using some simplifying modelling approaches; e.g. the local-repository scale model is solved for a fixed time adopting boundary conditions from the regional model. Results propagated to radionuclide transport calculations are taken from the local-repository scale simulations.

Results of regional scale analyses – Forsmark

A more comprehensive set of sensitivities have been considered in the SR-Can application of Forsmark /Hartley et al. 2006a/ than was possible in the site-modelling study for Forsmark /**Site description, Forsmark**/. A full list of the sensitivities considered and the variants used to quantify them is listed in Table 3-4 of /Hartley et al. 2006a/.

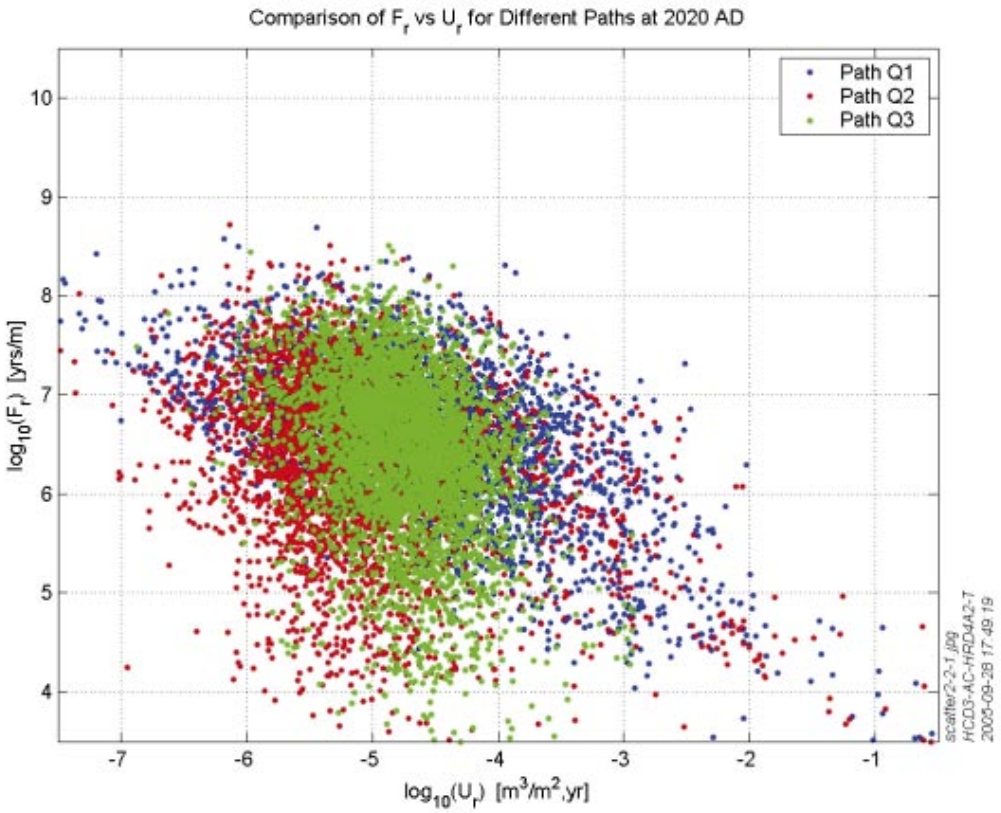

Figure 6-13. *Scatter plot between transport resistance in rock and initial Darcy velocity at starting points for different release paths for the combined Forsmark DFN/CPM local-repository scale model with lower transmissivity below ZFMNE00A2.*

The sensitivities found to be most important are:

- The choice between a multi-component CPM model and an ECPM model based on an underlying DFN concept results in big differences in performance measures. Travel-times and *F*-factors are about an order of magnitude higher for the CPM model. Part of the explanation for this is obvious from the fact that the CPM model takes a more optimistic view of hydraulic conductivity in rock domains RFM029/017 by using the PSS measurement limit. However, there are also more subtle differences such as flow being more channelised in the ECPM model due to heterogeneities, and that flow tends to be shallower in the ECPM model. The *F*-factor tends to be lower in the ECPM model since the flow-paths are often shorter, and more importantly, the flow-wetted surface, a_r, is computed based on the connected fracture intensity in each element in the ECPM model whereas a single value is used in the CPM model. In the CPM model, an a_r value of 0.25 m^2/m^3 is used, whereas in the ECPM model the average resulting flow-wetted surface is around 0.08 m^2/m^3 in the volume surrounding the repository.
- The choice of geological model has an effect mainly at future times, since the presence and properties of deformation zones outside the candidate area in the alternative case deformation zone model affect flow velocities downstream of the repository area. Flow paths are generally longer for the base case geological model than in the alternative case model. However, the location of discharge points is only moderately sensitive to the deformation zone model, presumably because the shoreline position has a stronger effect than the deformation zones.

- It is observed that the match against hydraulic conductivity is greatly improved by using a multi-component DFN model; i.e. a model with different DFN statistics in different parts of the model. This is achieved by using either a lower transmissivity around the repository, or alternatively, by using a lower fracture intensity around the repository. These two variants are more realistic interpretations of site conditions around the repository based on Forsmark 1.2 borehole data. The resulting *F*-factors are also increased for these two cases.
- Alternative relationships between fracture transmissivity and length are shown to influence the results. Cases with semi-correlated and uncorrelated models are applied. However, based on arguments presented in subsection 6.3.5 concerning fracture shape and surface roughness (the discussion on shape and roughness indicates that a dependence between shape and aperture exists, and hence a correlation between size and transmissivity seems plausible), it is deemed reasonable not to consider the uncorrelated case for further radionuclide transport analyses. The semi-correlated case results in travel times and *F*-factors that are more than an order of magnitude lower for many paths, and a significantly larger spread in flow paths and exit locations are observed. The reasons are slightly higher block-scale hydraulic conductivities and more vertical paths rather than longer path to the shoreline as observed in the perfectly correlated case. A lack of correlation thus tends not only to disperse particles and exit locations, but also to shorten paths by making long horizontal flow paths less likely. Based on the above, the semi-correlated model needs to be further analyzed on the local-repository scales. The fully correlated model is the one suggested by the site-descriptive model, but the semi-correlated model may provide poorer performance.

The sensitivities found to be less important are:

- Results are moderately sensitive to modifying the fracture length distribution (using a variant Geo-DFN). The reason is thought to be that both the reference case ECPM model and the variant Geo-DFN are calibrated against the hydraulic data for KFM03A. This meant that the numbers and magnitudes of flowing features are adjusted in both cases to be about the same, and hence the connectivity and bulk flows in both cases are likely to be very similar.
- A lower kinematic porosity in the deformation zones is considered since it is possible that flows within the zones are limited to a small volume of the zones, e.g. a thin layer near the top. This case results in only moderate effects on the performance measures. The reason is likely that larger proportions of travel-time and *F*-factor are accumulated in the background rock during the initial part of transport between release points and the first deterministic deformation zones.

The sensitivities found to be least important are:

- A layer of enhanced hydraulic conductivity in the top 100 m is thought to be possible and needs to be considered since the cored boreholes are cased in the top 100 m. However, this is found to have almost no effect on results.
- Changing the flow-wetted surface, within plausible ranges of values, of the deformation zones has little effect on results.

It is finally observed that different realisations of the stochastic DFN do not result in significantly different performance measures in terms of ensemble statistics over all canisters. This result suggests that the uncertainty in where stochastic fractures are located and uncertainty in their properties can be captured to a large extent by considering the spatial variability in the fracture network in a single realisation. Furthermore, the deterministic deformation zones create a system where the influence of the DFN variability may be of minor importance.

Results of local-repository scale analyses – Forsmark

Only a sub-set of the variants performed for the regional scale simulations are analysed on the more detailed scales. The choice of variants to propagate is based on the results from the regional scale analysis, with some additional variants motivated by the repository implementation. The resulting distributions of performance measures from the local-repository scale analyses are subsequently used in radionuclide transport modelling. Thus, the modelling described in this section provides the hard input data propagated in the model chain. The suggested variants in this section are also discussed in a hydrogeological context in Section 6.5. The suggested variants are:

- A realistic case, which is based on the DFN representation above, but with reduced transmissivity below zone ZFMNE00A2 (A2).
- The so-called reference case, which is identical to the case above but with unmodified transmissivity below zone A2.
- The realistic case with modified EDZ properties (100 time higher conductivity in EDZ).
- Realistic case with modified tunnel backfill properties (100 time higher conductivity in backfill).
- The realistic case with modified transmissivity-length correlation (semi-correlated and uncorrelated).
- A CPM representation of the realistic case, including variants with modified EDZ and tunnel backfill properties.
- An alternative nesting strategy where a local-scale DFN model is nested in a regional scale ECPM model.

The CPM and DFN models yield quite different results. This stems from the fact that the bedrock within the repository candidate area is very sparsely fractured with generally poor connectivity. In consequence, a DFN model predicts a very disjoint flow system with poor connections, areas of stagnant flow, tortuous flow paths such that significant flow and transport is restricted to the deterministic deformation zones and the larger stochastic fractures. The lack of connectivity horizontally over long distances restricts long flow paths from forming, and hence flow tends to be much localised and discharge from the repository is mainly to the immediate surface above. Transport is mainly sensitive to the structural model and occurrence of large stochastic fractures, while transient processes such as shoreline retreat are less influential. In contrast, a CPM model with isotropic hydraulic properties allows flow connections in all directions, and although the CPM bulk hydraulic properties are equivalent on a large-scale (100 m), the detailed flow and transport is very different. In the CPM model, flow is more homogeneous with flow around all deposition holes and longer flow paths, many of which reach the shoreline. In this case, results are sensitive to the position of the shoreline, and flow paths are less dominated by the geological structural model. In the DFN model, flow is thus more localised and vertical than in the corresponding regional up-scaled ECPM model which by definition is more connected. On average, the flow-wetted surface in the DFN model is around 0.2 m^2/m^3, which thus is close to the CPM value of 0.25 m^2/m^3 which is used in both regional and local-repository scale CPM models.

In terms of the performance measures, the CPM model predicts travels times with a median over 10^3 years, while the DFN model median is less than 10^2 years, see Figure 6-14. Also, the CPM model has a tail of long travel times. Initial Darcy velocity has a median around 10^{-6} m/y in the CPM model with small variability, while the DFN predicts a median around 10^{-5} m/y but with a larger standard deviation close to unity in log-scale, see Figure 6-15. In the CPM model, initial Darcy velocity (flux at deposition hole location) is used for calculating the near-field equivalent flow rate; in the DFN model, the Darcy velocity is only calculated for comparative purposes, see subsection 6.6.3 above. In the CPM model, the F-factor has a median value just under 10^8 y/m whereas the corresponding value for the DFN model is under 10^7 y/m, see Figure 6-16. In both the DFN and CPM models, travel-time and F-factors are almost identical for each of the release points around the canister, which suggests that the flow path is the same for each release point and that flow does not diverge down different flow conduits around the repository.

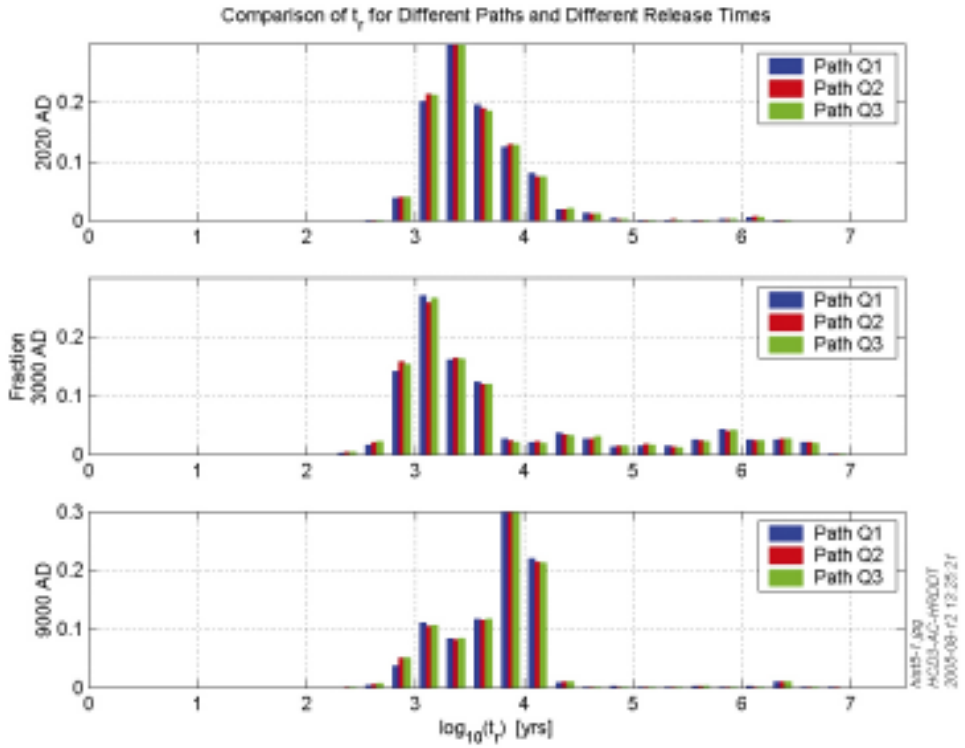

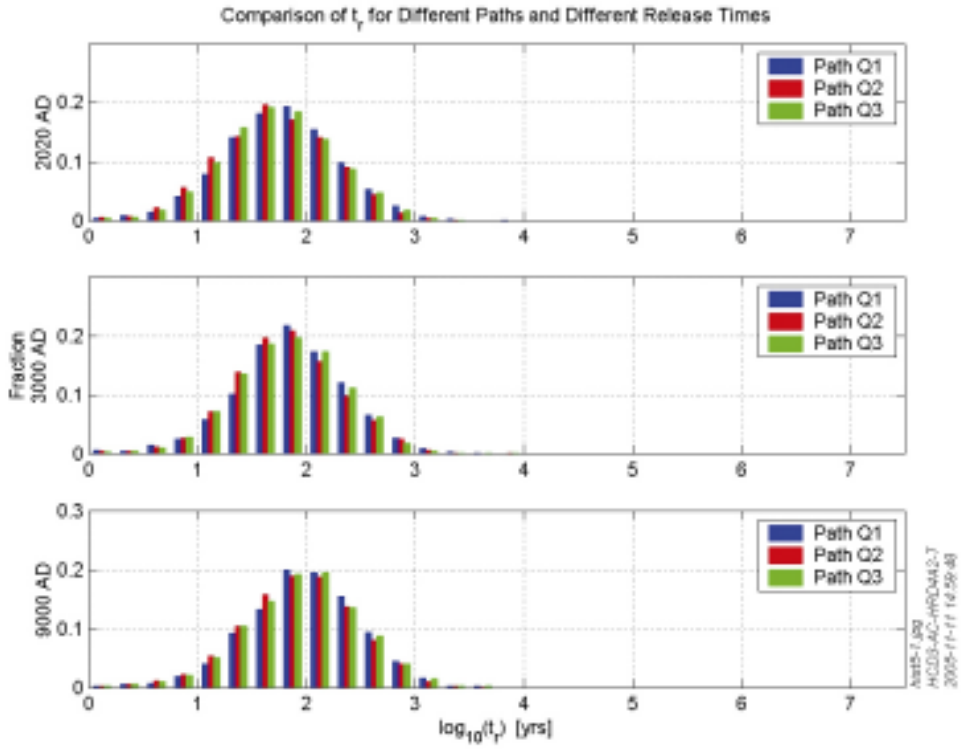

Figure 6-14, a and b. *Advective travel time in the rock for different paths and release times for a) CPM model and b) DFN model. Realistic case.*

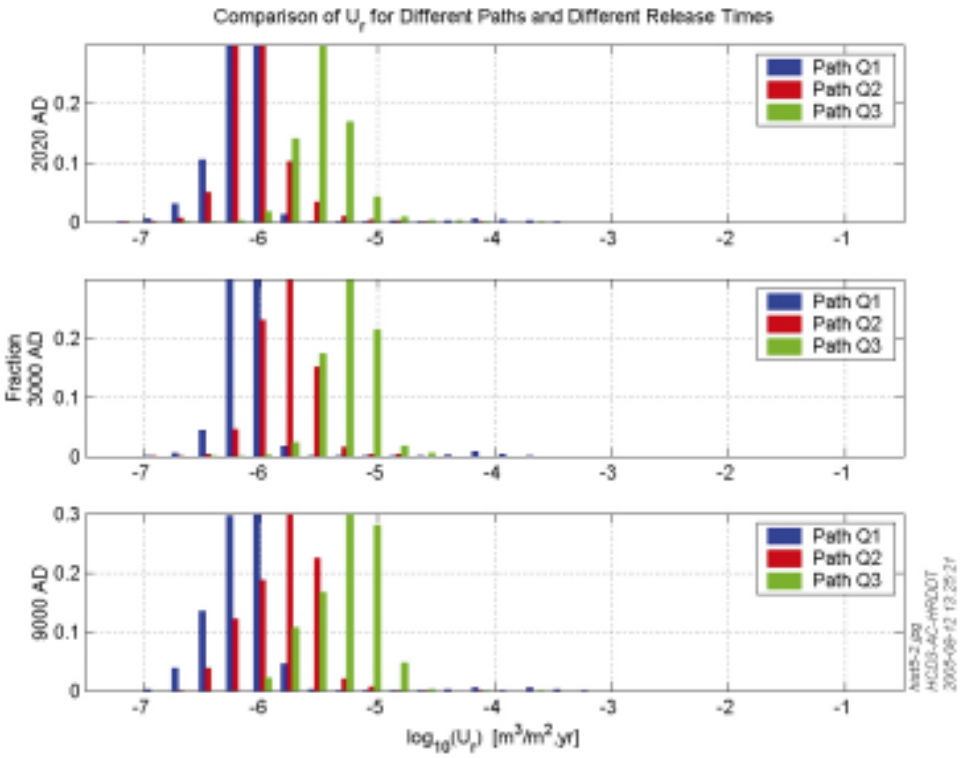

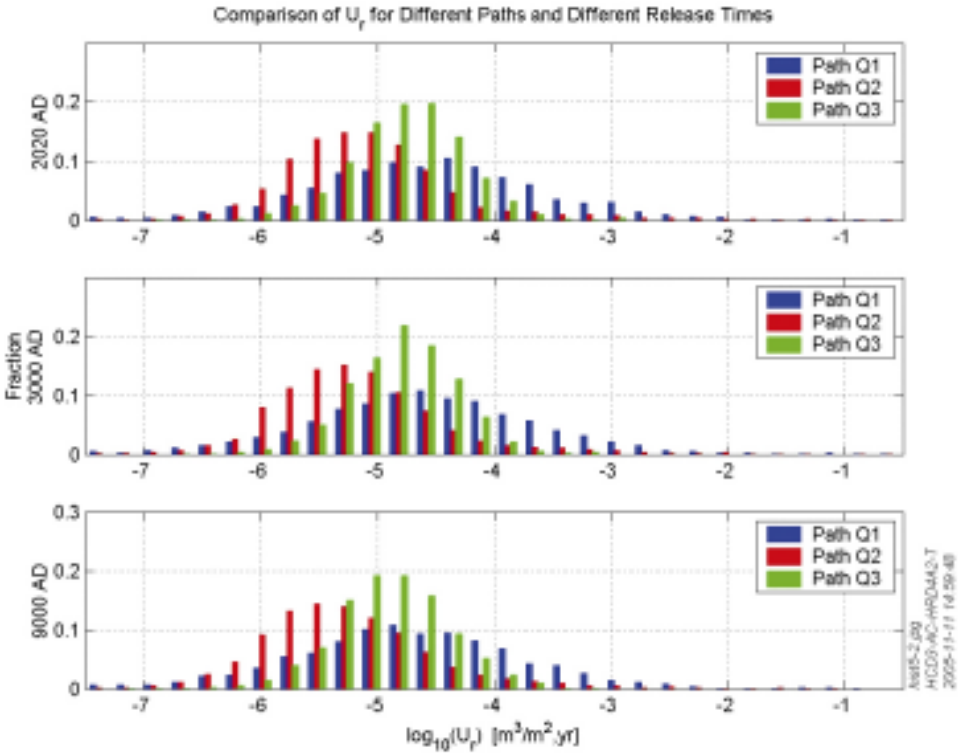

Figure 6-15, a and b. *Darcy velocity for different paths and release times for a) CPM model and b) DFN model. Realistic case.*

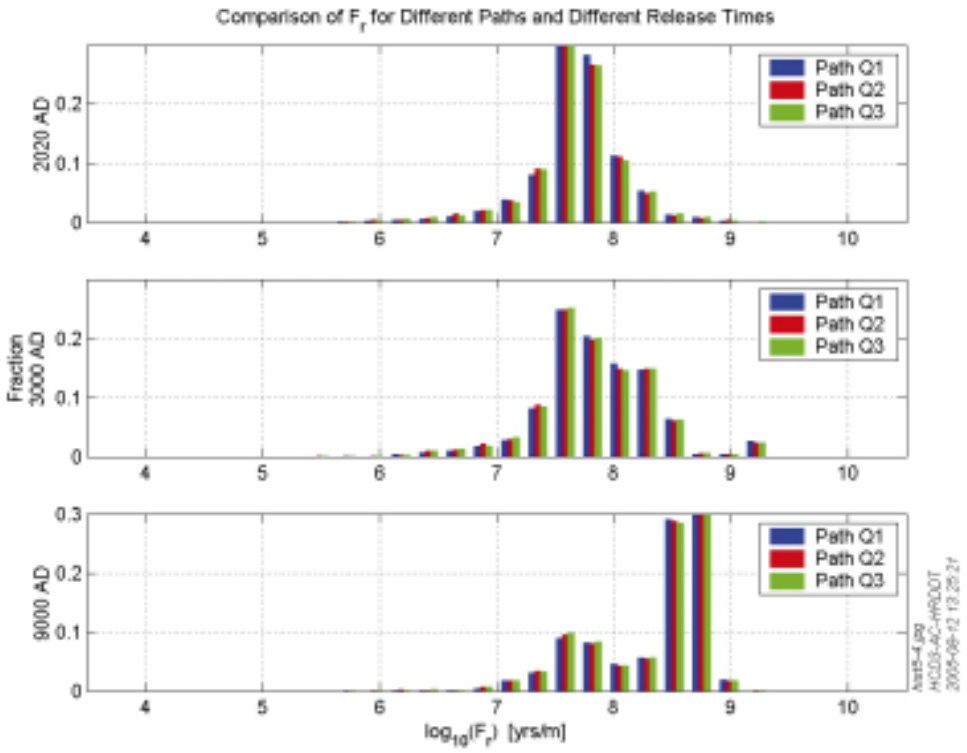

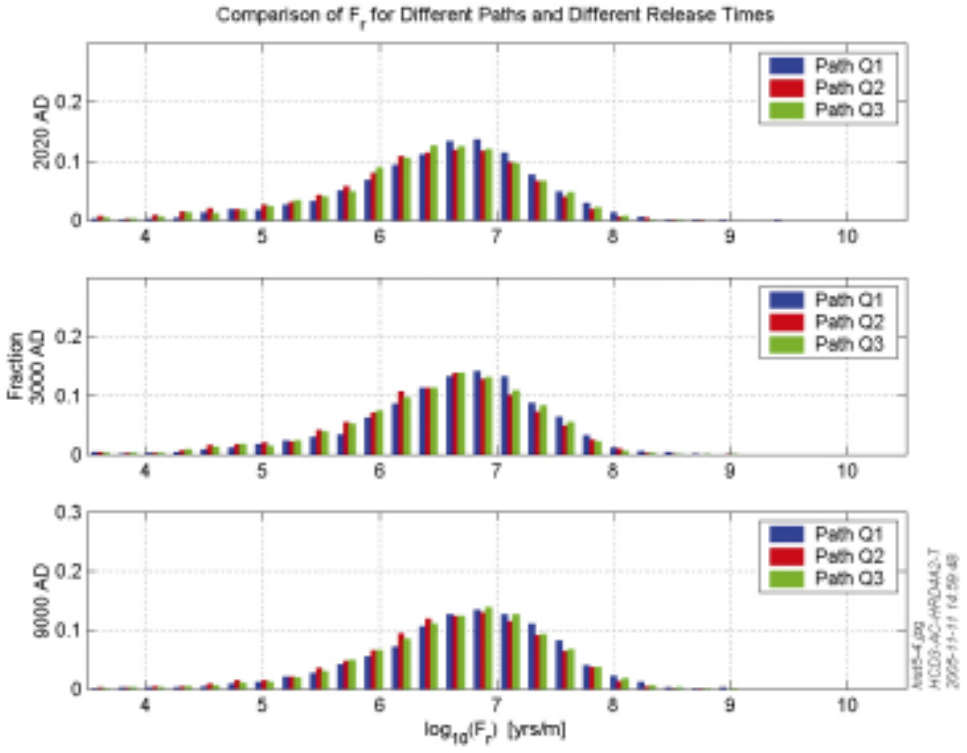

Figure 6-16, a and b. *Transport resistance in the rock (F-factor) for different paths and release times for a) CPM model and b) DFN model. Realistic case.*

Generally, the DFN representation is a worse scenario from a radionuclide transport perspective with the lower *F* values and higher initial Darcy velocities, but it does have some beneficial aspects too. For example, the DFN model predicts that there is advection away from the canister via a fracture that intersects the deposition hole for only about 40% of canisters, and of these only about 15% have a significant transmissivity (greater than 10^{-9} m^2/s). Similarly, there are stagnant flow conditions in parts of the EDZ and tunnel that amounts to about 40% of the canisters. Hence, for many canisters there is essentially no flow enabling radionuclides to escape.

Concerning the variants, the sensitivity to the backfill and EDZ properties is not great since the system of deposition tunnels is arranged orthogonal to the head gradient. Therefore flow tends to be limited by what the fracture system can supply and paths have to leave the tunnel or EDZ after relatively short distance to find a flow path to the surface through the fracture network.

The greatest sensitivities are observed in the DFN representation for the different transmissivity-length correlation models. For the semi-correlated and uncorrelated transmissivity DFN variants, the percentage of particles starting in stagnant flow areas increases to 67%–74% (compared to 60% for realistic case); however, in the non-stagnant areas, a higher percentage of deposition holes are connected to fractures of significant transmissivity (greater than 10^{-9} m^2/s), 18–20% compared to 15% in the realistic case. This is indicative of flow being more heterogeneous for the semi- and un-correlated variants with fewer advective pathways through the model. The semi-correlated and uncorrelated models also result in somewhat lower *F*-factors, see Figure 6-17, and may thus give moderately worse results than the correlated model in terms of input to radionuclide transport calculations. However, fewer particles escape to the surface for these cases. As discussed above, the uncorrelated case is not propagated to further radionuclide transport calculations.

The alternative nesting procedure, i.e. a local scale DFN model inside a regional scale ECPM, confirms that the paths calculated in the local-repository scale DFN/CPM model are representative, and that discharge areas are generally localised vertically above the site for present and future times. It also confirms that the local-repository scale DFN/CPM model gives a good estimate of transport resistance and path-length.

Results of regional scale analyses – Laxemar

Also for Laxemar a comprehensive set of sensitivities have been considered in the SR-Can application. A full list of the sensitivities considered and the variants used to quantify them are listed in Table 3-5 of /Hartley et al. 2006a/.

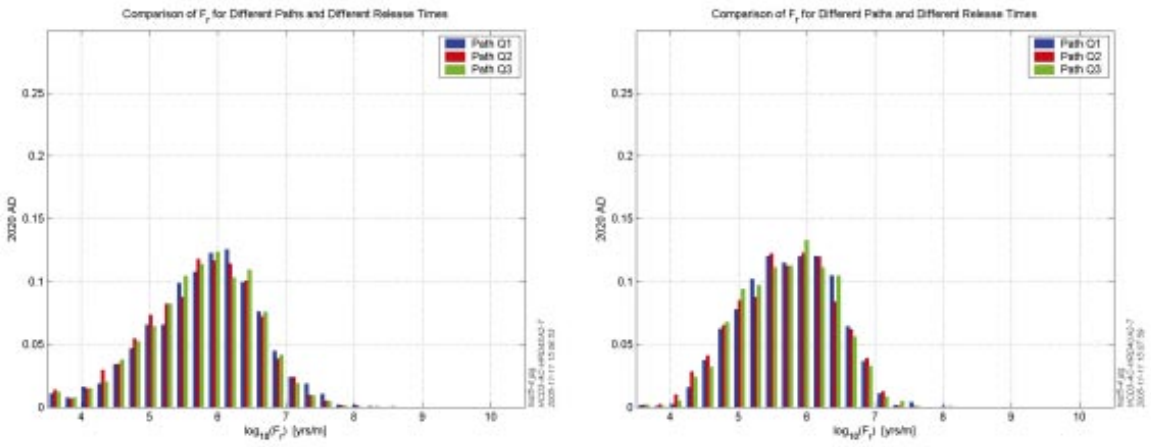

Figure 6-17, a and b. *Transport resistance in the rock (F-factor) for different paths and release times for a) DFN model with semi-correlated and b) uncorrelated transmissivity-length models.*

It was found that least favourable performance measures are found between about 2,000 BC and 1,000 BC. This time-frame coincides with that at which the coastline is directly above the starting positions. After the present-day, the performance measures are generally very constant. The only significant changes take place in the 20–30% of flow paths that discharge at the shoreline which slowly retreats in the future. Based on the evolution of performance measures and exit locations, 6,000 BC, 2,000 BC, 2,020 AD, and 6,000 AD were chosen as representative times to be used in the more detailed local-repository scale modelling.

Among the variants, one that stood out has a higher transmissivity in one of the sub-vertical sets giving greater heterogeneity than the reference case, since it gave the least favourable performance measures of the cases explored, although the predicted salinities for this case suggest it perhaps has implausibly high hydraulic conductivities. The variants with stochastic variability within the deformation zones gave a large spread in the results. Some performance measures in the simulations were worse than in the reference case, whereas the converse also occurred for these stochastic cases. However, when a large stochastic variability was used, unrealistic salinity profiles were predicted. More plausible variants are found when the standard deviation in transmissivity is around unity or less in log space. A variant with a correlated relationship between fracture transmissivity-size resulted in slightly worse performance measures than the reference case with a semi-correlated model. The case with low confidence deformation zones removed gave improved performance measures.

Results of local-repository scale analyses – Laxemar

The same approach as in Forsmark was adopted where the most important variants on the regional scale where propagated to the local-repository scale, but supplemented with cases describing the engineered system, i.e. the tunnel and EDZ.

In /Hartley et al. 2006b/ all cases on local-repository scale are analyzed in detail providing a full set of performance measures. However, large uncertainties are associated with the Laxemar SDM version 1.2; specifically, more recent data indicate that the rock properties within the potential repository volume are more favourable than those incorporated in the current model. Due to this limitation, a comprehensive consequence analysis incorporating radionuclide transport calculations for all variants is not deemed appropriate at this stage. Thus, only the reference case is considered for further analysis within SR-Can in conjunction with the cases with degraded properties of the backfill and EDZ.

First order evaluation of transport resistance

The transport resistance is also assessed using very simple back-of-the-envelope calculations. These are reported in the Preliminary Safety Evaluation (PSE) for Forsmark /SKB 2005b/. Below a short summary is provided.

Consider a fracture of transmissivity T. The flow over a width W is then given by $Q = W \cdot T \cdot grad(H)$, where $grad(H)$ is the hydraulic gradient. If flow is considered to be evenly distributed in the fracture, the transport resistance is given by:

$$F = 2WL/Q = 2WL/(WTgrad(H)) = 2L/(Tgrad(H)) \qquad \text{Equation 6.6.14}$$

i.e. in this case the transport resistance is independent of the width of the migration path. Assuming a gradient of 0.5 percent, which is certainly higher than found at the site at 400 m depth, and a migration distance of 100 m results in the transport resistances listed in Table 6-3.

The measured transmissivities at repository depth range between $3.9 \cdot 10^{-10}$ m^2/s and $2.2 \cdot 10^{-9}$ m^2/s /SKB, 2005b/. If these transmissivity values are typical, the transport resistance would be in the order of 10^6 yr/m to 10^7 yr/m. It is seen that these values are consistent with the estimates from the more elaborate modelling presented above.

Table 6-3. Transport resistance F for different fracture transmissivities assuming a gradient of 0.005 and 100 m migration length.

T (m^2/s)	F (s/m)	F (y/m)	Log_{10}(F) y/m
10^{-6}	$4 \cdot 10^{10}$	$1.3 \cdot 10^{3}$	3.1
10^{-7}	$4 \cdot 10^{11}$	$1.3 \cdot 10^{4}$	4.1
10^{-8}	$4 \cdot 10^{12}$	$1.3 \cdot 10^{5}$	5.1
10^{-9}	$4 \cdot 10^{13}$	$1.3 \cdot 10^{6}$	6.1
10^{-10}	$4 \cdot 10^{14}$	$1.3 \cdot 10^{7}$	7.1

Cases to propagate for radionuclide transport calculations – judgement by SR-Can team

Based on the analyses and findings presented above, the following Forsmark cases are suggested to be considered for subsequent radionuclide transport calculations:

- The so-called realistic DFN case, implemented on the repository-local scale, constitutes the main case for radionuclide transport calculations. The reasons for this choice are twofold; first, this representation provides block properties that are hydraulically consistent with measured values in the repository region, and second, the discrete nature of the representation provides flow paths that do not exhibit a likely over-emphasized lateral component, i.e. the model is not over-connected.
- The main variants to consider are the cases with increased backfill and/or EDZ permeability. Both cases are expected to provide similar results, so it may be sufficient to explore just one of these variants. In this case, the preference is the backfill case, since the EDZ case is considered less realistic (due to the assumed continuous properties).
- The realistic case with modified transmissivity-length correlation (semi-correlated) constitutes the next variant to consider. The motivation for this case is that it provides input to transport calculations that may affect results in dual fashion. On the one hand, the transport resistance is reduced, but on the other hand, the number of deposition holes being connected with a flow path to the surface is reduced.
- The final case to consider for the transport calculations is the continuum representation of the system. Also in this model the hydraulic block properties are reproduced; however, the lateral transport is deemed over-emphasized due to the connectivity in the model. Still, the model produces an alternative set of discharge points (further away from the repository, following the shore-line displacement) to the biosphere that need to be considered. For this case, it may also be of interest to address different release times since the discharge areas change with time. The transport resistance is also higher in this model relative to the models above.

In Table 6-4 below, the performance measure statistics for the realistic case are given as an example. For a full set of statistical results, the reader is referred to the Appendix of /Hartley et al. 2006a/.

In radionuclide transport calculations, the actual resulting distributions are used rather than the statistics in Table 6-4. In doing so, the inherent correlation between *F*-factor, advective travel and Darcy velocity are honoured since triplets rather than individual values are sampled (i.e. a triplet of *F*-factor, advective travel time and Darcy velocity for the same flow path is sampled).

For Laxemar, it is suggested that only the reference case as implemented on the local-repository scale and variants with degraded backfill and EDZ properties are propagated for further analyses. This is motivated by the low confidence in the Laxemar SDM version 1.2, see discussion above.

In Table 6-5 below, the performance measure statistics for the reference case are given as an example. For a full set of statistical results, the reader is referred to the Appendix of /Hartley et al. 2006b/.

It is emphasized that the judgment for only considering the reference case description of the geosphere is made at the consequence analysis stage of SR-Can. Both at the site-descriptive modelling stage and at the stage of implementation of the Site descriptive model for SR-Can applications, as described in /Hartley et al. 2006b/, all the variants are addressed without consideration of subsequent judgements.

Table 6-4. Distribution of $log_{10}(F_r)$ for each path Q1, Q2 and Q3 at different release times for the combined DFN/CPM repository scale model with lower transmissivity below ZFMNE00A2.

Log_{10}(Fr) (y/m)	2,020 AD			3,000 AD			9,000 AD		
	Q1	Q2	Q3	Q1	Q2	Q3	Q1	Q2	Q3
Mean	6.549	6.359	6.414	6.632	6.482	6.515	6.747	6.601	6.657
Median	6.647	6.475	6.506	6.722	6.575	6.623	6.819	6.682	6.738
5th percentile	5.025	4.649	4.853	5.188	4.940	4.997	5.386	5.162	5.283
10th percentile	5.522	5.182	5.305	5.607	5.443	5.485	5.759	5.590	5.684
25th percentile	6.112	5.893	5.975	6.219	6.045	6.083	6.326	6.162	6.215
75th percentile	7.077	6.968	6.978	7.146	7.023	7.063	7.268	7.142	7.173
90th percentile	7.465	7.340	7.374	7.523	7.420	7.419	7.619	7.521	7.555
95th percentile	7.707	7.551	7.573	7.710	7.615	7.599	7.845	7.726	7.754
Std deviation	0.794	0.856	0.813	0.767	0.794	0.780	0.750	0.776	0.758
Variance	0.631	0.733	0.662	0.588	0.631	0.608	0.563	0.603	0.575
Max value	9.371	8.719	8.451	8.686	9.055	9.045	8.971	8.660	8.976
Min value	3.372	3.218	3.041	3.427	3.024	3.051	3.658	2.923	2.903
Fraction OK	0.398	0.581	0.577	0.389	0.572	0.551	0.392	0.567	0.568

Table 6-5. Distribution of $log_{10}(F_r)$ for each path Q1, Q2 and Q3 at different release times for the combined DFN/CPM repository Laxemar model.

Log_{10}(Fr) [yrs/m]	6,000BC			2,000BC			2,020AD			6,000AD		
	Q1	Q2	Q3	Q1	Q2	Q3	Q1	Q2	Q3	Q1	Q2	Q3
Mean	6.133	5.979	6.014	5.622	5.440	5.521	5.655	5.463	5.541	5.679	5.495	5.573
Median	6.126	5.968	6.027	5.683	5.528	5.600	5.731	5.550	5.601	5.732	5.564	5.655
5th percentile	4.849	4.759	4.748	3.929	3.697	3.839	3.853	3.762	3.864	3.938	3.758	3.937
10th percentile	5.160	5.044	5.067	4.405	4.195	4.314	4.456	4.312	4.419	4.478	4.287	4.448
25th percentile	5.648	5.500	5.543	5.079	4.910	4.991	5.116	4.962	5.072	5.152	4.980	5.069
75th percentile	6.623	6.462	6.489	6.227	6.033	6.113	6.240	6.033	6.098	6.269	6.073	6.125
90th percentile	7.117	6.913	6.954	6.746	6.568	6.603	6.817	6.517	6.584	6.811	6.541	6.607
95th percentile	7.462	7.215	7.262	7.097	6.893	6.939	7.129	6.795	6.889	7.159	6.900	6.951
Std deviation	0.790	0.758	0.755	0.943	0.950	0.925	0.969	0.908	0.908	0.963	0.928	0.913
Variance	0.625	0.575	0.570	0.889	0.903	0.856	0.938	0.824	0.824	0.928	0.862	0.833
Max value	9.411	9.299	9.880	9.073	8.534	8.746	9.356	9.283	9.868	10.424	10.424	10.061
Min value	3.303	3.329	3.422	2.294	2.270	2.308	2.207	2.335	2.233	2.031	2.389	2.220
Fraction OK	0.479	0.714	0.751	0.511	0.742	0.791	0.524	0.768	0.806	0.474	0.694	0.723

6.7 Migration properties of the rock (non flow related)

Migration of solutes through fractured rock depends on several parameters. Some of these, such as the effective diffusivity, porosity, and sorption partitioning coefficients, are related to the rock matrix properties themselves, whereas others are closely related to the groundwater flow, i.e. are "flow related". This section evaluates the rock matrix related properties, whereas the flow related ones are discussed in subsection 6.6.8.

Sorption and diffusion properties may be highly site-specific, depending on the groundwater speciation and the geology of the site.

6.7.1 Modelling in SR-Can

Migration of dissolved radionuclides in the rock matrix occurs predominantly by diffusive transport, which is commonly modelled using Fick's laws. The diffusive transport will occur in the porewater that saturates the microporous system of rock at depth. Species will also, to different degrees, interact with the mineral surfaces surrounding the microporous system. Sorption of radionuclides in the far-field may be modelled using a linear relation (justified by a low radionuclide concentration) between sorbed species and solute concentrations. The proportionality coefficient is the sorption partitioning coefficient K_d (m^3/kg).

Both diffusion and sorption properties of the rock depend on a number of conditions, such as groundwater speciation, rock type, degree of fracturing, rock stress, etc. These conditions do not necessarily influence diffusion and sorption properties in the same manner. Many of the entities controlling radionuclide transport through the rock matrix are site-specific and conversion procedures of experimental data derived at other conditions may be necessary. At present, some of the site-specific conditions are unknown and therefore, the sorption and diffusion background data used are partly generic. However, care has been taken to use site-specific information when available.

Radionuclide migration through the far-field is in SR-Can mainly modelled by the transport simulation code FARF31 /Norman and Kjellbert 1990/. Other supporting models are ConnectFlow, DarcyTools, Chan3D, and FVFARF /Liu et al. 2006/. The modelling parameters that are used to describe migration in the rock matrix are the effective diffusivity D_e (m^2/s), the porosity ε (–), and the partitioning coefficient K_d. From these entities, the apparent diffusivity D_a (m^2/s) can be obtained.

$$D_a = \frac{D_e}{\varepsilon + K_d \rho_d} \qquad \text{Equation 6.7.1}$$

In this report D_e, ε, and K_d data have not been used to compile apparent diffusivities. The rational for this is to not lose valuable information from the two separate reports on matrix diffusion properties /Liu et al. 2006/ and sorption properties /Crawford et al. 2006/ and to be able to investigate the effect of each on the assessment results. For this reason, diffusion and sorption is from here on handled separately.

Furthermore, the connectivity of the porous system is an important parameter when modelling radionuclide retention /Liu et al. 2006/.

6.7.2 Sensitivity to assessment results

Sorption

An analysis on how retention in the far-field affects the radionuclide release to the biosphere can be found in SR 97 /Lindgren and Lindström 1999, SKB 1999ab/. In /Crawford et al. 2006/ no detailed sensitivity analysis has been made of the impact of K_d uncertainty in assessment calculations. However, it is pointed out that the retention of weakly and moderately sorbing nuclides, that have a transport time less than perhaps 0.1 to 5 half-lives, may be strongly

influenced by uncertainty in the K_d-value used in simulations. For strongly sorbing substances, that have transport times corresponding to some tens of half-lives, uncertainty in the actual K_d-value may not have a significant impact on far-field activity release. The same can be said for weakly or moderately sorbing substances that have sufficiently long transport times compared to their half-lives that their activity decays to negligible levels during transport to the biosphere.

Diffusion

By far the most important mechanism for retardation of radionuclide transport compared to the water movement is matrix diffusion. For sorbing radionuclides, interactions with mineral surfaces further dramatically enhance retardation /Liu et al. 2006/. An increased porosity and effective diffusivity will give rise to an increased retention. In a broader perspective, the tracer residence time depends also on "flow related" parameters that are discussed in subsection 6.5.8 of this report.

An identified entity that may influence the safety assessment is the pore connectivity, i.e. how far into the rock matrix from a water-bearing fracture the microporous system is connected /Liu et al. 2006/. The results from a number of experiments indicate that unaltered rock have a pore connectivity over at least several metres and possibly more.

In /Liu et al. 2006/, the presence of altered rock, as well as the rock heterogeneity is discussed. Around many fractures, alteration of the rock adjacent to the fracture has been observed. The extent of alteration can vary from practically nothing to millimetres and sometimes several centimetres. Commonly the altered rock has an increased porosity and diffusivity. This could enhance the uptake of nuclides into the matrix. However, as flow paths are not known in detail, it cannot be assured that these positive effects can be included in assessment calculations.

When it comes to the heterogeneity of rock, Liu et al. /Liu et al. 2006/ have observed that the variation in the diffusivity typically is larger for the smaller samples in the laboratory than for the larger samples in situ and draw the conclusion that the scale of the heterogeneity is on the same scale, or smaller, as that of the laboratory samples. This will lead to an extensive averaging along a flow path and thus, the variation of D_e and ε distributions will be much smaller on a scale applicable for assessment calculations. Here it should be clarified that even if an attempt is made to perform flow path averaging over assessment length scales in /Liu et al. 2006/, such averaged distributions are not given in the present report. The rational for this is to avoid the risk that delivered averaged distributions will be averaged once more in the subsequent modelling.

6.7.3 Source of information

Sorption

A designated data report assessing K_d-values for radionuclides in granitic rock has been prepared /Crawford et al. 2006/. Details about sources of information and how they were used are found there.

/Crawford et al. 2006/ have examined sorption data for a subgroup of nuclides in detail in order to provide updated estimates of K_d. This subgroup includes Ni(II), Sr(II), Cs (I), Ra(II), Th(IV), Np(IV,V), U(IV,V), and Am(III). Most of the data presented are derived from primary literature references in the form of journal articles and peer-reviewed conference proceedings. A smaller subset of data was only available in the form of secondary references (i.e. cited "second-hand" in other sorption compilations). Secondary references were largely obtained from the JNC sorption database /Shibutani et al. 1999/, although some data were also taken from the Nagra sorption database /Stenhouse 1995/.

Data for nuclides not covered by Crawford et al. /Crawford et al. 2006/ have been taken from the previous compilation of radionuclide sorption coefficients by /Carbol and Engkvist 1997/ which was used as supporting document for the SR 97 assessment. The data taken from /Carbol and Engkvist 1997/ have been adjusted in /Crawford et al. 2006/.

Little sorption data from the site investigations conducted by SKB are presently available and subsequently, mostly generic data have been used in /Crawford et al. 2006/.

Diffusion

A designated data report, /Liu et al. 2006/, assessing D_e- and ε-values in granitic rock has been prepared. Details about sources of information and how they were used are found there.

In /Liu et al. 2006/ both site-specific and generic data are presented. For D_e, both laboratory and in situ data are used. For ε, only laboratory data are used. D_e data are mainly presented in the form of formation factors F_f (–).

- For the Forsmark site, in situ and laboratory formation factors for the boreholes KFM01A and KFM02A have been taken from /Löfgren and Neretnieks 2005b/ and /Thunehed 2005/. The porosities for KFM01A, KFM02A, KFM03A, KFM04A, and KFM05A were supplied by Johan Byegård, Geosigma AB, Kungälv, Sweden. For further information concerning porosity measurements /Savukoski 2004abc/ and /Savukoski and Carlsson 2004a/ are referred to.
- For the Laxemar site, *in-situ* and laboratory formation factors for the borehole KLX02 have been taken from /Löfgren, 2001/. Porosities were taken from /Löfgren 2001/.
- For the Simpevarp site, in situ and laboratory formation factors for the boreholes KSH01A and KSH02 have been taken from /Löfgren and Neretnieks 2005a/. The porosities for KSH01A and KSH02 are tabulated in /Savukoski and Carlsson 2004b/ and /Carlsson 2004/, respectively.

Generic data, both for effective diffusivities (or formation factors) and porosities, were taken from the open literature, in the form of journal articles, peer-reviewed conference proceedings, theses and reports. Mainly data on granitic rock from Sweden, but also from Finland, the United Kingdom, and Switzerland, are used.

6.7.4 Conditions for which data are supplied

Sorption

In /Crawford et al. 2006/, the conditions that are deemed to be important for the K_d-values are listed as following: Water type; rock type; mineral surface area; redox state; radionuclide concentration.

- Water type: The sorption data in the literature are in /Crawford et al. 2006/, roughly categorised into two groups relating to the water composition (non-saline and saline). The limit for this classification is set to 500 mg/l Cl- (i.e. 0.014 mol/L). Most sorption experiments use synthetic groundwater with a pH within the range of 7–9. Carbonate concentrations are typically in the range 10–300 mg/l with a median of about 80 mg/l. The Kd-values given in this report consider the two main water types: non-saline and saline.
- Rock type: Crawford et al. /Crawford et al. 2006/ consider both the basic rock type (i.e. granite, granodiorite, etc) as well as any relevant descriptors that describe alteration and weathering. As there is a continuum of mineralogical compositions spanning different rock types, this introduces a taxonomic uncertainty in rock type identification. For this reason, Crawford et al. /Crawford et al. 2006/ do not attempt to strongly delineate different rock types, but treat them as indistinct property classes unless there are very clear differences apparent in the literature data. Rock is normally heterogeneous on a small scale. As most sorption data are typically derived from experiments using crushed rock samples consisting of perhaps 0.1–10 g, the variation between samples is high. In assessment modelling, where block sizes on the order of some tens of metres are considered, the potential stochastic variation on the block-scale is expected to be much reduced.

- Mineral surface area: The mineral surface area is thought to be a strong correlating parameter that appears to be more important than rock type for determining sorption properties. Owing to the paucity of data where surface area measurements have been made, Crawford et al. /Crawford et al. 2006/ have adopted the approach of presenting both K_d data, as well as K_a-data when available.
- Redox state: Redox conditions at repository depth are expected to be either strongly reducing, or oxidising at atmospheric intensity (dissolved $O_2 > 30\mu M$).. Owing to the rapid kinetics and on-off nature of aqueous redox states in deep groundwater, it is thought that these can also be handled efficiently in a conditional K_d framework. In /Crawford et al. 2006/, data are supplied for both oxidising and reducing conditions when appropriate.
- Radionuclide concentration: Certain radionuclides exhibit non-linear K_d behaviour down to very low concentrations. In these particular cases, Crawford et al. /Crawford et al. 2006/ have included the radionuclide concentration as a correlating parameter. Such non-linear concentration dependency is typically described by way of a Freundlich isotherm in the literature data. Owing to the empirical nature of Freundlich isotherm data, K_d-values should not be extrapolated too far outside the concentration range over which they were calculated.

Furthermore, temperature is described in /Crawford et al. 2006/ as only having a weak influence upon partitioning coefficients within the limited temperature range of interest and no attempt has been made to introduce temperature as a correlating parameter.

Diffusion

In /Liu et al. 2006/, the conditions that are deemed to be important for the effective diffusivity and/or porosity are listed as following: Rock type; rock type heterogeneity; fracture heterogeneity; groundwater chemistry; temperature; degree of alteration; rock stress.

- Rock type: Results from recent studies suggest that there may be a correlation between the rock type and the formation factor and porosity. Even though this correlation may be weak and rock type classification is not an absolutely clear-cut science, the rock type is deemed to be an important condition for both the formation factors and porosities presented in /Liu et al. 2006/. It is considered, in /Liu et al. 2006/, to be outside the scope of the report to present results for each single rock type identified within the site investigation program. Therefore, the site-specific formation factor and porosity distributions delivered include all rock types present at the site.
- Rock heterogeneity: Rock is heterogeneous on a small scale. Depending on the ratio between the scale of heterogeneity and the scale of the sample, the obtained results may differ. If the scale of the sample is on the same scale as the heterogeneity, it is more likely that "extreme" formation factors and porosities are obtained. If the scale of the sample is much larger than the scale of the heterogeneity, some averaging will occur and the variance of the parameter will be smaller. The sample size in the in situ formation factor measurements is on the order of 1 m^3 and the characteristic length (vertical resolution) of the measurements is about 0.1 m. The sample size in the laboratory porosity and formation factor measurements is on the order of 10^{-4} m^3 with the characteristic length (sample thickness) of about 0.03 m /Liu et al. 2006/.
- Fracture heterogeneity: The degree of fracturing relates both to advective and diffusive transport of solutes in fractured crystalline rock. The water flow is very unevenly distributed in the fractures. When there is very slowly flowing or even stagnant water in the fracture adjacent to more rapidly flowing water, solutes will diffuse into the stagnant water. The fracture characteristic that relates to advective transport is discussed in subsection 6.5.8. For the diffusive transport, fractures that hold stagnant water will increase the storage capacity of the rock matrix. Firstly, the porosity of the rock matrix is increased. Secondly, more rock matrix may be utilised for sorption and storage in the porewater, especially if limited pore connectivity is assumed. Therefore, the extent of which the fractures, holding stagnant water, are included in the rock matrix is an important condition both for the formation factor and porosity /Liu et al. 2006/.

For this reason two types of site-specific in situ formation factors are discussed in /Liu et al. 2006/; the rock matrix formation factor and the fractured rock formation factor. When obtaining the rock matrix formation factor, care has been taken to exclude all data that could be affected by water-bearing fractures. This formation factor thus represents the non-fractured rock matrix. When obtaining the fractured rock formation factor, care has been taken to exclude all data that could be affected by hydraulically conductive fractures detected in the site investigations. The fractured rock formation factor thus represents rock including fractures with stagnant water where no advective transport occurs. The laboratory porosities and formation factors have predominantly been obtained on non-fractured rock.

- Groundwater chemistry: For certain species, the matrix diffusivity may be changed by the groundwater chemistry, or more correctly by the porewater chemistry. For non-sorbing species this especially applies to anions, which are subjected to anion exclusion. The anion exclusion is more important in porewaters of low ionic strength than in porewaters of high ionic strength. For some sorbing cations, the diffusive flux through the rock matrix may be enhanced by diffusion in the electrical double layer. The flux may be more or less enhanced depending on the ionic strength of, and concentration of solute in, the porewater.

Due to the uncertainty induced by surface conduction in the in situ formation factor measurements, data have only been obtained where the electrical conductivity of the groundwater, at a corresponding depth, has been ≥ 0.5 S/m. Therefore, in situ formation factor data from the upper one or two hundred meters are not available. The site-specific laboratory formation factors are obtained using high ionic strength porewater (1.0 M NaCl).

Porosities are generally not affected by the groundwater chemistry /Liu et al. 2006/ unless dissolution or precipitation occur, which is conceivable adjacent to water-bearing fractures.

- Temperature: The effective diffusivity is to some extent dependent on the temperature. However, as the temperatures of interest range only over a few degrees, corrections due to the temperature would only influence the results in a minor way. The in situ results in /Liu et al. 2006/ are obtained at in situ temperature and the laboratory results are not corrected for temperature.

The porosity is generally not influenced by the temperature.

- Degree of alteration: The rock adjacent to water-bearing fractures could have been altered in different processes including hydrothermal alteration, metamorphism, and weathering. It is frequently reported that the rock in the alteration zone has a higher porosity and formation factor than the undisturbed rock. The diffusive properties of rock suggested in /Liu et al. 2006/ concern mainly unaltered rock at some distance from water-bearing fractures.
- Rock stress: In situ rock is subjected to stress that derives from the pressure of the overburden as well as from lateral stress induced by tectonic processes. The higher the rock stress, the more likely it is that the porous system is compressed /Liu et al. 2006/. Therefore, both the formation factor and the porosity are likely to be reduced in stressed rock compared to de-stressed rock. The in situ formation factors presented in /Liu et al. 2006/ are obtained in rock subjected to in situ stress while the laboratory formation factors and porosities are obtained on de-stressed rock.

6.7.5 Conceptual uncertainties

Input from experts

Sorption

According to /Crawford et al. 2006/ it is often presumed that mechanistic models that simulate ion exchange and surface complexation phenomena using fundamental principles of mass action, electrostatics, and aqueous speciation are reliable and accurate. For well-defined systems studied in a controlled laboratory environment this may be true. However, it is not currently possible to apply such models directly in transport simulation codes in a rigorous manner given the complexity of field conditions.

For the Swedish KBS-3 repository and projected environmental conditions it is thought that a K_d-based approach is sound and scientifically defensible in a broad sense, provided appropriate values are chosen for modelled repository conditions /Crawford et al. 2006/. Large changes in pH, for example, are not likely to occur in the natural barrier surrounding a KBS-3 type repository for spent nuclear fuel. At repository depth, there is the possibility of freshwater-saltwater intrusion and mixing events in the wake of glaciation periods. This can be handled in a conditional K_d framework. In a similar fashion, redox conditions at repository depth are expected to be either strongly reducing, or oxidising at atmospheric intensity. Owing to the rapid kinetics and on-off nature of aqueous redox states in deep groundwater, it is thought that these can also be handled efficiently in a conditional K_d framework. There is no reason at this point in time to suspect that the K_d methodology is unrealistic or non-conservative from a safety assessment perspective /Crawford et al. 2006/.

In /Crawford et al. 2006/, uncertainties are distinguished at the following levels:

- Uncertainty in the compiled *Kd*-data itself: This uncertainty relates to experimental errors and will be discussed in subsection 6.7.6 of the present report.
- Uncertainty related to the use of generic data in site-specific assessment calculations: This uncertainty relates to the need to use experimentally derived data in safety assessment applications where the conditions, such as groundwater speciation or rock type, may not exactly match the conditions under which the experimental data have been obtained.
- Uncertainty in the application conditions themselves: If there are significant uncertainties associated with the application conditions themselves, it is critical to take into account the conditional nature of the K_d-data. K_d-values chosen to be conservative under a given set of repository conditions can quickly become non-conservative if the porewater chemistry changes in such a way that the sorption of radionuclides is adversely affected. Additionally, K_d-data may not necessarily address issues related to variation of material properties along a flow path.

Crawford et al. /Crawford et al. 2006/ give the following general caveats on the use of conditional K_d data.

- A *Kd* based modelling approach is inappropriate when mechanisms other than ion exchange and surface complexation govern the radionuclide partitioning between the aqueous and solid phases. This may occur at concentrations much lower than that predicted by the solubility of pure mineral phases, owing to surface precipitation or co-precipitation phenomena.
- Given constant redox conditions, pH, and ionic strength over the considered temporal and spatial scales, a K_d based modelling approach, using appropriately selected conditional K_d-values, is applicable for describing sorption reactions. If the conditions vary, the response of sorption behaviour to changes in chemical and physicochemical conditions may need to be considered.
- In order to have as wide a range of applicability as possible, conditional K_d-values should be determined at conditions that mimic those in the field as closely as possible. This is particularly important with respect to redox condition, ionic strength, pH, colloids and the presence of ligands. If there are ligands or colloids present under in situ conditions that have not been considered in the formulation of synthetic groundwaters used for K_d-data acquisition, the "carrying capacity" of these substances may need to be estimated and the K_d-value adjusted to reflect this.
- For scenarios where radionuclide partitioning into the solid phase is considered to be reversible, a "conservative estimate" of the retention strength and capacity will possibly underestimate the load of radionuclides available upon remobilization. If an excessively low K_d-value (although conservatively estimated for retention) is used, for example, the actual amount of radionuclide that is remobilized may be subsequently underestimated.

Diffusion

Liu et al. /Liu et al. 2006/ did not find any conceptual uncertainties that could have a serious influence on the proposed data on the formation factor and porosity for use in safety assessment work.

Judgement by the SR-Can team

Sorption

The judgments made by /Crawford et al. 2006/ are accepted by the SR-Can team. Using the K_d approach is suggested to be appropriate for SA-modelling, even though there are issues involved when choosing appropriate data. Such issues are discussed in depth in /Crawford et al. 2006/. Crawford et al. /Crawford et al. 2006/ suggest that changes in groundwater chemistry, e.g. due to a freshwater-saltwater intrusion, can be handled by using conditional K_d-values. It is pointed out by the SR-Can team that this does not only require that one has to be able to foreseen such changes in groundwater chemistry. One also needs to have K_d values for all the foreseen conditions. In many cases, however, differences in groundwater chemistry parameters, such as ionic strength, do not affect the K_d greatly. In such cases it may suffice to know that the K_d does not change substantially over a range of reasonable groundwater chemistries.

Crawford et al. /Crawford et al. 2006/ suggest that there is a lack of applicability of mechanistic sorption models in granitic rock, due to its complexity. The SR-Can team supports this opinion but recognises that there is a debate within the scientific community on this issue.

Diffusion

The judgements made by Liu et al. /Liu et al. 2006/ are generally accepted by the SR-Can team. However, additional considerations are made:

In /Liu et al. 2006/ anion exclusion is mentioned as a phenomenon that excluded anions from accessing the region of the pore near the mineral surface, due to electrostatic interaction. This will reduce the diffusion available porosity of the rock matrix. However, it is not properly examined to what extent the available porosity is reduced for anions at different rock stresses. In the in situ formation factor measurements, which are based on electrical methods using alternating current, one can not separate a current propagated through the rock by cations and anions from a current propagated only by cations. As some anions are deemed to be troublesome in SR 97 e.g. /Lindgren and Lindström 1999/, this issue may deserve closer attention. In the few tracer tests carried out in situ e.g. /Birgersson and Neretnieks 1990/ or in the laboratory using an artificial rock stress /Skagius and Neretnieks 1986/ the anion iodide has been transported though the rock matrix without major influences from anion exclusion. Therefore, the data presented in /Liu et al. 2006/ are accepted.

Liu et al. /Liu et al. 2006/ suggest that a proper multicomponent mass transfer model should be used when translating the formation factor to effective diffusivity. At present it is widespread to use an improper binary mass transfer model for this purpose. The uncertainty in the effective diffusivity arising from this is subjectively set to be less than a factor of two in /Liu et al. 2006/. However, there is no estimate made of the uncertainty arising from not using a proper multicomponent mass transfer model when modelling radionuclide retention as a whole in a safety assessment.

6.7.6 Data uncertainty, spatial and temporal variation

Input from experts

Sorption

In /Crawford et al. 2006/, a number of data uncertainties that relate to experimental errors are discussed at length. Among these, the following are included: Random error, sample variability, systematic errors, methodological flaws, interpretation flaw, documentation flaws, and "frame shift" bias. Many of these errors give rise to an increased variability of the K_d-data. Some errors that relate to lack of knowledge and understanding of the system and to methodological flaws may give rise to a frame shift of the central value of the K_d-distribution.

Crawford et al. /Crawford et al. 2006/ suggest that there is good reason to believe that frame shifting is a real phenomenon and it has broad implications for the use of experimentally derived K_d-data in safety assessment applications. Some of these frame shift uncertainties are such that the central value of a variable could be shifted well outside the range of uncertainty as described by the probability density function. In /Crawford et al. 2006/ a number possibly frame shifting errors are deemed to be of importance.

- The foremost frame shift uncertainty of concern for sorption data relates to the fact that most sorption measurements are carried out on crushed rock. The experiment may be carried out with a single size fraction, or the crushed material may be sieved into different size fractions. Certain minerals of great importance for sorption, such as micas and clays, that are present in small amounts in most granitic rock, tend to occupy the lower end of the size distribution owing to their initially fine-grained nature.

An important effect of using crushed rock relates to the fact that in the crushing, new mineral surfaces are created that can provide additional sorption capacity. The additional surface area is a significant and serious source of bias that results in a substantial overestimation of K_d-values, particularly for moderately sorbing radionuclides. The main problem is that almost all the data in the literature are biased in this way. For some radionuclides, the "true" *Kd* appropriate for safety assessment modelling may lie outside the probability density function /Crawford et al. 2006/.

- Another source of frame shift concerns the fact that many times, sorption experiments are not carried out for long enough time periods to allow the system to equilibrate. This problem relates specifically to strongly sorbing species. For a radionuclide with $Kd \approx 1.0$ m^3/kg, the sorption may be underestimated by a factor of as much as 2.0–40 or more, if assuming a standard model of spherical diffusion, a contact time of one month, and an average particle size in the range 0.063–1.0 mm /Crawford et al. 2006/.
- Another uncertainty discussed in /Crawford et al. 2006/ is that it is not clear whether the sorption surface area of in situ rock at formation pressure is different to that in large pieces of de-stressed rock in the laboratory. Drill bit damage and subsequent sawing may also influence the sorption surface area in bore cores brought to the surface.
- The use of synthetic groundwater compositions is brought up as a source of bias in /Crawford et al. 2006/, owing to that very few experimental data have been derived using authentic groundwater samples. The K_d obtained using synthetic groundwater may be higher than that for authentic groundwater, owing to the absence of ligands such as humic and fulvic acids, as well as bacterial siderophores and colloids.

Concerning the spatial variability, Crawford et al. /Crawford et al. 2006/ suggest that variation of material properties along a transport flow path must be dealt with by some form of flow path averaging procedure. Most sorption data are derived from crushed rock samples where the total amount of solid may be on the order of 0.1–10 g. On a 30-metre block scale, the dissimilarity due to random mineralogical variation for lithologically comparable blocks could be as much as 10,000–100,000 times less than that of the original data uncertainty.

The application geochemical conditions, which are the future conditions that are predicted by modelling, may also have variability and uncertainty associated with them. These may be both spatial and temporal in nature. The impact that spatial variability will have upon the overall uncertainty at the block scale depends upon whether the geochemical conditions are conceptualised to vary locally over small scales or over larger scales. Local scale random variations tend to be evened out when averaged over the block, while large-scale variations may not. An additional complicating factor is that we may not know exactly how geochemical conditions will evolve over time. This is an additional epistemic uncertainty that is difficult to deal with in the framework of standard safety assessment codes /Crawford et al. 2006/.

Temporal variation over long time scales can be treated as a sequence of punctuated steady states in codes that, for example, model glacial rebound effects or post glacial intrusion scenarios. In these codes K_d-values can be chosen at run time to suit the prevailing conditions, although this may not always be strictly correct. Random temporal variations over short time scales should be dealt with using a PDF description of variability. Geochemical uncertainty over brief time scales and over short distance scales are epistemically similar and can be, in principle, dealt with in a similar fashion /Crawford et al. 2006/.

Diffusion

In /Liu et al. 2006/, different data uncertainties are discussed depending on whether the data are obtained in the laboratory or in situ. Uncertainties for laboratory data relate to the stress release and to the mechanical damage induced in excavation and sample preparation, when the sample is taken to the laboratory. Furthermore the uncertainties relate to the sample size in the laboratory. For both laboratory and in situ data, uncertainties relate to subjective sampling and to different properties of different tracers. For in situ data there is an additional uncertainty that relates to the approximation made that the in situ matrix porewater is in equilibrium with freely flowing groundwater at a corresponding depth.

When bringing a rock sample to the laboratory, the lithostatic pressure is released. In /Liu et al. 2006/ it is suggested that both laboratory porosities and formation factors may be overestimated several times, compared to those in situ, due to this stress release. Furthermore, it suggested that the porosity and formation factor obtained in the laboratory may be overestimated due to mechanical damage induced in the excavation and sample preparation. The porosity of a bore core sample could be overestimated by as much as a factor of two or more due to the excavation damage.

Uncertainties concerning the sample size in the laboratory relate to the fact that one may underestimate the tortuosity and constrictivity effects if using too short samples. Small samples also give a larger fraction of excavation damaged rock, which will lead to an overestimation of the formation factor and porosity /Liu et al. 2006/.

Uncertainties concerning subjective sampling relates from the fact that one often uses rock samples in the laboratory that are free of fractures and other unwanted features. Also in the in situ measurements, data points obtained in sparsely fractured rock may be overrepresented /Liu et al. 2006/.

Different species may have different effective diffusivities in the same rock. This gives rise to uncertainties, as the effective diffusivity is presented in the form of formation factor in /Liu et al. 2006/. Phenomena that are discussed are size exclusion, anion exclusion, and surface diffusion, where the two former decrease D_e and the latter increases D_e.

In the in situ formation factor measurements, the approximation is made that the in situ porewater is in equilibrium with freely flowing groundwater at a corresponding depth. The unknown porewater composition directly induces an uncertainty in the evaluation of the formation factor. This effect can be important if the porewater actually has a low salinity when it is assumed that it has a high salinity based on water extracted from nearby flowing fractures, or vice versa. Partly this can be remedied by measurements on the cores at the same locations.

The spatial variation of the formation factor is evident from the downhole measurements. Temporal variations are not expected to have a major influence on matrix diffusion or porosity /Liu et al. 2006/.

Judgement by the SR-Can team

Sorption

The judgements made by Crawford et al. /Crawford et al. 2006/ are accepted by the SR-Can team. An extensive job has been made to identify sources of data uncertainties in /Crawford et al. 2006/. Many of the sources of uncertainties identified may be significantly reduced when using site-specific data that are obtained with a carefully planned and well thought through methodology.

Diffusion

The judgements made by Liu et al. /Liu et al. 2006/ are accepted by the SR-Can team. However, concerning the uncertainties introduced in the in situ formation factor measurements, it is important to further justify the assumption that data obtained on freely flowing groundwater adequately represents that of the porewater. Furthermore, there may be a need to further investigate how anion exclusion is affected by the in situ stress situation.

6.7.7 Correlations

Input from experts

Sorption

In /Crawford et al. 2006/, two core groups of correlated parameters are identified:

correlations between major groundwater species

correlations in the sorption of chemically related radionuclides

The correlation between major species in groundwater is important when reducing the number of conditional K_d-values needed in a safety assessment. Such correlations may be used if extrapolating K_d-data to other, but similar, conditions. Furthermore, considerations of correlations between groundwater species could be of great importance for the application of mechanistic models for K_d predictions under site-specific conditions.

There are a number of specific correlations between chemically related radionuclides. Some of these relate to direct similarities in sorption behaviour while others relate to the way in which the sorption of certain radionuclides responds to speciation effects etc. This was considered previously in /Ochs and Talerico 2004/ and the main aspects are repeated in /Crawford et al. 2006/. Certain radionuclides share chemical similarities that enable them, in varying degrees, to be used interchangeably as sorption "analogues" for each other. This is useful for estimating sorption properties where there are gaps in the literature data, or for combining data sets from closely related radionuclides to obtain a more detailed picture of variability. Analogous radionuclides can be grouped into a number of categories where group members have similar sorption characteristics. Some of these are (excluding non-sorbing species):

1. Alkali elements: Cs, K, Na, Rb
2. Alkaline earth elements: Ba, Ra, Sr
3. Divalent transition elements: Cd, Co, Ni, Pb, Pd
4. Trivalent elements: Ac, Am, Ce, Cm, Eu, Ho, Pu(III), Pm, Sm
5. Tetravalent elements: Np(IV), Pa(IV), Pu(IV), Sn, Th, U(IV), Zr
6. Pentavalent elements: Nb, Np(V), Pa(V), Pu(V)
7. Hexavalent elements: Pu(VI), U(VI)

Not all of the analogies listed above are very good and there can be some deviation between individual members in the groups listed above. Although, having roughly the same chemistry, many of them have sufficiently dissimilar hydrolysis and stability constants for complexation that there can be significant uncertainty concerning their "analogous" behaviour /Crawford et al. 2006/.

Diffusion

Porosity and matrix diffusion are mainly positively correlated but variations are very large. Correlations are expected between rock stress and porosity as well as rock stress and matrix diffusion. These correlations are not properly quantified, although higher stress decreases matrix porosity and formation factors /Liu et al. 2006/.

Judgement by the SR-Can team

Sorption

The judgements made by Crawford et al. /Crawford et al. 2006/ are accepted by the SR-Can team. Although it is deemed as acceptable to use the suggested correlations, it should be noted that Crawford et al. /Crawford et al. 2006/ caution that there are uncertainties introduced in using them.

Diffusion

Except for the fact that the formation factor and effective diffusivity is directly correlated, no other correlations could be quantified by Liu et al. /Liu et al. 2006/. It is common to correlate the porosity and formation factor through Archie's law. However, the applicability of Archie's law in granitic rock has recently been questioned /e.g Löfgren 2004/ and the SR-Can team suggest that it should not be generally used without further justification.

6.7.8 Quantification

Input from experts

Sorption

Crawford et al. /Crawford et al. 2006/ have examined sorption data for a subgroup of nuclides in detail in order to provide updated estimates of K_d. This subgroup includes Ni(II), Sr(II), Cs (I), Ra(II), Th(IV), Np(IV,V), U(IV,V), and Am(III). Data for nuclides that /Crawford et al. 2006/ have not examined in detail have been taken from /Carbol and Engkvist 1997/.

According to /Crawford et al. 2006/ the data reported for most solutes reflect a broad range of experimental conditions, which tends to give large scatter in the aggregate data set. Major factors influencing this variability are choices of water composition, spike concentration, liquid/solid ratio, rock type, particle size, and contact time. The partitioning coefficients measured for certain solutes may also be influenced by choice of phase separation technique (e.g. centrifugation, filtration, etc). Some data sets may be heavily biased by the way in which data has been reported as some experimenters report mean values (occasionally also with error estimates), some report ranges, while others report values given as less than (<) or greater than (>) a given value. Owing to the generally poor quality of the data and confounding factors, no robust statistical analysis has been attempted to provide non-biased best estimates of the data distributions.

As the compiled data are based upon reported data from literature sources it is also difficult to establish rigorously whether the measured data represent true sorption processes or precipitation/co-precipitation phenomena. The high end of the ranges (i.e. $K_d \geq 1$) given for some of the strongly sorbing nuclides, (particularly in the case of redox sensitive solutes) should therefore be treated with some caution.

In addition to scatter in the experimental data, there is strong evidence to suggest that the use of crushed material may give results that systematically overestimate in situ K_d-values by at least an order of magnitude and possibly more for sorbing species. For this reason, the recommended data presented are reduced by a factor of 10 relative to the raw data used as a basis for the statistical analyses. For consistency, the same correction factor is used for solutes taken from /Carbol and Engkvist 1997/.

For strongly sorbing species, disequilibrium effects arising due to short contact times may potentially give underestimated in situ K_d-values. However, as the mechanistic basis for this effect is unclear, it has not been accounted for in /Crawford et al. 2006/.

The outcome of /Crawford et al. 2006/ is K_d-values at saline or non-saline groundwater conditions. Data derivation and assessment of uncertainties were carried out in the following steps:

- Step 1: A radionuclide was selected.
- Step 2: A water type was selected. This step includes a selection from the two main water types non-saline and saline. In this step the pH range is also defined (pH 7–9), as well as whether there is strongly reducing conditions or oxidising conditions at atmospheric intensity.
- Step 3: From the detailed information gathered, rock types that are most appropriate for Simpevarp, Laxemar or Forsmark were selected.
- Step 4: Preference was given to experimental data that were best documented and had longest contact times.

R_d-values were corrected for the increased surface area due to crushing by a multiplying factor *f*cr. At present Crawford et al. /Crawford et al. 2006/ use *f*cr = 0.1, which is based upon approximately known data for generic rock types as well as data from the ongoing site investigations. In measurements from the Laxemar site investigation the BET area was about one order of magnitude larger for the smallest size fractions compared to the larger (Figure 6-18).

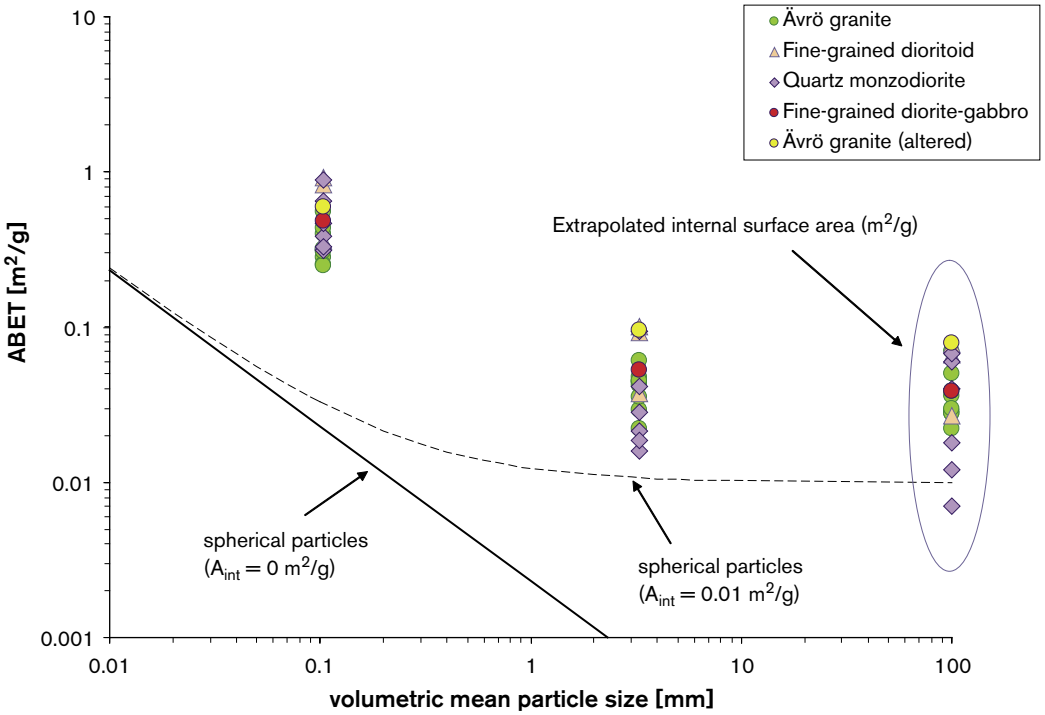

Figure 6-18. *BET surface area for different size fractions. Taken from /Crawford et al. 2006/.*

Crawford et al. /Crawford et al. 2006/ suggest that there may be a need to perform other corrections. The additional correction factors mentioned are:

- f_{ls} that should correct for the fact that some mineral surfaces may be less accessible in situ, comparing to the laboratory, due to the higher in situ stress
- f_{eq} that should correct for the fact that larger experimental K_d-values may be obtained if the experiments run for a longer period of time, allowing for better equilibration
- f_{chem} that should correct for deviations in experimental K_d-values originating in the fact that synthetic groundwater has been used in the experiments.

Crawford et al. /Crawford et al. 2006/ choose not to give numerical values for such correction factors, due to the present lack of knowledge on the subject.

- Step 5: A statistical analysis of the data set was made for each species. The median K_d-value of the data set was given, This K_d is noted as $K_{d,BE}$ (best estimate). Two sets of upper and lower limits were used in the statistical analysis. The first set of limits represent the 25% and 75% quartiles of the data set. The K_d-values at these limits are noted as $K_{d,25\%}$ and $K_{d,75\%}$, respectively. The *F*-range, bound by the other set of limits, comprises roughly 99% of the data set, with the underlying assumption that the data set is normally distributed. The Kd-values at these limits are noted as the $K_{d,low}$ and $K_{d,high}$. In addition to setting these limits, and attempt was made to investigate the distribution of each species. In most cases the data set did not appear to follow any well-defined distribution. Figure 6-19 shows two examples of data set histograms obtained by Crawford et al. /Crawford et al. 2006/.

The upper histogram in Figure 6-19 is based on the data set for Am(III). It is suggested in /Crawford et al. 2006/ that the data set might be log-normally distributed. However, due to the poor quality of the data set and the possibility of bias it is not possible to conclude that K_d-values for Am(III) generally are log-normally distributed. The lower histogram in Figure 6-19 is based on the data set for Ni(II), which do not follow any well-defined distribution.

The sorption data presented by Crawford et al. /Crawford et al. 2006/ are compiled in Table A-40–Table A-42 in Appendix A10.

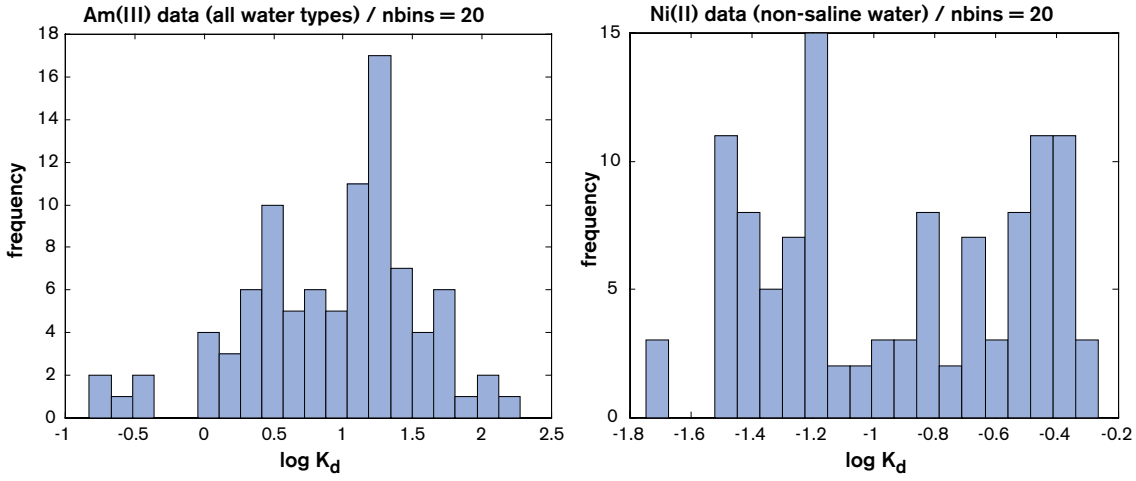

Figure 6-19. *Sorption data set histograms for upper image: Am(III), lower image: Ni(II). Images taken from /Crawford et al. 2006/*

Diffusion

Liu et al. /Liu et al. 2006/ have examined formation factor data and porosity data. Both site-specific data and generic data are presented, where the generic data have the function of validating the magnitude of the site-specific data. Regarding the site-specific data, both laboratory and in situ formation factors have been compiled, while all porosities were obtained in the laboratory. Data derivation and assessment of uncertainties were carried out in the following steps:

- Step 1: The parameter, Ff or ε, was selected.
- Step 2: The site, Forsmark, Simpevarp, or Laxemar, was selected.
- Step 3: The conditions were selected.

Site-specific formation factors were obtained from all depths and from all boreholes available at a site. All rock types present were included. For the laboratory data, no data were excluded on the basis of sample heterogeneity, even if subjective sampling may have excluded heterogeneities in an earlier stage. For the in situ data, rock matrix formation factors were used, where data adjacent to any fracture were excluded. Due to this, data from altered rock is most likely underrepresented. In situ data were taken from all depths with their corresponding groundwater composition, with the exception of the upper few hundred meters, where the electrical conductivity of the groundwater was lower than 0.5 S/m. Laboratory data were obtained at atmospheric pressure while in situ data were obtained at all present in situ rock stresses.

The sample size in the laboratory was on the order of 10^{-4} m^3 with the characteristic length of about 0.03 m. The in situ sample size was on the order of 1 m^3 with the characteristic length of about 0.1 m /Liu et al. 2006/.

Site-specific porosities were obtained from all depths and from all boreholes available at a site. All rock types present were included, with the exception of strongly altered samples in Forsmark. No data were excluded on the basis of sample heterogeneity, even if subjective sampling may have excluded heterogeneities in an earlier stage. The sample size was on the order of 10^{-4} m^3 with the characteristic length of about 0.03 m /Liu et al. 2006/.

- Step 4: In situ data were separated from laboratory data.
- Step 5: Site-specific in situ and laboratory formation factor distributions were obtained. Site-specific laboratory porosity distributions were obtained.
- Step 6: Liu et al. /Liu et al. 2006/ make the recommendation to use in situ formation factors distributions over laboratory formation factors distributions for SA-modelling. The in situ data need no correction. The log-normal distribution was recommended. Logarithmic and arithmetic mean values and standard deviations were obtained for the distributions. As an example, a histogram of in situ formation factors obtained in the borehole KFM02A, together with the best fitted log-normal distribution, is shown in Figure 6-20.

It was recommended to use laboratory porosity distributions for assessment modelling. A correction for the fact that the laboratory rock samples are de-stressed in the laboratory was made. All obtained porosities were divided by a factor of 2.5. The log-normal distribution was used. Logarithmic and arithmetic mean values and standard deviations were obtained for the distributions.

- Step 7: It was investigated to what extent varying the conditions may affect the recommended values. Major rock types were found to have comparable formation factor distributions. The strongly altered rock examined had a significantly increased formation factor. In situ formation factors distributions obtained at different depths (rock stresses) did not differ significantly. By performing statistical analyses on the rock type 101057 (granite to granodiorite, metamorphic, medium-grained) from several 100 long sections in KMF01A, mean values and standard deviations of the logarithm of the formation factor were obtained. In Figure 6-21, the obtained mean values and standard deviations are shown against borehole length (centre of section). The laboratory samples were taken from the entire borehole but measured on at atmospheric pressure at the surface. They are therefore lumped into one distribution at the depth zero.

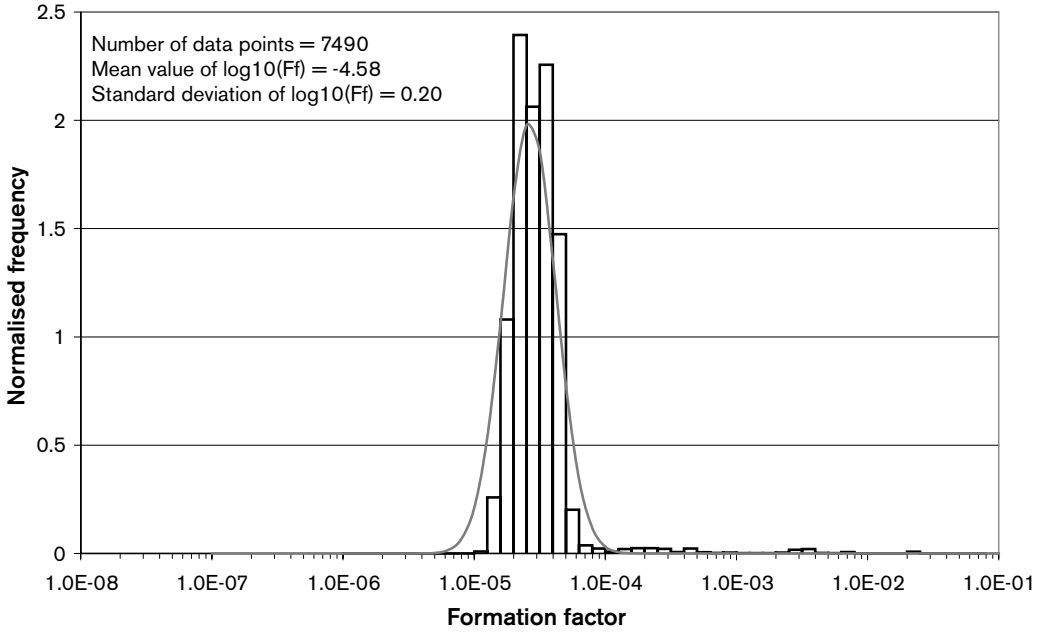

Figure 6-20. *Example of formation factor probability distribution. Image taken from /Liu et al. 2006/.*

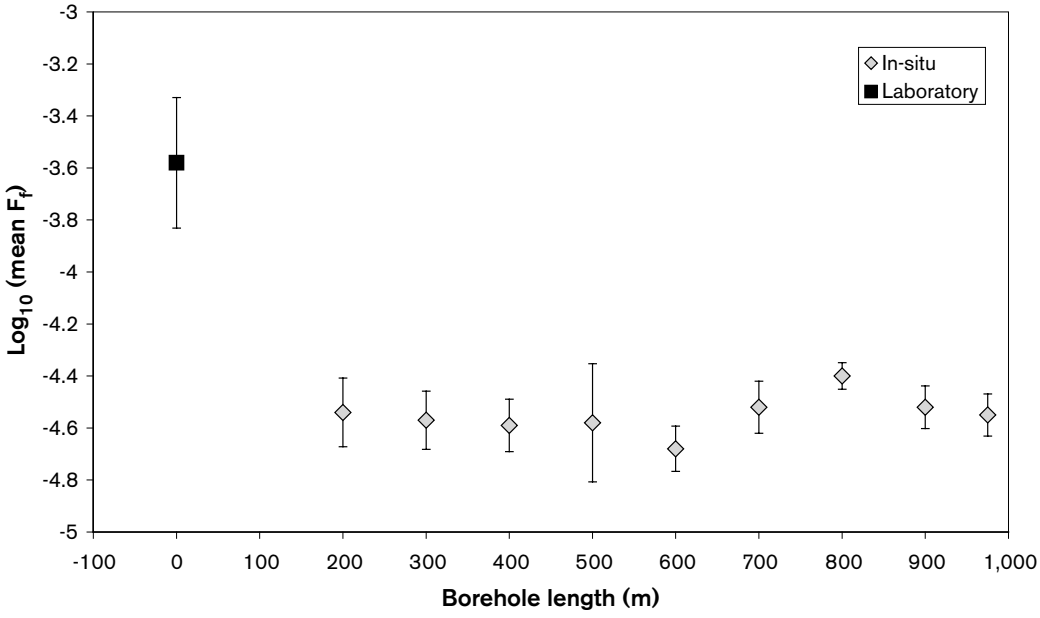

Figure 6-21. *Formation factor against borehole depth in KFM01A. Image taken from /Liu et al. 2006/.*

The arithmetic mean value for the fractured rock formation factor was found to be about a factor of two larger than that of the rock matrix formation factor. Thus, using the rock matrix formation factor may be overly conservative. The rock heterogeneity was found to be on the same or on a smaller scale as that of the laboratory samples. As a result of this, the variability of the formation factor distributions obtained in the laboratory was larger than those obtained in situ. Figure 6-22 shows a suggested decrease in variability with characteristic length of sample. The data are taken from Simpevarp. The variabilities for respective characteristic length of the samples use in the laboratory (0.03 m) and *in-situ* (0.1 m) are marked with diamonds.

In /Liu et al. 2006/ it is urged not to take Figure 6-22 too quantitatively. There seems to be a need for more investigations on how the rock heterogeneity affects the results.

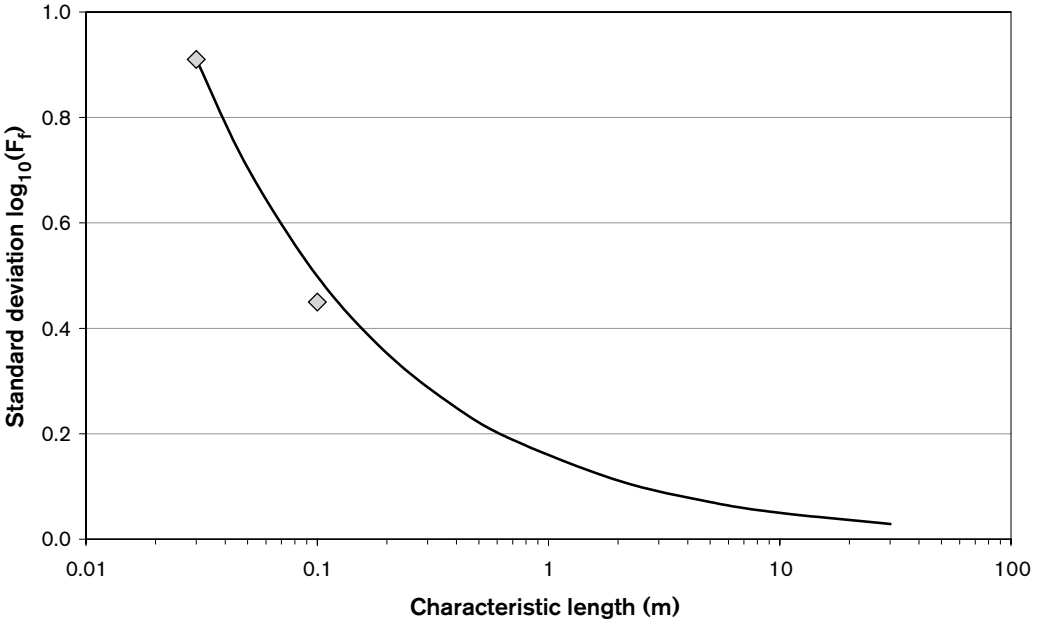

Figure 6-22. *Variability in formation factor distribution vs sample size (extrapolated beyond 0.1 m). Image taken from /Liu et al. 2006/.*

- Step 8: A table of diffusivities in free solution for a number of species /Ohlsson and Neretnieks 1997/ was given. These can be multiplied by the suggested formation factors to obtain effective diffusivities.

The diffusion and porosity data presented by Liu et al. /Liu et al. 2006/ are compiled in Table A-40–Table A-42. On the issue of pore connectivity Liu et al. /Liu et al. 2006/ suggest that the microporous system of the rock matrix is connected over all scales relevant for the safety assessment.

Judgement by the SR-Can team

Sorption

The judgements made by Crawford et al. /Crawford et al. 2006/ are generally accepted by the SR-Can team. However, additional considerations are made:

The concept of correcting sorption data by introducing the correction factors f_{cr} and f_{ls} is conceptually interesting. Although the correction factors seem reasonable, there may be need for future work in order to more accurately assess their numerical values. It is judged by the SR-Can team that the correction factor system used in /Crawford et al. 2006/ is conservative and acceptable.

In /Crawford et al. 2006/ frame shift errors are discussed. It is stated that "some of these uncertainties are such that the central value of a variable is shifted well outside the range of uncertainty as described by the PDF", where PDF is the probability density function. Still such frame shift errors may not necessarily be adequately handled by multiplying correction factors only. Some of the frame shift errors could possibly be handled by e.g. addition or subtraction. Furthermore, the underlying mechanisms for these proposed frame shift errors may need to be more properly evaluated in future work, as well as discussed within the scientific community.

The sets of upper and lower limits for the suggested K_d-values are based on statistical analyses. However, before making the analyses a number of data points were sorted out, potentially on subjective grounds. In addition, the obtained distributions may be biased if the data sets comprise more data points from one experiment than from another. Using a proper experimental methodology in obtaining the sorption partitioning coefficients would facilitate the sorting process and makes it less subjective.

In /Crawford et al. 2006/ it is suggested that the experimental errors may be large compared to the natural variability of the sorption partitioning coefficient. However, if that is the case, also the central (best estimate) value chosen could depend more on the experimental methodology used than on sorption properties of the system. The central value may then need to be more properly evaluated. The SR-Can team suggests that subsequent users of the sorption data presented in this report use them as "best estimates", until further methodical evaluation of site-specific data has been carried out within the SKB site investigation program.

Concerning a possible reduction of available surface area for in situ sorption, due to increased stress comparing to the laboratory, Crawford et al. /Crawford et al. 2006/ choose not to quantify such a reduction factor. It is judged by the SR-Can team as most likely that this effect do not exceed the effect of stress on porosity. The factor suggested by the SR-Can team for reducing laboratory to in situ porosities is 2.5.

Crawford et al. /Crawford et al. 2006/ deliver, for each species investigated, five K_d-values: $K_{d,low}$, $K_{d,25\%}$, $K_{d,BE}$, $K_{d,75\%}$, and $K_{d,high}$. Due to the poor quality of the underlying data sets, assigning K_d distribution is a somewhat subjective task. It was judged that assigning log-normal K_d-distributions could not be justified. The rational for this is that if using such a well defined distribution, one may be given the impression that we know more about the natural variation of K_d than we actually do. Two other distributions discussed within the SR-Can team were rectangular distributions, either ranging from $K_{d,low}$ to $K_{d,high}$ or from $K_{d,25\%}$, to $K_{d,75\%}$ (Figure 6-23 a and b). The rational for not using either of these distributions was that the former give to much weight to the low K_d-values and the latter to little weight.

Another distribution discussed was the triangular distribution (Figure 6-23c). However, even though the median value of a K_d-data set was known, the median value would not necessarily represent the central value of the K_d-distribution. Hybrids of the former distributions are presented graphical in Figure 6-23 (d and e). In the discussions, it could not be judged which of these hybrids would represent the data sets, as well as present knowledge of the entity, best.

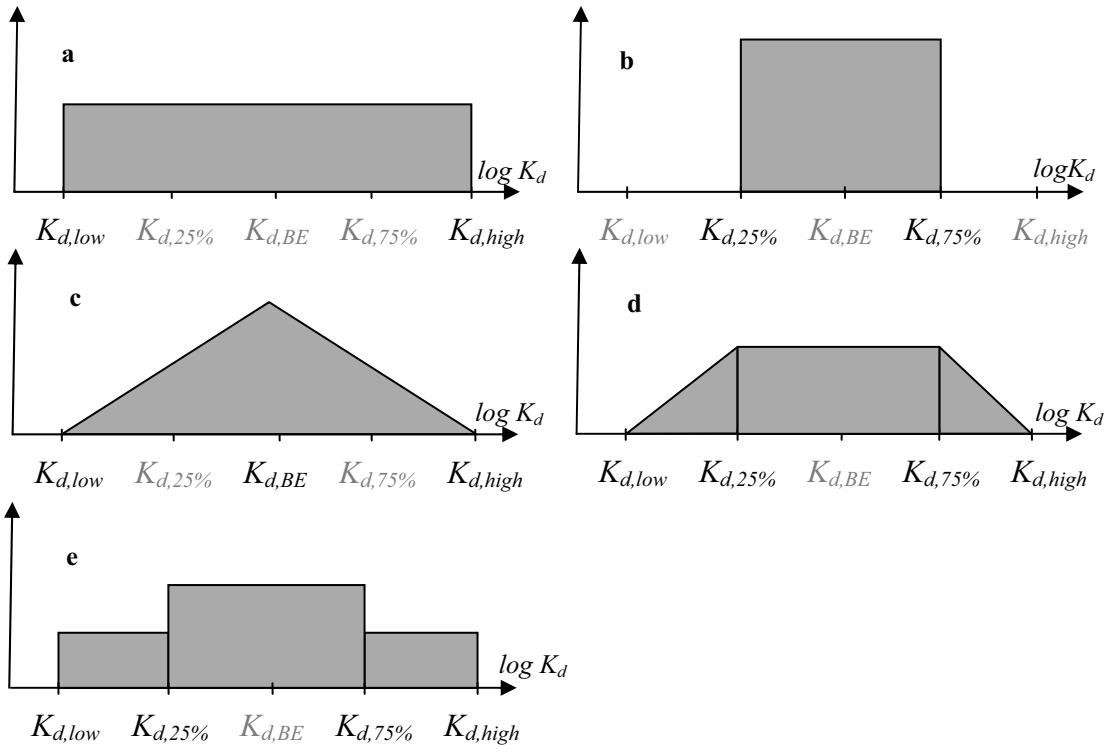

Figure 6-23. *Different distributions discussed. Values in grey on x-axes are not used.*

Finally it was judged to use the piecewise uniform distribution (Figure 6-23c), as it is easier to describe mathematically. In the recommended distribution, the centre piece should hold 50% of the area while the other pieces should hold 25% each, as the K_d-values ($K_{d,low}$, $K_{d,25\%}$, $K_{d,BE}$, $K_{d,75\%}$, and $K_{d,high}$) are set symmetrically. The suggested K_d-values can be found in Table A-43.

For the K_d-data based on /Carbol and Engkvist 1997/, but modified in /Crawford et al. 2006/, a triangular distribution is suggested by the SR-Can team. The suggested K_d-values can be found in Table A-44.

In Table A-44, no lower value is given for Sn(IV). This presents a problem when making a distribution in log-space. For this reason, a lower K_d-value of $1.2 \cdot 10^{-7}$ m^3/kg can be used for the distribution. This value is 10% of the storage capacity of the rock due to the porosity, using the porosity 0.003 and dry density 2,600 kg/m^3.

Diffusion

The judgements made by Liu et al. /Liu et al. 2006/ are accepted by the SR-Can team. However, additional considerations are made:

In /Liu et al. 2006/ an attempt to average the porosity and formation factor along a flow path is made. However, to avoid the risk that the delivered flow path averaged distributions will be averaged once more in the subsequent modelling, this step has been disregarded by the SR-Can team. Liu et al. /Liu et al. 2006/ make an interesting attempt to show how the natural variability of the formation factor varies with sample size. Based on this reasoning the variability is reduced to values of minor significance on the block scale used in hydro modelling. However, the authors themselves urge the readers not to take the reasoning too quantitatively. Therefore, the SR-Can team has chosen to use the variability obtained in situ for the formation factor and in the laboratory for the porosity.

In /Liu et al. 2006/ effective diffusivities are obtained by multiplying the given formation factors by the diffusivity of species in free solution. No quantitative information on possible corrections needed in this operation, due to e.g. anion exclusion, is given. With exception for anions exclusion, corrections for such effects are judged to be minor by the SR-Can team, and the method of obtaining effective diffusivities is accepted.

In the SR 97 safety assessment it was suggested to reduce the effective diffusivity for anions by a factor of 10 /Andersson 1999/. In the light of recent electrical conductivity measurements in the laboratory, this factor may seem to be too large. If comparing formation factors obtained in through diffusion experiments using anions with those obtained by electrical conductivity methods, where both anions and cations propagate the current, they are in general only a factor of about two smaller. However, as there is a lack of knowledge on e.g. how in situ stress affect anion exclusion, the reduction factor of 10 for anions suggested in the SR 97 safety assessment is also suggested for SR-Can.

The SR-Can team judge that porosities suggested by /Liu et al. 2006/ are acceptable for all solutes, including anions.

In /Liu et al. 2006/ it is suggested that the porous system of the rock matrix is connected over all scales relevant for a safety assessment. However, no maximum penetration depth for solutes diffusing into the rock matrix is given. It is suggested by the SR-Can team that the central value of the maximum penetration depth should be based on half the spacing of hydraulically conductive fractures. It is suggested in subsection 6.5.8 that the typical spacing between two hydraulically conductive fractures should be set to 10 m, without further uncertainty, for all sites.

Furthermore, it is suggested that the lower value of the maximum penetration depth is based on the conceivable possibility that some small fraction of the rock mass has a porous system with limited pore connectivity. Basing the lower value for the maximum penetration depth on the

concept of limited pore connectivity may be over-conservative, as limited pore connectivity has not been properly substantiated. It also presents a problem when choosing a representative value for the limited pore connectivity. The bore core pieces that are taken to the laboratory for measuring the formation factor within the SKB site investigation program have a length of 3 cm. On that scale, they all demonstrate a connected porous network /e.g. Löfgren and Neretnieks 2005b/. It is argued by the SR-Can team that the lower value for the maximum penetration depth should not be set to lower than 3 cm. Without further justification, it is suggested by the SR-Can team to use a triangular distribution in the normal space with 3 cm as the lower value and 10 m as both the peak and the upper value for the maximum penetration depth at all sites.

7 References

Aaaltonen P, Varis P, 1993. Long term corrosion tests of OFHC-coppers in simulated repository conditions – Final report. YJT-93-05, Nuclear Waste Commission of Finnish Power Companies.

Ageskog L, Jansson P, 1999. Heat propagation in and around the deep repository. Thermal calculations applied to three hypothetical sites: Aberg, Beberg and Ceberg. SKB TR-99-02, Svensk Kärnbränslehantering AB.

Allègre C J, Le Mouel J L, Provost A, 1982. Scaling rules in rock fracture and possible implications for earthquake prediction. Nature (London) 297(5861): 47–49.

Andersson C-G, Andersson M, Erixon B, Björkegren L-E, Dillström P, Minnebo P, Nilsson K-F, Nilsson F, 2005. Probabilistic analysis and material characterisation of canister insert for spent nuclear fuel. Summary report. SKB TR-05-17 Svensk Kärnbränslehantering AB.

Andersson J, 1999. SR 97 – Data and data uncertainties. Compilation of data and data uncertainties for radionuclide transport calculations. SKB TR-99-09, Svensk Kärnbränslehantering AB.

Auqué Sanz L F, Gimeno Serrano M J, Gómez Jiménez J B, Puigdomenech I, Smellie J, Tullborg E-L, 2006. Modelling of groundwater chemistry over a glacial cycle. Background data for SR-Can. SKB TR-06-31, Svensk Kärnbränslehantering AB.

Avila R, Bergström U, 2006. Methodology for calculation of doses to man and implementation in Pandora. SKB-R-06-68, Svensk Kärnbränslehantering AB.

Avila R, Ekström P A, Kautsky U, 2006. Development of Landscape dose factors for dose-assessments in SR-Can. SKB-TR-06-15, Svensk Kärnbränslehantering AB.

Aydin A, Johnson A M, 1978. Development of faults as zones of deformation bands and as slip surfaces in sandstone. Pure and Applied Geophysics 116(4–5): 931–942.

Baecher G B, Einstein H H, Lanney N A, 1977. Statistical description of rock properties and sampling, Colo. Sch. Mines Press, Golden, Colo., United States (USA).

Barton N, 1978. Suggested methods for the quantitative description of discontinuities in rock masses. International Journal of Rock Mechanics and Mining Sciences; Geomechanics Abstracts 15(6): 319–368.

Barton C C, Larsen E, Baechle P E, 1985. Fractal geometry of two-dimensional planar sections through fracture networks at Yucca Mountain, southwestern Nevada. Eos, Transactions, American Geophysical Union 66(46): 1089.

Berkowitz B, Adler P, 1998. Stereological analysis of fracture network structure in geological formations. J. Geophys. Res. 103(B7): 15339–15360.

Birgersson L, Neretnieks I, 1990. Diffusion in the matrix of granitic rock: Field test in the Stripa mine. Water Resources Research 26(11): 2833–2842.

Bond A E, Hoch A R, Jones G D, Tomczyk A J, Wiggin R M, Worraker W J, 1997. Assessment of a spent fuel disposal canister. Assessment studies for a copper canister with cast steel inner component. SKB TR 97-19, Svensk Kärnbränslehantering AB.

Bour O, Davy P, Darcel C, Odling N, 2002. A statistical scaling model for fracture network geometry, with validation on a multiscale mapping of a joint network (Hornelen Basin, Norway). J. Geophys. Res.

Bradbury M H, Baeyens B, 2003. Near-field sorption data bases for compacted MX-80 bentonite for performance assessment of a high-level radioactive waste repository in Opalinus clay host rock. NAGRA NTB 02-18, Nagra Wettingen Switzerland.

Brantberger M, 2004. Forsmark pilot layout. Personal communication with Harald Hökmark Clay Technology AB.

Buffer and backfill process report, 2006. Buffer and backfill process report for the safety assessment SR-Can. SKB TR-06-18, Svensk Kärnbränslehantering AB.

Bäckblom G, Christiansson R, Lagerstedt L, 2004. Choice of rock excavation methods for the Swedish deep repository for spent nuclear fuel. SKB R-04-62, Svensk Kärnbränslehantering AB.

Börgesson L, Fredrikson A, Johannesson L-E, 1994. Heat conductivity of buffer materials. SKB TR 94-29, Svensk Kärnbränslehantering AB.

Börgesson L, Johannesson L-E, 1995. Thermo-hydro-mechanical modelling of water unsaturated buffer material. Status 1995. SKB AR 95-32, Svensk Kärnbränslehantering AB.

Börgesson L, Johannesson L-E, Sandén T, Hernelind J, 1995. Modelling of the physical behaviour of water saturated clay barriers. Laboratory tests, material models and finite element application. SKB TR 95-20, Svensk Kärnbränslehantering AB.

Börgesson L, Hernelind J, 1999. Coupled thermo-hydro-mechanical calculations of the water saturation phase of a KBS-3 deposition hole. Influence of hydraulic rock properties on the water saturation phase. SKB TR-99-41, Svensk Kärnbränslehantering AB.

Börgesson L, Johannesson L-E, Hernelind J, 2003. Earthquake induced rock shear through a deposition hole. Effect on the canister and the buffer. SKB TR-04-02, Svensk Kärnbränslehantering AB.

Börgesson L, Fälth B, Hernelind J, 2006. Water saturation phase of the tunnel backfill in the KBS-3V concept and its influence on the wetting of the buffer. SKB TR-06-14. Svensk Kärnbränslehantering AB.

Börgesson L, Hernelind J, 2006. Canister displacement in KBS-3V. A theoretical study. SKB TR-06-04, Svensk Kärnbränslehantering AB.

Carbol P, Engkvist I, 1997. Compilation of radionuclide sorption coefficients for performance assessment. SKB R-97-13, Svensk Kärnbränslehantering AB.

Carlsson L, 2004. Drill hole KSH02. Determining of porosity by water saturation and density by buoyancy technique. Oskarshamn site investigation. SKB P-04-57, Svensk Kärnbränslehantering AB.

Chilès J-P, Delfiner P, 1999. Geostatistics. Modeling spatial uncertainty, A Wiley-Interscience publication John Wiley & Sons Inc. USA.

Cliffe K A, Kelly M, 2004. COMP23 v1.2.2 Users manual. SKB R-04-64, Svensk Kärnbränslehantering AB.

Climate report, 2006. Climate related issues for the safety assessment SR-Can. SKB TR-06-23, Svensk Kärnbränslehantering AB.

Crawford J, Neretnieks I, Malmström M, 2006. SR-Can Data and uncertainty assessment for radionuclide Kd partitioning coefficients in granitic rock for use in SR-Can calculations. SKB R-06-75, Svensk Kärnbränslehantering AB.

Darcel C, Bour O, Davy P, 2003. Stereological analysis of fractal fracture networks. J. Geophys. Res.

Dershowitz W, Baecher G, Einstein H, 1979. Prediction of rock mass deformability. Proceedings of the Congress of the International Society for Rock Mechanics (4, Vol. 1): 605–611.

Dershowitz W, Lee G, Geier J, Foxford T, La Pointe P, Thomas A, 1995. FRACMAN-Interactive Discrete Feature Data Analysis, Geometric Modeling, and Exploration Simulation. User Documentation, version 2.5. Golder Associates Inc.

Dershowitz W, Winberg A, Hermansson J, Byegård J, Tullborg E-L, Andersson P, Mazurek M, 2003. Äspö Hard Rock Laboratory. Äspö Task Force on modelling of groundwater flow and transport of solutes. Task 6c. A semi-synthetic model of block scale conductive structures at the Äspö HRL. SKB IPR-03-13, Svensk Kärnbränslehantering AB.

DHI, 2004. MIKE SHE User Guide.

Dillström P, 2005. Probabilistic analysis of canister inserts for spent nuclear fuel. SKB TR-05-19, Svensk Kärnbränslehantering AB.

Drake H, Sandström B, Tullborg E-L, 2006. Mineralogy and geochemistry of rocks and fracture fillings from Forsmark and Oskarshamn: Compilation of data for SR-Can. SKB R-06-109, Svensk Kärnbränslehantering AB.

Duro L, Grivé M, Cera E, Domènech C, B J, 2005. Update of a thermodynamic database for radionuclides to assist solubility limits calculation for PA. Enviros Report

Duro L, Grivé M, Cera E, Gaona X, Domènech C, Bruno J, 2006. Determination and assessment of the concentration limits to be used in SR-Can. SKB TR-06-32, Svensk Kärnbränslehantering AB.

Edenius M, Ekberg K, Forssén B-H, Knott D, 1993. CASMO-4. A Fuel Assembly Burnup Program. Users Manual. STUDSVIK/SOA-93/1

Elert M, Gylling B, Lindgren M, 2004. Assessment model validity document FARF31. SKB R-04-51, Svensk Kärnbränslehantering AB.

Emsley S, Olsson O, Stenberg L, Alheid H-J, Falls S, 1997. ZEDEX – A study of damage and disturbance from tunnel excavation by blasting and tunnel boring. SKB TR 97-30, Svensk Kärnbränslehantering AB.

Evans M, Hastings N, Peacock B, 2000. Statistical distributions, John Wiley & Sons, Inc., New York.0-471-37124-6.

FEP report, 2006. FEP report for the safety assessment SR-Can. SKB TR-06-20, Svensk Kärnbränslehantering AB.

Fisher R, 1953. Dispersion on a sphere, Royal Society of London Proceedings.

Fisher N I, Lewis T, Embleton B J, 1987. Statistical Analysis of Spherical Data, Cambridge University Press. Cambridge, U. K.

Follin S, Stigsson M, Svensson U, 2005. Regional hydrogeological simulations for Forsmark – Numerical modelling using DarcyTools. Preliminary site description Forsmark area – version 1.2. SKB R-05-60, Svensk Kärnbränslehantering AB.

Follin S, Stigsson M, Svensson U, 2006. Hydrogeological DFN modelling using structural and hydraulic data from KLX04. Preliminary site description Laxemar subarea – version 1.2. SKB R-06-24, Svensk Kärnbränslehantering AB.

Fuel and canister process report, 2006. Fuel and canister process report for the safety assessment SR-Can. SKB TR-06-22, Svensk Kärnbränslehantering AB.

Geosphere process report, 2006. Geosphere process report for the safety assessment SR-Can. SKB TR-06-19, Svensk Kärnbränslehantering AB.

Glamheden R, 2004. Simpevarp pilot layout. Personal communication with Harald Hökmark Clay Technology AB.

Grenthe I, Stumm W, Laaksoharju M, Nilsson A C, Wikberg P, 1992. Redox potentials and redox reactions in deep groundwater systems. In: Chemical Geology 98: Pp 131–150.

Gunnarsson D, Börgesson L, Hökmark H, Johannesson L-E, Sandén T, 2001. Äspö Hard Rock Laboratory. Report on the installation of the Backfill and Plug Test. SKB International Progress Report IPR-01-17, Svensk Kärnbränslehantering AB.

Gunnarsson D, Börgesson L, Keto P, Tolppanen P, Hansen J, 2004. Backfilling and closure of the deep repository. Assessment of backfill concepts. SKB R-04-53, Svensk Kärnbränslehantering AB.

Hartley L, Cox I, Holton D, Hunter F, Joyce S, Gylling B, Lindgren M, 2004. Groundwater flow and radionuclide transport modelling using CONNECTFLOW in support of the SR Can assessment. SKB R-04-61, Svensk Kärnbränslehantering AB.

Hartley L, Cox I, Hunter F, Jackson P, Joyce S, Swift B, Gylling B, Marsic N, 2005a. Regional hydrogeological simulations for Forsmark – numerical modelling using CONNECTFLOW. Preliminary site description Forsmark area – version 1.2. SKB R-05-32, Svensk Kärnbränslehantering AB.

Hartley L, Hoch A, Hunter F, Jackson P, Marsic N, 2005b. Regional hydrogeological simulations – numerical modelling using ConnectFlow. Preliminary site description Simpevarp sub area – version 1.2. SKB R-05-12, Svensk Kärnbränslehantering AB.

Hartley L, Hoch A, Jackson P, Joyce S, McCarthy R, Rodwell W, Swift B, 2006a. Groundwater flow and transport modelling during the temperate period for the SR-Can assessment: Forsmark area – Version 1.2. SKB R-06-98, Svensk Kärnbränslehantering AB.

Hartley L, Hoch A, Jackson P, Joyce S, McCarthy R, Swift B, Gylling B, Marsic N, 2006b. Groundwater flow and transport modelling during the temperate period for the SR-Can assessment: Laxemar area – Version 1.2. SKB R-06-99, Svensk Kärnbränslehantering AB.

Hartley L, Hunter F, Jackson P, McCarthy R, Gylling B, Marsic N, 2006c. Regional hydrogeological simulations using CONNECTFLOW. Preliminary site description Laxemar subarea – version 1.2. SKB R-06-23, Svensk Kärnbränslehantering AB.

Hedin A, 2002. Safety Assessment of a Spent Nuclear Fuel Repository: Sensitivity Analyses for Prioritisation of Research. In: Proceedings of the 6th International Conference on Probabilistic Safety Assessment and Management PSAM6. Elsevier Science Ltd.

Hedin A, 2003. Probabilistic dose calculations and sensitivity analyses using analytic models. In: Reliability Engineering & System Safety 79:2 pp 195–204.

Hedin A, 2004. Integrated near-field evolution model for a KBS-3 repository. SKB R-04-36, Svensk Kärnbränslehantering AB.

Hedin A, 2005. An analytic method for estimating the probability of canister/fracture intersections in a KBS-3 repository. SKB R-05-29, Svensk Kärnbränslehantering AB.

Hermanson J, Forssberg O, Fox A, La Pointe P, 2005. Statistical model of fractures and deformation zones. Preliminary site description, Laxemar subarea, version 1.2. SKB R-05-45 Svensk Kärnbränslehantering AB.

Hirata T, 1989. Fractal dimension of fault systems in Japan; fractal structure in rock fracture geometry at various scales. Pure and Applied Geophysics 131(1–2): 157–170.

Hora S, 2002. Expert opinion in SR 97 and the SKI/SSI joint review of SR 97. SSI Rapport 2002 20, Department of Waste Management and Environmental Protection SSI – Statens strålskyddsinstitut (Swedish Radiation Protection Authority) Stockholm Sweden.

Hora S, Jensen M, 2002. Expert judgement elicitation. SSI Rapport 2002 19, Department of Waste Management and Environmental Protection SSI – Statens strålskyddsinstitut (Swedish Radiation Protection Authority) Stockholm Sweden.

Hummel W, Berner U, Curti E, Pearson F J, Thoenen T, 2002. NAGRA/PSI Chemical Thermodynamic Data Base 01/01, Nagra.

Håkansson R, 2000. Beräkning av nuklidinnehåll, resteffekt, aktivitet samt doshastighet för utbränt kärnbränsle. SKB R-99-74, Svensk Kärnbränslehantering AB.

Hökmark H, Fälth B, 2003. Thermal dimensioning of the deep repository. Influence of canister spacing, canister power, rock thermal properties and nearfield design on the maximum canister surface temperature. SKB TR-03-09, Svensk Kärnbränslehantering AB.

Hökmark H, 2004. Hydration of the bentonite buffer in a BS-3 repository. Applied Clay Science 26 219–233.

Hökmark H, Fälth B, Wallroth T, 2006. T-H-M couplings in rock. Overview of results if importance to the SR-Can safety assessment. SKB TR-06-88, Svensk Kärnbränslehantering AB.

Initial state report, 2006. Initial state report for the safety assessment SR-Can. SKB TR-06-21, Svensk Kärnbränslehantering AB.

Itasca Consulting Group Inc, 2003. 3DEC – 3 Dimensional Distinct Element Code, User's Guide.

Johannesson L-E, Börgesson L, Sandén T, 1999. Äspö Hard Rock Laboratory. Backfill materials based on crushed rock (part 2). Geotechnical properties determined in laboratory. SKB International Progress Report IPR-99-23, Svensk Kärnbränslehantering AB.

Johannesson L-E, Nord S, Pusch R, Sjöblom R, 2000. Isostatic compaction of beaker shaped bentonite blocks on the scale 1:4. SKB TR-00-14, Svensk Kärnbränslehantering AB.

Johannesson L-E, Börgesson L, 2002. Äspö Hard Rock Laboratory. Laboratory tests on Friedland Clay. Friedland Clay as backfill material. Results of laboratory tests and swelling/compression calculations. SKB International Progress Report IPR-02-50, Svensk Kärnbränslehantering AB.

Johannesson L-E, Nilsson U, 2006. Deep repository – Engineered barrier systems. Geotechnical properties of candidate backfill materials – Laboratory tests and calculations for determining performance. SKB TR-06-73, Svensk Kärnbränslehantering AB.

Johansson R S, 2005. A comparison of two independent interpretations of lineaments from geophysical and topographic data at the Forsmark site. SKB R-05-23, Svensk Kärnbränslehantering AB.

Johnson L H, Tait J C, 1997. Release of segregated nuclides from spent fuel. SKB TR 97-18, Svensk Kärnbränslehantering AB.

Johnson L, Poinssot C, Ferry C, Lovera P, 2004. Estimates of the instant release fraction for UO2 and MOX fuel at t = 0. A report of the spent fuel stability (SFS) project of the 5th Euratom framework program. Nagra NTB 04-08, Nagra Wettingen Switzerland.

Jones J, Vahlund F, Kautsky U, 2004. Tensit – a novel probabilistic simulation tool for safety assessments. Tests and verifications using biosphere models. SKB TR-04-07, Svensk Kärnbränslehantering AB.

Jones J, Kautsky U, Vahlund F, 2005. Tensit – a simulation tool for nuclide transport, risk and dose calculations. In: Radioprotection volume 1(2005): S933–S938.

Karnland O, Sandén T, Johannesson L-E, Eriksen T E, Jansson M, Wold S, Pedersen K, Motamedi M, Rosborg B, 2000. Long term test of buffer material. Final Report on the pilot parcels. SKB TR-00-22, Svensk Kärnbränslehantering AB.

Karnland O, Nilsson U, Olsson S, Sellin P, 2005. Experimental study on sealing properties of commercial bentonites related to bentonite mineralogy and water solution composition.

Kelly M, Cliffe K A, 2006. Validity Document for COMP23. SKB R-06-76, Svensk Kärnbränslehantering AB.

King F, Ahonen L, Taxén C, Vuorinen U, Werme L, 2001. Copper corrosion under expected conditions in a deep geologic repository. SKB TR-01-23, Svensk Kärnbränslehantering AB.

Kjellberg N, 1999a. Säkerhet och Vetenskap. Proper Monitor User`s Manual. SKB Arbetsrapport TS-99-09, Svensk Kärnbränslehantering AB.

Kjellberg N, 1999b. Säkerhet och Vetenskap. Proper Programmer`s Manual. SKB Arbetsrapport TS-99-11, Svensk Kärnbränslehantering AB.

Kjellberg N, 1999c. Säkerhet och Vetenskap. Proper Submodel Designer`s Manual. SKB Arbetsrapport TS-99-10, Svensk Kärnbränslehantering AB.

Knuutila A, 2001. Long-term creep of nuclear fuel disposal canister shroud. POSIVA Working Report 2001-13, Posiva Oy Helsinki Finland.

La Pointe P R, Olofsson I, Hermanson J, 2005. Statistical model of fractures and deformation zones for Forsmark. Preliminary site description Forsmark area – version 1.2. SKB R-05-26, Svensk Kärnbränslehantering AB.

Laaksoharju M, Gurban I, Skårman C, 1998. Summary of hydrochemical conditions at Aberg, Beberg and Ceberg. SKB TR 98-03, Svensk Kärnbränslehantering AB.

LBNL, 1999. LBNL Isotopes Project Nuclear Data Dissemination Home Page. version 2/28/99, http://ie.lbl.gov/toi.html.

Lindgren M, Gylling B, Elert M, 2002. FARF31 Version 1-2 – User´s Guide. SKB Arbetsrapport TS-02-03, Svensk Kärnbränslehantering AB.

Lindgren M, Lindström F, 1999. SR 97 – Radionuclide transport calculations. SKB TR-99-23, Svensk Kärnbränslehantering AB.

Litke C D, Ryan S R, King F, 1992. A mechanistic study of the uniform corrosion of copper in compacted clay-sand soil,. AECL-10397, COG-91-304, Atomic Energy of Canada Limited.

Liu L, Neretnieks I, 2005. Analysis of fluid flow and solute transport in a fracture intersecting a canister with variable aperture fractures and arbitrary intersection angles. Nuclear Technology, 132–144.

Liu J, Löfgren M, Neretnieks I, 2006. SR-Can – Data and uncertainty assessment, Matrix diffusivity and porosity in situ. SKB R-06-111, Svensk Kärnbränslehantering AB.

Long J C S, Gilmour P, Witherspoon P A, 1985. A model for steady fluid flow in random three-dimensional networks of disc-shaped fractures. Water Resources Research 21(8): 1105–1115.

Lund B, 2005. Effects of deglaciation on the crustal stress field and implications for endglacial faulting: a parametric study of simple Earth and ice models. SKB TR-05-04, Svensk Kärnbränslehantering AB.

Löfgren M, 2001. Formation factor logging in igneous rock by electrical methods. Department of Chemical Engineering and Technology, Division of Chemical Engineering, Royal Institute of Technology, Stockholm, Sweden, Department of Chemical Engineering and Technology Division of Chemical Engineering Royal Institute of Technology Stockholm Sweden.

Löfgren M, 2004. Diffusive properties of granitic rock as measured by in situ electrical methods., Royal Institute of Technology, Stockholm, Sweden. Doctoral Thesis.

Löfgren M, Neretnieks I, 2005a. Formation factor logging in situ and in the laboratory by electrical methods in KSH01A and KSH02. Measurements and evaluation of methodology. Oskarshamn site investigation. SKB P-05-27, Svensk Kärnbränslehantering AB.

Löfgren M, Neretnieks I, 2005b. Formation factor logging in situ by electrical methods in KFM01A and KFM02A. Measurements and evaluation of methodology. Forsmark site investigation. SKB P-05-29, Svensk Kärnbränslehantering AB.

Main report, 2006. Long-term safety for KBS-3 repositories at Forsmark and Laxemar – a first evaluation Main report of the SR-Can project. SKB TR-06-09, Svensk Kärnbränslehantering AB.

Marsic N, Hartley L, Jackson P, Poole M, Morvik A, 2001. Development of hydrogeological modelling tools based on NAMMU. SKB R-01-49, Svensk Kärnbränslehantering AB.

Marsic N, Hartley L, Sanchez-Friera P, Morvik A, 2002. Embedded regional/local-scale model of natural transients in saline groundwater flow: Illustrated using the Beberg site. SKB R-02-22, Svensk Kärnbränslehantering AB.

Mishra S, 2002. Assigning probability distributions to input parameters of performance assessment models. SKB TR-02-11, Svensk Kärnbränslehantering AB.

Model summary report, 2006. Model summary report for the safety assessment SR-Can. SKB TR-06-26, Svensk Kärnbränslehantering AB.

Moreno L, Crawford J, Neretnieks I, 2006. Modelling radionuclide transport for time varying flow in a channel network. J Contaminant Hydrology, 86, 215–238.

Munier R, 2004. Statistical analysis of fracture data, adapted for modelling Discrete Fracture Networks-Version 2. SKB R-04-66, Svensk Kärnbränslehantering AB.

Munier R, Hökmark H, 2004. Respect distances. Rationale and means of computation. SKB R-04-17, Svensk Kärnbränslehantering AB.

Nagra, 2002. Project Opalinus Clay. Safety report. Demonstration of disposal feasibility for spent fuel, vitrified high-level waste and long-lived intermediate-level waste (Entsorgungsnachweis). NAGRA NTB 02-05, Nagra Wettingen Switzerland.

Neretnieks I, 2006. Flow and solute transport in a zone damaged due to spalling. SKB R-06-91, Svensk Kärnbränslehantering AB.

Newman J, Mitra G, 1993. Lateral variations in mylonite zone thickness as influenced by fluid-rock interactions, Linville Falls Fault, North Carolina. Journal of Structural Geology 15(7): 849–863.

Nilsson K-F, Lofaj F, Burström M, Andersson C-G, 2005. Pressure tests of two KBS-3 canister mock-ups. SKB TR-05-18, Svensk Kärnbränslehantering AB.

Norman S, Kjellbert N, 1990. FARF31 – A far field radionuclide migration code for use with the PROPER package. SKB TR-90-01, Svensk Kärnbränslehantering AB.

Ochs M, Talerico C, 2004. SR-Can. Data and uncertainty assessment. Migration parameters for the bentonite buffer in the KBS-3 concept. SKB TR-04-18, Svensk Kärnbränslehantering AB.

Ochs M, 2006. SR-Can – Data and uncertainty assessment Migration parameters for a backfill of Friedland Clay in the KBS-3 concept. SKB TR-06-85, Svensk Kärnbränslehantering AB.

Ohlsson Y, Neretnieks I, 1997. Diffusion data in granite. Recommended values. SKB TR 97–20, Svensk Kärnbränslehantering AB.

Okubo P G, Aki K, 1987. Fractal geometry in the San Andreas fault system. Journal of Geophysical Research, B, Solid Earth and Planets 92(1): 345–355.

Olsson R, 1998. Mechanical and hydromechanical behaviour of hard rock joints. A laboratory study, PhD thesis. Department of Geotechnical Engineering, Chalmers University of Technology, Göteborg, Sweden.

Olsson M, Niklasson B, Wilson L, Andersson C, Christiansson R, 2004. Äspö HRL. Experiences of blasting of the TASQ tunnel. SKB R-04-73, Svensk Kärnbränslehantering AB.

ORNL, 1996. Modular Code System for Performing Standardized Computer Analyses for Licensing Evaluation. CCC-545, Oak Ridge National Laboratory.

Painter S, 2006a. Effect of Single-Fracture Aperture Variability on Field-Scale Transport. SKB R-06-25, Svensk Kärnbränslehantering AB.

Painter S, 2006b. Time-domain random walk methods for simulating radionuclide transport in fractured porous rock. Proceedings of the 11th International High-level Radioactive Waste Management Conference, April 30–May 4, 2006, Las Vegas, Nevada.

Palisade Corporation, 2004. Palisade Corporation 798 Cascadilla Street Ithaca, NY 14850 USA 800432 7475 US/Canada. www.palisade.com

Parkhurst D L, Appelo C A J, 1999. User's guide to PHREEQC (version 2) – a computer program for speciation, batch-reaction, one-dimensional transport and inverse geochemical calculations. USGS Water resources investigations report 99-4259, 312 p.

Parkhurst D L, Kipp K L, Engesgaard P, Charlton S R, 2004. PHAST – A program for simulating ground-water flor, solute transport, and multicomponent geochemical reactions. U.S.Geological Techniques and methods 6-A8, 154 p.

Poinssot C, Toulhoat P, Piron J-P, Cappelare C, Desgranges L, Gras J-M, 2000. Operational and scientific questions related to the long term evolution of spent nuclear fuel in dry conditions. Current status of the French research. Embedded Topical Meeting on DOE Spent Nuclear Fuel and Fissile Material Management, San Diego, Materials Research Society Pittsburgh Pennsylvania.

Poinssot C, Jegou C, Toulhoat P, Piron J-P, Gras J-M, 2001. A new approach to the RN source term for spent nuclear fuel under geological disposal conditions,, Materials Research Soceity

Poinssot C, Lovera P, Faure M-H, 2002. Assessment of the evolution with time of the instant release fraction of spent nuclear fuel in geological disposal conditions. Materials Research Soceity.

Power W L, Tullis T E, Brown S R, Boitnott G N, Scholz C H, 1987. Roughness of natural fault surfaces. Geophysical Research Letters 14(1): 29–32.

Power W L, Tullis T E, 1991. Euclidean and fractal models for the description of rock surface roughness. Journal of Geophysical Research, B, Solid Earth and Planets 96(2): 415–424.

Pusch R, 1990. Radionuclide transport paths in the nearfield – a KBS-3 concept study. SKB TR 90-32, Svensk Kärnbränslehantering AB.

Pusch R, Stanfors R, 1992. The zone of disturbance around blasted tunnels at depth. Clay Technology AB, Lund, Sweden 1); Roy Stanfors Consulting AB, Lund, Sweden 2), In: Int. J. Rock Mech. Min. Sci. & Geomech. Abstr. 29:No. 5 pp 447–456.

Pusch R, 2001. The Buffer and Backfill Handbook. Part 2: Materials and techniques. SKB TR-02-12, Svensk Kärnbränslehantering AB.

Pusch R, 2003a. The buffer and backfill handbook. Part 1: definitions, basic relationships, and laboratory methods. SKB TR-02-20, Svensk Kärnbränslehantering AB.

Pusch R, 2003b. The Buffer and Backfill Handbook. Part 3: Models for calculation of processes and behaviour. SKB TR-03-07, Svensk Kärnbränslehantering AB.

Rippon J H, 1985. Contoured patterns of the throw and hade of normal faults in the Coal Measures (Westphalian) of north-east Derbyshire. Proceedings of the Yorkshire Geological Society 45(3): 147–161.

Romero L, Thompson A, Moreno L, Neretnieks I, Widén H, Boghammar A, 1999. Comp23/ Nuctran user`s guide. Proper version 1.1.6. SKB R-99-64, Svensk Kärnbränslehantering AB.

Roos and Gelin, 2003. Letter Report to Lars Werme, SKB.

Savukoski M, 2004a. Drill hole KFM01A Determination of porosity by water saturation and density by buoyancy technique. Forsmark site investigation. SKB P-04-166, Svensk Kärnbränslehantering AB.

Savukoski M, 2004b. Drill hole KFM03A Determination of porosity by water saturation and density by buoyancy technique. Forsmark site investigation. SKB P-04-168, Svensk Kärnbränslehantering AB.

Savukoski M, 2004c. Drill hole KFM04A Determination of porosity by water saturation and density by buoyancy technique. Forsmark site investigation. SKB P-04-169, Svensk Kärnbränslehantering AB.

Savukoski M, Carlsson L, 2004a. Drill hole KFM02A Determination of porosity by water saturation and density by buoyancy technique. Forsmark site investigation. SKB P-04-167, Svensk Kärnbränslehantering AB.

Savukoski M, Carlsson L, 2004b. Drill hole KSH01A. Determining of porosity by water saturation and density by buoyancy technique. Oskarshamn site investigation. SKB P-04-56, Svensk Kärnbränslehantering AB.

Schrire D, Matsson I, Grapengiesser B, 1997. Fission gas release in ABB SVEA 10X10 BWR fuel. International Topical Meeting on Light Water Reactor Fuel Performance, Portland, Oregon.

Serco Assurance, 2005. CONNECTFLOW Release 9.0 Technical Summary Document. Serco Assurance Report SA/ ENV/CONNECTFLOW/15

Shibutani T, Suyama T, Shibata M, 1999. Sorption database for radionuclides on bentonite and rocks. JNC Technical Report (in Japanese with English abstract) TN8410 99-050, Japan Nuclear Cycle Development Institute

Site descriptive report, Forsmark, 2005. Preliminary site description. Forsmark area – version 1.2. SKB R-05-18, Svensk Kärnbränslehantering AB.

Site descriptive report, Laxemar, 2006. Preliminary site description. Laxemar area – version 1.2. SKB R-06-10, Svensk Kärnbränslehantering AB.

Site descriptive report, Simpevarp, 2005. Preliminary site description. Simpevarp subarea – version 1.2. SKB R-05-08, Svensk Kärnbränslehantering AB.

Skagius K, Neretnieks I, 1986. Diffusivity measurements and electrical-resistivity measurements in rock samples under mechanical-stress. Water Resources Research 22(4): 570–580.

SKB, 1992. SKB 91 – Final disposal of spent nuclear fuel. Importance of the bedrock for safety. SKB TR 92-20, Svensk Kärnbränslehantering AB.

SKB, 1995. SR 95. Template for safety reports with descriptive example. SKB TR 96-05, Svensk Kärnbränslehantering AB.

SKB, 1999a. Deep repository for spent nuclear fuel. SR 97 – Post-closure safety. Main report – Volume I, Volume II and Summary. SKB TR-99-06, Svensk Kärnbränslehantering AB.

SKB, 1999b. SR 97 – Processes in the repository evolution. Background report to SR 97. SKB TR-99-07, Svensk Kärnbränslehantering AB.

SKB, 2004a. Deep repository. Underground design premises. Edition D1/1. SKB R-04-60, Svensk Kärnbränslehantering AB.

SKB, 2004b. Hydrogeochemical evaluation for Simpevarp model version 1.2. Preliminary site description of the Simpevarp area. SKB R-04-74, Svensk Kärnbränslehantering AB.

SKB, 2004c. Interim data report for the safety assessment SR-Can. SKB R-04-34, Svensk Kärnbränslehantering AB.

SKB, 2004d. Interim FEP report for the safety assessment SR-Can. SKB R-04-32, Svensk Kärnbränslehantering AB.

SKB, 2004e. Interim initial state report for the safety assessment SR-Can. SKB R-04-35, Svensk Kärnbränslehantering AB.

SKB, 2004f. Interim main report of the safety assessment SR-Can. SKB TR-04-11, Svensk Kärnbränslehantering AB.

SKB, 2004g. Interim process report forthe safety assessment SR-Can. SKB R-04-33, Svensk Kärnbränslehantering AB.

SKB, 2005a. Hydrogeochemical evaluation. Preliminary site description Forsmark area – version 1.2. SKB R-05-17, Svensk Kärnbränslehantering AB.

SKB, 2005b. Preliminary safety evaluation for the Forsmark area. Based on data and site descriptions after the initial site investigation stage. SKB TR-05-16, Svensk Kärnbränslehantering AB.

SKB, 2005c. Preliminary site description. Forsmark area – version 1.2. SKB R-05-18, Svensk Kärnbränslehantering AB.

SKB, 2005d. Preliminary site description. Simpevarp subarea – version 1.2. SKB R-05-08, Svensk Kärnbränslehantering AB.

SKB, 2006a. The Biosphere at Forsmark. Data, assumptions and models used in the SR-Can assessment. SKB R-06-82, Svensk Kärnbränslehantering AB.

SKB, 2006b. The Biosphere at Laxemar. Data, assumptions and models used in the SR-Can assessment. SKB R-06-83, Svensk Kärnbränslehantering AB.

SKB, 2006c. Buffer and backfill process report for the safety assessment SR-Can. SKB TR-06-18, Svensk Kärnbränslehantering AB.

SKB, 2006d. Climate and climate related issues for the safety assessment SR-Can. SKB TR-06-23, Svensk Kärnbränslehantering AB.

SKB, 2006e. FEP report for the safety assessment SR-Can. SKB TR-06-20, Svensk Kärnbränslehantering AB.

SKB, 2006f. Fuel and canister process report for the safety assessment SR-Can. SKB TR-06-22, Svensk Kärnbränslehantering AB.

SKB, 2006g. Geosphere process report for the safety assessment SR-Can. SKB TR-06-19, Svensk Kärnbränslehantering AB.

SKB, 2006h. Initial state report for the safety assessment SR-Can. SKB TR-06-21, Svensk Kärnbränslehantering AB.

SKB, 2006i. Long-term safety for KBS-3 repositories at Forsmark and Laxemar – a first evaluation Main report of the SR-Can project. SKB TR-06-09, Svensk Kärnbränslehantering AB.

SKB, 2006j. Model summary report for the safety assessment SR-Can. SKB TR-06-26, Svensk Kärnbränslehantering AB.

SKB, 2006k. Preliminary Site Description. Laxemar area version 1.2. SKB R-06-10, Svensk Kärnbränslehantering AB.

SKB, 2006l. Tillförlitlighet i delsystem Förslutning, underlagsrapport för SR-Can. SKB R-06-04, Svensk Kärnbränslehantering AB.

SKI/SSI, 2001. SKI's and SSI's joint review of SKB's safety assessment report, SR 97. Summary. SKI Report 01 3, SSI-report 2001 2, SKI – Statens kärnkraftinspektion (Swedish Nuclear Power Inspectorate); SSI – Statens strålskyddsinstitut (Swedish Radiation Protection Institute).

Smart N R, Blackwood D J, Werme L, 2002a. Anaerobic corrosion of carbon steel and cast iron in artificial groundwaters: Part 1 – Electrochemical aspects. In: Corrosion 58(2002):7 pp 547–559.

Smart N R, Blackwood D J, Werme L, 2002b. Anaerobic corrosion of carbon steel and cast iron in artificial groundwaters: Part 2 – Gas generation. In: Corrosion 58(2002):8 pp 627–637.

Smart N R, Rance A P, Fennell P A H, 2005. Galvanic corrosion of copper-cast iron couples. SKB TR-05-06, Svensk Kärnbränslehantering AB.

Stenhouse M J, 1995. Sorption database for crystalline, marl and bentonite for performance assessment. NAGRA Technical Report NTB 93-06, NAGRA Wettingen Switzerland.

Stroes-Gascoyne S, Tait J C, Porth R J, McConnel J L, Lincoln W J, 1994. Release of 14C from the gap and grain-boundary regions of used CANDU fuels to aqueous solutions. Waste Management, 14, 385–392.

Stråhle A, 2001. Definition och beskrivning av parametrar för geologisk, geofysisk och bergmekanisk kartering av berg. SKB R-01-19, Svensk Kärnbränslehantering AB.

Sundberg J, 2002. Determination of thermal properties at Äspö HRL. Comparison and evaluation of methods and methodologies for borehole KA 2599 G01. SKB R-02-27, Svensk Kärnbränslehantering AB.

Sundberg J, Back P-E, Bengtsson A, Ländell M, 2005a. Thermal modelling. Preliminary site description Forsmark area – version 1.2. SKB R-05-31, Svensk Kärnbränslehantering AB.

Sundberg J, Back P-E, Bengtsson A, Ländell M, 2005b. Thermal modelling. Preliminary site description Simpevarp area – version 1.2. SKB R-05-24, Svensk Kärnbränslehantering AB.

Sundberg J, Back P-E, Hellström G, 2005c. Scale dependence and estimation of rock thermal conductivity. Analysis of upscaling, inverse thermal modelling and value of information with the Äspö HRL prototype repository as an example. SKB R-05-82, Svensk Kärnbränslehantering AB.

Sundberg J, Wraster J, Back P-E, Ländell M, 2006. Thermal modelling. Preliminary site description Laxemar subarea – version 1.2. SKB R-06-13, Svensk Kärnbränslehantering AB.

Svensson U, Kuylenstierna H-O, Ferry M, 2002a. Säkerhet och Vetenskap. DarcyTools. Concepts, methods, equations and tests. Version 1.0. SKB Arbetsrapport TS-02-06, Svensk Kärnbränslehantering AB.

Svensson U, Kuylenstierna H-O, Ferry M, 2002b. Säkerhet och Vetenskap. DarcyTools. Software description and documentation. Version 1.0. SKB Arbetsrapport TS-02-05, Svensk Kärnbränslehantering AB.

Svensson U, 2004. DarcyTools, Version 2.1. Verification and validation. SKB R-04-21, Svensk Kärnbränslehantering AB.

Svensson U, Kuylenstierna H-O, Ferry M, 2004a. DarcyTools, Version 2.1. Concepts, methods, equations and demo simulations. SKB R-04-19, Svensk Kärnbränslehantering AB.

Svensson U, Kuylenstierna H-O, Ferry M, 2004b. DarcyTools, Version 2.1. User´s guide. SKB R-04-20, Svensk Kärnbränslehantering AB.

Takase H, Benbow S, Grindrod P, 1999. Mechanical failure of SKB spent fuel disposal canisters. Mathematical modelling and scoping calculations. SKB TR-99-34, Svensk Kärnbränslehantering AB.

Thunehed H, 2005. Resistivity measurements on samples from KFM01A and KFM02A. Forsmark site investigation. SKB P-05-26, Svensk Kärnbränslehantering AB.

Tsang C-F, Bernier F, Davies C, 2005. Geohydromechanical processes in the Excavation Damaged Zone in crystalline rock, rock salt, and indurated and plastic clays—in the context of radioactive waste disposal. Int. J, Rock Mech. Min. Sci., 109–125.

Turcotte D L, 1986. Fractals and fragmentation. JGR. Journal of Geophysical Research. B 91(2): 1921–1926.

Turcotte D L, 1990. Implications of chaos, scale-invariance, and fractal statistics in geology. Geosphere fluctuations; short term instabilities in the Earth's system. S. Cloetingh. Amsterdam, Netherlands, Elsevier. 3; 3: 301–308.

Vahlund F, Hermansson H, 2006. Compulink – Implementing the COMP23 conceptualisation in Simulink. SKB TR 06-86, Svensk Kärnbränslehantering AB.

Walsh J J, Watterson J, 1988. Analysis of the relationship between displacements and dimensions of faults. Journal of Structural Geology 10(3): 239–247.

Warburton P M, 1980. Stereological interpretation of joint trace data; influence of joint shape and implications for geological surveys. International Journal of Rock Mechanics and Mining Sciences & Geomechanics Abstracts 17(6): 305–316.

Werme L, Johnson L H, Oversby V M, King F, Spahiu K, Grambow B, Shoesmith D W, 2004. Spent fuel performance under repository conditions: A model for use in SR-Can. SKB TR-04-19, Svensk Kärnbränslehantering AB.

Vermilye J M, Scholz C H, 1995. Relation between vein length and aperture. Journal of Structural Geology 17(3): 423–434.

Vesterlund G, Cosetti L V, 1994. Recent ABB fuel design and performance experience. 1994 International Topical Meeting on Light Water Reactor Fuel Performance,, West Palm Beach, Florida.

Wilmot R D, Galson D A, 2000. Expert judgement in performance assessment. SKI Report 00 4, SKI Statens kärnkraftinspektion (Swedish Nuclear Power Inspectorate) Stockholm Sweden.

Wilmot R D, Galson D A, Hora S C, 2000. Expert judgements in performance assessments. Report of an SKI/SSI seminar. SKI Report 00 35, SKI – Statens kärnkraftinspektion (Swedish Nuclear Power Inspectorate) Sweden.

Winberg A, 1991. The role of the disturbed rock zone in radioactive waste repository safety and performance assessment. A topical discussion and international overview. SKB TR 91-25, Svensk Kärnbränslehantering AB.

Yu J-W, Neretnieks I, 1997. Diffusion and sorption properties of radionuclides in compacted bentonite. SKB TR 97-12, Svensk Kärnbränslehantering AB.

Appendix A

Data

A1 Inventory

Table A-1, inventory for BWR fuel with a burn-up of 38 MWd/kg U after 40 years /Håkansson 2000, Table A1-7 and A1-9/.

Activation products Activity (Bq/t U)		Actinides Activity (Bq/t U)		Fission products. Activity (Bq/tU)	
H-3	$1.11 \cdot 10^{12}$	Th-234	$1.17 \cdot 10^{10}$	H-3	$2.07 \cdot 10^{12}$
C-14	$5.00 \cdot 10^{10}$	Pa-233	$1.50 \cdot 10^{10}$	Se-79	$2.82 \cdot 10^{9}$ [1, 2]
Ca-41	$6.94 \cdot 10^{6}$ [1]	Pa-234m	$1.17 \cdot 10^{10}$	Kr-85	$2.73 \cdot 10^{13}$
Cl-36	$5.46 \cdot 10^{8}$	U-234	$4.64 \cdot 10^{10}$	Sr-90	$1.20 \cdot 10^{15}$
Fe-55	$9.29 \cdot 10^{9}$	U-236	$1.04 \cdot 10^{10}$	Y-90	$1.20 \cdot 10^{15}$
Co-60	$8.92 \cdot 10^{11}$	U-237	$1.85 \cdot 10^{10}$	Zr-93	$5.03 \cdot 10^{10}$
Ni-59	$8.79 \cdot 10^{10}$	U-238	$1.17 \cdot 10^{10}$	Nb-93m	$4.21 \cdot 10^{10}$
Ni-63	$9.29 \cdot 10^{12}$	Np-237	$1.50 \cdot 10^{10}$	Tc-99	$5.72 \cdot 10^{11}$
Sr-90	$2.55 \cdot 10^{7}$	Np-239	$1.17 \cdot 10^{12}$	Ru-106	$2.66 \cdot 10^{4}$
Y-90	$2.55 \cdot 10^{7}$	Pu-238	$9.45 \cdot 10^{13}$	Rh-106	$2.66 \cdot 10^{4}$
Zr-93	$5.62 \cdot 10^{9}$	Pu-239	$9.50 \cdot 10^{12}$	Pd-107	$4.86 \cdot 10^{4}$ [1]
Nb-93m	$2.33 \cdot 10^{10}$	Pu-240	$1.18 \cdot 10^{13}$	Cd-113m	$1.69 \cdot 10^{11}$
Nb-94	$2.88 \cdot 10^{9}$	Pu-241	$7.72 \cdot 10^{14}$	Sn-121	$4.39 \cdot 10^{10}$
Mo-93	$4.42 \cdot 10^{7}$	Pu-242	$1.01 \cdot 10^{11}$	Sn-121m	$5.65 \cdot 10^{10}$
Ag-108	$4.34 \cdot 10^{7}$	Am-241	$1.51 \cdot 10^{14}$	Sb-125	$1.11 \cdot 10^{10}$
Ag-108m	$4.98 \cdot 10^{8}$ [3]	Am-242m	$4.53 \cdot 10^{11}$	Te-125m	$2.70 \cdot 10^{9}$
Cd-113m	$3.43 \cdot 10^{10}$	Am-242	$4.51 \cdot 10^{11}$	Sn-126	$2.25 \cdot 10^{10}$
Sn-121	$1.35 \cdot 10^{10}$	Am-243	$1.17 \cdot 10^{12}$	Sb-126m	$2.25 \cdot 10^{10}$
Sn-121m	$1.74 \cdot 10^{10}$	Cm-242	$3.73 \cdot 10^{11}$	I-129	$1.32 \cdot 10^{6}$ [1]
Sb-125	$1.21 \cdot 10^{9}$	Cm-243	$4.44 \cdot 10^{11}$	Cs-134	$9.10 \cdot 10^{9}$
Te-125m	$2.96 \cdot 10^{8}$	Cm-244	$2.84 \cdot 10^{13}$	Cs-135	$2.05 \cdot 10^{10}$
Eu-154	$3.17 \cdot 10^{11}$	Cm-245	$9.37 \cdot 10^{9}$	Cs-137	$1.79 \cdot 10^{15}$
Eu-155	$1.33 \cdot 10^{10}$	Cm-246	$2.89 \cdot 10^{9}$	Ba-137m	$1.69 \cdot 10^{15}$
Ho-166m	$7.47 \cdot 10^{7}$			Pm-146	$9.84 \cdot 10^{8}$
				Pm-147	$1.54 \cdot 10^{11}$
				Sm-151	$9.36 \cdot 10^{12}$
				Eu-152	$3.28 \cdot 10^{10}$
				Eu-154	$1.81 \cdot 10^{13}$
				Eu-155	$7.62 \cdot 10^{11}$

[1] Obtained by extrapolating data from /Håkansson 2000, Table A1-9/.

[2] Activity calculated using $t_{1/2} = 3.29 \cdot 10^{5}$ years /Håkansson 2000/, updated $t_{1/2} = 1.13 \cdot 10^{6}$ years /LBNL 1999/.

[3] Activity calculated using $t_{1/2} = 127$ years /Håkansson 2000/, updated $t_{1/2} = 418$ years /LBNL 1999/.

Table A-2. Inventory for BWR fuel with a burn-up of 38 MWd/kg U after 40 years after discharging the fuel elements calculated per canister (2.04 tonnes U).

	Moles/canister		Moles/canister		Moles/canister
Ag-108	$3.02 \cdot 10^{-14}$	H3	0.006054	Rh-106	$3.89 \cdot 10^{-18}$
Ag-108m	$9.75 \cdot 10^{-6}$ [1]	Ho166m	$1.38 \cdot 10^{-5}$	Ru-106	$4.14 \cdot 10^{-12}$
Am-241	10.06	I-129	3.196	Sb-125	$5.26 \cdot 10^{-6}$
Am-242	$1.27 \cdot 10^{-7}$	Kr-85	0.04513	Sb-126m	$1.25 \cdot 10^{-10}$
Am-242m	0.01062	Mo-93	$2.38 \cdot 10^{-5}$	Se-79	0.143 [2]
Am-243	1.332	Nb-93m	0.0001372	Sm-151	0.1299
Ba-137m	$1.26 \cdot 10^{-6}$	Nb-94	0.009015	Sn-121	$2.71 \cdot 10^{-8}$
C-14	0.04417	Ni-59	1.084	Sn-121m	0.0005695
Ca-41	$1.1 \cdot 10^{-4}$	Ni-63	0.1318	Sn-126	0.347
Cd-113m	0.0004572	Np-237	4.952	Sr-90	5.389
Cl-36	0.02534	Np-239	$1.16 \cdot 10^{-6}$	Tc-99	18.79
Cm-242	$2.57 \cdot 10^{-5}$	Pa-231	$9.15 \cdot 10^{-6}$	Te-125m	$7.34 \cdot 10^{-8}$
Cm-243	0.001951	Pa-233	$1.71 \cdot 10^{-7}$	Th-229	$1.15 \cdot 10^{-8}$
Cm-244	0.0793	Pa-234m	$4.01 \cdot 10^{-12}$	Th-230	0.00019
Cm-245	0.01228	Pd-107	4.869	Th-234	$1.19 \cdot 10^{-7}$
Cm-246	0.002108	Pm-146	$8.39 \cdot 10^{-7}$	U-233	$7.58 \cdot 10^{-5}$
Co-60	0.0007249	Pm-147	$6.23 \cdot 10^{-5}$	U-234	1.749
Cs-134	$2.89 \cdot 10^{-6}$	Pu-238	1.279	U-235	48.84
Cs-135	7.271	Pu-239	35.25	U-236	37.55
Cs-137	8.28	Pu-240	11.89	U-237	$5.27 \cdot 10^{-8}$
Eu-152	$6.88 \cdot 10^{-5}$	Pu-241	1.715	U-238	8061
Eu-154	0.02442	Pu-242	6.026	Y-90	0.001351
Eu-155	0.0005929	Ra-226	$3.45 \cdot 10^{-8}$	Zr-93	13.19
Fe-55	$3.73 \cdot 10^{-6}$				

[1] Using $t_{1/2}$ = 127 years.

[2] Using $t_{1/2} = 3.29 \cdot 10^{6}$ years.

Table A-3. Inventory for BWR fuel with a burn-up of 38 MWd/kg U at 1,000 years after deposition, calculated per canister (2.04 tonnes U).

Nuclide	Mol/canister	Nuclide	Mol/canister	Nuclide	Mol/canister
Ag-108m	$1.86 \cdot 10^{-6}$ [1]	I-129	3.1959	Sr-90	$1.54 \cdot 10^{-9}$
Am-241	2.4031	Nb-94	0.008712	Tc-99	18.729
Am-242m	0.00012	Ni-59	1.0746	Th-229	$6.80 \cdot 10^{-6}$
Am-243	1.2126	Ni-63	$8.61 \cdot 10^{-5}$	Th-230	0.008284
C-14	0.039139	Np-237	14.3213	Th-232	0.00113
Ca-41	$1.1 \cdot 10^{-4}$	Pa-231	$5.70 \cdot 10^{-5}$	U-233	0.00358
Cl-36	0.025282	Pd-107	4.8685	U-234	3.0291
Cm-242	$2.90 \cdot 10^{-7}$	Pu-238	0.000721	U-235	49.8426
Cm-243	$3.58 \cdot 10^{-13}$	Pu-239	34.3687	U-236	38.7524
Cm-244	$1.56 \cdot 10^{-16}$	Pu-240	10.7658	U-238	8061.01
Cm-245	0.011319	Pu-242	6.0173	Zr-93	13.184
Cm-246	0.001821	Ra-226	$3.21 \cdot 10^{-5}$		
Cs-135	7.2688	Se-79	0.143 [2]		
Cs-137	$4.30 \cdot 10^{-9}$	Sm-151	$7.22 \cdot 10^{-5}$		
Ho-166m	$7.77 \cdot 10^{-6}$	Sn-126	0.3446		

[1] Using $t_{1/2}$ = 418 years.

[2] Using $t_{1/2} = 1.13 \cdot 10^{6}$ years.

Am-242m is added to the Cm-246 inventory.

Cm-242 is added to the Pu-242 inventory.

Pu-238 is added to the U-238 inventory.

Cm-243 is added to the Am-243 inventory.

A2 Instant release fraction

Table A-4. Instant release fractions, pessimistic values are interpreted to be related to high burn-ups while realistic values are related to normal burn-up. Only normal burn-ups are suggested to be used in the assessment calculations, see Section 3.2.

Nuclide		Lower (%)	Central (%)	Upper (%)	Note
Actinides		0	0	0	1
Ag108m	Realistic	0	1	2.5	2
	Pessimistic	0	2	5	
C14		0.1	5	10	3
Ca41		100	100	100	4
Cl36		1	5	10	3
Cs135	Realistic	0	1	2.5	3
	Pessimistic	0	2	5	
Cs137	Realistic	0	1	2.5	5
	Pessimistic	0	2	5	
Ho166m					6
I-129	Realistic	0	1	2.5	3
	Pessimistic	0	2	5	
Nb94		100	100	100	7
Ni59		100	100	100	7
Ni63		100	100	100	7
Pd-107		0	0.2	1	3
Se-79		0	0.03	0.1	3
Sm151		0	0	0	6
Sn126		0	0.003	0.01	3
Sr90	Realistic	0.25	0.25	0.25	6
	Pessimistic	1	1	1	
Tc99		0	0.2	1	3
Zr93		0	0	0	6

1) Fuel and canister process report.

2) Corresponding values as I-129 and Cs135 /Johnson and Tait 1997/.

3) /Werme et al. 2004/.

4) Pessimistic assumption by the SR-Can team.

5) Corresponding values as for Cs135.

6) /Johnson and Tait 1997/.

7) Appears mainly in metal parts which are assumed to be instantly released /Johnson and Tait 1997, Håkansson 2000, **Fuel and canister process report**/.

A3 Solubilities

Table A-5. Solubility limiting phases used in the analysis of the solubility limits.

	Limiting specie	Reaction
Ag(0)	Ag(s)	$Ag(s)+H^{+}+0.25O_2 = Ag^{+}+0.5H_2O$
Ag(I)	AgCl(cr)	$AgCl(cr) = Ag^{+}+Cl^{-}$
Am(III)	$Am(OH)_3$(am)	$Am(OH)_3(am)+3H^{+} = Am^{+3}+3H_2O$
Am(III)	$Am(CO_3)(OH)$(s)	$Am(CO_3)(OH)(s)+H^{+} = Am^{+3}+CO_3^{-2}+H_2O$
Am(III)	$Am_2(CO_3)_3$(s)	$Am_2(CO_3)_3(s) = 2Am^{+3}+3CO_3^{-2} =$
Am(III)	$Am(CO_3)_2Na{\cdot}5H_2O$(s)	$Am(CO_3)_2Na5H_2O(s) = Am^{+3}+2CO_3^{-2}+5H_2O+Na^{+}$
Cm(III)	$Cm(OH)_3$(am)	$Cm(OH)_3(am)+3H^{+} = Cm^{+3}+3H_2O$
Cm(III)	$Cm(CO_3)(OH)$(s)	$Cm(CO_3)(OH)(s)+H^{+} = Cm^{+3}+CO_3^{-2}+H_2O$
Ho(III)	$Ho(OH)_3$(am)	$Ho(OH)_3(am)+3H^{+} = Ho^{+3}+3H_2O$
Ho(III)	$Ho_2(CO_3)_3$(s)	$Ho_2(CO_3)_3(s) = 2Ho^{+3}+3CO_3^{-2}$
Ni(II)	$Ni(OH)_2$(s)	$Ni(OH)_2(s)+2H^{+} = Ni^{+2}+2H_2O$
Ni(II)	$NiCO_3$(s)	$NiCO_3(cr) = Ni^{+2}+CO_3^{-2}$
Nb(V))	Nb_2O_5(s)	$Nb_2O_5(s)+H_2O = 2NbO_3-+2H^{+}$
Np(IV)	$NpO_2{\cdot}2H_2O$(am)	$NpO_2{\cdot}2H_2O(am)+4H^{+} = Np^{+4}+4H_2O$
Np(V)	Np_2O_5(s)	$Np_2O_5(s)+8H^{+} = 2Np^{+4}+0.5O_2+4H_2O$
Np(V)	$NpO_2(CO_3)Na{\cdot}3.5$aq	$NpO_2CO_3Na{\cdot}3.5aq+3H^{+} = Np^{+4}+0.25O_2+5H_2O+CO_3^{-2}+Na^{+}$
Pa(V)	Pa_2O_5(s)	$Pa_2O_5(s)+2H^{+} = 2PaO_2^{+}+H_2O$
Pu(III)	$Pu(OH)_3$(s)	$Pu(OH)_3(cr)+3H^{+} = Pu^{+3}+3H_2O$
Pu(III)	$PuCO_3OH$(s)	$PuCO_3OH(s)+H^{+} = Pu^{+3}+CO_3^{-2}+H_2O$
Pu(IV)	$Pu(OH)_4$(s)	$Pu(OH)_4(s)+3H^{+} = Pu^{+3}+0.25O_2+3.5H_2O$
Pd(II)	$Pd(OH)_2$s	$Pd(OH)_2s+2H^{+} = Pd^{+2}+2H2O$
Ra(II)	$RaCO_3$(s)	$RaCO_3(s) = Ra^{+2}+CO_3^{-2}$
Ra(II)	$Ra(SO_4)$s	$Ra(SO_4)(s) = Ra^{+2}+SO_4^{-2}$
Se(-II)	FeSe(s)	$FeSe(s)+2O_2 = SeO_4^{-2}+Fe^{+2}$
Sm(III)	$Sm(OH)_3$(am)	$Sm(OH)_3(am)+3H^{+} = Sm^{+3}+3H_2O$
Sm(III)	$Sm_2(CO_3)_3$(s)	$Sm_2(CO_3)_3(s) = 2Sm^{+3}+3CO_3^{-2}$
Sm(III)	$SmOHCO_3$(s)	$SmOHCO_3(s) = Sm^{+3}+CO_3^{-2}+H_2O$
Sn(IV)	SnO_2(am)	$SnO_2(am)+4H^{+} = Sn^{+4}+2H_2O$
Sn(IV)	$Ca[Sn(OH)_6]$(s)	$Ca[Sn(OH)_6](s)+6H^{+} = Sn^{+4}+6H_2O+Ca^{+2}$
Sr(II)	$SrCO_3$(strontianite)	$SrCO_3(s) = Sr^{+2}+CO_3^{-2}$
Sr(II)	$SrSO_4$(celestite)	$SrSO_4(s) = Sr^{+2}+SO_4^{-2}$
Tc(0)	Tc(s)	$Tc(cr)+H_2O+O_2 = TcO(OH)_2$
Tc(IV)	$TcO_2{\cdot}1.63H_2O$	$TcO_2 1.63H_2O = TcO(OH)_2+0.63H_2O$
Th(IV)	$ThO_2{\cdot}2H_2O$(am)	$ThO_2{\cdot}2H_2O(am)+4H^{+} = Th^{4+}+4H_2O$
U(IV)	$UO_2{\cdot}2H_2O$(am)	$UO_2{\cdot}2H_2O(am)+2H^{+}+0.5O_2 = UO_2^{+2}+3H_2O$
U(IV)	Coffinite	$USiO_4(s)+2H^{+}+0.5O_2 = UO_2^{+2}+H_4SiO_4$
U(VI)	Schoepite	$UO_3{\cdot}2aq(s)+2H^{+} = UO_2^{+2}+3H_2O$
U(VI)	$CaUO_4$(s)	$CaUO_4(s)+4H^{+} = UO_2^{+2}+Ca^{+2}+2H_2O$
U(VI)	Becquerelite	$Ca(UO_2)_6O_4(OH)_6{\cdot}8aq+14H^{+} = Ca^{+2}+6UO_2^{+2}+18H_2O$
U(VI)	Uranophane	$Ca((UO_2)_2SiO_3OH)_2{\cdot}5aq+6H^{+} = Ca^{+2}+2UO_2^{+2}+2H_4SiO_4+5H_2O$
Zr(IV)	$Zr(OH)_4$(s)	$Zr(OH)_4(s)+4H^{+} = Zr^{+4}+4H_2O$

Table A-6. Main type of uncertainty affecting to each one of the radionuclides under study.

Element	Associated uncertainty
C	Reduction to $CH_4(g)$
Cs	
Sr	SO_4^{2-} to HS^- reduction possibility of coprecipitation with other elements' carbonates
Ra	SO_4^{2-} to HS^- reduction; possibility of coprecipitation with other elements' carbonates
Sn	SO_4^{2-} to HS^- reduction;
Se	Formation of native Se^0; SO_4^{2-} to HS^- reduction;
Zr	Crystallinity of the solid phase
Nb	Scarcity of TDB
Tc	Formation of metallic Tc^0
Ni	SO_4^{2-} to HS^- reduction;
Pd	Formation of metallic Pd^0
Ag	Formation of metallic Ag^0; SO_4^{2-} to HS^- reduction;
Sm	Effect of phosphates in water; Stability of the solid hydroxo-carbonate
Ho	Effect of phosphates in water; Stability of the solid hydroxo-carbonate
Th	Cristallinity of the solid phase; Uncertain thermodynamic data for aqueous carbonates
Pa	Lack of thermodynamic data
U	Silicate solid precipitation TDB data on solid stability
Np	Crystallinity of the solid phase
Pu	Effect of phosphates in water; Stability of the solid hydroxo-carbonate; SO_4^{2-} to HS- reduction;
Am/Cm	Effect of phosphates in water; Stability of the solid hydroxo-carbonate;

Table A-7. Redox states given by the chosen groundwaters and solubility calculations described in Section 3.4.

Ag	Ag(I)
Am	Am(III)
C	C, methane
Ca	Ca(II)
Cl	Cl(-I)
Cm	Cm(III)
Cs	Cs(I)
Ho	Ho(III)
I	I(-I)
Nb	Nb(V)
Ni	Ni(II)
Np	Np(IV)
Pa	Pa(IV)
Pd	Pd(II)
Pu	Pu(IV)
Ra	Ra(II)
Se	Se(-II)
Sm	Sm(III)
Sn	Sn(IV)
Sr	Sr(II)
Tc	Tc(IV)
Th	Th(IV)
U	U(IV)
Zr	Zr(IV)

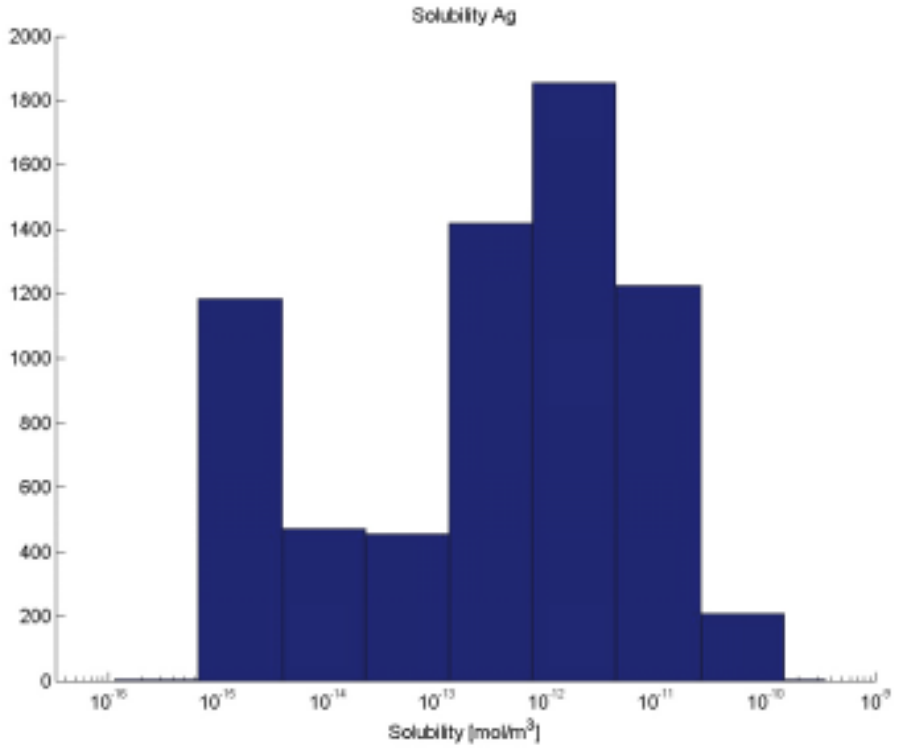

Figure A-1. *Solubility limits for Ag calculated using the methods explained in Section 3.4 using groundwater data from Section 6.1, y-axis shows the number of realisations in each bin.*

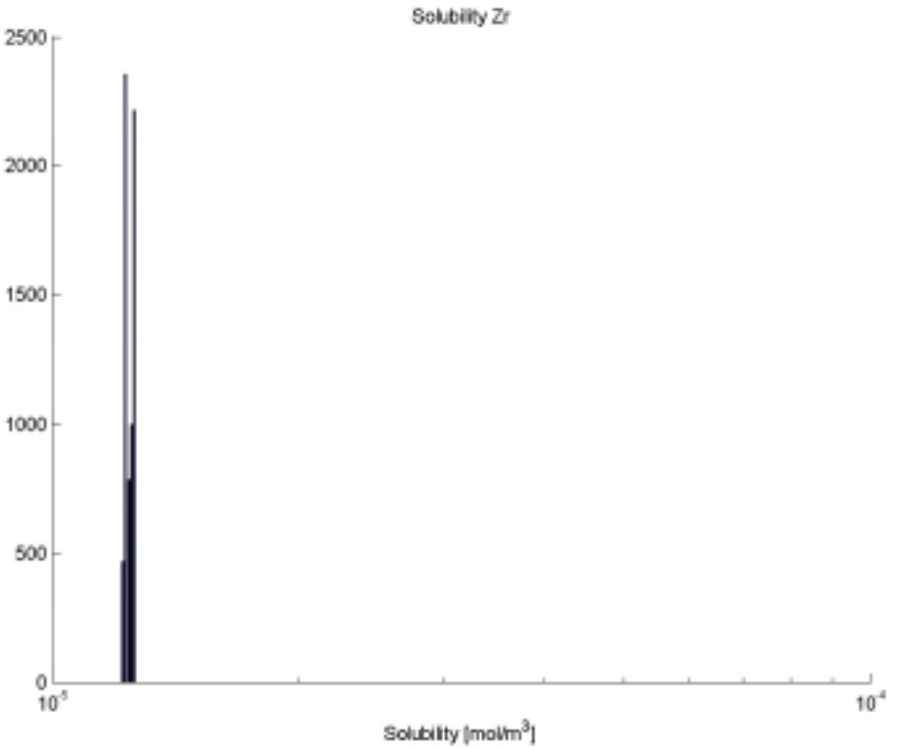

Figure A-2. *Solubility limits for Zr calculated using the methods explained in Section 3.4 using groundwater data from Section 6.1, y-axis shows the number of realisations in each bin.*

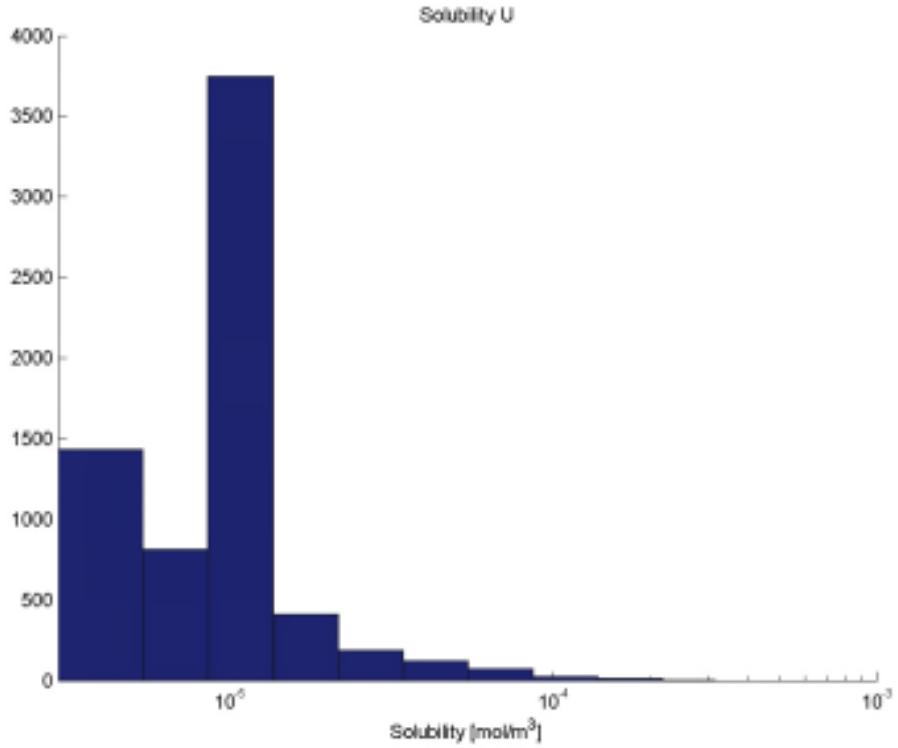

Figure A-3. *Solubility limits for U calculated using the methods explained in Section 3.4 using groundwater data from Section 6.1, y-axis shows the number of realisations in each bin.*

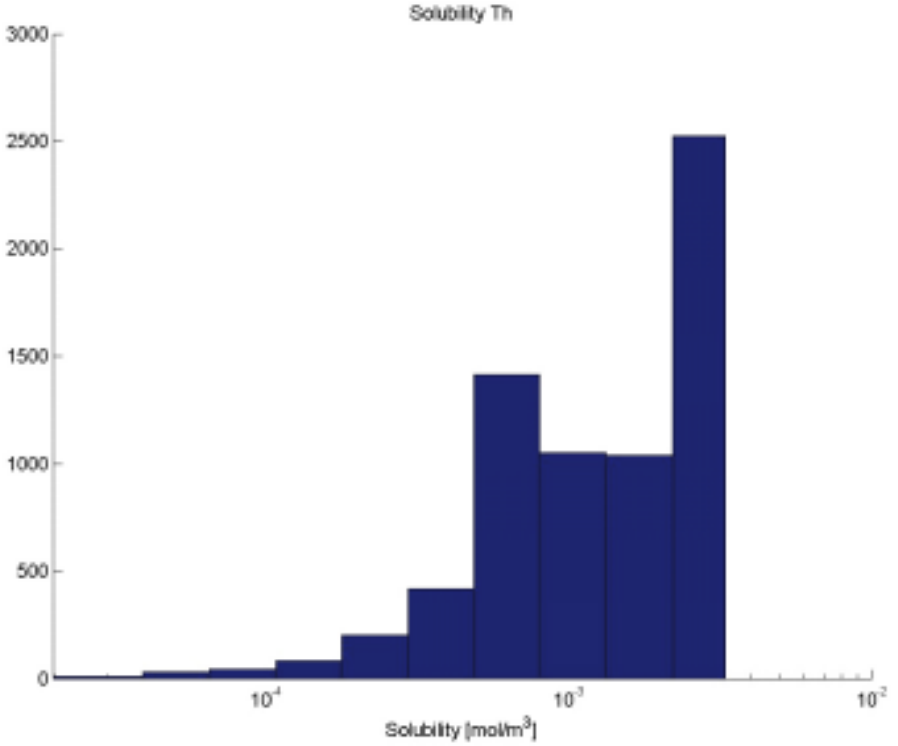

Figure A-4. *Solubility limits for Th calculated using the methods explained in Section 3.4 using groundwater data from Section 6.1, y-axis shows the number of realisations in each bin.*

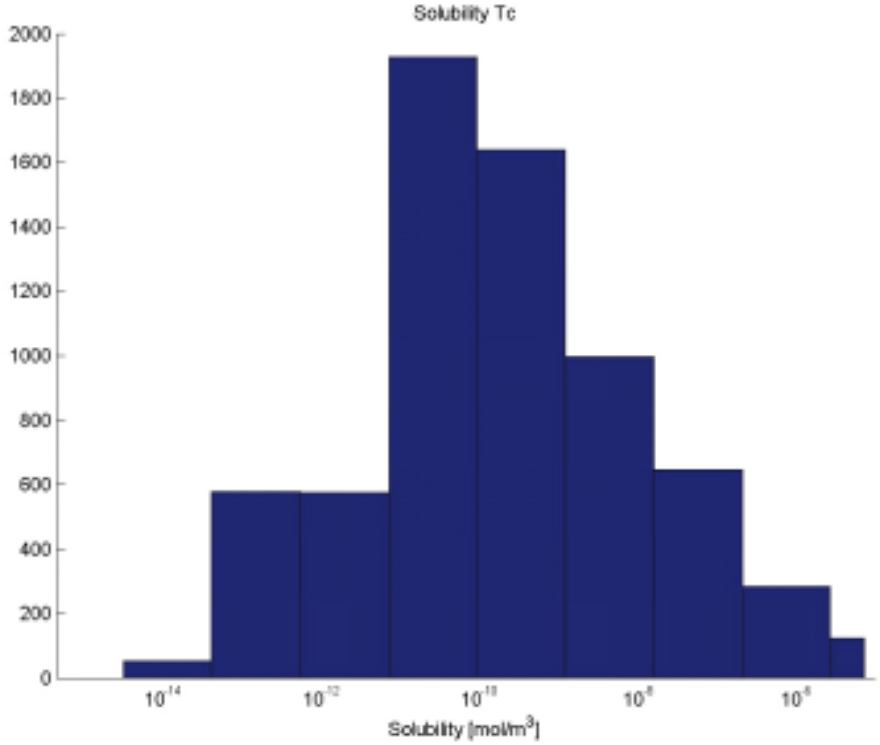

Figure A-5. *Solubility limits for Tc calculated using the methods explained in Section 3.4 using groundwater data from Section 6.1, y-axis shows the number of realisations in each bin.*

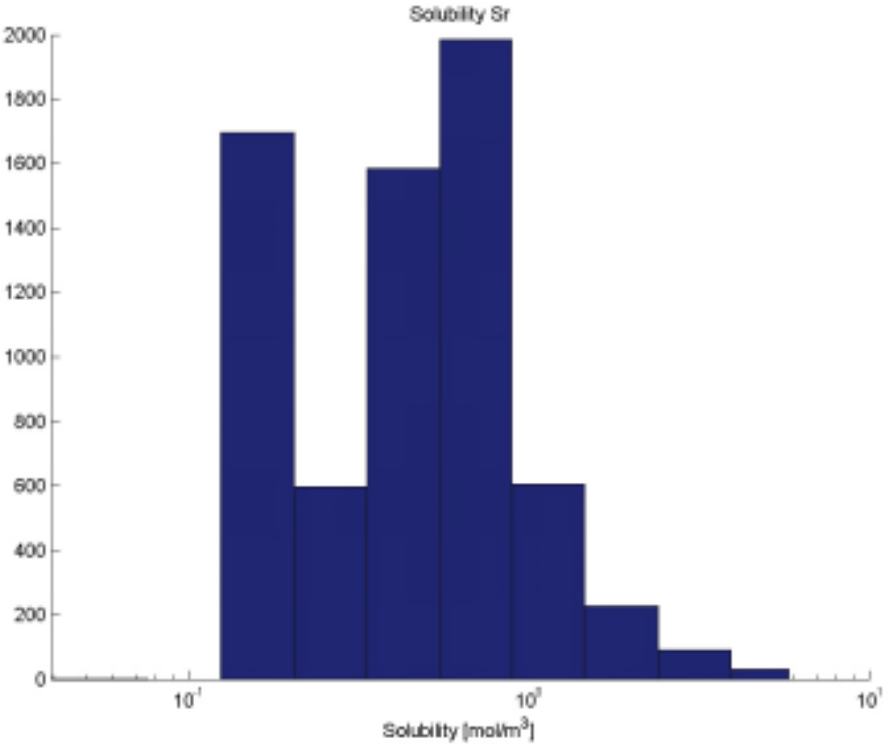

Figure A-6. *Solubility limits for Sr calculated using the methods explained in Section 3.4 using groundwater data from Section 6.1, y-axis shows the number of realisations in each bin.*

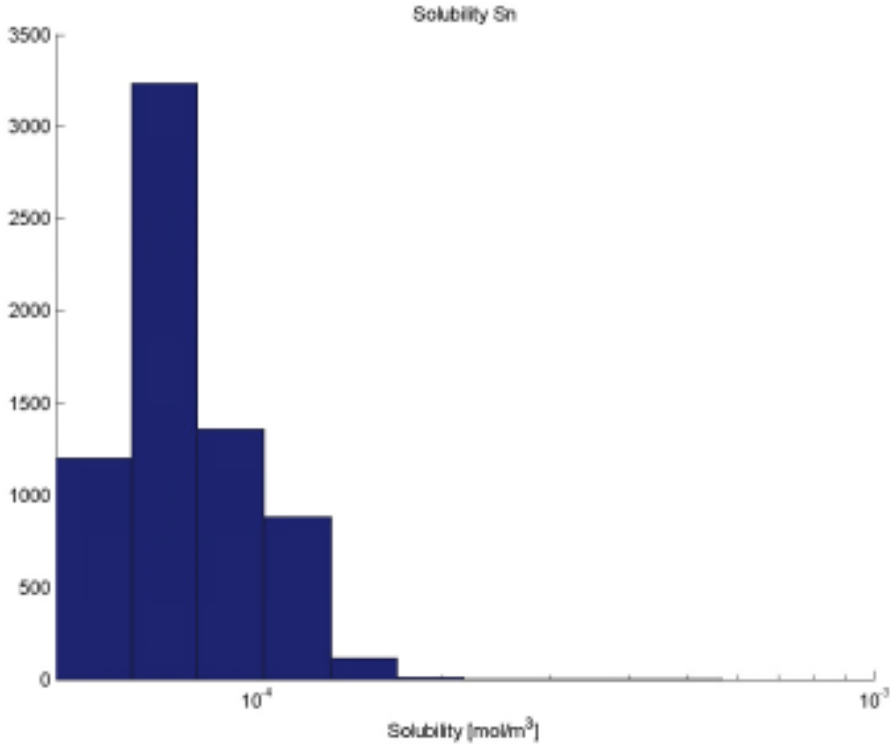

Figure A-7. *Solubility limits for Sn calculated using the methods explained in Section 3.4 using groundwater data from Section 6.1, y-axis shows the number of realisations in each bin.*

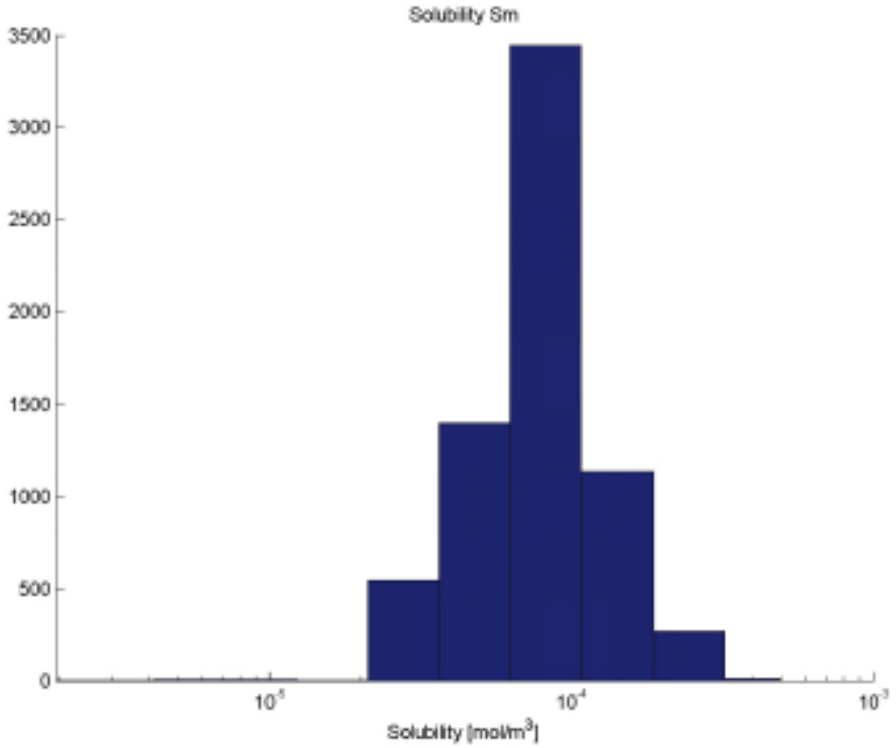

Figure A-8. *Solubility limits for Sm calculated using the methods explained in Section 3.4 using groundwater data from Section 6.1, y-axis shows the number of realisations in each bin.*

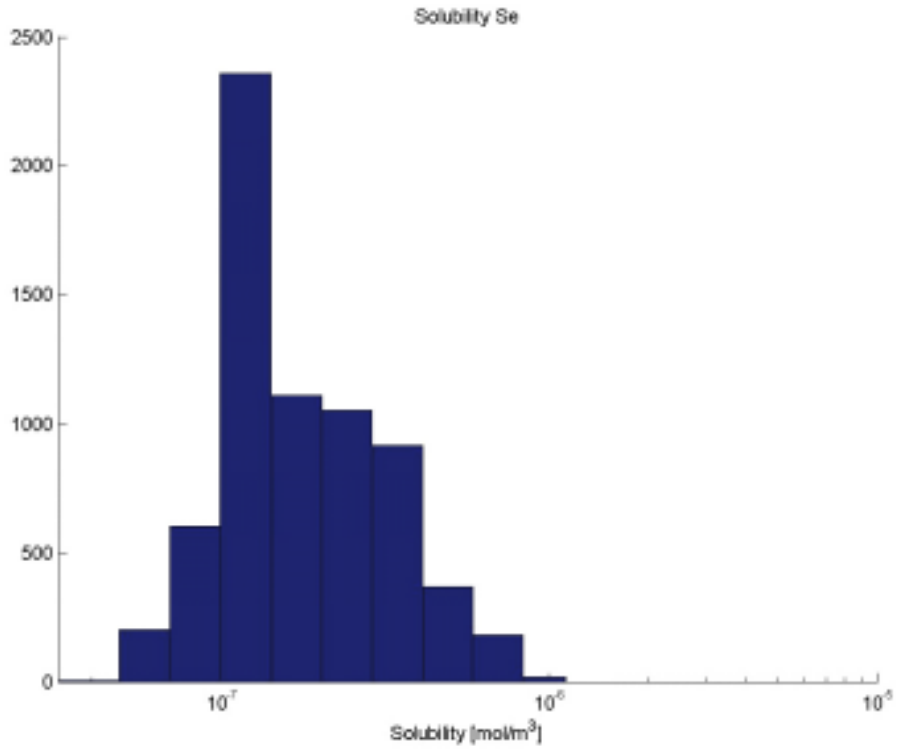

Figure A-9. *Solubility limits for Se calculated using the methods explained in Section 3.4 using groundwater data from Section 6.1, y-axis shows the number of realisations in each bin.*

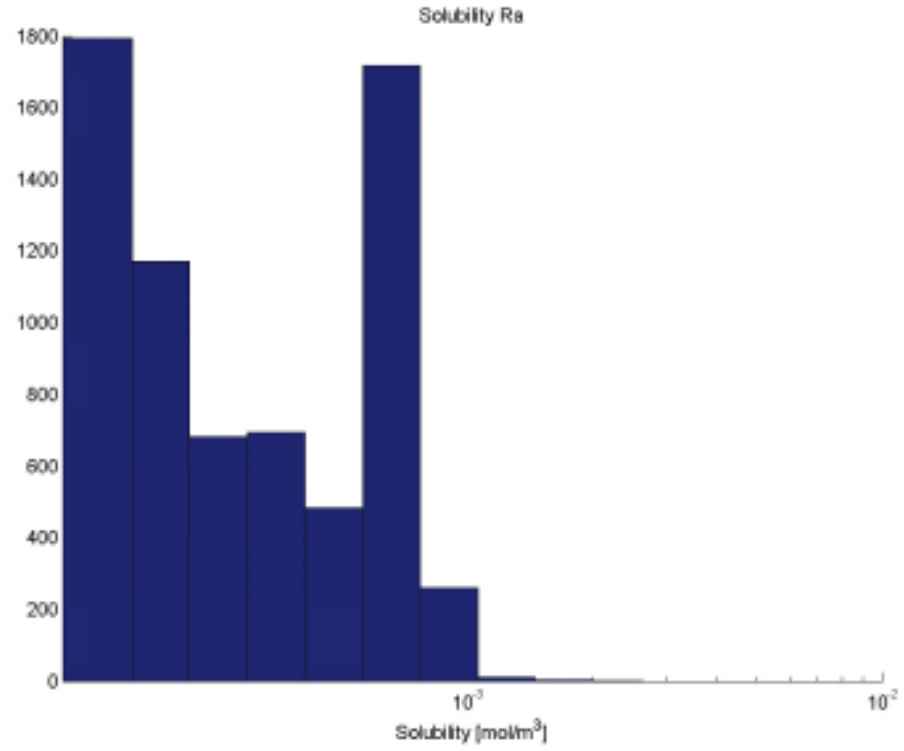

Figure A-10. *Solubility limits for Ra calculated using the methods explained in Section 3.4 using groundwater data from Section 6.1, y-axis shows the number of realisations in each bin.*

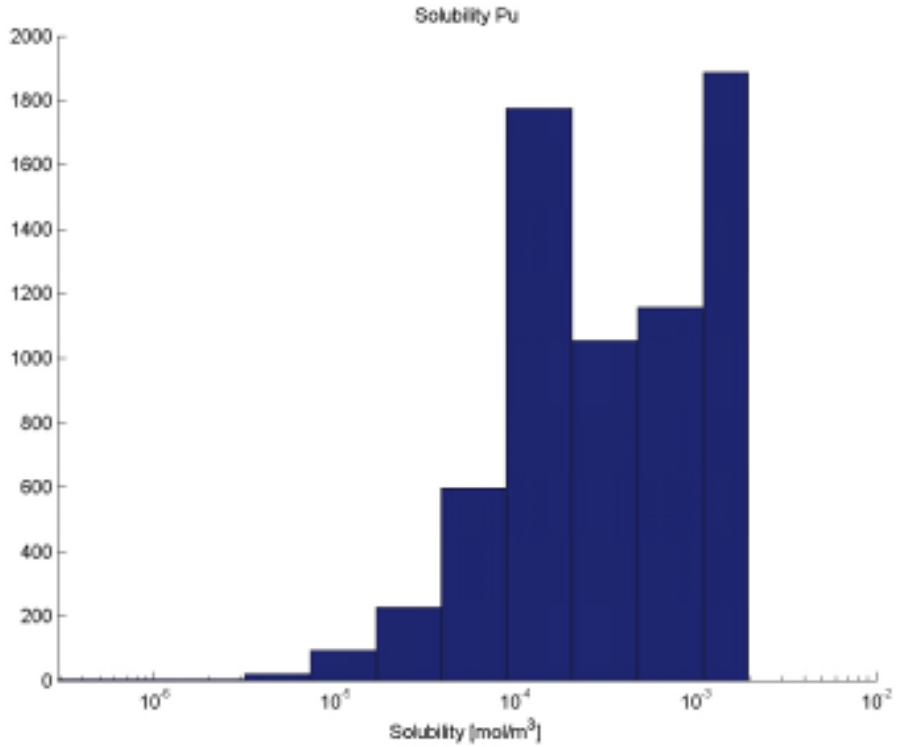

Figure A-11. *Solubility limits for Pu calculated using the methods explained in Section 3.4 using groundwater data from Section 6.1, y-axis shows the number of realisations in each bin.*

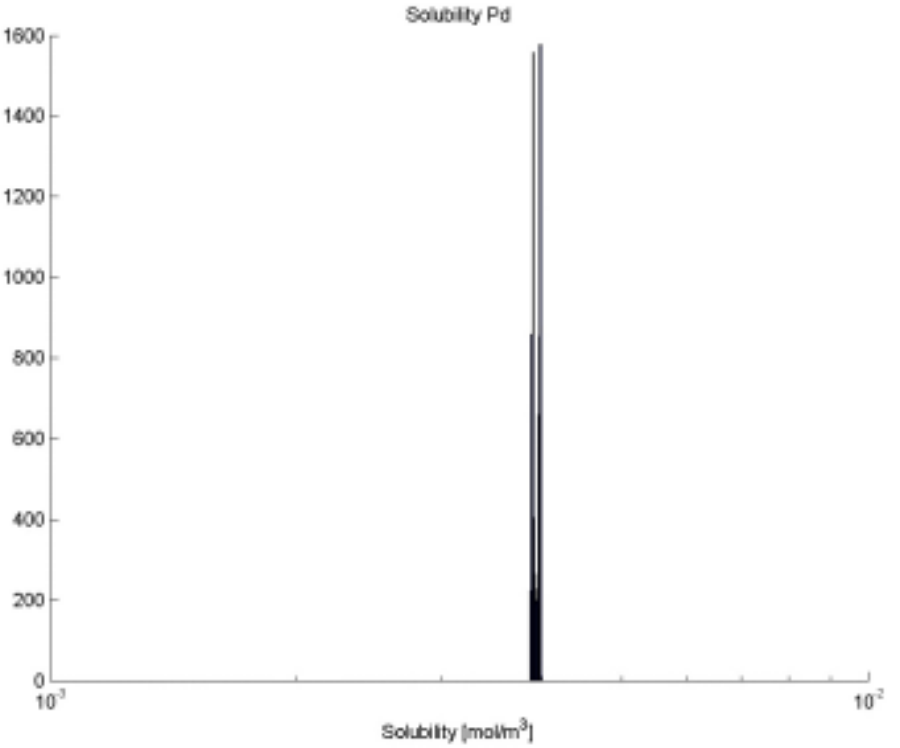

Figure A-12. *Solubility limits for Pd calculated using the methods explained in Section 3.4 using groundwater data from Section 6.1, y-axis shows the number of realisations in each bin.*

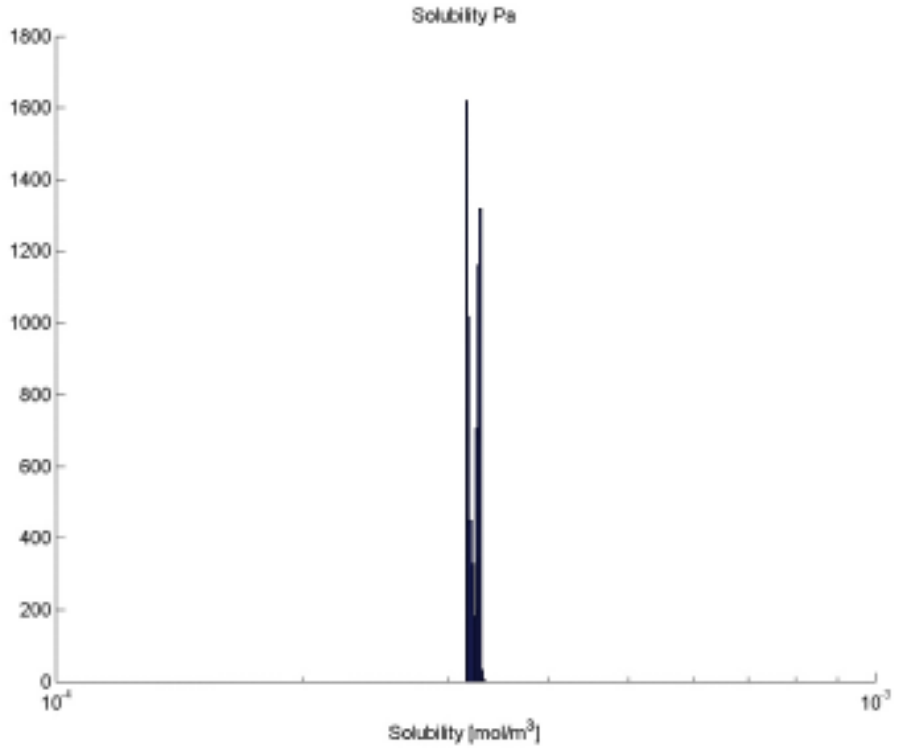

Figure A-13. *Solubility limits for Pa calculated using the methods explained in Section 3.4 using groundwater data from Section 6.1, y-axis shows the number of realisations in each bin.*

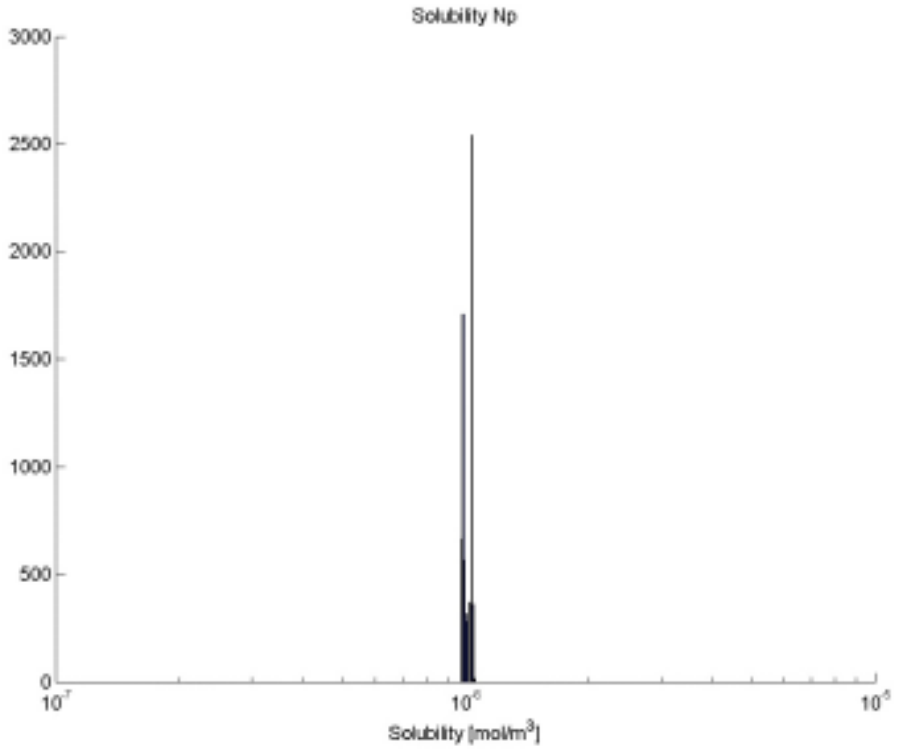

Figure A-14. *Solubility limits for Np calculated using the methods explained in Section 3.4 using groundwater data from Section 6.1, y-axis shows the number of realisations in each bin.*

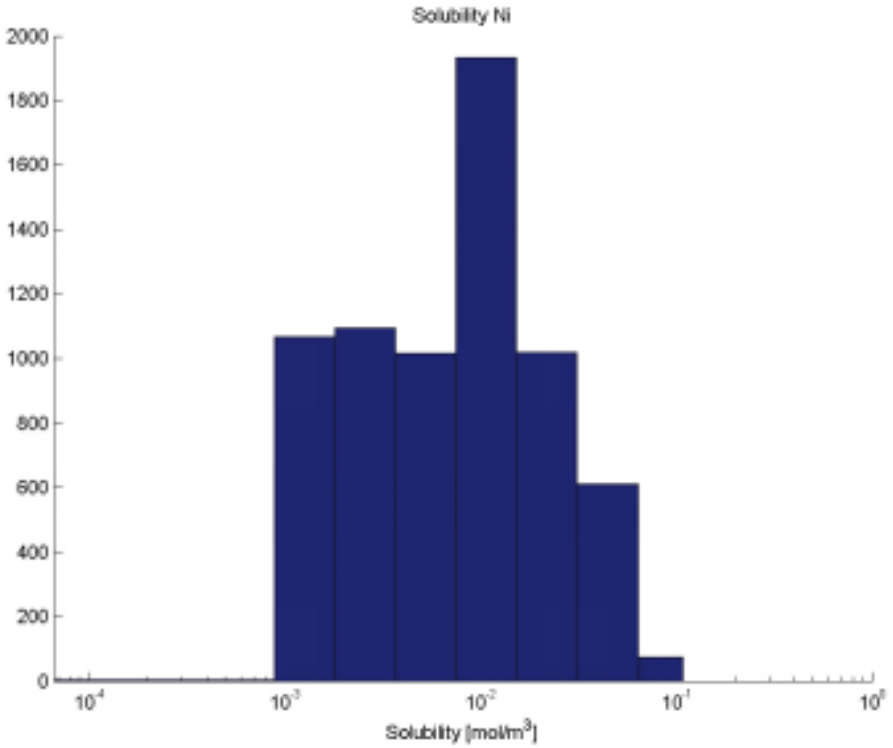

Figure A-15. *Solubility limits for Ni calculated using the methods explained in Section 3.4 using groundwater data from Section 6.1, y-axis shows the number of realisations in each bin.*

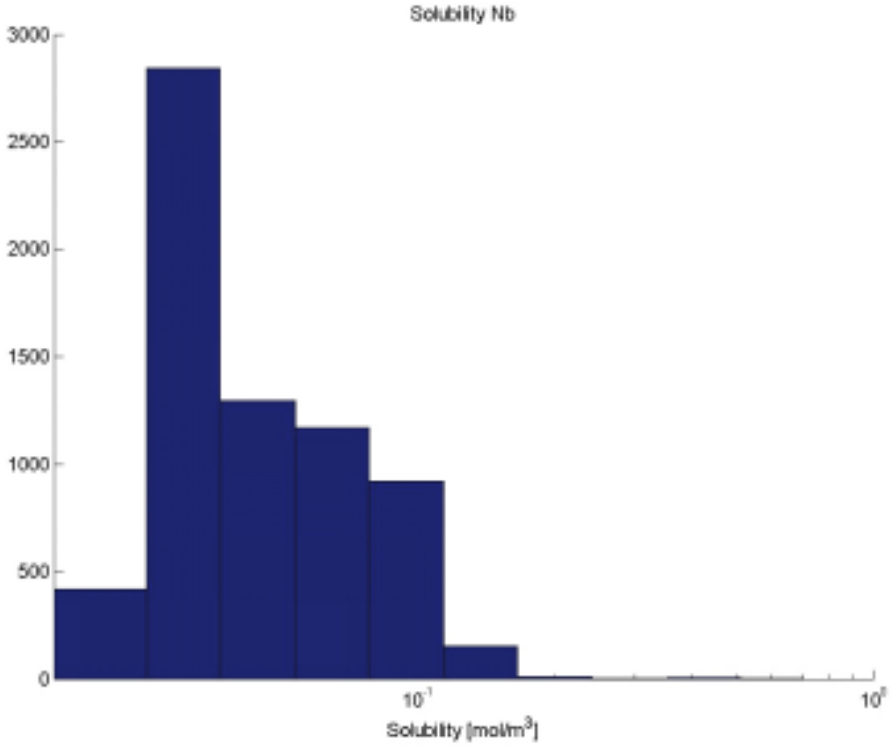

Figure A-16. *Solubility limits for Nb calculated using the methods explained in Section 3.4 using groundwater data from Section 6.1, y-axis shows the number of realisations in each bin.*

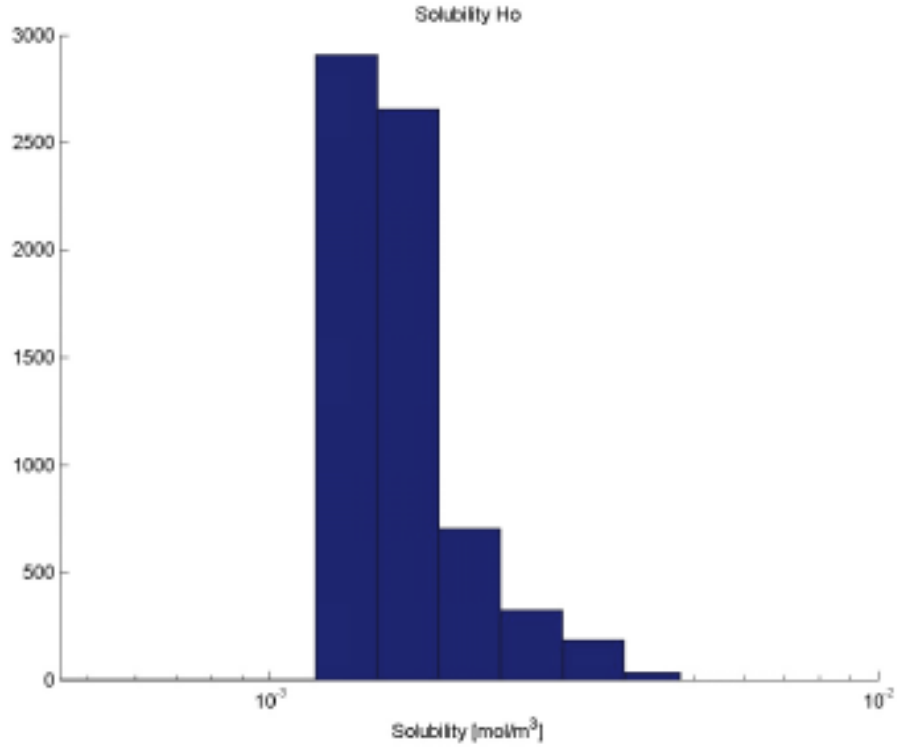

Figure A-17. *Solubility limits for Ho calculated using the methods explained in Section 3.4 using groundwater data from Section 6.1, y-axis shows the number of realisations in each bin.*

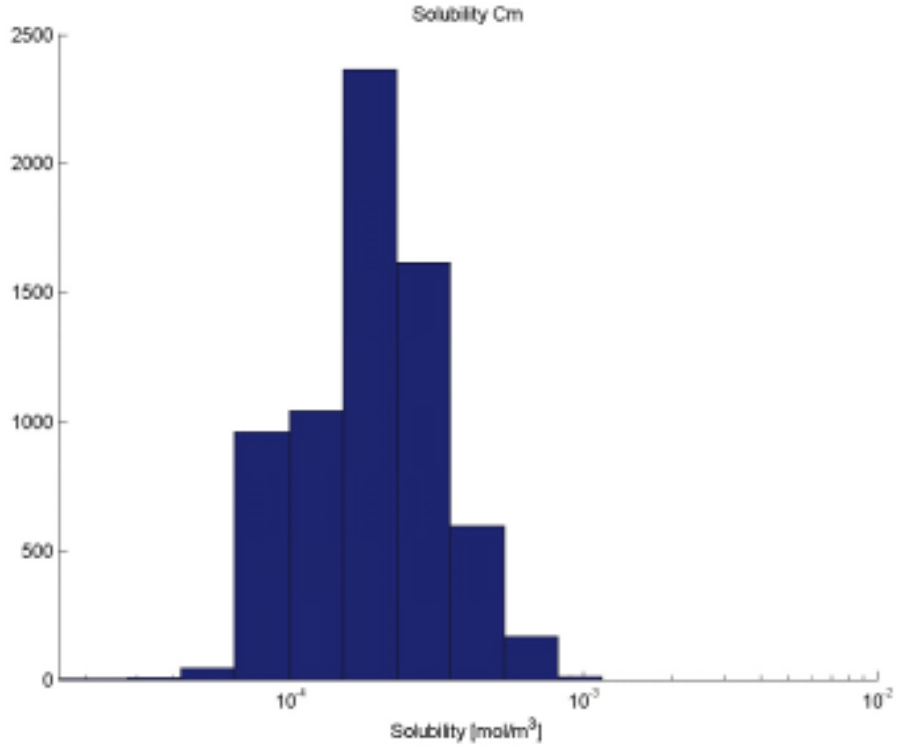

Figure A-18. *Solubility limits for Cm calculated using the methods explained in Section 3.4 using groundwater data from Section 6.1, y-axis shows the number of realisations in each bin.*

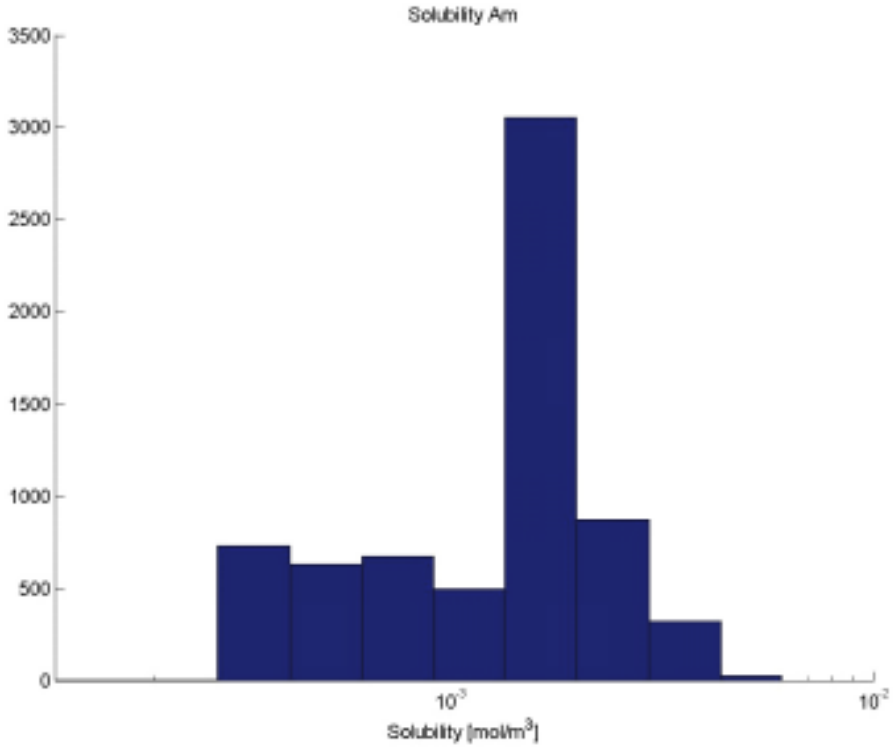

Figure A-19. *Solubility limits for Am calculated using the methods explained in Section 3.4 using groundwater data from Section 6.1, y-axis shows the number of realisations in each bin.*

A4 Buffer

Table A-8. Density and porosity distributions for MX-80 and Deponite CA-N bentonite buffer.

Distribution parameter	Value
Central fully saturated density	$2.00 \cdot 10^3$ kg/m^3
Standard deviation	$0.05 \cdot 10^3$ kg/m^3
Central porosity	0.44
Standard deviation	0.03

Table A-9. Reference groundwater used when determining the porewater composition based on saline Beberg water (BFI01) /Laaksoharju et al. 1998/ and the composition of the "highly saline" alternative groundwater.

Species/entity	"Saline" reference groundwater	"Highly saline" groundwater
Na^+ (mol/l)	$7.39 \cdot 10^{-2}$	$5.74 \cdot 10^{-1}$
K^+ (mol/l)	$3.32 \cdot 10^{-4}$	$3.32 \cdot 10^{-4}$
Ca^{+2} (mol/l)	$4.12 \cdot 10^{-2}$	$4.12 \cdot 10^{-2}$
Mg^{+2} (mol/l)	$4.53 \cdot 10^{-3}$	$4.53 \cdot 10^{-3}$
CO_3^{-2} (mol/l)	$7.70 \cdot 10^{-4}$	$7.25 \cdot 10^{-4}$
H^+ (mol/l)	$8.59 \cdot 10^{-4}$	$7.7 \cdot 10^{-4}$
Cl^- (mol/l)	$1.56 \cdot 10^{-1}$	$6.55 \cdot 10^{-1}$
SO_4^{-2} (mol/l)	$3.85 \cdot 10^{-3}$	$3.85 \cdot 10^{-3}$
pH	7.00	7.18
pCO_2	–2.56	–2.79
Change balance (%)	0.99	0.34
Ionic strength (mol/l)	0.208	0.706

Table A-10. Reference porewater (RPW) composition in bentonite based on reference groundwater Table A-9 and open CO_2 system.

Species/entity	Reference porewater
Na^+ (mol/m^3)	$2.57 \cdot 10^{-1}$
K^+ (mol/m^3)	$5.50 \cdot 10^{-4}$
Ca^{2+} (mol/m^3)	$1.44 \cdot 10^{-2}$
Mg^{2+} (mol/m^3)	$4.08 \cdot 10^{-3}$
CO_3^{2-} (mol/m^3)	$1.48 \cdot 10^{-3}$
H^+ (mol/m^3)	$-4.55 \cdot 10^{-2}$
Cl^- (mol/m^3)	$1.60 \cdot 10^{-1}$
SO_4^{2-} (mol/m^3)	$4.36 \cdot 10^{-2}$
$H_2SiO_4^{2-}$ (mol/m^3)	$1.08 \cdot 10^{-4}$
SOH (mol/m^3)	$8.57 \cdot 10^{-2}$
LAX (mol/m^3)	$3.31 \cdot 10^{0}$
pH	7.38
pCO_2	–2.6
Ionic Strength	0.29
System	Open
Solids	Quartz
	Calcite
	Gypsum

Table A-11. Buffer, recommended D_e and ε values for reference density and all groundwater types.

Species (Redox state)	D_e (m^2/s)	Upper D_e limit (m^2/s)	Lower D_e limit (m^2/s)	ε (−)	Lower ε limit (−)	Upper ε limit (−)
Ag(I)	$1.2 \cdot 10^{-10}$	$1.91 \cdot 10^{-10}$	$4.94 \cdot 10^{-11}$	0.43	–	–
Am(III)	$1.2 \cdot 10^{-10}$	$1.91 \cdot 10^{-10}$	$4.94 \cdot 10^{-11}$	0.43	–	–
C, carbonate species	$1.0 \cdot 10^{-11}$	$3.0 \cdot 10^{-11}$	$3.0 \cdot 10^{-12}$	0.17	0.12	0.24
C, methane	$1.2 \cdot 10^{-10}$	$1.91 \cdot 10^{-10}$	$4.94 \cdot 10^{-11}$	0.43		
C, organic acids	$1.0 \cdot 10^{-11}$	$3.0 \cdot 10^{-11}$	$3.0 \cdot 10^{-12}$	0.17	0.12	0.24
Ce(III)	$1.2 \cdot 10^{-10}$	$1.91 \cdot 10^{-10}$	$4.94 \cdot 10^{-11}$	0.43	–	–
Cl(–I)	$1.0 \cdot 10^{-11}$	$3.0 \cdot 10^{-11}$	$3.0 \cdot 10^{-12}$	0.17	0.12	0.24
Cm(III)	$1.2 \cdot 10^{-10}$	$1.91 \cdot 10^{-10}$	$4.94 \cdot 10^{-11}$	0.43	–	–
Cs(I)	$3.0 \cdot 10^{-10}$	$3.0 \cdot 10^{-10}$	$4.94 \cdot 10^{-11}$	0.43	–	–
Eu(III)	$1.2 \cdot 10^{-10}$	$1.91 \cdot 10^{-10}$	$4.94 \cdot 10^{-11}$	0.43	–	–
Ho(III)	$1.2 \cdot 10^{-10}$	$1.91 \cdot 10^{-10}$	$4.94 \cdot 10^{-11}$	0.43	–	–
I(–I)	$1.0 \cdot 10^{-11}$	$3.0 \cdot 10^{-11}$	$3.0 \cdot 10^{-12}$	0.17	0.12	0.24
Nb(V)	$1.2 \cdot 10^{-10}$	$1.91 \cdot 10^{-10}$	$4.94 \cdot 10^{-11}$	0.43	–	–
Ni(II)	$1.2 \cdot 10^{-10}$	$1.91 \cdot 10^{-10}$	$4.94 \cdot 10^{-11}$	0.43	–	–
Np(IV)	$1.2 \cdot 10^{-10}$	$1.91 \cdot 10^{-10}$	$4.94 \cdot 10^{-11}$	0.43	–	–
Np(V)	$1.2 \cdot 10^{-10}$	$1.91 \cdot 10^{-10}$	$4.94 \cdot 10^{-11}$	0.43	–	–
Pa(IV)	$1.2 \cdot 10^{-10}$	$1.91 \cdot 10^{-10}$	$4.94 \cdot 10^{-11}$	0.43	–	–
Pa(V)	$1.2 \cdot 10^{-10}$	$1.91 \cdot 10^{-10}$	$4.94 \cdot 10^{-11}$	0.43	–	–
Pb(II)	$1.2 \cdot 10^{-10}$	$1.91 \cdot 10^{-10}$	$4.94 \cdot 10^{-11}$	0.43	–	–
Pd(II)	$1.2 \cdot 10^{-10}$	$1.91 \cdot 10^{-10}$	$4.94 \cdot 10^{-11}$	0.43	–	–
Pu(III)	$1.2 \cdot 10^{-10}$	$1.91 \cdot 10^{-10}$	$4.94 \cdot 10^{-11}$	0.43	–	–
Pu(IV)	$1.2 \cdot 10^{-10}$	$1.91 \cdot 10^{-10}$	$4.94 \cdot 10^{-11}$	0.43	–	–
Pu(V)	$1.2 \cdot 10^{-10}$	$1.91 \cdot 10^{-10}$	$4.94 \cdot 10^{-11}$	0.43	–	–
Pu(VI)	$1.2 \cdot 10^{-10}$	$1.91 \cdot 10^{-10}$	$4.94 \cdot 10^{-11}$	0.43	–	–
Ra(II)	$1.2 \cdot 10^{-10}$	$1.91 \cdot 10^{-10}$	$4.94 \cdot 10^{-11}$	0.43	–	–
Rn(–)	$1.2 \cdot 10^{-10}$	$1.91 \cdot 10^{-10}$	$4.94 \cdot 10^{-11}$	0.43	–	–
Se(–II)	$1.0 \cdot 10^{-11}$	$3.0 \cdot 10^{-11}$	$3.0 \cdot 10^{-12}$	0.17	0.12	0.24
Se(IV)	$1.0 \cdot 10^{-11}$	$3.0 \cdot 10^{-11}$	$3.0 \cdot 10^{-12}$	0.17	0.12	0.24
Se(VI)	$1.0 \cdot 10^{-11}$	$3.0 \cdot 10^{-11}$	$3.0 \cdot 10^{-12}$	0.17	0.12	0.24
Sm(III)	$1.2 \cdot 10^{-10}$	$1.91 \cdot 10^{-10}$	$4.94 \cdot 10^{-11}$	0.43	–	–
Sn(IV)	$1.2 \cdot 10^{-10}$	$1.91 \cdot 10^{-10}$	$4.94 \cdot 10^{-11}$	0.43	–	–
Sr(II)	$1.2 \cdot 10^{-10}$	$1.91 \cdot 10^{-10}$	$4.94 \cdot 10^{-11}$	0.43	–	–
Tc(IV)	$1.2 \cdot 10^{-10}$	$1.91 \cdot 10^{-10}$	$4.94 \cdot 10^{-11}$	0.43	–	–
Tc(VII)	$1.0 \cdot 10^{-11}$	$3.0 \cdot 10^{-11}$	$3.0 \cdot 10^{-12}$	0.17	0.12	0.24
Th(IV)	$1.2 \cdot 10^{-10}$	$1.91 \cdot 10^{-10}$	$4.94 \cdot 10^{-11}$	0.43	–	–
U(IV)	$1.2 \cdot 10^{-10}$	$1.91 \cdot 10^{-10}$	$4.94 \cdot 10^{-11}$	0.43	–	–
U(VI)	$1.2 \cdot 10^{-10}$	$1.91 \cdot 10^{-10}$	$4.94 \cdot 10^{-11}$	0.43	–	–
Zr(IV)	$1.2 \cdot 10^{-10}$	$1.91 \cdot 10^{-10}$	$4.94 \cdot 10^{-11}$	0.43	–	–

Table A-12. Buffer, recommended K_d values for reference porewater (RPW), to be used for saline and non-saline groundwater (see composition in Table A-9).

Species (Redox State)	K_d (m^3/kg)	Upper K_d limit (m^3/kg)	Lower K_d limit (m^3/kg)	Correlation group
Ag(I)	0	15	0	–
Am(III)	61	378	10	3
C, carbonate species	Isotope exchange	–	–	–
C, methane	0	0	0	–
C, organic acids	0	0	0	–
Ce(III)	8	93	0.8	3
Cl(–I)	0	0	0	7
Cm(III)	61	378	10	3
Cs(I)	0.11	0.6	0.018	1
Eu(III)	8	93	0.8	3
Ho(III)	8	93	0.8	3
I(–I)	0	0	0	7
Nb(V)	3	45	0.2	–
Ni(II)	0.30	3.3	0.03	2
Np(IV)	63	1,113	4	4
Np(V)	0.02	0.2	0.004	5
Pa(IV)	3	45	0.2	–
Pa(V)	3	45	0.2	–
Pb(II)	74	457	12	2
Pd(II)	5	75	0.3	–
Pu(III)	100	984	10	3
Pu(IV)	63	1,111	4	4
Pu(V)	0.02	0.2	0.002	5
Pu(VI)	3	28	0.3	6
Ra(II)	0.005	0.03	0.001	1
Rn(–)	0	0	0	–
Se(–II)	0	0	0	
Se(IV)	0.04	0.4	0.003	–
Se(VI)	0	0	0	7
Sm(III)	8	93	0.8	3
Sn(IV)	63	1,764	2.3	4
Sr(II)	0.005	0.031	0.0009	1
Tc(IV)	63	1,764	2.3	4
Tc(VII)	0	0	0	7
Th(IV)	63	700	6	4
U(IV)	63	1,113	3.6	4
U(VI)	3	18	0.5	6
Zr(IV)	4	103	0.1	4

Correlation groups according to Section 5.4.7.

Table A-13. Buffer, recommended K_d values for highly saline porewater (HSPW), corresponding to highly saline groundwater.

Species (Redox State)	K_d (m^3/kg)	Upper K_d limit (m^3/kg)	Lower K_d limit (m^3/kg)	Correlation group
Ag(I)	0	15	0	–
Am(III)	24	152	4	3
C, carbonate species	Isotope exchange	–	–	–
C, methane	0	0	0	–
C, organic acids	0	0	0	–
Ce(III)	5	57	0.5	3
Cl(–I)	0	0	0	7
Cm(III)	24	152	4	3
Cs(I)	0.03	0.2	0.006	1
Eu(III)	5	57	0.5	3
Ho(III)	5	57	0.5	3
I(–I)	0	0	0	7
Nb(V)	3	45	0.2	–
Ni(II)	0.07	0.8	0.01	2
Np(IV)	40	702	2	4
Np(V)	0.02	0.1	0.004	5
Pa(IV)	3	45	0.2	–
Pa(V)	3	45	0.2	–
Pb(II)	46	287	7	2
Pd(II)	5	75	0.3	–
Pu(III)	43	421	4	3
Pu(IV)	40	700	2	4
Pu(V)	0.02	0.2	0.002	5
Pu(VI)	3	28	0.3	6
Ra(II)	0.001	0.01	0.0002	1
Rn(–)	0	0	0	–
Se(–II)	0	0	0	
Se(IV)	0.05	0.6	0.005	–
Se(VI)	0	0	0	7
Sm(III)	5	57	0.5	3
Sn(IV)	40	1,113	1.4	4
Sr(II)	0.001	0.008	0.0002	1
Tc(IV)	40	1,113	1.4	4
Tc(VII)	0	0	0	7
Th(IV)	40	442	4	4
U(IV)	40	703	2.3	4
U(VI)	3	18	0.5	6
Zr(IV)	5	134	0.2	4

Correlation group according to Section 5.4.7.

A5 Backfill

Table A-14. Density and porosity distributions for Friedland Clay backfill.

Distribution parameter	Value
Central fully saturated density	$2.19 \cdot 10^3$ kg/m^3
Standard deviation	$0.08 \cdot 10^3$ kg/m^3
Central porosity	0.41
Standard deviation	0.03

Table A-15. Density and porosity distributions for pre-compacted 30/70 bentonite/ballast backfill.

Distribution Parameter	Value
Central fully saturated density	$2.30 \cdot 10^3$ kg/m^3
Standard deviation	$0.08 \cdot 10^3$ kg/m^3
Central porosity	0.37
Standard deviation	0.03

Table A-16. Density and porosity distributions for in situ compacted 30/70 bentonite/ballast backfill.

Distribution Parameter	Value
Central fully saturated density	$2.23 \cdot 10^3$ kg/m^3
Standard deviation	$0.08 \cdot 10^3$ kg/m^3
Central porosity	0.33
Standard deviation	0.03

Table A-17. Friedland Clay backfill: Recommended D_e and ε values for reference density and for all groundwater types.

Species (Redox State)	D_e (m^2/s)	Upper D_e limit(m^2/s)	Lower D_e limit(m^2/s)	ε (−)	Upper ε limit (−)	Lower ε limit (−)
Ag(I)	$7.00 \cdot 10^{-11}$	$1.10 \cdot 10^{-10}$	$2.90 \cdot 10^{-11}$	0.36		
Am(III)	$7.00 \cdot 10^{-11}$	$1.10 \cdot 10^{-10}$	$2.90 \cdot 10^{-11}$	0.36		
C, carbonate species	$5.60 \cdot 10^{-12}$	$1.70 \cdot 10^{-11}$	$1.70 \cdot 10^{-12}$	0.14	0.2	0.1
C, methane	$7.00 \cdot 10^{-11}$	$1.10 \cdot 10^{-10}$	$2.90 \cdot 10^{-11}$	0.36		
C, organic acids	$5.60 \cdot 10^{-12}$	$1.70 \cdot 10^{-11}$	$1.70 \cdot 10^{-12}$	0.14	0.2	0.1
Ce(III)	$7.00 \cdot 10^{-11}$	$1.10 \cdot 10^{-10}$	$2.90 \cdot 10^{-11}$	0.36		
Cl(–I)	$5.60 \cdot 10^{-12}$	$1.70 \cdot 10^{-11}$	$1.70 \cdot 10^{-12}$	0.14	0.2	0.1
Cm(III)	$7.00 \cdot 10^{-11}$	$1.10 \cdot 10^{-10}$	$2.90 \cdot 10^{-11}$	0.36		
Cs(I)	$2.10 \cdot 10^{-10}$	$2.10 \cdot 10^{-10}$	$2.90 \cdot 10^{-11}$	0.36		
Eu(III)	$7.00 \cdot 10^{-11}$	$1.10 \cdot 10^{-10}$	$2.90 \cdot 10^{-11}$	0.36		
Ho(III)	$7.00 \cdot 10^{-11}$	$1.10 \cdot 10^{-10}$	$2.90 \cdot 10^{-11}$	0.36		
I(–I)	$5.60 \cdot 10^{-12}$	$1.70 \cdot 10^{-11}$	$1.70 \cdot 10^{-12}$	0.14	0.2	0.1
Nb(V)	$7.00 \cdot 10^{-11}$	$1.10 \cdot 10^{-10}$	$2.90 \cdot 10^{-11}$	0.36		
Ni(II)	$7.00 \cdot 10^{-11}$	$1.10 \cdot 10^{-10}$	$2.90 \cdot 10^{-11}$	0.36		
Np(IV)	$7.00 \cdot 10^{-11}$	$1.10 \cdot 10^{-10}$	$2.90 \cdot 10^{-11}$	0.36		
Np(V)	$7.00 \cdot 10^{-11}$	$1.10 \cdot 10^{-10}$	$2.90 \cdot 10^{-11}$	0.36		
Pa(IV)	$7.00 \cdot 10^{-11}$	$1.10 \cdot 10^{-10}$	$2.90 \cdot 10^{-11}$	0.36		
Pa(V)	$7.00 \cdot 10^{-11}$	$1.10 \cdot 10^{-10}$	$2.90 \cdot 10^{-11}$	0.36		
Pb(II)	$7.00 \cdot 10^{-11}$	$1.10 \cdot 10^{-10}$	$2.90 \cdot 10^{-11}$	0.36		
Pd(II)	$7.00 \cdot 10^{-11}$	$1.10 \cdot 10^{-10}$	$2.90 \cdot 10^{-11}$	0.36		
Pu(III)	$7.00 \cdot 10^{-11}$	$1.10 \cdot 10^{-10}$	$2.90 \cdot 10^{-11}$	0.36		
Pu(IV)	$7.00 \cdot 10^{-11}$	$1.10 \cdot 10^{-10}$	$2.90 \cdot 10^{-11}$	0.36		
Pu(V)	$7.00 \cdot 10^{-11}$	$1.10 \cdot 10^{-10}$	$2.90 \cdot 10^{-11}$	0.36		
Pu(VI)	$7.00 \cdot 10^{-11}$	$1.10 \cdot 10^{-10}$	$2.90 \cdot 10^{-11}$	0.36		
Ra(II)	$7.00 \cdot 10^{-11}$	$1.10 \cdot 10^{-10}$	$2.90 \cdot 10^{-11}$	0.36		
Rn(–)	$7.00 \cdot 10^{-11}$	$1.10 \cdot 10^{-10}$	$2.90 \cdot 10^{-11}$	0.36		
Se(–II)	$5.60 \cdot 10^{-12}$	$1.70 \cdot 10^{-11}$	$1.70 \cdot 10^{-12}$	0.14	0.2	0.1
Se(IV)	$5.60 \cdot 10^{-12}$	$1.70 \cdot 10^{-11}$	$1.70 \cdot 10^{-12}$	0.14	0.2	0.1
Se(VI)	$5.60 \cdot 10^{-12}$	$1.70 \cdot 10^{-11}$	$1.70 \cdot 10^{-12}$	0.14	0.2	0.1
Sm(III)	$7.00 \cdot 10^{-11}$	$1.10 \cdot 10^{-10}$	$2.90 \cdot 10^{-11}$	0.36		
Sn(IV)	$7.00 \cdot 10^{-11}$	$1.10 \cdot 10^{-10}$	$2.90 \cdot 10^{-11}$	0.36		
Sr(II)	$7.00 \cdot 10^{-11}$	$1.10 \cdot 10^{-10}$	$2.90 \cdot 10^{-11}$	0.36		
Tc(IV)	$7.00 \cdot 10^{-11}$	$1.10 \cdot 10^{-10}$	$2.90 \cdot 10^{-11}$	0.36		
Tc(VII)	$5.60 \cdot 10^{-12}$	$1.70 \cdot 10^{-11}$	$1.70 \cdot 10^{-12}$	0.14	0.2	0.1
Th(IV)	$7.00 \cdot 10^{-11}$	$1.10 \cdot 10^{-10}$	$2.90 \cdot 10^{-11}$	0.36		
U(IV)	$7.00 \cdot 10^{-11}$	$1.10 \cdot 10^{-10}$	$2.90 \cdot 10^{-11}$	0.36		
U(VI)	$7.00 \cdot 10^{-11}$	$1.10 \cdot 10^{-10}$	$2.90 \cdot 10^{-11}$	0.36		
Zr(IV)	$7.00 \cdot 10^{-11}$	$1.10 \cdot 10^{-10}$	$2.90 \cdot 10^{-11}$	0.36		

Table A-18. Bentonite/ballast backfill: Recommended D_e and ε values for all groundwater types.

Species (Redox State)	D_e (m^2/s)	Upper D_e limit (m^2/s)	Lower D_e limit (m^2/s)	ε (−)	Upper ε limit (−)	Lower ε limit (−)
Ag(I)	$5.0 \cdot 10^{-11}$	$8.0 \cdot 10^{-11}$	$2.1 \cdot 10^{-11}$	0.23	0.26	0.21
Am(III)	$5.0 \cdot 10^{-11}$	$8.0 \cdot 10^{-11}$	$2.1 \cdot 10^{-11}$	0.23	0.26	0.21
C, carbonate species	$4.2 \cdot 10^{-12}$	$1.3 \cdot 10^{-11}$	$1.3 \cdot 10^{-12}$	0.092	0.13	0.066
C, methane	$5.0 \cdot 10^{-11}$	$8.0 \cdot 10^{-11}$	$2.1 \cdot 10^{-11}$	0.23	0.26	0.21
C, organic acids	$4.2 \cdot 10^{-12}$	$1.3 \cdot 10^{-11}$	$1.3 \cdot 10^{-12}$	0.092	0.13	0.066
Ce(III)	$5.0 \cdot 10^{-11}$	$8.0 \cdot 10^{-11}$	$2.1 \cdot 10^{-11}$	0.23	0.26	0.21
Cl(–I)	$4.2 \cdot 10^{-12}$	$1.3 \cdot 10^{-11}$	$1.3 \cdot 10^{-12}$	0.092	0.13	0.066
Cm(III)	$5.0 \cdot 10^{-11}$	$8.0 \cdot 10^{-11}$	$2.1 \cdot 10^{-11}$	0.23	0.26	0.21
Cs(I)	$1.3 \cdot 10^{-10}$	$1.3 \cdot 10^{-10}$	$2.1 \cdot 10^{-11}$	0.23	0.26	0.21
Eu(III)	$5.0 \cdot 10^{-11}$	$8.0 \cdot 10^{-11}$	$2.1 \cdot 10^{-11}$	0.23	0.26	0.21
Ho(III)	$5.0 \cdot 10^{-11}$	$8.0 \cdot 10^{-11}$	$2.1 \cdot 10^{-11}$	0.23	0.26	0.21
I(–I)	$4.2 \cdot 10^{-12}$	$1.3 \cdot 10^{-11}$	$1.3 \cdot 10^{-12}$	0.092	0.13	0.066
Nb(V)	$5.0 \cdot 10^{-11}$	$8.0 \cdot 10^{-11}$	$2.1 \cdot 10^{-11}$	0.23	0.26	0.21
Ni(II)	$5.0 \cdot 10^{-11}$	$8.0 \cdot 10^{-11}$	$2.1 \cdot 10^{-11}$	0.23	0.26	0.21
Np(IV)	$5.0 \cdot 10^{-11}$	$8.0 \cdot 10^{-11}$	$2.1 \cdot 10^{-11}$	0.23	0.26	0.21
Np(V)	$5.0 \cdot 10^{-11}$	$8.0 \cdot 10^{-11}$	$2.1 \cdot 10^{-11}$	0.23	0.26	0.21
Pa(IV)	$5.0 \cdot 10^{-11}$	$8.0 \cdot 10^{-11}$	$2.1 \cdot 10^{-11}$	0.23	0.26	0.21
Pa(V)	$5.0 \cdot 10^{-11}$	$8.0 \cdot 10^{-11}$	$2.1 \cdot 10^{-11}$	0.23	0.26	0.21
Pb(II)	$5.0 \cdot 10^{-11}$	$8.0 \cdot 10^{-11}$	$2.1 \cdot 10^{-11}$	0.23	0.26	0.21
Pd(II)	$5.0 \cdot 10^{-11}$	$8.0 \cdot 10^{-11}$	$2.1 \cdot 10^{-11}$	0.23	0.26	0.21
Pu(III)	$5.0 \cdot 10^{-11}$	$8.0 \cdot 10^{-11}$	$2.1 \cdot 10^{-11}$	0.23	0.26	0.21
Pu(IV)	$5.0 \cdot 10^{-11}$	$8.0 \cdot 10^{-11}$	$2.1 \cdot 10^{-11}$	0.23	0.26	0.21
Pu(V)	$5.0 \cdot 10^{-11}$	$8.0 \cdot 10^{-11}$	$2.1 \cdot 10^{-11}$	0.23	0.26	0.21
Pu(VI)	$5.0 \cdot 10^{-11}$	$8.0 \cdot 10^{-11}$	$2.1 \cdot 10^{-11}$	0.23	0.26	0.21
Ra(II)	$5.0 \cdot 10^{-11}$	$8.0 \cdot 10^{-11}$	$2.1 \cdot 10^{-11}$	0.23	0.26	0.21
Rn(–)	$5.0 \cdot 10^{-11}$	$8.0 \cdot 10^{-11}$	$2.1 \cdot 10^{-11}$	0.23	0.26	0.21
Se(–II)	$4.2 \cdot 10^{-12}$	$1.3 \cdot 10^{-11}$	$1.3 \cdot 10^{-12}$	0.092	0.13	0.066
Se(IV)	$4.2 \cdot 10^{-12}$	$1.3 \cdot 10^{-11}$	$1.3 \cdot 10^{-12}$	0.092	0.13	0.066
Se(VI)	$4.2 \cdot 10^{-12}$	$1.3 \cdot 10^{-11}$	$1.3 \cdot 10^{-12}$	0.092	0.13	0.066
Sm(III)	$5.0 \cdot 10^{-11}$	$8.0 \cdot 10^{-11}$	$2.1 \cdot 10^{-11}$	0.23	0.26	0.21
Sn(IV)	$5.0 \cdot 10^{-11}$	$8.0 \cdot 10^{-11}$	$2.1 \cdot 10^{-11}$	0.23	0.26	0.21
Sr(II)	$5.0 \cdot 10^{-11}$	$8.0 \cdot 10^{-11}$	$2.1 \cdot 10^{-11}$	0.23	0.26	0.21
Tc(IV)	$5.0 \cdot 10^{-11}$	$8.0 \cdot 10^{-11}$	$2.1 \cdot 10^{-11}$	0.23	0.26	0.21
Tc(VII)	$4.2 \cdot 10^{-12}$	$1.3 \cdot 10^{-11}$	$1.3 \cdot 10^{-12}$	0.092	0.13	0.066
Th(IV)	$5.0 \cdot 10^{-11}$	$8.0 \cdot 10^{-11}$	$2.1 \cdot 10^{-11}$	0.23	0.26	0.21
U(IV)	$5.0 \cdot 10^{-11}$	$8.0 \cdot 10^{-11}$	$2.1 \cdot 10^{-11}$	0.23	0.26	0.21
U(VI)	$5.0 \cdot 10^{-11}$	$8.0 \cdot 10^{-11}$	$2.1 \cdot 10^{-11}$	0.23	0.26	0.21
Zr(IV)	$5.0 \cdot 10^{-11}$	$8.0 \cdot 10^{-11}$	$2.1 \cdot 10^{-11}$	0.23	0.26	0.21

Table A-19. Friedland Clay backfill: Recommended K_d values for reference porewater (RPW-FC), to be used for non-saline, saline and highly saline groundwater.

Species (Redox State)	K_d (m^3/kg)	Upper K_d limit (m^3/kg)	Lower K_d limit (m^3/kg)	Correlation group
Ag(I)	0	4.40	0	–
Am(III)	17.7	110	3	3
C, carbonate species	isotope exchange	–	–	–
C, methane	0	0	0	–
C, organic acids	0	0	0	–
Ce(III)	10	60	2	3
Cl(–I)	0	0	0	7
Cm(III)	18	110	3	3
Cs(I)	0.03	0.2	0.004	1
Eu(III)	10	60	1.7	3
Ho(III)	10	60	1.7	3
I(–I)	0	0	0	7
Nb(V)	0.9	13.2	0.06	–
Ni(II)	1.47	8.80	0.24	2
Np(IV)	18.2	322	1.0	4
Np(V)	0.007	0.041	0.0011	5
Pa(IV)	0.9	13.2	0.06	–
Pa(V)	0.9	13.2	0.06	–
Pb(II)	22	134	3.5	2
Pd(II)	1.5	22	0.1	–
Pu(III)	17.7	276	1.1	3
Pu(IV)	18.2	322	1	4
Pu(V)	0.007	0.065	0.0007	5
Pu(VI)	0.9	9.0	0.1	6
Ra(II)	0.0013	0.0078	0.0002	1
Rn(–)	0	0	0	–
Se(–II)	0	0	0	
Se(IV)	0.01	0.12	0.001	–
Se(VI)	0	0	0	7
Sm(III)	10	60	1.7	3
Sn(IV)	18.2	510	0.7	4
Sr(II)	0.0013	0.0078	0.0002	1
Tc(IV)	18.2	510	0.7	4
Tc(VII)	0	0	0	7
Th(IV)	18.2	202	1.6	4
U(IV)	18.2	322	1.0	4
U(VI)	0.9	5.7	0.15	6
Zr(IV)	1.2	30	0.03	4

Correlation group according to subsection 5.5.7.

Table A-20. Bentonite/ballast backfill: Recommended K_d values to be used for saline and non-saline groundwater.

Species (Redox State)	K_d (m^3/kg)	Lower K_d limit (m^3/kg)	Upper K_d limit (m^3/kg)	Correlation group
Ag(I)	0.0035	$7.0 \cdot 10^{-4}$	4.5	–
Am(III)	19	3.2	$1.1 \cdot 10^{2}$	3
C, carbonate species[2]	$7.0 \cdot 10^{-5}$	$3.5 \cdot 10^{-5}$	$1.4 \cdot 10^{-4}$	–
C, methane[1]	0	0	0	–
C, organic acids[1]	0	0	0	–
Ce(III)[1]	2.4	0.24	28	3
Cl(–I)	0	0	0	7
Cm(III)	19	3.1	$1.2 \cdot 10^{2}$	3
Cs(I)	0.036	0.0061	0.19	1
Eu(III)	2.5	0.31	28	3
Ho(III)	2.5	0.31	28	3
I(–I)	0	0	0	7
Nb(V)	0.97	0.095	14	–
Ni(II)	0.091	0.0096	0.99	2
Np(IV)	19	1.2	$3.3 \cdot 10^{2}$	4
Np(V)[1]	0.0073	0.0020	0.063	5
Pa(IV)	0.97	0.095	14	–
Pa(V)	0.97	0.095	14	–
Pb(II)[1]	22	3.6	$1.4 \cdot 10^{2}$	2
Pd(II)	1.5	0.090	23	–
Pu(III)	30	3.1	$3.0 \cdot 10^{2}$	3
Pu(IV)	19	1.3	$3.3 \cdot 10^{2}$	4
Pu(V)[1]	0.0060	$6.0 \cdot 10^{-4}$	0.060	5
Pu(VI)[1]	0.90	0.090	8.4	6
Ra(II)	0.15	0.007	0.17	1
Rn(–)[1]	0	0	0	–
Se(–II)	$7.0 \cdot 10^{-5}$	$3.5 \cdot 10^{-5}$	$3.5 \cdot 10^{-4}$	
Se(IV)	0.012	$9.4 \cdot 10^{-4}$	0.12	–
Se(VI)	$7.0 \cdot 10^{-5}$	$3.5 \cdot 10^{-5}$	$3.5 \cdot 10^{-4}$	7
Sm(III)	2.5	0.31	28	3
Sn(IV)	19	0.69	$5.3 \cdot 10^{2}$	4
Sr(II)	0.0015	$2.8 \cdot 10^{-4}$	0.0097	1
Tc(IV)	19	0.73	$5.3 \cdot 10^{2}$	4
Tc(VII)	0	0	0	7
Th(IV)	19	1.9	$2.1 \cdot 10^{2}$	4
U(IV)	19	1.2	$3.3 \cdot 10^{2}$	4
U(VI)	0.90	0.15	5.4	6
Zr(IV)	1.3	0.065	31	4

Correlation groups according to subsection 5.5.7.

[1] Assumed non-sorbing on rock.

[2] Assumed non-sorbing on bentonite.

A6 Thermal properties for the geosphere

Table A-21. Mean value, standard deviation and two-sided 99% confidence intervals of thermal conductivity (W/(m·K)) at canister scale valid at 20°C. At higher temperatures the thermal conductivity for the dominating rock type, Granite, decreases with about 10%/100°C /Table 7-13 in *Site descriptive report, Forsmark*/.

Rock domain	Mean	St. dev.	Lower confidence limit	Upper confidence limit
RFM029	3.55	0.22	2.9	3.8
RFM012	3.46	0.28	2.9	3.8

Table A-22. Recommended mean, standard deviation and lower tail percentiles of thermal conductivity (W/(m·K)) at 0.8 m scale valid at 20°C. For RSME and RSMM, a rough correction has been applied to percentiles estimated from Monte Carlo simulated distributions, which are based on a < 0.1 m scale. The thermal conductivity decreases slightly at higher temperatures, 1–5% per 100°C temperature increase. /Table 7-13 in *Site descriptive report, Laxemar*/.

Rock domain	Mean	St. dev	0.5 percentile	2.5 percentile
RSMA	2.82	0.29	2.20	2.32
RSMBA	2.87	0.29	2.24	2.37
RSMD	2.70	0.17	2.32	2.44
RSME	2.45	–	2.0	2.2
RSMM	2.58	–	2.2	2.3

Table A-23. Thermal properties to be used in canister peak temperature calculations in SR-Can. Temperature calculations in repository scale can use the mean values given by Table A-21 and Table A-22.

Site	Temperature at repository depth (°C)	Thermal conductivity at 80°C (W/(m·K))	Standard deviation in thermal conductivity (W/(m·K))	Suggested lowest value in thermal conductivity (W/(m·K))	Heat capacity (MJ/(m³·K))
Forsmark	11 (400 m)	3.34	0.22	–	2.17
RSMA	13.8 (500 m)	2.77	0.29	2.20	2.24
RSMBA	13.8 (500 m)	2.82	0.29	2.24	2.23
RSMD	13.8 (500 m)	2.65	0.17	2.32	2.29
RSME	13.8 (500 m)	2.40	0.2	2.0	2.25
RSMM	13.8 (500 m)	2.53	0.2	2.2	2.25

A7 Fracture data

Table A-24. DFN size model for Forsmark, v.1.2. Minimum and maximum estimates for k_r were computed by SR-Can.

SIZE PFM_DFN_1.2_SIZ_rev_4.0 Forsmark, Domain 29		Date: 2006-05-17	
Set name	**Probability Distribution**	**k_r**	**r_0**
NS (L1)	Power Law	2.88	0.28
NE (L2)	Power Law	3.02	0.25
NW (L3)	Power Law	2.81	0.14
EW (L4)	Power Law	2.95	0.15
Horizontal	Power Law	2.92	0.25

Table A-25. DFN intensity model for Forsmark, v.1.2.

INTENSITY PFM_DFN_1.2_INT_rev_1.0		Date:	2005-03-24		
P_{32}Intensity (m^2/m^3)	**Set name**	**Partly open**	**Open**	**Sealed**	**Total**
Domain 29	NS (L1)	0.01	0.12	0.47	0.60
	NE (L2)	0.05	0.46	1.56	2.07
	NW (L3)	0.01	0.16	0.27	0.44
	EW (L4)	0.00	0.05	0.17	0.22
	Horizontal	0.01	0.34	0.26	0.61
	All	0.08	1.13	2.73	3.94
Domain 18	NS (L1)	0.05	0.26	0.43	0.74
	NE (L2)	0.18	1.01	1.43	2.62
	NW (L3)	0.05	0.36	0.25	0.66
	EW (L4)	0.02	0.11	0.15	0.28
	Horizontal	0.04	0.73	0.24	1.01
	All	0.34	2.47	2.50	5.31
Domain 17	NS (L1)	0.01	0.01	0.51	0.53
	NE (L2)	0.04	0.02	1.70	1.76
	NW (L3)	0.01	0.01	0.30	0.32
	EW (L4)	0.00	0.00	0.18	0.18
	Horizontal	0.01	0.02	0.28	0.31
	All	0.07	0.06	2.97	3.10
Domain 12	NS (L1)	0.10	0.22	1.04	1.36
	NE (L2)	0.37	0.84	3.46	4.67
	NW (L3)	0.11	0.30	0.60	1.01
	EW (L4)	0.04	0.09	0.37	0.50
	Horizontal	0.09	0.61	0.57	1.27
	All	0.71	2.06	6.04	8.81

Table A-26. Mean values and standard deviation of P_{32} for Open, Partly open and Sealed fractures in different sampled rock domains /from La Pointe et al. 2005, Table 6-25/.

	Mean			Standard deviation		
	Open	Partly open	Sealed	Open	Partly open	Sealed
RFM012	2.06	0.71	6.05	1.56	0.74	4.01
RFM017	0.06	0.08	2.98	–	–	–
RFM018	2.47	0.34	2.5	–	–	–
RFM029	1.13	0.08	2.73	2.41	0.11	1.6

Table A-27. DFN orientation model for Forsmark, v.1.2.

ORIENTATION **PFM_DFN_1.2_ORI_rev_1.0** **Forsmark**					**Date:2005-03-24**		
Set name	**Probability distribution**	**Mean pole**		**Dispersion**		**Goodness of fit**	
		Trend	**Plunge**	***K1**	**K2**	**K-S**	**Sig.**
NS (L1)	Bivariate Fisher	92.4	5.9	19.31	19.69	0.067	3.9%
NE (L2)	Bingham	137.3	3.7	–17.09	–9.1	0.045	10.7%
NW (L3)	Univariate Fisher	40.6	2.2	23.9	–	0.038	8.5%
EW (L4)	Univariate Fisher	190.4	0.7	30.63	–	0.051	2.9%
Horizontal	Univariate Fisher	342.9	80.3	8.18	–	0.041	54.6%
Major axis orientation		**Trend**	**Plunge**	**–**		**K-S**	**Sig.**
NS (L1)		355.3	50.2	–		0.06	8.80%
NE (L2)		38.1	68.2	–		0.045	10.30%

* For univariate Fisher distributions, K1 in this table stands for Fisher k.

ORIENTATION-Fisher alternative **PFM_DFN_1.2_ORI_Fisher_rev 1** **Forsmark**						
Set name	**Probability distribution**	**Mean pole**		**Dispersion**	**Goodness of fit**	
		Trend	**Plunge**	**k**	**K-S**	**Sig.**
NS (L1)	Univariate Fisher	87.2	1.7	21.66	0.078	0.01%
NE (L2)	Univariate Fisher	135.2	2.7	21.54	0.0531	2.53E–5%

Table A-28. DFN size model for Laxemar, v.1.2 /Hermanson et al. 2005 Tables 6-9, 7-5 and 7-6/.

SIZE LAX_DFN_1.2_SIZ_rev6.0 Laxemar Subarea, Domain A		Date:	2006-05-17	
Set name	**Probability distribution**	**k_r**	**r_0**	**P_{32}**
S_A	Power Law	2.85	0.328	1.31[a]
S_B	Power Law	3.04	0.977	1.026[a]
S_C	Power Law	3.01	0.858	0.974[a]
S_d	Exponential	–	4[c]	2.32[b]
S_d[d]	Power Law	2.90	0.208	2.32[b]
S_e	Power Law	3.600	0.400	1.4[b]

[a] From Table 7-5 in /Hermanson et al. 2005/.

[b] From Table 7-6 in /Hermanson et al. 2005/.

[c] Refers to the parameter λ of the exponential distribution. The mean and standard deviation are both equal to 1/λ.

[d] Refers to an alternative size model for the set. From Table 6-9 in /Hermanson et al. 2005/.

Table A-29. DFN orientation model for Laxemar, v.1.2.

ORIENTATION ALTERNATIVE 1 LAX_DFN_1.2_ORI_rev2.00 Laxemar Subarea				Date:	2005-05-03
Set name	**Probability distribution**	**Mean pole Trend**	**Plunge**	**Dispersion k**	**Goodness of fit K-S**	**% Sig.**
S_A	Univ. Fisher	338.1	4.5	13.06	0.031	55.60%
S_B	Univ. Fisher	100.4	0.2	19.62	0.058	10.70%
S_C	Univ. Fisher	212.9	0.9	10.46	0.076	15.70%
S_d	Univ. Fisher	3.3	62.1	10.13	0.021	99.70%
S_f	Univ. Fisher	243.0	24.4	23.52	0.216	N/S

A.8 Hydraulic properties and the EDZ

Table A-30. Issues explored in the different simulation cases for Forsmark analysed by /Hartley et al. 2006a/. A full listing of the variants explored are given in Table A-31– Table A-33.

Issue	Parameter variation formulated to explore issue
Deformation Zone Geometry	Alternative Case (AC) geometry as suggested by site model
Representation of the low permeability volumes at depth	Rock mass between the deformation zones is either a • low transmissivity DFN, with parameters as given by /Hartley et al. 2006a/ • poorly connected DFN, with parameters as given by /Hartley et al. 2006a/ • a low permeability porous medium as suggested by /Follin et al. 2005/.
DFN properties in different subdomains	Volume E DFN properties throughout entire volume as a variant to the base case
Correlation between fracture size and T	Three cases explored: • Correlated T/L • Semicorrelated T/L • Uncorrelated T/L
Representation of rock mass permeability	Different cases with ECPM, nested ECPM/DFN or nested CPM/DFN descriptions.
EDZ	Alternative with continuous and high transmissivity EDZ.

Table A-31. Task 3 nested CPM cases for Forsmark.

Case description SR-Can Forsmark v1.2	Sensitivity	Properties	Description
HCD3_AC_HRDDT	Alternative 1	CPM	DarcyTools description (no Hydro-DFN), check FWS
HCD3_AC_HRDDT_EDZ	EDZ	CPM	100 times high conductivity in EDZ
HCD3_AC_HRDDT_T1	Tunnel	CPM	10 times higher conductivity in tunnel backfill (10^{-9}m/s)
HCD3_AC_HRDDT_T2	Tunnel	CPM	100 times higher conductivity in tunnel backfill (10^{-8}m/s)
HCD3_AC_HRDDT_T3	Tunnel	CPM	1,000 times higher conductivity in tunnel backfill (10^{-7}m/s)

Note: All CPM cases are defined by 3 blocks; **_b1, _b2, _b3** multiplied by 3 times **2,020 AD, 3,000 AD and 9,000 AD**

Table A-32. Task3 nested ECPM cases for Forsmark.

Case Description SR-Can Forsmark v1.2	Sensitivity	Properties	Description
HCD3_AC_HRD3EC	Alternative 2	ECPM – Correlated T/L	CF Base Case (Volume *E* DFN)
HCD3_AC_HRD3EC_EDZ	EDZ	ECPM – Correlated T/L	100 times high conductivity in EDZ
HCD3_AC_HRD3EC_T2	Tunnel	ECPM – Correlated T/L	100 times higher conductivity in tunnel backfill (10^{-8}m/s)
HCD3_AC_HRD3A2_T	DFN with lower T below zone A2	ECPM – Correlated T/L	Lower open fracture T below ZFMNE00A2
HCD3_AC_HRD3A2_T_ EDZ	DFN with lower T below zone A2, EDZ	ECPM – Correlated T/L	Lower open fracture T below ZFMNE00A2, 100 times high conductivity in EDZ
HCD3_AC_HRD3A2_T_T2	DFN with lower T below zone A2, EDZ	ECPM – Correlated T/L	Lower open fracture T below ZFMNE00A2, 100 times higher conductivity in tunnel backfill (10^{-8}m/s)

Note: All ECPM cases are defined by 3 blocks; _b1, _b2, _b3 multiplied by 3 times 2,020 AD, 3,000 AD and 9,000 AD

Table A-33. Task 3 combined DFN/CPM cases for Forsmark.

Case Description SR-Can Forsmark v1.2	Sensitivity	Properties	Description
HCD3_AC_HRD4A2_T	Realistic base case	DFN – Correlated T/L	Lower open fracture T below ZFMNE00A2
HCD3_AC_HRD4	Reference case	DFN – Correlated T/L	CF Base Case (Volume *E* DFN)
HCD3_AC_HRD4_EDZ	Reference case+ EDZ	DFN – Correlated T/L	100 times high conductivity in EDZ
HCD3_AC_HRD4_T2	Reference case + Tunnel	DFN – Correlated T/L	100 times higher conductivity in tunnel backfill (10^{-8}m/s)
HCD3_AC_HRD4A2_T_ EDZ	Realistic base case + EDZ	DFN – Correlated T/L	100 times high conductivity in EDZ
HCD3_AC_HRD4A2_T_T2	Reference case + Tunnel	DFN – Correlated T/L	100 times higher conductivity in tunnel backfill (10^{-8}m/s)
HCD3_AC_HRD4SA2_T	Realistic base case + DFN	DFN – semi-correlated T/L	Semi-correlated T model
HCD3_AC_HRD4UA2_T	Realistic base case + DFN	DFN – Uncorrelated T/L	Uncorrelated T model
HCD3_AC_HRD3EC	Alternative 2	DFN – Correlated T/L	CF Base Case (Volume *E* DFN)

Note: HCD3_AC_HRD4 combined cases are defined by 3 blocks; **_b1, _b2, _b3** multiplied by 3 times **2,020 AD, 3,000 AD and 9,000 AD.** All other combined cases are defined by 3 blocks; **_b1, _b2, _b3** at **2,020 AD** only.

Table A-34. List of cases modelled in the Laxemar ECPM regional-scale modelling of f /Hartley et al. 2006b/.

Cases for SR-can Laxemar v1.2	Properties or characteristics
SC_HCD1P3_HRD3a_ddKhalf_ani_HSD1_BC3_MD1_IC1_1	Reference Case adopted from SDM L1.2
SC_HCD1P3S1_HRD3a_ddKhalf_ani_HSD1_BC3_MD1_IC1	Stochastic HCD, std = (0.90, 0.58, 1.21), rel. 1
SC_HCD1P3S2_HRD3a_ddKhalf_ani_HSD1_BC3_MD1_IC1	Stochastic HCD, std = (0.90, 0.58, 1.21), rel. 2
SC_HCD1P3S3_HRD3a_ddKhalf_ani_HSD1_BC3_MD1_IC1	Stochastic HCD, std = (0.90, 0.58, 1.21), rel. 3
SC_HCD1P3S1i_HRD3a_ddKhalf_ani_HSD1_BC3_MD1_IC1	Stochastic HCD, std = (1.40, 1.08, 1.71), rel. 1
SC_HCD1P3S2i_HRD3a_ddKhalf_ani_HSD1_BC3_MD1_IC1	Stochastic HCD, std = (1.40, 1.08, 1.71), rel. 2
SC_HCD1P3S3i_HRD3a_ddKhalf_ani_HSD1_BC3_MD1_IC1	Stochastic HCD, std = (1.40, 1.08, 1.71), rel. 3
SC_HCD5P3_HRD3a_ddKhalf_ani_HSD1_BC3_MD1_IC1	Low confidence zones removed
SC_HCD1P3_HRD3a_ddKhalf_ani-S_C_HSD1_BC3_MD1_IC1	10 times higher T in Set_C
SC_HCD1P3_HRD3b_ddKhalf_ani_HSD1_BC3_MD1_IC1	Realisation 2 of DFN model
SC_HCD1P3_HRD3c_ddKhalf_ani_HSD1_BC3_MD1_IC1	Realisation 3 of DFN model
SC_HCD1P3_HRD4_ddKhalf_ani_HSD1_BC3_MD1_IC1	Correlated
SC_HCD1P3_HRD5_ddKhalf_ani_HSD1_BC3_MD1_IC1	Un-correlated
SC_HCD1P3_HRD3a_ddKhalf_ani_HSD2_BC1_MD1_IC1	Elaborate Overburden model
SC_HCD1P3_HRD3a_ddKhalf_ani_HSD1_BC3_MD1_MP_IC1	Lower matrix porosity
SC_HCD1P3_HRD3a_ddKhalf_ani_HSD1_BC1_MD1_FWS_IC1	Modified FWS in HRD
SC_HCD1P3_HRD3a_ddKhalf_ani_HSD1_BC4_MD1_IC1	Flux boundary condition
SC_HCD1P3_HRD3a_ddKhalf_ani_HSD1_BC1_MD1_IC1_DT	Darcy Tools DFN model

Table A-35. ist of cases modelled in the Laxemar DFN/CPM repository-scale modelling of /Hartley et al. 2006b/.

Case Name	Sensitivity	Properties	Description
HCD1P3_HRD3a_ddKhalf_ani_ HSD1_BC3	Reference case	DFN – Semi-correlated *T*/*r*	SDM Reference Case
HCD1P3_HRD3a_ddKhalf_ani_ HSD1_BC3_EDZ	Reference case + EDZ	DFN – Semi-correlated *T*/*r*	10 times higher conductivity in EDZ (3 10^{-7}m/s)
HCD1P3_HRD3a_ddKhalf_ani_ HSD1_BC3_T	Reference case + Tunnel	DFN – Semi-correlated *T*/*r*	100 times higher conductivity in tunnel backfill (10^{-8}m/s)
HCD1P3_HRD3a_ddKhalf_ani_ cubic_HSD1_BC3	Reference case + transport aperture	DFN – Semi-correlated T/r	Cubic law transport aperture
HCD1P3_HRD3a_ddKhalf_ani_ S-C_HSD1_BC3	Reference case + DFN	DFN – Semi-correlated T/r	Transmissivity for Set_C 10 times higher
HCD1P3_HRD4_ddKhalf_ani_ HSD1_BC3	Reference case + DFN	DFN – Correlated T/r	Correlated *T* model

A9 Rock mechanics

Table A-36. 3DEC Base case parameter values.

Component	3DEC parameter	Unit	Forsmark	Simpevarp	Note
Intact rock	Density	kg/m^3	2,600		1
	Young's modulus	GPa	76	80	2
	Poisson ratio	–	0.24	0.27	2
	Heat conductivity	W/(m·K)	3.65	2.61	3
	Heat diffusivity	m^2/s	$1.75 \cdot 10^{-6}$	$1.25 \cdot 10^{-6}$	3
	Heat expansion coefficient	K^{-1}	$7.7 \cdot 10^{-6}$	$6.2 \cdot 10^{-6}$	4
Fractures	Joint normal stiffness	GPa/m	128	100	5
	Joint shear stiffness,	GPa/m	39	29	5
	Friction angle	deg	34		6
	Cohesion	MPa	0.6		6
	Dilation angle	deg	10		7
Rock mass	Young's modulus	MPa	68	62	8
	Poisson ratio	–	0.22	0.28	8

Notes to Table A-36

1) Approximate and generic value used in all models.

2) Site model data. Mean values given for rock type *"granite to granodiorite"* (Forsmark area) and "*quartz monzonite to monzodiorite and Ävrö granite"* (Simpevarp subareara). For Young's modulus the site reports give min-max ranges of 70–90 GPa (*granite to granodiorite*) and 70–82 GPa (*Ävrö granite*).

3) Values of heat conductivity were obtained from early deliveries of site data to preliminary design projects /Brantberger 2004, Glamheden 2004/. These data were used to set the canister spacing in pilot layout work and have been kept in the 3DEC models, although the thermal site models have been updated such that the RFM012 rock domain mean value is 3.46 W/(m·K) rather than 3.65 W/(m·K) /Sundberg et al. 2005b/ and the RSMA01 value is 2.80 W/(m·K) rather than 2.61 W/(m·K) /Sundberg et al. 2005a/. The thermal diffusivities are calculated from generic values of density (2,600 kg/m^3) and specific heat (800 J/(kg·K)). These values correspond to a volumetric heat capacity of 2.08 MJ/m^3, while the RFM012 and RSMA01 rock domains mean values are 2.15 MJ/m^3 and 2.23 MJ/m^3, respectively /Sundberg et al. 2005ab/.

4) Values of heat expansion were obtained from draft site model versions. For the Forsmark model this value agrees with the one given for *granite to granodiorite* and, on the domain level, for domains RFM012 and RFM029 in /**Site descriptive report, Forsmark**/. For the Simpevarp model, the value now given for *Ävrö granite* is $6.0 \cdot 10^{-6}$ K^{-1} /SKB 2005d/.

5) Site model data. In the site models, there are no differences between fractures belonging to different fracture sets or different domains within the sites. In the 3DEC model mean values are used throughout. For the normal stiffness the site reports give min-max ranges of 60–230 GPa/m (Forsmark) and 49–179 GPa/m (Simpevarp). For the shear stiffness corresponding ranges are 10–55 GPa/m and 10–49 GPa/m, respectively.

6) Values of Mohr-Coulomb parameters given here are approximated from data given in the site reports. Similar to the stiffness values, the given strength data is not differentiated with regard to borehole or joint set. The data given for the two sites are sufficiently similar that the same parameter values are used for both sites. These average values are based on the mean value given for the two sites.

7) Draft versions of the two site reports (and the borehole primary data reports) did not include any values of the dilation angle. For the Simpevarp subarea there are no values in the final version /SKB 2005d/. Previous investigations of rock joints in *Ävrö granite* have indicated that the dilation angle should be about 10 degrees or more /Olsson 1998/, which is the value used in the 3DEC models for both sites. The values now the given for the Forsmark area ranges between 4° (for fractures in low compression) and 19.5° (for fractures in high compression) /**Site descriptive report, Forsmark**/.

8) Site model data. Mean values given for rock domain RFM012 (Forsmark) and rock domain A (Simpevarp) /**Site descriptive report, Forsmark and Simpevarp**/. The site reports give min-max ranges of 40–80 GPa (RFM012, Forsmark) and 45–79 GPa (Rock domain A, Simpevarp).

Table A-37. Fractures in rock mechanics.

Fracture	
#1	Vertical and perpendicular to tunnel, at 0.4 m distance from the wall of the central deposition hole
#2	Vertical and parallel to tunnel at 0.75 m distance from the tunnel wall
#3	Vertical, intersecting tunnel at 45° at 0.54 m distance from the wall of the central deposition hole.
#4	Dipping 20° with strike normal to tunnel
#5	Dipping 45° with strike normal to tunnel
#6	Dipping 45° with strike 45° relative to tunnel

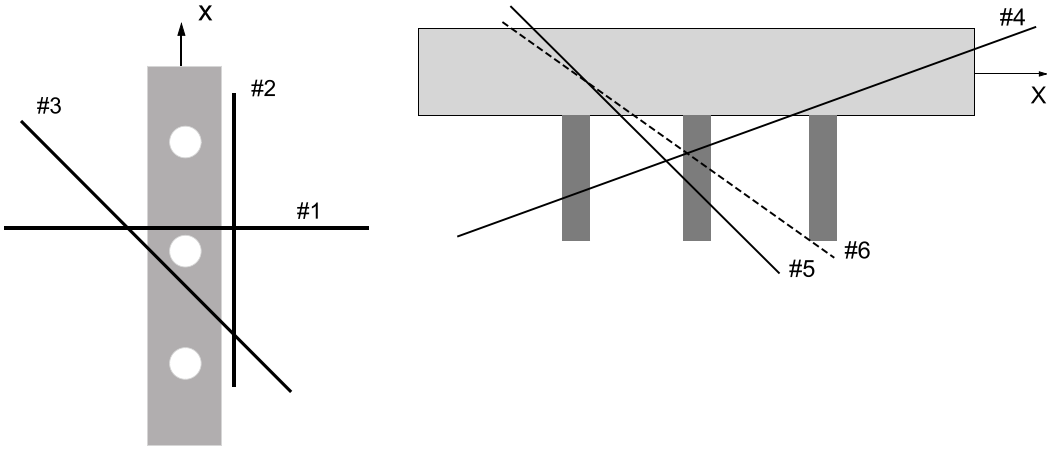

Table A-38. Principal stress and stress orientation relative to tunnels in 3DEC near-field models.

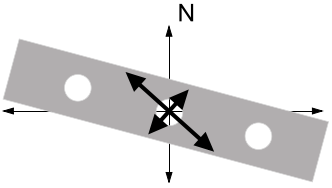

Angle between tunnel axis and σ_H = 15°

	Forsmark	Simpevarp 1		Simpevarp 2
σ_H	45	32	σ_H	16
σ_h	18 [1]	9.5	σ_h	5.5
σ_v	13	14	σ_v	9

[1] The σ_h value used for the Forsmark 3DEC model at 500 m depth (18 MPa) differs from the one given in the final site report (31.5 MPa)

A10 Hydraulic properties and the EDZ

Table A-39. Parameter values suggested by /Hartley et al. 2005a/ for the uncorrelated, correlated and semi-correlated transmissivity models in Volumes E – G /Table 8-10 in *Site descriptive report, Forsmark*/.

Object	Uncorrelated		Correlated		Semi-correlated		
	$\mu_{log(T)}$	$\sigma_{log(T)}$	a	b	a	b	$\sigma_{log(T)}$
Volume E	–6.5	0.9	$1.8 \cdot 10^{-9}$	1	$5.3 \cdot 10^{-8}$	0.6	1
Volume F	–6.5	0.9	$1.8 \cdot 10^{-9}$	1	$5.3 \cdot 10^{-8}$	0.6	1
Volume G	–	–	$8.9 \cdot 10^{-10}$	1	–	–	–

A11 Migration properties of the rock

Table A-40. Recommended value for diffusivities in free solution /Ohlsson and Neretnieks 1997/.

Element/specie	Diffusivity in free solution $D_w \cdot 10^9$ (m^2/s)	Possible ion exclusion/surface diffusion effects in low salinity waters
Ag	1.7	
Br	2.0	Anion exclusion
C/CO_3	1.2	Anion exclusion
Cd	0.72	
Cl	2.0	Anion exclusion
Co	0.7	
Cs	2.1	Surface diffusion
HTO	2.4	
I	0.83	Anion exclusion
Na	1.3	Surface diffusion
Ni	0.68	
Ra	0.89	Surface diffusion
Sr	0.79	Surface diffusion
Th	0.15	
All other nuclides	1.0	

Table A-41. Recommended log_{10}-normal formation factor distributions.

Site	Mean value $log_{10}(F_f)$	Standard deviation $log_{10}(F_f)$
Forsmark	–4.74	0.25
Simpevarp	–4.70	0.45
Laxemar	–4.60	0.23

Effective diffusivities D_e (m^2/s) are obtained from the product of the formation factors F_f (–) given Table A-41 in and the diffusivities in free solution D_w (m^2/s) given in Table A-40. When doing this for species subjected to anion exclusion, as stated in Table A-42, the product should be divided by a factor of 10.

Characteristic length of samples equals 0.1 m.

Table A-42. Recommended *log$_{10}$*-normal porosity distributions.

Site	Mean value $\log_{10}(\varepsilon)$	Standard deviation $\log_{10}(\varepsilon)$
Forsmark	–3.03	0.20
Simpevarp	–3.17	0.38
Laxemar	–2.84	0.18

Characteristic volume of samples equals $6 \cdot 10^{-5}$ m^3.

Table A-43. Far-field: K_d values for granitic rock, to be used in Forsmark. Simpevarp, and Laxemar as recommended values after multiplying with correction factors.

Nuclide/redox state		Non-saline K_d (m^3/kg)	Saline K_d (m^3/kg)	Correction factors	Corr. group
Ni(II)[1]	best estimate	$1.2 \cdot 10^{-1}$	$1.0 \cdot 10^{-2}$	$f_{cr} = 0.1$	3
	$K_{d,25\%} – K_{d,75\%}$	$5.5 \cdot 10^{-2}$–$3.0 \cdot 10^{-1}$	$8.0 \cdot 10^{-3}$–$2.8 \cdot 10^{-2}$		
	$K_{d,low} – K_{d,high}$	$1.8 \cdot 10^{-2}$–$5.4 \cdot 10^{-1}$	$2.0 \cdot 10^{-3}$–$8.7 \cdot 10^{-2}$		
Sr(II)[1]	best estimate	$1.3 \cdot 10^{-2}$	$3.1 \cdot 10^{-4}$	$f_{cr} = 0.1$	2
	$K_{d,25\%} – K_{d,75\%}$	$6.5 \cdot 10^{-3}$–$4.1 \cdot 10^{-2}$	$8.4 \cdot 10^{-5}$–$5.4 \cdot 10^{-3}$		
	$K_{d,low} – K_{d,high}$	$1.0 \cdot 10^{-3}$–$6.1 \cdot 10^{-1}$	$1.4 \cdot 10^{-5}$–$2.6 \cdot 10^{-2}$		
Cs(I)[1]	best estimate	$1.8 \cdot 10^{-1}$	$4.2 \cdot 10^{-2}$	$f_{cr} = 0.1$	1
	$K_{d,25\%} – K_{d,75\%}$	$4.9 \cdot 10^{-2}$–$7.2 \cdot 10^{-1}$	$1.0 \cdot 10^{-2}$–$1.4 \cdot 10^{-1}$		
	$K_{d,low} – K_{d,high}$	$1.7 \cdot 10^{-3}$–9.6	$4.0 \cdot 10^{-4}$–2.0		
Ra(II)[1]	best estimate	1.3	2.1	$f_{cr} = 0.1$	2
	$K_{d,25\%} – K_{d,75\%}$	$1.4 \cdot 10^{-1}$–1.9	$9.9 \cdot 10^{-2}$–2.3		
	$K_{d,low} – K_{d,high}$	$6.3 \cdot 10^{-2}$–11	$6.4 \cdot 10^{-3}$–2.6		
Th(IV)	best estimate	1.0	1.0	$f_{cr} = 0.1$	5
	$K_{d,25\%} – K_{d,75\%}$	$7.9 \cdot 10^{-1}$–2.4	$7.9 \cdot 10^{-1}$–2.4		
	$K_{d,low} – K_{d,high}$	$5.0 \cdot 10^{-1}$–10	$5.0 \cdot 10^{-1}$–10		
U(IV)[2]	best estimate	6.3	6.3	$f_{cr} = 0.1$	5
	$K_{d,25\%} – K_{d,75\%}$	1.1–13	1.1–13		
	$K_{d,low} – K_{d,high}$	$4.8 \cdot 10^{-2}$–$2.8 \cdot 10^{2}$	$4.8 \cdot 10^{-2}$–$2.8 \cdot 10^{2}$		
U(VI)[2]	best estimate	$6.3 \cdot 10^{-3}$	$6.3 \cdot 10^{-3}$	$f_{cr} = 0.1$	7
	$K_{d,25\%} – K_{d,75\%}$	$1.5 \cdot 10^{-3}$–$1.6 \cdot 10^{-2}$	$1.5 \cdot 10^{-3}$–$1.6 \cdot 10^{-2}$		
	$K_{d,low} – K_{d,high}$	$5.0 \cdot 10^{-4}$–$1.2 \cdot 10^{-1}$	$5.0 \cdot 10^{-4}$–$1.2 \cdot 10^{-1}$		
Np(IV)[2]	best estimate	$9.6 \cdot 10^{-1}$	$9.6 \cdot 10^{-1}$	$f_{cr} = 0.1$	5
	$K_{d,25\%} – K_{d,75\%}$	$3.2 \cdot 10^{-1}$–2.8	$3.2 \cdot 10^{-1}$–2.8		
	$K_{d,low} – K_{d,high}$	$4.7 \cdot 10^{-2}$–20	$4.7 \cdot 10^{-2}$–20		
Np(V)[2]	best estimate	$1.8 \cdot 10^{-2}$	$1.8 \cdot 10^{-2}$	$f_{cr} = 0.1$	6
	$K_{d,25\%} – K_{d,75\%}$	$1.1 \cdot 10^{-2}$–$4.4 \cdot 10^{-2}$	$1.1 \cdot 10^{-2}$–$4.4 \cdot 10^{-2}$		
	$K_{d,low} – K_{d,high}$	$2.0 \cdot 10^{-3}$–$2.2 \cdot 10^{-1}$	$2.0 \cdot 10^{-3}$–$2.2 \cdot 10^{-1}$		
Am(III)	best estimate	13	13	$f_{cr} = 0.1$	4
	$K_{d,25\%} – K_{d,75\%}$	3.2–21	3.2–21		
	$K_{d,low} – K_{d,high}$	$2.2 \cdot 10^{-1}$–$1.9 \cdot 10^{2}$	$2.2 \cdot 10^{-1}$–$1.9 \cdot 10^{2}$		

Non-saline groundwater: [Cl-] < 500 mg/l, pH 7–9, oxidising (atmospheric) or reducing (Eh < 200 mV) conditions.
Saline groundwater: [Cl-] ≥ 500 mg/l, pH 7–9, oxidising (atmospheric) or reducing (Eh < 200 mV) conditions.

[1] Solutes that exhibit sensitivity to ionic strength.

[2] Solutes that exhibit sensitivity to redox conditions. Correlation groups according to subsection 6.7.7

Table A-44. K_d values for granitic rock, to be used in Forsmark. Simpevarp, and Laxemar as recommended values after multiplying with correction factors.

Nuclide/redox state		Non-saline K_d (m^3/kg)	Saline K_d (m^3/kg)	Correction factors	Corr. group
HCO_3^-	best estimate	$1 \cdot 10^{-3}$	$1 \cdot 10^{-3}$	$f_{cr} = 0.1$	
	$K_{d,low} – K_{d,high}$	$5 \cdot 10^{-4} – 2 \cdot 10^{-3}$	$5 \cdot 10^{-4} – 2 \cdot 10^{-3}$		
Cl^-	best estimate	0	0		
	$K_{d,low} – K_{d,high}$	–	–		
Co(II)	best estimate	0.1	$2 \cdot 10^{-2}$	$f_{cr} = 0.1$	3
	$K_{d,low} – K_{d,high}$	$5 \cdot 10^{-2} – 5 \cdot 10^{-1}$	$1 \cdot 10^{-2} – 0.1$		
Se(-II, IV,VI)	best estimate	$1 \cdot 10^{-3}$	$1 \cdot 10^{-3}$	$f_{cr} = 0.1$	
	$K_{d,low} – K_{d,high}$	$5 \cdot 10^{-4} – 5 \cdot 10^{-3}$	$5 \cdot 10^{-4} – 5 \cdot 10^{-3}$		
Kr	best estimate	0	0		
	$K_{d,low} – K_{d,high}$	–	–		
Zr(II)	best estimate	1	1	$f_{cr} = 0.1$	5
	$K_{d,low} – K_{d,high}$	0.5−3	0.5−3		
Nb(V)	best estimate	1	1	$f_{cr} = 0.1$	6
	$K_{d,low} – K_{d,high}$	0.5−3	0.5−3		
Tc(IV)	best estimate	1	1	$f_{cr} = 0.1$	
	$K_{d,low} – K_{d,high}$	0.5−3	0.5−3		
Tc(VII)	best estimate	0	0		
	$K_{d,low} – K_{d,high}$	–	–		
Pd(II)	best estimate	0.1	$1 \cdot 10^{-2}$	$f_{cr} = 0.1$	3
	$K_{d,low} – K_{d,high}$	$1 \cdot 10^{-2} – 0.5$	$1 \cdot 10^{-3} – 5 \cdot 10^{-2}$		
Ag(I)	best estimate	0.5	$5 \cdot 10^{-2}$	$f_{cr} = 0.1$	
	$K_{d,low} – K_{d,high}$	0.1−1	$1 \cdot 10^{-2} – 0.1$		
Cd(II)	best estimate	0.1	0.02	$f_{cr} = 0.1$	3
	$K_{d,low} – K_{d,high}$	$5 \cdot 10^{-2} – 0.5$	0.01−0.1		
Sn(IV)	best estimate	$1 \cdot 10^{-3}$	$1 \cdot 10^{-3}$	$f_{cr} = 0.1$	5
	$K_{d,low} – K_{d,high}$	$0 – 1 \cdot 10^{-2}$	$0 – 1 \cdot 10^{-2}$		
I^-	best estimate	0	0		
	$K_{d,low} – K_{d,high}$	–	–		
Sm(III)	best estimate	2	2	$f_{cr} = 0.1$	4
	$K_{d,low} – K_{d,high}$	1−5	1−5		
Eu(III)	best estimate	2	2	$f_{cr} = 0.1$	4
	$K_{d,low} – K_{d,high}$	1−5	1−5		
Ho(III)	best estimate	2	2	$f_{cr} = 0.1$	4
	$K_{d,low} – K_{d,high}$	1−5	1−5		
Ac(III)	best estimate	3	3	$f_{cr} = 0.1$	4
	$K_{d,low} – K_{d,high}$	1−5	1−5		
Pa(IV, V)	best estimate	1	1	$f_{cr} = 0.1$	5.6
	$K_{d,low} – K_{d,high}$	0.5−5	0.5−5		
Pu(III, IV)	best estimate	5	5	$f_{cr} = 0.1$	4.5
	$K_{d,low} – K_{d,high}$	1−10	1−10		
Cm(III)	best estimate	3	3	$f_{cr} = 0.1$	4
	$K_{d,low} – K_{d,high}$	1−5	1−5		

Based on /Carbol and Engkvist 1997/. Correlation groups according to subsection 6.7.7.

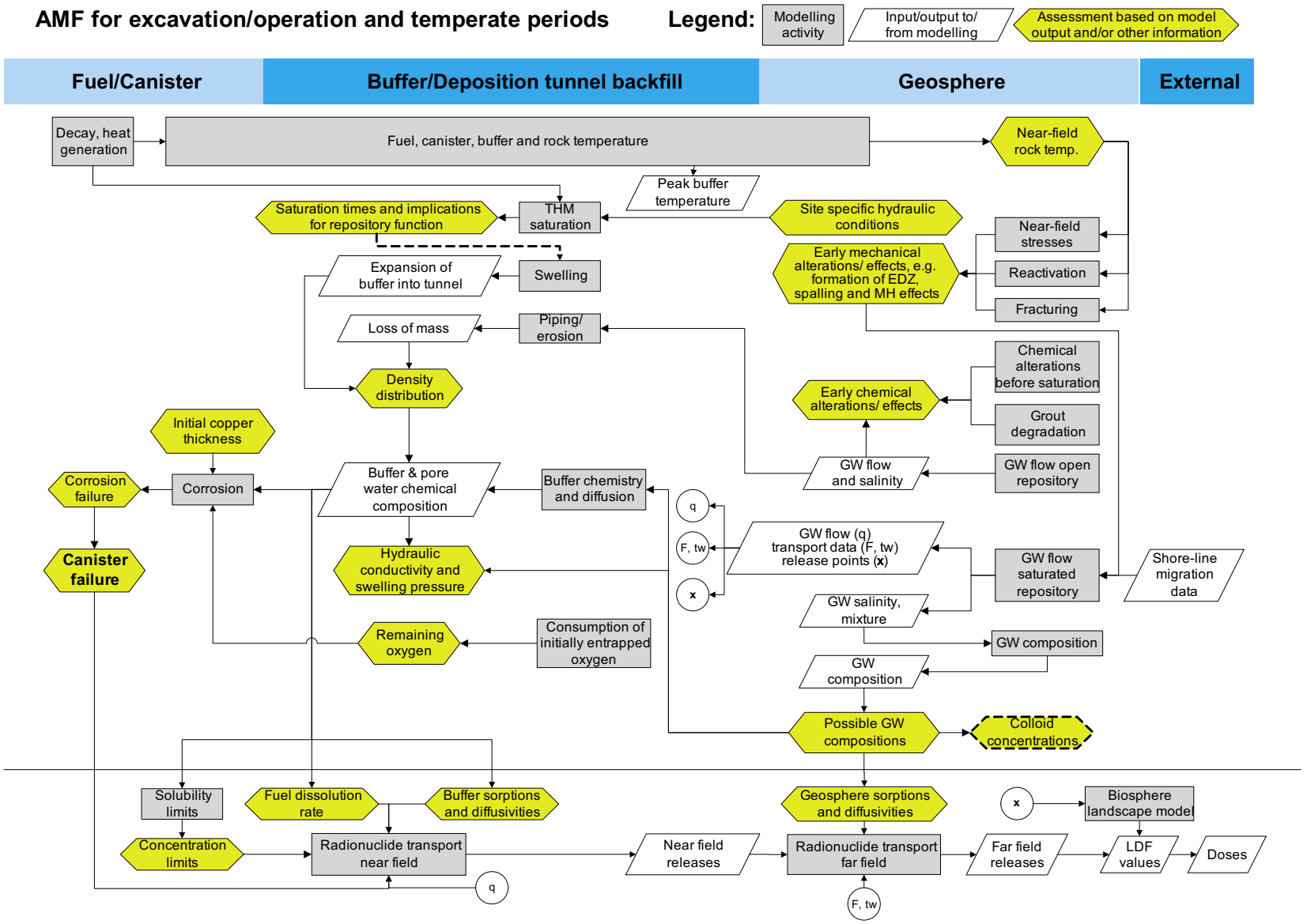

Figure B-1. *Assessment model flow chart for the excavation/operation period and the initial temperate period after closure.*

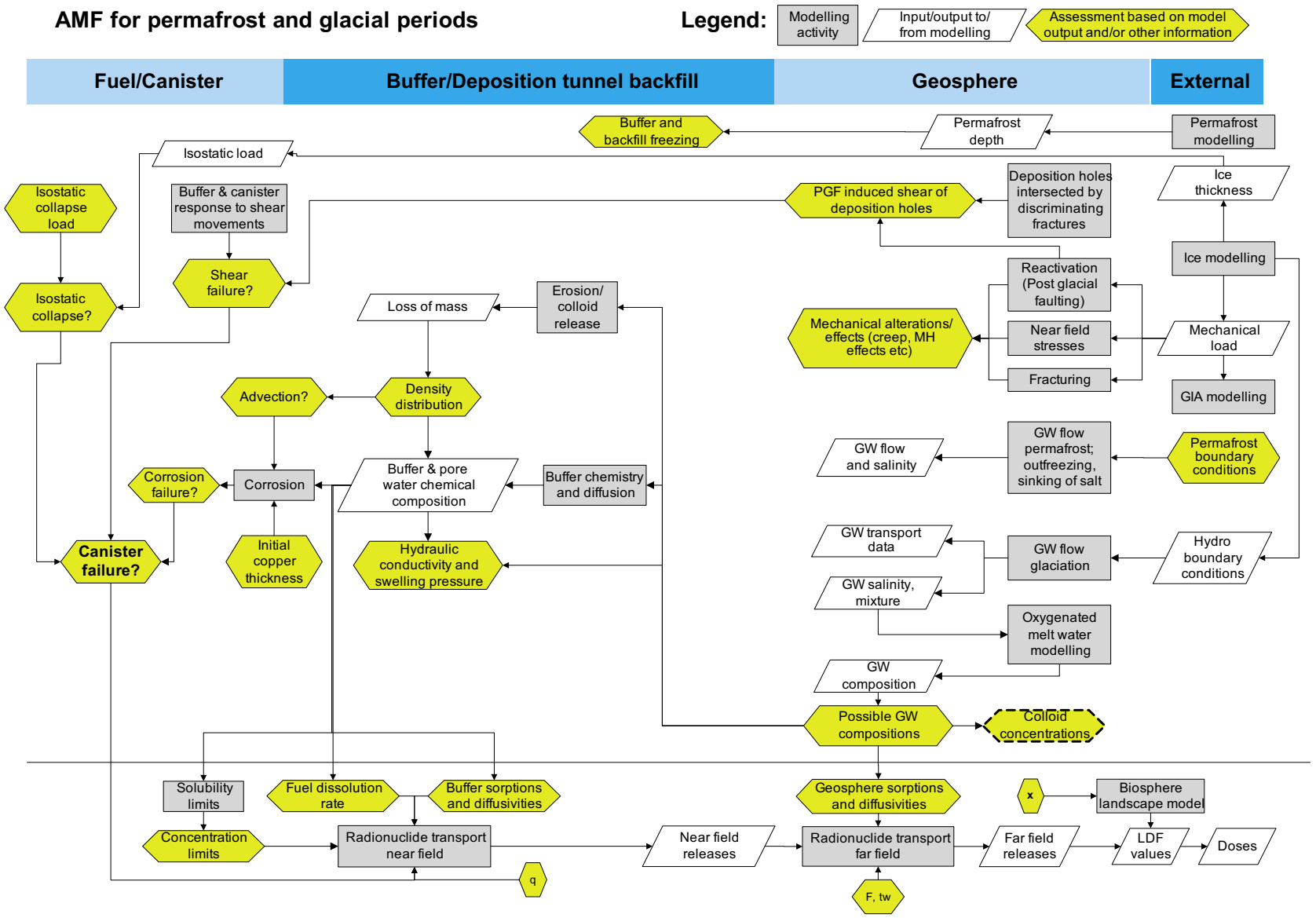

Figure B-2. *Assessment model flow chart for permafrost and glacial conditions.*

ISSN 1404-0344
CM Digitaltryck AB, Bromma, 2006